INFORMATION TO USERS

This manuscript has been reproduced from the microfilm master. UMI films the text directly from the original or copy submitted. Thus, some thesis and dissertation copies are in typewriter face, while others may be from any type of computer printer.

The quality of this reproduction is dependent upon the quality of the copy submitted. Broken or indistinct print, colored or poor quality illustrations and photographs, print bleedthrough, substandard margins, and improper alignment can adversely affect reproduction.

In the unlikely event that the author did not send UMI a complete manuscript and there are missing pages, these will be noted. Also, if unauthorized copyright material had to be removed, a note will indicate the deletion.

Oversize materials (e.g., maps, drawings, charts) are reproduced by sectioning the original, beginning at the upper left-hand corner and continuing from left to right in equal sections with small overlaps. Each original is also photographed in one exposure and is included in reduced form at the back of the book.

Photographs included in the original manuscript have been reproduced xerographically in this copy. Higher quality 6" x 9" black and white photographic prints are available for any photographs or illustrations appearing in this copy for an additional charge. Contact UMI directly to order.

UMI

A Bell & Howell Information Company
300 North Zeeb Road, Ann Arbor MI 48106-1346 USA
313/761-4700 800/521-0600

Synthesis, Characterization and Reactivity Studies of Group 2, 3 and 4 Metal Complexes Bearing Chelating Amino Siloxide and Alkoxide Ligands

by

Pengcheng Patrick Shao
B.Sc., East China University of Chemical Technology, 1988

A Dissertation Submitted in Partial Fulfillment of the
Requirements for the Degree of

DOCTOR OF PHILOSOPHY

in the Department of Chemistry

We accept this dissertation as conforming
to the required standard

Dr. D.J. Berg, Supervisor (Department of Chemistry)

Dr. A. McAuley (Department of Chemistry)

Dr. C. Qian (Department of Chemistry)

Dr. B.J. Hawkins, Outside Member (Department of Biology)

Dr. D.H. McConville, External Examiner (Department of Chemistry, U.B.C)

© Pengcheng Patrick Shao, 1997

University of Victoria

All rights reserved. This dissertation may not be reproduced in whole or in part, by photocopying or other means, without the permission of the author

Supervisor: Dr. David J. Berg

ABSTRACT

A series of chelating amino siloxide and alkoxide ligands have been prepared. Barium, lanthanide and zirconium complexes bearing these new ligands have been synthesized and characterized by NMR or X-ray crystallography. Reactivity of the zirconium complexes has been studied.

The tris(siloxide) lanthanide(III) complexes are all monomeric in both solution and solid-state. A yttrium tris(siloxide) and a zwitterionic ytterbium tetrakis(siloxide) complexes have been characterized by X-ray crystallography. The yttrium complexes have shown high volatility. Mono(siloxide) barium(II) silamide complexes are dimeric as determined by X-ray crystallography, and barium bis(siloxide) exists as a monomer-dimer equilibrium in hydrocarbon solvents. Although highly soluble in hydrocarbon solvents, the barium complexes are non-volatile.

A new aryl(siloxide) ligand has been synthesized and used as an ancillary ligand for the preparation of lanthanide dialkyl complexes. Although ligand redistribution was not observed, "ate"-complexes were isolated instead of neutral dialkyl complexes.

Zirconium bis(aminodiolate) complexes were synthesized by reaction of tetrabenzyl zirconium and two equivalents of the ligands. The substituents on nitrogen were found to have a great effect on the structure. Mono(aminodiolate) zirconium dialkyl complexes were successfully synthesized by three different methods: protonolysis, ligand redistribution and metathesis. Thermal decomposition of these zirconium dialkyl complexes was found to show a marked dependence on the substituents at nitrogen. The

α-methyl benzyl derivative decomposed by *ortho*-metallation of phenyl group exclusively and resulted in clean formation of a metallacyclic complex.

The reaction of primary amines with the metallacycle allowed isolation of amide intermediates protonolysis of the benzyl group, and eventually resulted in formation of bridging imide complexes. The insertion reaction of carbonyl groups (C=O) into the metallacycle Zr-carbon bond proceeds regio- and stereoselectively. The first insertion products of carbonyl insertion were isolated, and the β-naphthaldehyde insertion product was characterized by X-ray crystallography.

The metallacycle exhibited catalytic activity towards alkyne cyclotrimerization without preactivation. Zirconium cationic complexes were generated by alkyl abstraction using $B(C_6F_5)_3$. The cationic complexes generated from the zirconium dibenzyl derivatives showed catalytic activity towards both ethylene and 1-hexene polymerization.

A new cyclopentadienyl ligand bearing pendant fluorinated alkoxide functionality was synthesized. The zirconium complexes bearing this ligand exhibited remarkably high Lewis acidity, and the dichloride complex was shown to be catalytically active towards vinylether polymerization.

Dr. D. Berg

Dr. A. McAuley

Dr. C. Qian

Dr. B.H. Hawkins

Dr. D.H. McConville

TABLE OF CONTENTS

LIST OF TABLES

LIST OF FIGURES

LIST OF ABBREVIATIONS

Me	methyl
Et	ethyl
i-Pr	*iso*-propyl
t-Bu	*tert*-butyl
Cy	cyclohexyl
Ph	phenyl
Bz	benzyl
Cp	cyclopentadienyl
Cp*	pentamethylcyclopentadienyl
MAO	methylaluminoxane
THF	tetrahydrofuran
R_f	alkyl or aryl group with fluorine substituents
s	singlet
d	doublet
t	triplet
q	quartet
m	multiplet
br	broad
vt	variable temperature
ppm	parts per million
ee	enatiomeric excess
de	diasteriomeric excess

ACKNOWLEDGEMENTS

I would like to thank my supervisor, Dr. D.J. Berg, for his encouragement and guidance throughout the course of this work. I would also like to thank the members of the Berg group: L. Lee and L. Clouston. The assistance of C. Greenwood with NMR spectroscopy, D. McGillivray and L. Schallig with mass spectroscopy, and K. Beveridge, B. Chak and D.J. Berg with crystallography is greatly appreciated.

To my parents and my wife, Jiang Liangbo.

CHAPTER 1

INTRODUCTION

1.1 Historical development of metal alkoxide chemistry

The first reported synthesis of an alkoxide compound was by Embelman[1] in 1846 who prepared silicon tetra-*iso*-amyloxide by a reaction between tetrachlorosilane and isoamyl alcohol. In the nineteenth century, an important discovery was the preparation of aluminum trialkoxides. Aluminum triethoxide was first prepared in 1881 by the reaction of aluminum metal with ethanol in the presence of iodine as a catalyst[2]. The first effort to synthesize zirconium alkoxide complexes was attempted by Hornberger in 1876[3]. Although he claimed that the reaction between zirconium tetrachloride and ethanol resulted in the formation of zirconium hydroxide and ethyl chloride, this was later shown to be in error by Bradley[4]. Meyer and Koss investigated the synthesis of lanthanum alkoxide complexes in 1902. They reported that addition of lanthanum trichloride to an ethanol solution resulted in formation of a solid which was assigned the formula $LaCl_3 \cdot 2EtOH$[5]. In the century since the initial synthesis of an alkoxide compound, the development of alkoxide chemistry progressed slowly and until 1950, the alkoxides of only a dozen of elements were known. Since 1950, however, alkoxide chemistry has developed rapidly, so that by the mid 1970's, alkoxides of almost all metallic and metalloidal elements were known. During this period, Bradley and Mehrotra contributed greatly to this area, and their work, as well as that of others, have been summarized in the book "Metal Alkoxides" by Bradley and Mehrotra[6].

The research goals in the early stages of alkoxide chemistry focused on the synthesis of their metal complexes and an understanding of their physical and chemical properties[6]. As far as applications were concerned, the aluminum alkoxide catalyzed reduction of aldehydes and ketones to their corresponding esters was discovered as early

as 1906 by Tischtschenko[7]. By the mid 1920's, aluminum iso-propoxide catalyzed reductions of aldehydes and ketones to their corresponding alcohols was discovered and became known as the "Meerwein-Ponndorf-Verley reduction". This reaction is still widely used as a selective reduction method in organic chemistry[8].

More recently, a resurgence in interest in alkoxide chemistry has been driven by the application of metal alkoxides as precursors to metal oxide based electronic ceramics by means of the MOCVD (Metal-Organic Chemical Vapor Deposition) and sol-gel techniques[9]. MOCVD is a method of film formation on solid substrates that relies upon the transport of the component elements in the gas phase as intact complexes, followed by deposition on the substrate and decomposition, often at elevated temperatures, to form a metal oxide film. The sol-gel technique consists of making a homogeneous solution of the component metal alkoxides in a suitable solvent, and then causing the hydrolysis under controlled conditions to produce a gel containing the hydrated metal oxide. The gel is then dried, compacted, and fired to produce a ceramic or glassy material at a temperature much lower than that required by the conventional melting process. The advantages of MOCVD and sol-gel techniques over other methods (physical deposition methods, such as laser ablation and electron plasma) include higher purity, better control over composition and microstructure, lower processing temperature and simpler equipment. The MOCVD method requires the alkoxides to be volatile while the sol-gel technique requires high solubility in organic solvents. These requirements have led to intensive research aimed at the design and synthesis of bulky and donor functionalized alkoxide ligands[10].

Another major motivation for developing alkoxide chemistry is to study organometallic chemistry with alkoxides as ancillary ligands. The alkoxide ligands are

especially suitable for early transition metals, lanthanides and actinides because they are considered hard Lewis donors, and the metal-oxygen bonds formed are extremely strong. Both academic interest and industrial applications have rendered alkoxide chemistry as one of the fastest growing areas in inorganic chemistry[11].

1.2 Coordination chemistry of lanthanide and group 4 metal alkoxide complexes

The alkoxide ligands used for group 4 elements and lanthanides have varied from simple nonchelating alkoxide, aryloxide and siloxide ligands to multidentate and donor functionalized ligands. Alkoxide ligands are less sterically demanding than amido or alkyl ligands because there is no possibility of α-branching (Figure 1). The Tolman cone angle

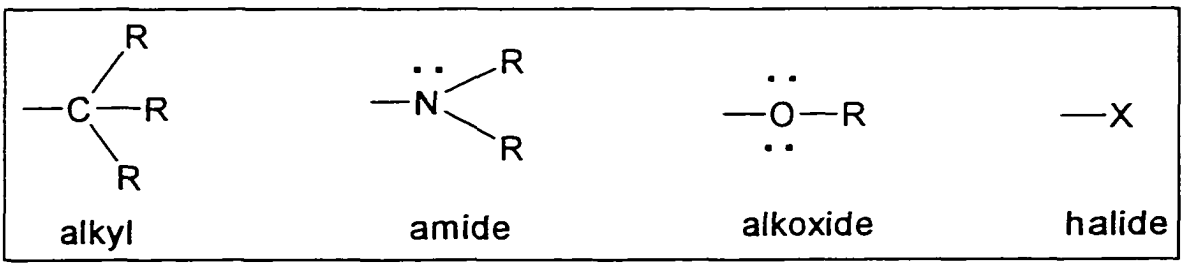

Figure 1 A comparison of the steric bulk of alkyl, amide, alkoxide and halide ligands

of $^tBuO^-$ is less than 90°, and tritox ($^tBu_3CO^-$) ligand, one of the bulkiest alkoxide ligands[12], has a cone angle of 125°; by comparison, the cone angles of all cyclopentadienyl ligands are over 130° as estimated by Tolman[13]. In the early stages of alkoxide chemistry, simple alkoxide ligands such as CH_3O^-, $CH_3CH_2O^-$, $(CH_3)_2CHO^-$, and $(CH_3)_3CO^-$ were commonly used, and the resulting alkoxide complexes often possess multinuclear structures. For example, the degree of aggregation of $Zr[OCH(CH_3)_2]_4$ in benzene

solution is 3.0 as determined by cryoscopy[14], and the lanthanides *iso*-propoxides exist as pentameric oxo-clusters[15]. Although zirconium tetra(*tert*-butoxide) is a monomer by cryoscopy[16], in order to isolate monomeric lanthanide alkoxide complexes, bulkier ligands such as $^{t}Pr^{t}Bu_2O^-$, $^{t}Bu_3CO^-$ or $^{t}Bu_3SiO^-$ must be used[17].

There is a direct relationship between volatility and degree of aggregation: the higher the degree of aggregation, the lower the volatility of the alkoxide complex (Table 1)[6]. Because the volatility is the most important factor to be considered when a alkoxide complex is to be used as a precursor for MOCVD, high aggregation must be avoided. Solubility of the alkoxide complexes also depends on the degree of aggregation, and monomeric complexes usually have high solubility.

Table 1 Molecular complexity and boiling point of group 4 metal alkoxides

$Ti(OR)_4$ and $Zr(OR)_4$	Molecular Complexity	B.P. (°C/mmHg)
$Ti(OEt)_4$	2.4	138.3/5.0
$Ti(O^{i}Pr)_4$	1.4	91.3/5.0
$Ti(O^{t}Bu)_4$	1.0	93.8/5.0
$Zr(OEt)_4$	3.6	234.8/5.0
$Zr(O^{i}Pr)_4$	3.0	203.8/5.0
$Zr(O^{t}Bu)_4$	1.0	89.1/5.0

The bond between early transition metals and oxygen contains a large ionic contribution because of the large difference in electronegativity between the elements. (the electronegativity of lanthanides is estimated by the Allred-Rochow method[18] to be in the range from 1.01-1.14; Ti: 1.32, Zr: 1.22, Hf: 1.23, and O: 3.50.). Lanthanide and group 4

metals are extremely electropositive elements and have large charge to radius ratios which render them strong Lewis acids. In order to achieve steric and electronic saturation, lanthanides and group 4 metal alkoxide complexes often form oligomeric and polymeric structures through oxygen bridging. The alkoxide oxygen has two lone pairs which are capable of $p\pi$-$d\pi$ donation to a metal center, so that an alkoxide can act as a $1e^-$, $3e^-$ or $5e^-$ electron donor (in a neutral sense). Although it is difficult to quantify the exact number of electrons donated to the metal from oxygen, structural information is often helpful in determining whether the metal to ligand bonds contain multiple bond character. A near linear M-O-C bond angle often indicates significant involvement of O(p) → M(d) π-donation; the shorter the M-O bond, the stronger this interaction[19]. However, large M-O-C angles and longer M-O bonds may also be due to steric congestion at the metal center, and these parameters are not always reliable indicators of the M-O bond order. For example, Rothwell has shown that there is no correlation between M-O-C bond angle and M-O bond distance[20].

In principle, alkoxide and cyclopentadienyl ligands are electronically analogous. Linear combinations of C p-orbitals comprise σ- and π-donor orbitals of cyclopentadienyl; while the alkoxide ligand binds to a metal principally through a σ-type orbital but π-donation via the two $p\pi$-orbitals that are perpendicular to the M-O vector can also occur (Figure 2). So that when required alkoxide ligands may act as $5e^-$ electron donors similar to a cyclopentadienyl ligand (in such a case the metal center must be extremely electron deficient and have a low coordination number). In most cases, alkoxide ligands do not donate all five electrons because the electronegativity of oxygen is much higher than that of carbon. As a result, metal complexes with alkoxide ligands often exhibit higher Lewis

acidity than cyclopentadienyl complexes[21]. Compared to cyclopentadienyl ligands, alkoxides are also sterically more flexible, which is important in some catalytic processes such as the zirconium-catalyzed alkyne cyclotrimerization reactions which will be discussed in Chapter 4.

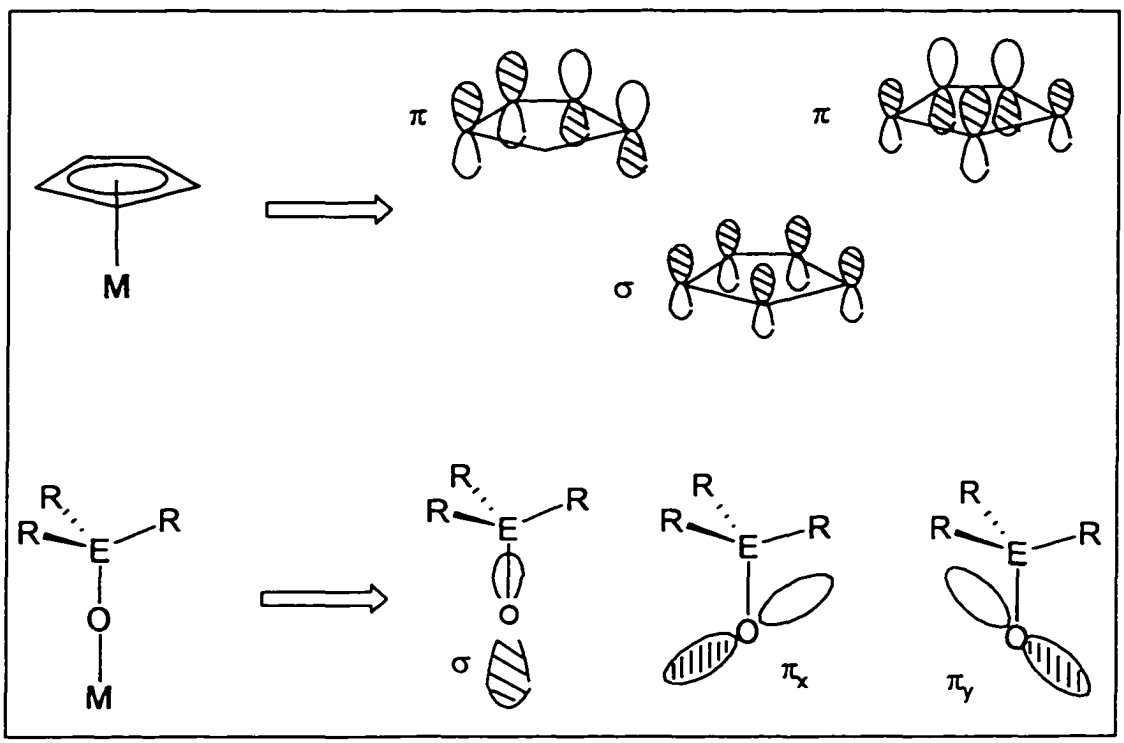

Figure 2 Donor orbital analogy of Cp to an alkoxide ($\sigma + 2\pi$).

1.3 Alkoxide, aryloxide and siloxide ligands

Alkoxide ligands have a conical shape while aryloxide ligands possess "wedge" shapes due to the flat nature of the aromatic ring (Figure 3)[11f]. It appears that the "wedge-like" aryloxide ligand is particularly good at packing around the metal center: Rothwell has shown that regardless of the initial $ZrCl_4/ArO^-$ (Ar: 2,6 di-*iso*-propyl or *t*-butyl phenyl) stoichiometry, the final product was always the zirconium tris-aryloxide complex[22]. An

additional advantage of the aryloxide ligand is that it is straightforward to place bulky groups such as *t*-butyl or cyclohexyl at the 2,6 position of the aromatic ring to construct a sterically demanding ligand. Rothwell has done a great deal of interesting chemistry with early transition metals using these sterically demanding aryloxide ligands[23].

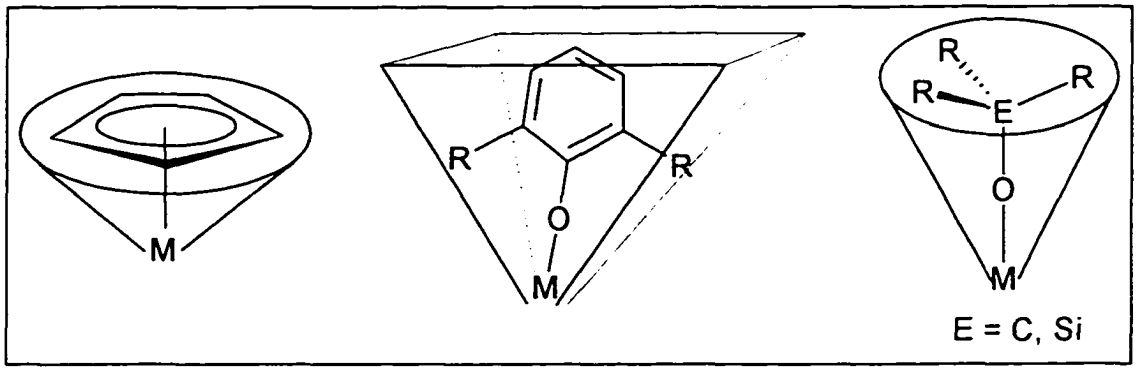

Figure 3 Spatial perceptions of an aryloxide "Wedge" and the conical displacements of Cp and a triangulated alkoxide or siloxide.

In comparison to alkoxides, siloxide ligands with the same substituents are less sterically hindered because the Si-O bond is longer than the C-O bond, and as a result, the steric bulk is farther away from the metal center. In terms of electron donating ability, siloxide ligands are less electron donating than alkoxide ligands. This is most easily seen by an examination of the pK_a values of related species. For example, Et_3SiOH (pK_a = 13.6, in water) [24a] exhibits a higher acid dissociation constant than Me_3COH (pK_a = 19, in water)[24b], reflecting the inductive influence of the more electropositive silicon. The R_3Si group possesses fairly low-lying, empty 3*d* fragment molecular orbitals that can interact with the $p\pi$-orbitals of oxygen. This means that the silicon competes with the metal for the oxygen electron density. As a result, the metal center receives less electron density from

the oxygen and exhibits greater electrophilicity. Although pertinent spectroscopic information is limited, siloxide ligands are believed to electronically influence a metal center in roughly the same manner as aryloxide ligands; both are substantially better at supporting reduced metal centers[25].

Siloxide complexes of the lanthanides and early transition metals usually exhibit higher stability than alkoxide analogues. For example, $(^tBu_3CO)_2ZrCl_2$ degrades within 24 h at 25 °C in C_6D_6, and $(^tBu_3CO)_2NbCl_3$ is too reactive to be isolated, while $(^tBu_3SiO)_3NbCl_3$ can be heated to its melting point (270 °C) without decomposition[26]. The high thermal stability of siloxide complexes can be attributed to both thermodynamic and kinetic effects. Thermodynamically, silicon-oxygen bond strengths are estimated to be in the 130 kcal mol^{-1} range[27], substantially greater than the 90 kcal mol^{-1} usually attributed to C-O single bonds. The mechanism of thermal decomposition of alkoxide complexes is outlined in Scheme 1. Heterolytic C-O bond scission of a bound alkoxide is considered to occur via an S_N1 type process to afford a transient cation R_3C^+ as shown in Scheme 1[28]. It is unlikely that the same mechanism is involved in the decomposition process of siloxide complexes since the pathway of generating silyl cation which eventually decomposes to a silene is highly unfavorable[29]. The high Si-O bond strength and lack of a low energy decomposition pathway render the siloxide complexes unusually stable.

Scheme 1

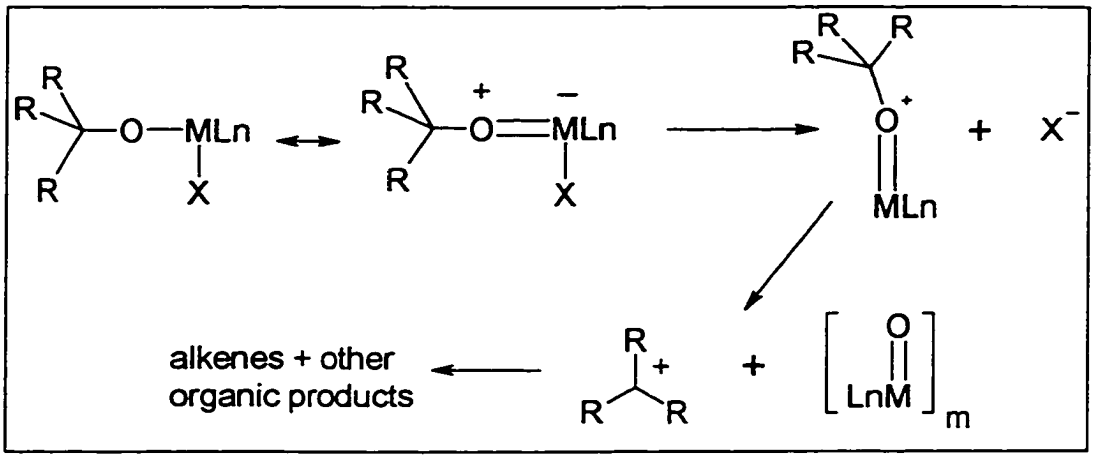

It is also interesting to note that siloxide complexes are usually much less volatile than their alkoxide analogues[30]. The reasons for this difference are less steric bulk for the siloxides and greater metal electrophilicity in the M-O-Si unit (*vide supra*). For example, $[Nd(OSi^tBu_3)_3]$ is nonvolatile and thermally stable at 250 °C/10^{-3} Torr and decomposes at temperatures above 340 °C, while $[Nd(OC^tBu_3)_3]$ decomposes at 150 °C to give the dinuclear derivative $\{Nd(OCH^tBu_2)_3\}_2$, which sublimes at 175 °C/10^{-3} Torr[31]. The aryloxide complexes usually exhibit high thermal stability and low volatility. For instance $Ln[O\text{-}2,6\text{-}^tBu_2\text{-}4\text{-}MeC_6H_2]_3$ (Ln = Sc, Y and La-Lu) only sublimes above 200-250 °C in high vacuum (10^{-4} Torr)[32]. The low volatility of aryloxide complexes is mainly due to the polarizing character of the aryl groups, which reduces the volatility by means of intermolecular π-π interactions. Despite the high thermal stability, the low volatility excludes their application as MOCVD precursors[10].

1.4 Fluorinated ligands

Metal complexes with perfluorinated or highly fluorinated ligands usually show high volatility and solubility[33]. For example, $[La_3\{OCCH_3(CF_3)_2\}_9]$ is much more volatile than $[La_3(OCMe_3)_9].2HOCMe_3$ (130 °C/10^{-2} Torr vs. 240 °C/10^{-3} Torr)[34]. The high volatility is due to the intermolecular repulsion of the extremely electronegative fluorine groups. Although high volatility is the most desired property in a MOCVD precursor, the draw back of using alkoxides with fluorinated ligands is that the final metal oxide products are often contaminated with undesired fluorides[10, 35].

The Van der Waals radius of fluorine is only approximately 10 % larger than that of hydrogen (135 pm vs. 120 pm)[36]. Hence, CF_3 is not much larger than CH_3, however, the electron withdrawing ability is totally different. The CF_3 group is one of the strongest electron withdrawing groups while CH_3 is considered to be an electron donating group. The strong electronic effect of fluorine is also evident in borane chemistry: $B(C_6F_5)_3$ is a much stronger Lewis acid than $B(C_6H_5)_3$ and capable of abstracting alkyls group from zirconium to generate cationic zirconium complexes. Introducing fluorinated groups reduces the pK_a of alcohols drastically[37] (pK_a value of CH_3CH_2OH[38a]: 16, CF_3CH_2OH: 11.4[38b], $(CF_3)_2CHOH$: 9.3, $(CF_3)_3COH$: 5.95[39]) which should increase both the Lewis acidity and stability of metal complexes derived from the corresponding alkoxides. In many cases, metal complexes with fluorinated ligands exhibit unique catalytic reactivities and have great application in organic synthesis (Chapter 5).

1.5 Application of donor functionalized alkoxide and siloxide ligands for MOCVD

Donor functionalized alkoxide ligands such as alkanolamines and alkoxyethanol have been extensively used for preparing group 13, 14 and transition metal complexes. Mehrotra and others have synthesized and studied the reactivity of boron, aluminum, silicon, germanium, tin, titanium and lanthanide complexes with alkanolamines ligands[6]. However, application of these complexes was not investigated during the early stages of this work. Research in this area has been spurred by the demand for volatile alkoxide complexes for MOCVD purposes, and it is significant to note that Mehrotra and Singh pointed out "that bulky ligands with side chains capable of donor functionality...appear to combine the advantage of steric crowding as well as coordinative saturation within the same species"[40]. In a recent review entitled "Volatile Metal Alkoxides According to the Concept of Donor Functionalization", Herrmann describes the recent developments in this area[10].

Because of the ionic character and highly polar nature of the M-O bond intermolecular dipolar interactions are usually strong. There are two ways to reduce this interaction and to achieve volatility of the alkoxide complexes: (1) increasing the distance between polar M-O units by means of large organic groups (concept of steric shielding); (2) reducing the polarizing strength of the metal ion by charge transfer from donor ligands (concept of donor functionalization). One problem in utilizing extremely bulky ligands such as $HOC(^tBu)_3$ is that "steric overcrowding" can result in alkoxide decomposition by homolytic (when metals are less electropositive)[41] or heterolytic (when metals are more electropositive)[42] cleavage as shown in Scheme 2. One of the best studied examples is the decomposition of $Ce(O^tCBu_3)_3$ which allows isolation of a X-ray crystallographically

characterized dimeric cerium alkoxide $[Ce(OCH^tBu_2)_3]_2$ as the main decomposition product.

Scheme 2

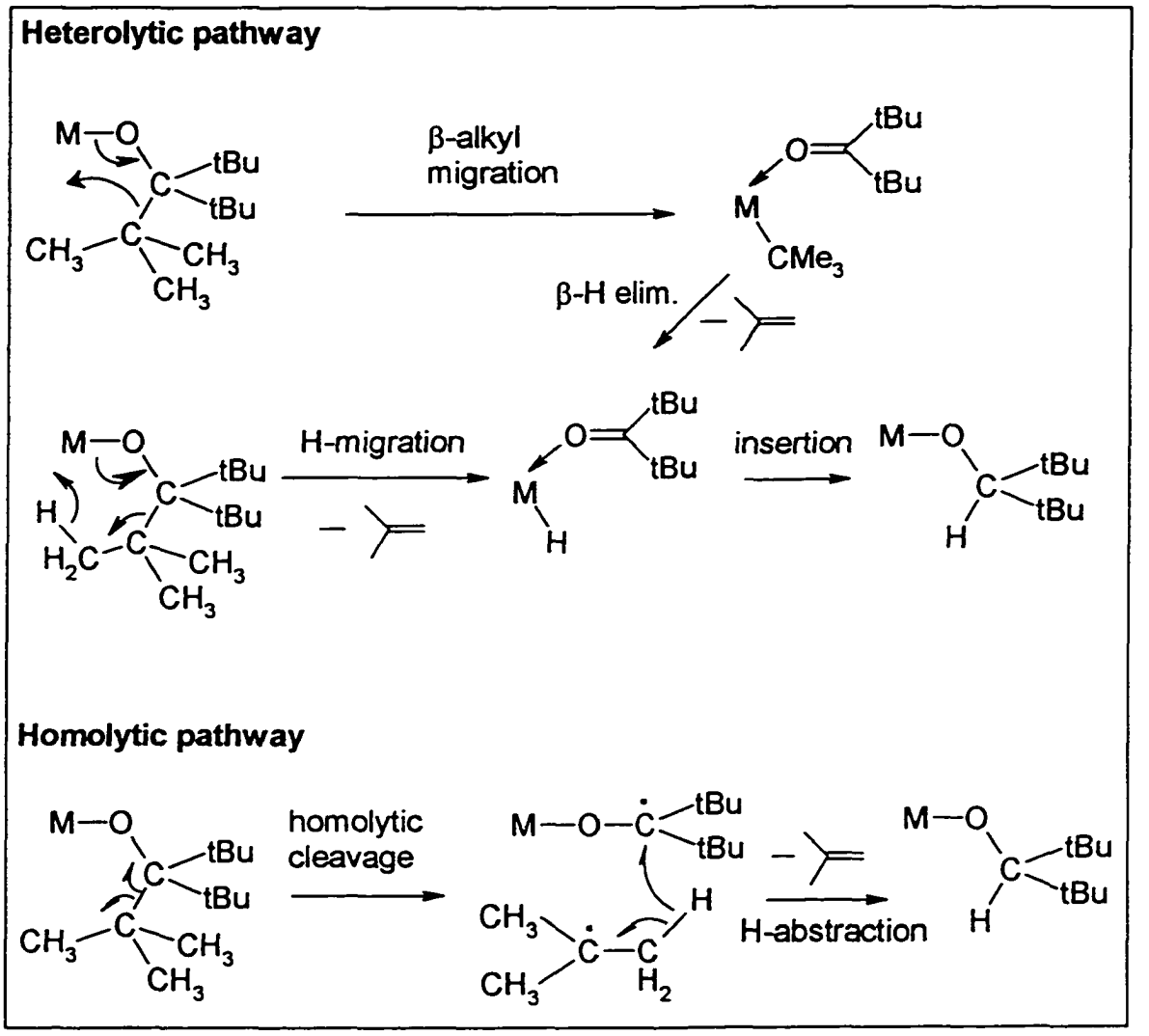

The copper complex, $[Cu(OCH_2CH_2NEt_2)_2]$, reported in1989, is volatile at 100 °C in high vacuum[43], and is the first example of a volatile metal complex containing a donor functionalized ligand. 2-Methoxyethanol $HOCH_2CH_2OCH_3$ is one of the most widely used donor functionalized ligands and has been used to prepare complexes of Ca, Ba, Pb, Bi,

Cu, Cd Y and Ce. Although these alkoxides often show good solubility in nonpolar organic solvents and are useful for sol-gel processes, they are nonvolatile[10].

When dealing with large and electropositive ions such as Ba^{2+}, neither principle alone leads to optimal volatility and thermal stability. However, a combination of high steric demand and donor functionalization in the same ligand can lead to high volatility and thermal stability. For example, this strategy has been used to generate the most volatile Cr^{III} complex to date, $Cr\{O(CH_3)_2CH_2OCH_3\}_3$, which sublimes at 65 °C/1.5 Torr without decomposition[44]. Barium is a very important component in high Tc superconductors, and the search for a suitable MOCVD precursor of Ba^{2+} represents an extremely difficult case because of the extremely large, electropositive and divalent nature. With $HOC(^tBu)(CH_2O^iPr)_2$, the barium derivative $[Ba_2\{OC(^tBu)(CH_2O^iPr)_2\}_4]$ sublimes at 150 °C /10^{-2} Torr. This is the first barium alkoxide that fully sublimes without any decomposition[45].

1.6 Application of chelating alkoxide ligands as ancillary ligands in lanthanide and early transition metal organometallic chemistry

Although organometallic chemistry of the lanthanides and group 4 metals is dominated by Cp and its derivatives as ancillary ligands, there is an increasing trend towards alternative ligands such as alkoxide and amido ligands since these ligands are sterically and electronically very different from Cp derivatives, and the metals complexes derived from these alternative ligands are expected to exhibit unique reactivities[46].

Alkoxides are very useful in organic synthesis, especially in asymmetric catalysis due to ease of access to a large variety of chiral alkoxide ligands. It is very important to

have the alkoxide ligand attached to the metal center during the catalytic process in order to achieve high stereoselectivity. This can be very difficult when the pK_as of the reaction substrates are comparable to alcohols. Additionally, since the pK_a of H_2O is lower than that of alcohols, these alkoxide complexes are all moisture sensitive. Several strategies have been employed to address this problem including use of phenols[47] or silanols[48] which have lower pK_a values to provide a thermodynamic stabilization of the metal ligand bonds and using sterically hindered ligands to kinetically retard the loss of a coordinated alkoxide ligand[49]. However in the area of asymmetric catalysis, these strategies are not totally satisfying, since there is no reaction in which high enantioselectivity (> 70% ee) has been achieved using a transition metal catalyst bearing monodentate alkoxide ligands[50]. The most successful strategy for preparing robust early transition metal alkoxides is the use of diols or polyols so that the metal complexes are stabilized via chelation. A familiar example is the Sharpless asymmetric epoxidation which utilizes bidentate diolate ligands derived from dialkyl tartrates[51]. Nearly perfect enantioselectivity has been achieved which indicates clearly that the ligand remains attached to the metal during the catalytic reaction.

With donor functionalized ligands, the pendant Lewis bases not only provide the metal center electronic and steric saturation, but they may also dissociate to open coordination sites for incoming substrates when it is required. Thus, donor functionalized alkoxides may possess interesting reactivities. For example, a dimeric titanium complex bearing an amino diol ligand prepared by the Nugent group is a excellent enatioselective alkyl transfer catalyst for the reaction of benzaldehyde and diethyl zinc (96% ee)[21]. The effect of the pendant Lewis bases has been well recognized, and many donor functionalized ligands have been successfully applied in organometallic chemistry[52].

However, the chemistry of lanthanide and group 4 metal organometallic complexes bearing donor functionalized alkoxide ligands has not yet been well explored, and the effect of the Lewis base donor on the stability and reactivity of the metal complexes is not well understood.

The most common problems in lanthanide and group 4 metal organometallic chemistry are ligand redistribution and formation of intermolecularly bridged oligomers. These problems are especially severe in the case of lanthanide because their ions are considerably larger and more electropositive than those of the group 4 metal ions, and only extremely bulky ligands such as Cp* and $[N(SiMe_3)_2]^-$ provide sufficient steric shielding to allow isolation of monomeric complexes. However even with these bulky ligands, redistribution may still occur. Thus it is extremely difficult to synthesize monoligand lanthanide dialkyl complexes. For example, Cp^*LnR_2 is very extremely difficult to prepare because it can undergo ligand redistribution to form Cp^*_2LnR as shown in Equation 1[53]. With donor-functionalized sterically demanding ligands, it may be possible to achieve sufficient electronic and steric saturation to prevent ligand redistribution. Recently, Takats has shown that bulky tris(pyrazolyl)borate ligands allow isolation of previously unknown divalent lanthanide alkyl and trivalent lanthanide dialkyl complexes[54]. In this case, the contribution of the Lewis base donors is clearly demonstrated.

$$2\ Cp^*LnR_2 \rightarrow Cp^*_2LnR + LnR_3 \text{ (often decomposes)} \qquad (1)$$

One of the most important applications of lanthanide and group 4 metal complexes is in Ziegler-Natta olefin polymerization. More than 40 years ago, Ziegler discovered that

ethylene could be polymerized with $TiCl_4$-$AlClEt_2$ catalyst[55], and shortly following that discovery, Natta discovered stereoselective propene polymerization[56]. Since then, polymerization of α-olefin has developed into a giant industry with worldwide annual polyolefin production of more than 54 million tons. Classical Ziegler-Natta catalysts are heterogeneous, and after four decades of development, these heterogeneous catalysts have become even more efficient. The modern $MgCl_2$-supported catalysts have tremendous activity and such minute amounts of catalysts are required that they can be left in the polyolefin product without affecting the polymer properties[57]. Heterogeneous catalysts also give highly stereoregular polypropene. Today, most industrial polyolefin production is still based on heterogeneous catalysts. Despite all the advantages of heterogeneous catalysis systems, because they are heterogeneous, there are many different types of active sites and the resulting polymers often have broad molecular weight distributions. In the case of copolymer synthesis, heterogeneous catalysts often lead to uneven incorporation of comonomer. These drawbacks can be overcome by using homogeneous metallocene catalysts.

Application of group 4 metallocene complexes in olefin polymerization was studied by Wilkinson *et al.*, shortly after the synthesis of the first group 4 metallocene complex[58]. However, the early results were not promising. It was only after the accidental discovery that trace H_2O dramatically enhanced catalytic activity of the Cp_2ZrR_2+$AlMe_3$ system and that addition of MAO (methylaluminoxane) had the same effect[59], that metallocene catalysts became practicable. At the present time, homogeneous metallocene catalysts can achieve comparable catalytic activity to heterogeneous systems and are capable of producing highly stereoregular polymer with very narrow molecular weight

distributions. Synthesis of high performance copolymers has become possible because metallocene catalysts are homogeneous and have a single type of catalytically active site. The real active species in metallocene-based polyolefin catalysts is believed to be Cp_2ZrR^+ which is generated through alkyl abstraction by MAO[60]. MAO is the most widely used cocatalyst. The drawback of this method is that MAO has to be used in large excess in order to achieve high activity, usually at Al:Zr ratios of 10^3-10^4:1. The high cost of MAO and the need to remove it from the polyolefin products adds to the cost of these systems. Because of the industrial importance of olefin polymerization and superior performance of metallocene catalysts, research on metallocene catalysts has attracted enormous interest. Several reviews have summarized recent achievements in this area[61].

Although metallocene catalysts exhibit the most promising performance, increasing efforts have been directed at new ligand environments and catalyst types for two primary reasons: first, to find a patentable ligand system which can rival or exceed the extensively patented Cp compounds (ca. 1400 patents on Cp-based catalysts have been filed); second, to eliminate the complications of a counteranion and to develop neutral analogues of cationic complexes[61a].

Among the numerous alternative ligands which have been employed, chelating cyclopentadienyl-amido ligands such as **I** and **II** have proven very successful in a range of polymerizations and copolymerizations[62]. Cationic complexes derived from bidentate[63] and tridentate[64] chelating amido ligands **III** and **IV** show catalytic activity towards olefin polymerization. Macrocyclic ligands such as **V** and **VI** have also been investigated. Although the zirconium dialkyl complexes derived from these ligands have a geometry

closely similar to zirconocene dialkyls and cationic alkyl complexes can be made, they are either inactive towards olefin polymerization (VI[65]) or poor catalysts (V[66]) (Figure 4).

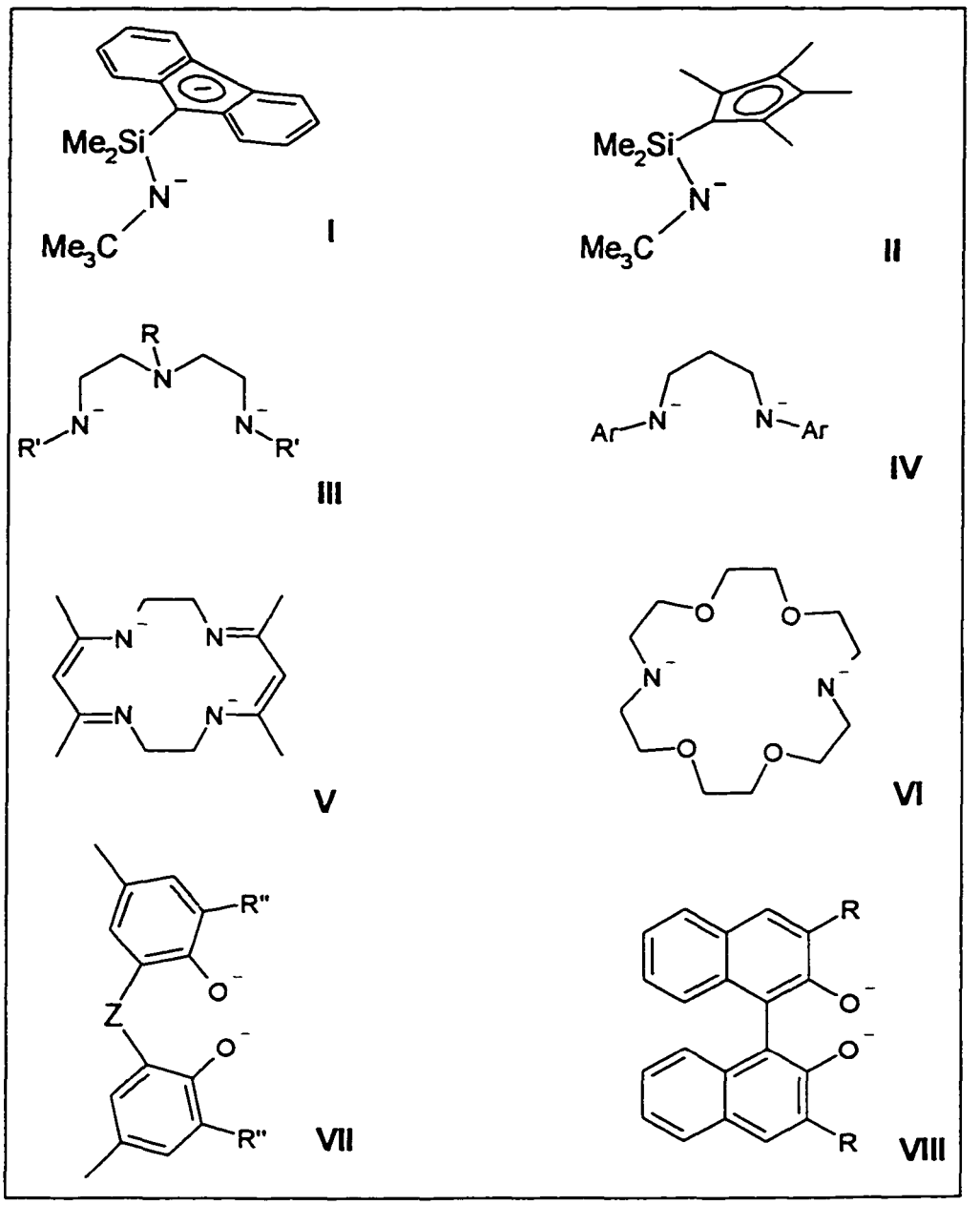

Figure 4 Examples of alternative ligand systems

Application of alkoxide (aryloxide) complexes in olefin polymerization have also been explored. There are reports showing that titanium phenoxide complexes in the presence of larger excess of MAO (5000 equivalent) were highly active olefin polymerization catalysts[67]. Schaverien has studied olefin polymerization activity of cationic titanium and zirconium complexes with sterically hindered chelating phenoxides (**VII** and **VIII**, Figure 4). These complexes showed moderate activity towards ethylene as well as α-olefin polymerization[68].

Lanthanide complexes (L_2LnR) are isoelectronic with cationic group 4 complexes. The chemistry and reactivity of both groups of metals should therefore be quite similar, and lanthanides have the advantage of being neutral species, thus eliminating complications due to the counteranion. Indeed, lanthanide metallocenes such as [$Cp^*_2LuCH_3$] are highly active ethylene polymerization catalysts; however, they are not useful in propene polymerization since they give only propene oligmers[69]. Besides the obvious Lewis acidity differences between neutral lanthanides and cationic group 4 metal complexes, the former are prone to formation of bridging dimers, which often possess much lower reactivity. It is possible that it is this dimer formation which is responsible for the low catalytic activity of most lanthanide complexes[70]. The catalytic activity of lanthanide complexes with cyclopentadienyl-alkoxide mixed ligand system have been investigated by the Schaverien group and were found to show only moderate activity towards ethylene and 1-hexene polymerization[71].

1.7 Methods for synthesis of alkoxide complexes

The general methods for synthesis of alkoxide complexes have been summarized in the book "Metal Alkoxides" by Bradley and Mehrotra[6]. Some of the most useful methods include (a) direct reaction of metals with alcohols; (b) metathesis reaction with metal halides; (c) reaction of metal alkyl or amide complexes with alcohols; (d) interchange reaction with esters or other alcohols.

(a) Direct reaction between metals and alcohols

This method involves the direct reaction of a metal with an alcohol as shown in equation 2:

$$M + n\,ROH \rightarrow M(OR)_n + n/2\,H_2 \qquad (2)$$

This method is limited to the strongly electropositive metals, such as the alkali and alkaline earth metals and the lanthanides. For the lanthanides, the direct reaction between the lanthanide metals and alcohols is extremely slow and is not practicable; instead, lanthanide amalgams or metal vapor deposition techniques are usually employed[72].

(b) Metathesis reactions with metal halides

Metal halides are common starting materials and many of them are available in anhydrous form. This is one of the most widely used methods as shown in equation 3, 4 and 5:

$$L_nM\text{-}X + HOR \rightarrow L_nM\text{-}OR + HX \qquad (3)$$

$$L_nM\text{-}X + HOR + NR_3 \rightarrow L_nM\text{-}OR + R_3NH^+X^- \qquad (4)$$

$$L_nM\text{-}X + Li(Na,K)OR \rightarrow L_nM\text{-}OR + Li(Na,K)X \qquad (5)$$

When a metal halide is dissolved in alcohol, the initial process must be solvation. For the electronegative elements like boron, silicon and phosphorus, solvolysis of the halide occurs completely with the replacement of the halogens by alkoxy groups and release of HCl[73]. However, in the case of the more electropositive elements like the lanthanides, no lanthanide alkoxides are formed and only alcohol solvated halides can be isolated[74]. When $TiCl_4$ and $ZrCl_4$ react with alcohols, only partially solvolysed products can be isolated (equation 6 and 7)[75]. However, addition of amine leads to clean formation of alkoxide complexes (equation 8)[76].

$$TiCl_4 + 3C_2H_5OH \rightarrow TiCl_2(OC_2H_5)_2 \cdot C_2H_5OH + 2HCl \quad (6)$$

$$ZrCl_4 + 3C_2H_5OH \rightarrow TiCl_2(OC_2H_5)_2 \cdot C_2H_5OH + TiCl_3(OC_2H_5) \cdot C_2H_5OH + 3HCl \quad (7)$$

$$TiCl_4 + 4ROH + 4NH_3 \rightarrow Ti(OR)_4 + 4NH_4Cl \quad (8)$$

Reaction of metal halides and alkali metal alkoxides has been used successfully for the synthesis of large numbers of alkoxide complexes including lanthanide and group 4 metal complexes (equation 9)[77]. The drawbacks of this method are the difficulty in removing alkali metal halides from the alkoxide products and the formation of ionic "ate"-complexes (equation 10)[78]. However these problems can be avoided by using less polar solvents such as hydrocarbons or through method (c) below.

$$MCl_n + n\,NaOR \rightarrow M(OR)_n + n\,NaCl \quad (9)$$

$$MO^tBu + Zr(O^tBu)_4 \rightarrow \underset{\text{"ate"-complex}}{M^+[Zr(O^tBu)_5]^-} \quad (M = Li, Na, K, Cs) \quad (10)$$

(c) Reaction of metal alkyl or amide complexes with alcohols

Because the pK_a of amines and alkyls are much higher than that of alcohols, there is a great thermodynamic driving force for the reaction between early transition metal amides and alkyls with alcohols. When volatile amines or alkyls are used, they can be easily removed by vacuum distillation leaving clean metal alkoxide products (equation 11 and 12). Because it gives clean products, this method was extensively used in preparing lanthanide and early transition metal complexes despite the fact that this necessitates preparation of suitable alkyl or amide metal complexes as starting materials. This is also the main method employed throughout the research described in this thesis. Lanthanide silamide[79], barium silamide[80], zirconium tetrabenzyl[81], zirconium dibenzyl dichloride[81] and zirconium bis(silamide) dichloride[82] complexes are the main starting materials used in this research because they are easy to prepare and purify.

$$M(NR'_2)_n + n\,ROH \rightarrow M(OR)_n + n\,R'_2NH \quad (11)$$

$$MR'_n + n\,ROH \rightarrow M(OR)_n + n\,R' \quad (12)$$

(d) Interchange reactions with esters or other alcohols

Interchange reactions of alkoxides with esters or alcohols are outlined in the following equations:

$$M(OR)_n + m\,R'OH \rightleftharpoons M(OR)_{n-m}(OR')_m + m\,ROH \quad (13)$$

$$M(OR)_n + m\,CH_3COOR' \rightleftharpoons M(OR)_{n-m}(OR')_m + m\,CH_3COOR \quad (14)$$

The simple alcohol and ester exchange reactions are nearly thermoneutral, and an equilibrium is obtained instead of a clean reaction. However, if the byproduct alcohols or esters can be removed from the reaction mixture, it is possible to push the equilibrium towards exclusive formation of the desired products. This is therefore a particularly useful method when the boiling point of the starting alcohol or ester is significantly higher than that of the product so that the latter can easily be removed by distillation[83].

In the case of chelating donor functionalized alkoxide ligands, the gain in free energy (negative enthalpy contribution from coordination of the Lewis base and positive entropy contribution from the chelate effect) is often high enough to drive the interchange reaction to completion. For example, treatment of a THF solution of titanium *iso*-propoxide with 1 equivalent of the aminotriol results in loss of 3 equivalents of *iso*-propanol and quantitative formation of the desired product (equation 13)[50a]. Although this method has not been used in this research, the similarity between this aminotriol and the ligands employed in this research suggests it is potentially useful.

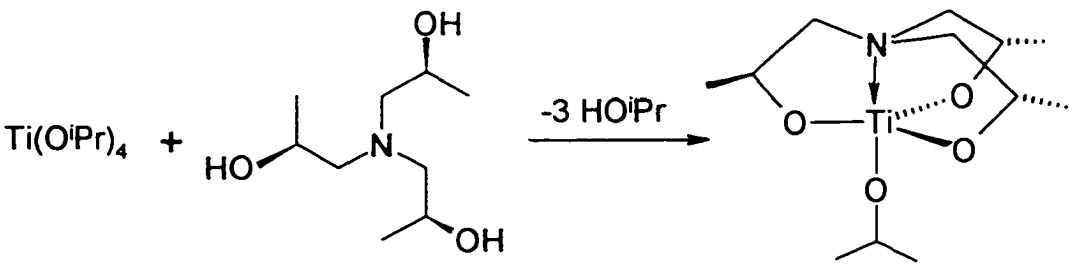

(15)

1.8 Objective of the research

The aim of this project is to develop new chelating, donor functionalized, sterically demanding alkoxide (siloxide) ligands and apply these ligands to lanthanide and group 4 metals. There are two main research directions in this project: (a) to synthesize lanthanide and barium complexes bearing chelating sterically demanding aminosiloxide ligands and investigate their possible applications as MOCVD precursors; (b) to utilize chelating aminodialkoxides as alternative ligands to cyclopentadienyl for zirconium chemistry and to study the applications of these complexes in organic synthesis and Ziegler-Natta olefin polymerization.

When we first started this project, there was tremendous interest in synthesis of volatile or highly soluble alkoxide complexes because of the application of these complexes in synthesis of high Tc superconductor materials[84]. It was an challenging task to prepare volatile lanthanide and barium alkoxides. In the following chapter, the synthesis, structural characterization and volatility investigation of lanthanide and barium complexes bearing bulky donor functionalized siloxide ligands **IX** and **X** will be presented; as well, in this chapter, our attempts at synthesizing lanthanide alkyl complexes with siloxide ligand **XI** will also be shown (Figure 5).

Organometallic chemistry of the group 4 metals has been dominated by Cp and its derivatives as ancillary ligands. However, alternative ligands such as amido, phosphino, alkoxide and thiolate ligands have seen increasing use. Chapter 3 details the synthesis of a series of new chelating amino alkoxide ligands (**XII** and **XIII**) and their zirconium complexes. Decomposition reactions of the zirconium dialkyl complexes will be discussed, and the effects of the Lewis base donor will be emphasized. Reaction of zirconium alkyl

complexes bearing the amino alkoxide ancillary ligands with various organic substrates including amines, carbonyl groups and alkynes will be presented in Chapter 4. Our preliminary results on application of the cationic zirconium complexes in Ziegler-Natta olefin polymerization are also included in this chapter. In Chapter 5, the synthesis and characterization of cyclopentadienyl alkoxide (fluorinated) ligands (XIV) and their zirconium complexes will be presented. Chapter 6 concludes the discussion with an evaluation of the ligand systems used in this project. Finally, full experimental details pertaining to the synthesis and characterization of the ligands and their metal complexes is presented in Chapter 7.

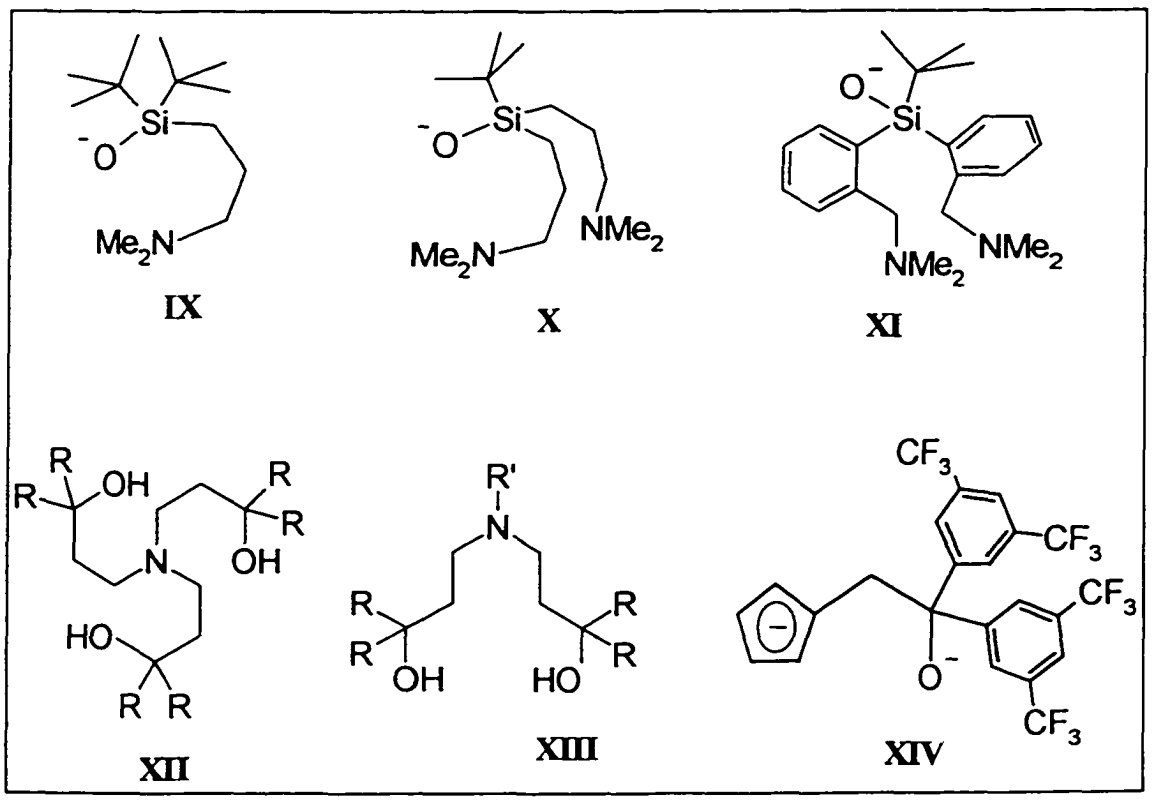

Figure 5 Ligand systems employed in this project.

CHAPTER 2

SYNTHESIS AND CHARACTERIZATION OF YTTRIUM AND BARIUM COMPLEXES BEARING AMINO SILOXIDE LIGANDS

2.1 Introduction

Metal alkoxides (siloxides) are excellent precursors for the deposition of metal oxides (MOCVD and sol-gel methods)[10], and the current interest in using metal oxides in optoelectronics, high-Tc superconductors, and other electronic ceramics has led to tremendous interest in the chemistry of the metal alkoxides[84]. Of particular interest, group 2 and 3 elements such as Ba and Y are the main components in the high Tc superconductor $YBa_2Cu_3O_7$. When this project began, volatile yttrium and barium alkoxides which could be employed in the growth of thin-film superconductors by MOCVD were synthetically challenging targets[85]. Although high volatility can be achieved by using fluorinated β-diketonate or alkoxide ligands, it often causes fluoride contamination in the final metal oxide products during the thermal decomposition of the alkoxides[86]. Among the nonfluorinated ligands, donor-functionalized sterically demanding alkoxide ligands are the most promising for this purpose[10]. The siloxide ligands (**3** and **4**, Scheme 3) used in this project have bulky *tert*-butyl group(s) on silicon to provide steric shielding and flexible pendant dimethylamino group(s) to provide extra steric and electronic saturation. Metal complexes of **3** and **4** are expected to have a low degree of aggregation and thus high volatility. Preceding this research work, there were several reports employing chelating alkoxide ligands in group 2, 3 and lanthanide chemistry. For example, Lappert's group utilized phosphinoalkoxide ligands with bulky *tert*-butyl groups on the alkoxide carbon to synthesize a series of lanthanide complexes (**XV**)[87a] (Figure 6). While this work was in progress, Herrmann reported the synthesis of a number of closely related lanthanide alkoxide complexes (**XVI**) bearing donor-functionalized alkoxide ligands for MOCVD purposes[87b]. These complexes showed high volatility.

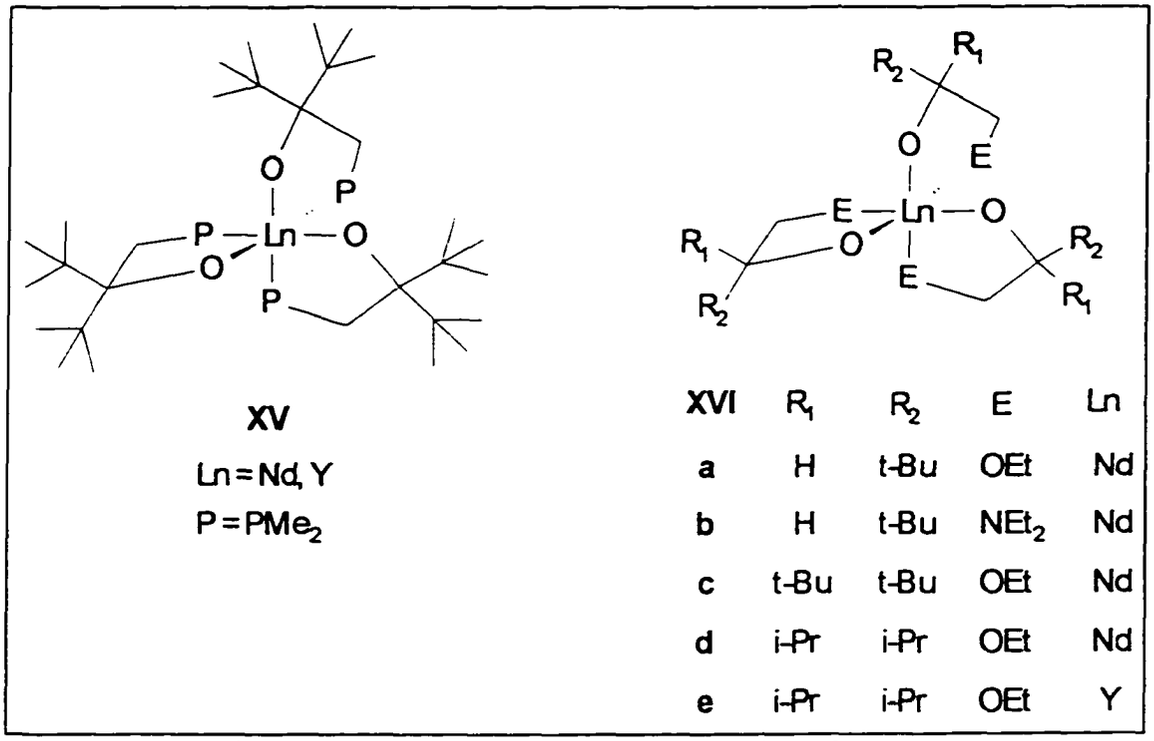

Figure 6 Lanthanide alkoxides with donor functionalized ligands

2.2 Ligand synthesis

The silanol ligands **3** and **4** were prepared in two steps from *tert*-butyl dichlorosilane or chloro-di-*tert*-butylsilane and the Grignard reagent as shown in Scheme 3. Preparation of the Grignard reagent must be carried out immediately after the ammonium salt has been free-based and dried over anhydrous $MgSO_4$, because free 3-chloropropyldimethylamine can undergo self-condensation. The silicon center is highly congested as indicated by the slow reactions of these chlorosilanes with the Grignard reagent. Thus in the case of chloro-di-*tert*-butylsilane, the reaction mixture must be refluxed in THF for 48 hours in order to complete the reaction; *tert*-butyldichlorosilane reacted more rapidly but overnight reflux in THF was still required. In both cases, the

Grignard reagent was used in slight excess (1.1 eq). The intermediate silanes **1** and **2** were isolated as very pure colorless liquids after vacuum distillation. Although silanes are generally moisture sensitive compounds, the purified silane products did not show any evidence of hydrolysis after exposure to air for days. Indeed, conversion of silanes **1** and **2** to silanols, **3** and **4**, proved quite difficult as prolonged reflux (in the case of **2**, it took one week!) in aqueous HCl (3M) was necessary. Silanols **3** and **4** showed remarkable stability to condensation and disiloxane products were not observed even under the harsh hydrolysis conditions. All these observations show that the silicon center is highly congested. Additionally, the mass spectra of **1-4** all revealed a base peak corresponding to loss of a *tert*-butyl fragment with the more bulky di-*tert*-butyl compounds **2** and **4** showing the greatest relative intensity for this peak.

Ligand **5** was synthesized by the reaction of *tert*-butyl trichlorosilane with the lithium reagent in 1:2 ratio followed by quenching with an aqueous solution of K_2CO_3. The lithium reagent was prepared by addition of one equivalent of n-butyl lithium to a hexane solution of benzyldimethylamine which led to selective metallation at the *ortho* position due to chelate formation[88]. The arylsilanol ligand **5** was isolated in high yield as yellow crystals after recrystallization from toluene. (Scheme 3)

Scheme 3

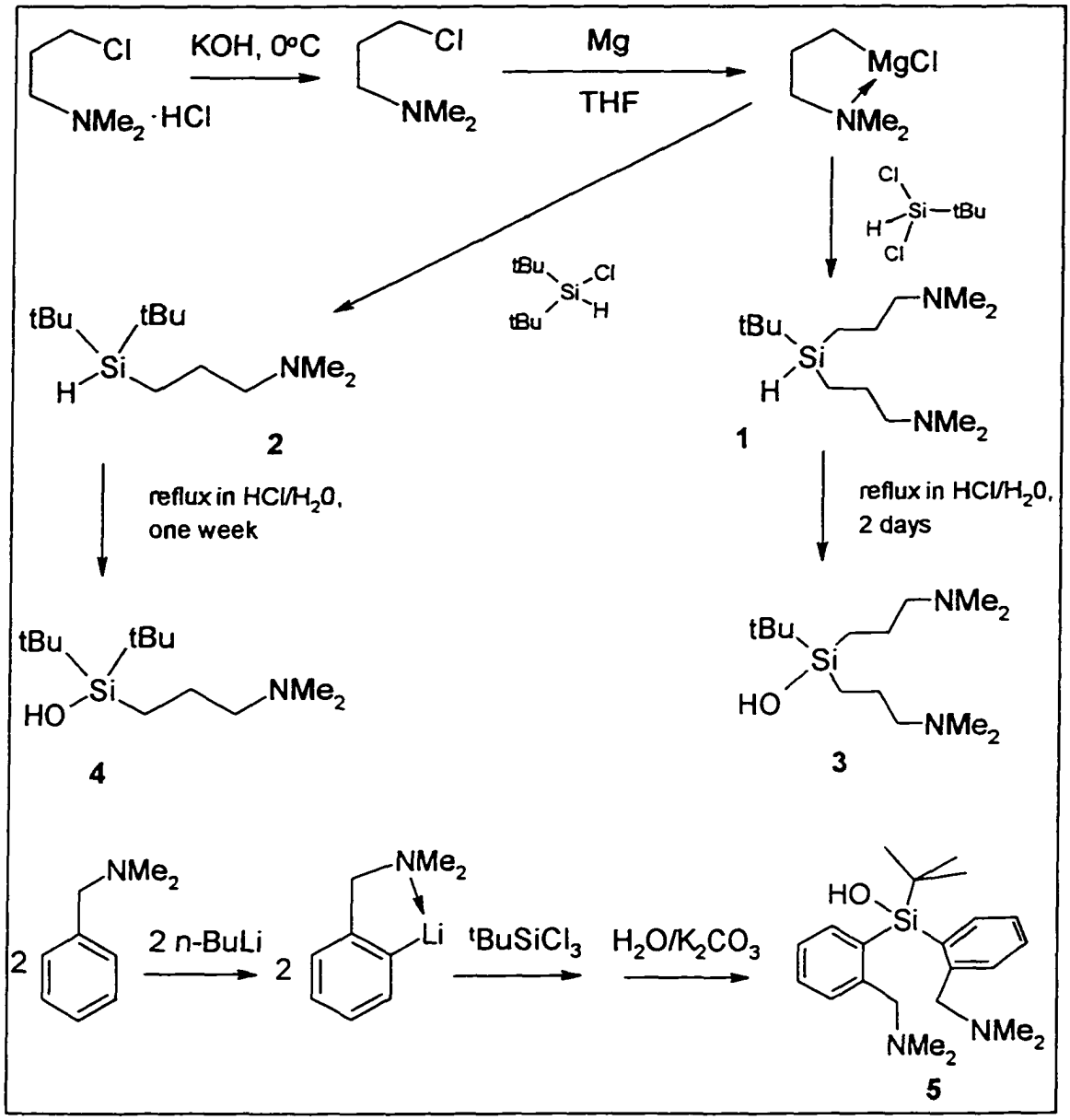

2.3 Lanthanide tris(siloxide) complexes

2.3.1 Synthesis and characterization

Reaction of **3** and **4** with $Ln[N(SiMe_3)_2]_3$ (Ln = Ce and Y) in a 3:1 molar ratio allowed isolation of the tris(siloxide) complexes **6, 7** and **8** (equation 16). Complexes derived from the tridentate silanol **3** were found to be viscous oils of high hexane solubility. Yttrium complex **6**

was isolated as a pure oil that slowly crystallized but the cerium analog could not be isolated in reasonable purity. In contrast **7** and **8**, derived from the bidentate silanol **4**, were isolated as crystalline compounds from toluene-hexane mixtures.

3 equiv. **3** or **4** + $Ln[N(SiMe_3)_2]_3$ →

$$Ln[OSiBu^t_{3-n}[(CH_2)_3NMe_2]_n]_3 + 3\ HN(SiMe_3)_2 \qquad (16)$$

6 n = 2 ; Ln = Y
7 n = 1 ; Ln = Y
8 n = 1 ; Ln = Ce

The NMR spectra of **6** - **8** show only one type of siloxide ligand. The yttrium complexes, **6** and **7**, show a small $^2J(^{29}Si\text{-}^{89}Y)$ coupling of 6 Hz. The ^{29}Si resonance shifts ca. 10 ppm upfield relative to the free silanol (**3** and **4**, respectively) for both **6** and **7**. The ^{89}Y NMR shift of 269 ppm in **7** is similar to that reported for $Y(OSiMe_2Bu^t)_3(THF)_3$ (266.6 ppm)[89] and $Y(OCPr^i_2CH_2OEt)_3$ (277.1 ppm) [87b]. With the exception of a small amount of broadening, the ^1H NMR spectra of **6** and **7** are invariant to -80 °C. Since these results are consistent with either a high symmetry static structure or rapid exchange of coordinated and free dimethylaminopropyl arms, an X-ray crystallographic study of **7** was carried out.

2.3.2 Solid-state structure of 7

The structure of **7** is shown in Figure 7. Fractional atomic coordinates are given in Appendix Table II and selected bond lengths and angles are collected in Table 2. The X-ray crystal structure reveals that **7** possesses a trigonal bipyramidal geometry at the central yttrium atom with the bulkier siloxide groups occupying the equatorial positions (mean O-Y-O angle 120°) and the two coordinated dimethylamino donors occupying the axial sites (N-Y-N angle 169.2(4)°). The third dimethylaminopropyl arm is not coordinated.

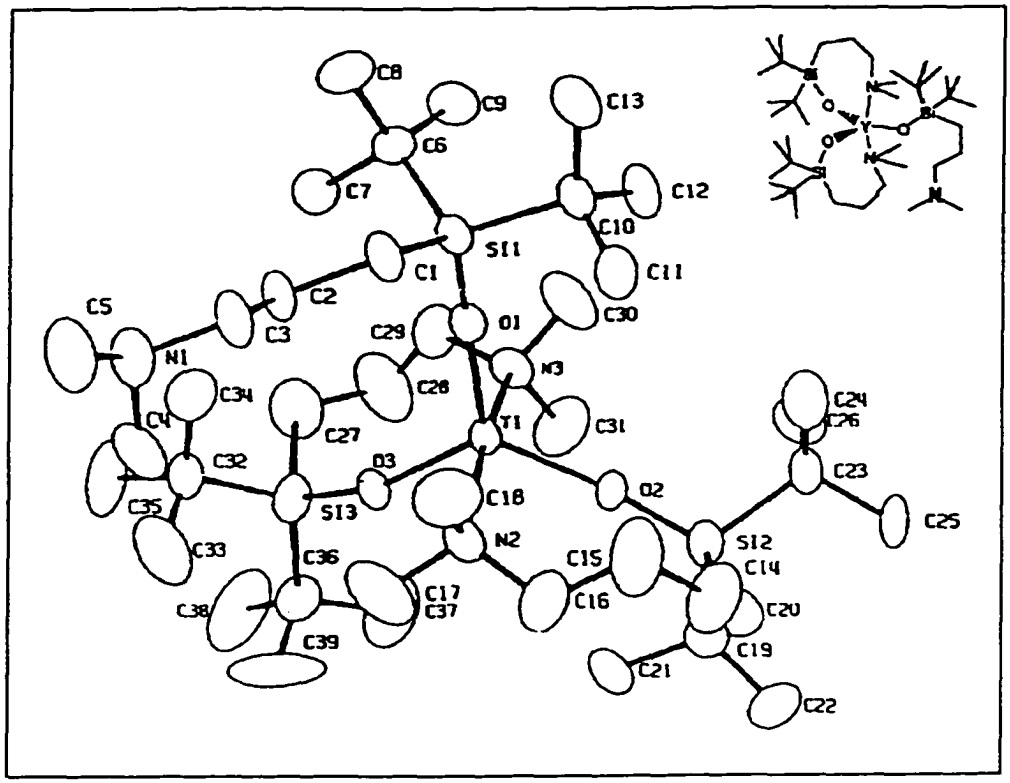

Figure 7 ORTEP diagram for $Y[OSi(t\text{-}Bu)_2(CH_2)_3NMe_2]_3$ (7)

The Y-O distances are all equivalent within experimental error (mean 2.097 Å) and very similar to the terminal Y-O distances (mean 2.09 Å) for the five-coordinate Y centre of $(ROH)(RO)_2Y(\mu\text{-}OR)_2Y(OR)_2$ (RO = t-$BuMe_2SiO$), **XVII**[89a]. The range of trivalent lanthanide-alkoxide oxygen bond distances reported in the literature is 2.03 - 2.12 Å[87a,89a,90], after correction for differences in metal ionic radii[91]. The Y-O distances in 7, while nearer the upper extreme, are still well within the expected range. The Y-O-Si angles are nearly linear for all three ligands and fall within the typical range found in early metal siloxides[92]. This angle is greatest (175.1(4)°) for the monodentate siloxide. The more pronounced bending of the bidentate Y-O-Si angles may reflect a requirement for chelation.

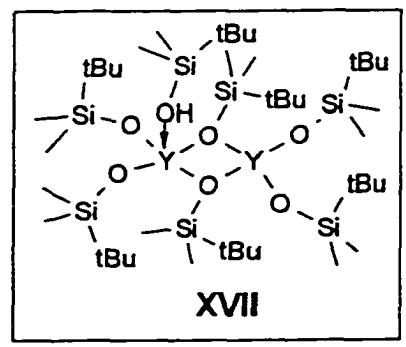

XVII

Table 2 Selected distances (Å) and angles (deg) for 7 [a]

		Distances	
Y(1)-O(1)	2.093(8)	Y(1)-O(2)	2.099(8)
Y(1)-O(3)	2.098(5)	Y(1)-N(2)	2.629(8)
Y(1)-N(3)	2.595(9)	O(1)-Si(1)	1.630(9)
O(2)-Si(2)	1.631(8)	O(3)-Si(3)	1.583(6)
		Angles	
O(1)-Y(1)-O(2)	121.5(3)	O(1)-Y(1)-O(3)	116.9(3)
O(2)-Y(1)-O(3)	121.6(3)	O(1)-Y(1)-N(2)	93.6(3)
O(1)-Y(1)-N(3)	97.2(3)	O(2)-Y(1)-N(2)	89.5(3)
O(2)-Y(1)-N(3)	84.1(3)	O(3)-Y(1)-N(2)	88.9(2)
O(3)-Y(1)-N(3)	87.0(3)	N(2)-Y(1)-N(3)	169.2(4)
Y(1)-O(1)-Si(1)	175.1(4)	Y(1)-O(2)-Si(2)	164.3(5)
Y(1)-O(3)-Si(3)	159.5(4)		

[a] estimated standard deviation in parentheses

The observation of a trigonal bipyramidal geometry in the solid state indicates that 7 is fluxional in solution. The most likely dynamic process is the interchange of mono- and bidentate siloxides by the dissociation and reassociation of dimethylamino donors (an "arm on - arm off" process). The fact that this exchange occurs rapidly on the NMR timescale even at -80 °C is consistent with the well-known lability of lanthanide-Lewis base adducts[93]. It is also noteworthy that Lappert [87a] isolated and structurally characterized **XV** (Figure 6). This is remarkable because the shorter C-O bond should result in increased steric pressure at Y in this compound. It is therefore probable that the considerably longer Y-P bond distances (3.045(2) Å) in **XV** are important in allowing formation of a six-coordinate geometry. Additionally, the presence of five-membered chelate rings in **XV**, versus seven-membered rings in 7, should favor formation of a six-coordinate geometry.

Herrmann has recently reported the synthesis of a number of closely related chelating alkoxide complexes of the lanthanides, **XVI** [87b] (Figure 6). Interestingly, these complexes also

show a single type of alkoxide in the room temperature NMR and a nearly identical ^{89}Y NMR shift to 7. A six coordinate geometry was assumed on the basis of the similarity in ^{89}Y chemical shift to $Y(OSiMe_2Bu^t)_3(THF)_3$ [89] but since a structural determination was not carried out, it is also possible that **XVIa-e** contain dangling donor arms which are in rapid exchange with coordinated donors. The shorter C-O bonds of these ligands should increase the steric crowding within the coordination sphere although this may be partially offset by the smaller size of OEt versus NMe_2.

Paramagnetic complex **8** exhibits very different ^1H NMR behavior compared with its Y analog 7. Upon cooling from room temperature to -60 °C, the single set of resonances collapsee and is finally replaced by a complex spectrum containing five large resonances (2:1:1:1:1 ratio) and several very broad peaks of smaller integrated intensity. Presumably, the five large resonances represent inequivalent t-butyl groups. This pattern is consistent with a *mer*-octahedral geometry (C_1 symmetry, mer-**XVIII**) as shown in Figure 8 assuming the accidental overlap of two t-butyl resonances. A *fac*-octahedral geometry (C_3 symmetry, fac-**XVIII**) can be ruled out since this can, at most, result in two inequivalent t-butyl groups. A five-coordinate structure similar to 7 should give rise to three t-butyl resonances (assuming free rotation about the Ce-O bond) and seems unlikely in view of the rapid fluxional behavior of 7 at low temperature. A six-coordinate geometry may be possible for **8**, the solid state structure of **7** notwithstanding, because the ionic radius of Ce^{3+} is approximately 0.11 Å larger than that of Y^{3+} in this coordination number [91]. On the basis of these considerations, a *mer*-octahedral geometry (mer-**XVIII**) seems most reasonable. The structure of **6** is not known but a fluxional six- or seven-coordinate geometry is reasonable given the smaller size of the $OSiBu^t[(CH_2)_3NMe_2]_2$ ligand.

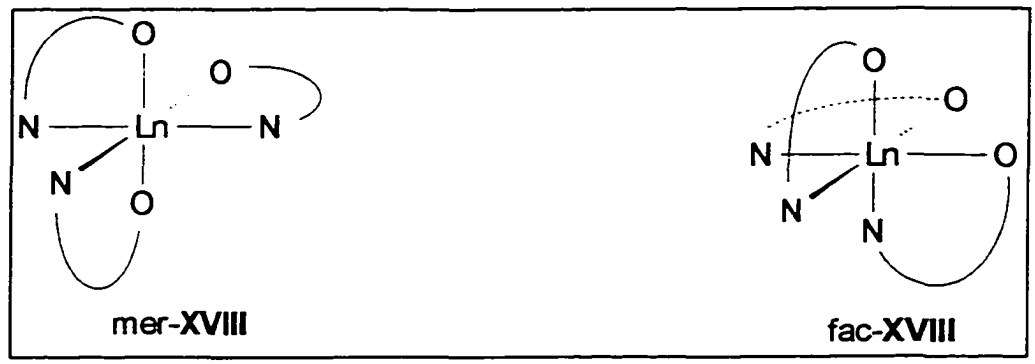

Figure 8 Two possible structures for **8**

2.4 Zwitterionic tetrakis(siloxide) complexes

2.4.1 Synthesis of zwitterionic tetrakis(siloxide) complexes

During the initial synthesis of **7**, a small amount of well-formed crystals were isolated which gave a more complex ^{1}H NMR spectrum. This impurity was traced to the presence of a slight excess of silanol **4** relative to $Y[N(SiMe_3)_2]_3$. Repeating the reaction using a 4:1 molar ratio of silanol to Y reproduced compound **9** in good yield (eq 17).

4 equiv. **4** + $Ln[N(SiMe_3)_2]_3$ →

$$Ln[OSiBu^t_2(CH_2)_3NMe_2]_3[OSiBu^t_2(CH_2)_3NMe_2H] + 3\ HN(SiMe_3)_2 \qquad (17)$$

9 Ln = Y
10 Ln = Yb

The ^{1}H NMR spectrum clearly showed the presence of free silanol **4** and complex **7** as well as a third component. It is well known that alcohols and lanthanide alkoxides can form adducts[94]. Thus this crystalline solid **9** was initially assigned as a simple silanol adduct of **7**. The elemental analysis was consistent with this formulation but a crystal structure was deemed desirable. We were unable to obtain X-ray quality crystals of **9** but preparation of the

ytterbium analog **10** provided crystals suitable for a structural study. Given the fact that Yb^{3+} is only 0.03 Å smaller than Y^{3+} [91], it is reasonable to assume that **10** and **9** have very similar structures.

2.4.2 Solid-state structure of 10

The structure of **10** is shown in Figure 9. Fractional atomic coordinates are given in Appendix Table V and selected bond distances and angles are presented in Table 3. Surprisingly, the crystal structure of **10** does not show a simple silanol adduct of **7**. It is very clear that all four silanols have been deprotonated and bind to the central ytterbium atom as a regular tetrahedron of siloxides (O-Yb-O angles range from 107.5(2)-111.2(2)° with an mean of 109.5°). All four Yb-O distances are similar (mean 2.076 Å). The best comparisons available in the literature are the terminal siloxide Y-O distances for the four-coordinate Y in **XVII** (section 2.3.2)[89a]. The distances of 2.046(20) and 2.060(19) Å observed in this compound predict Yb-O distances in **10** of 2.02 Å after correction for the ca. 0.03 Å smaller ionic radius of Yb^{3+} versus Y^{3+}. The Yb-O distance in **10** compares well with that in the crowded Ce^{4+} alkoxide, $[(tritox)_3Ce]_2(\mu\text{-}p\text{-}C_6H_4O_2)$ [90c]. The nearly linear Yb-O-Si angles are typical for lanthanide siloxide complexes and similar to those observed in **7**.

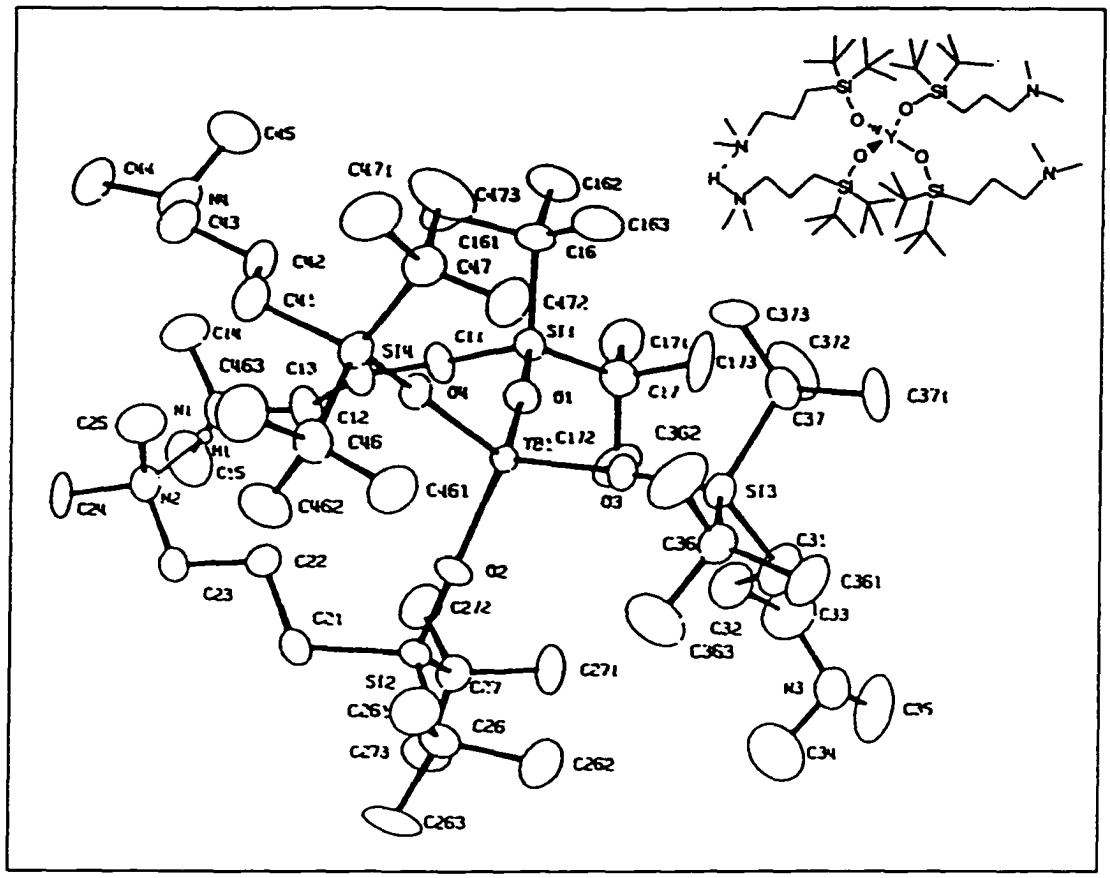

Figure 9 ORTEP diagram of $Yb[OSi(t\text{-}Bu)_2(CH_2)_3NMe_2]_3[OSi(t\text{-}Bu)_2(CH_2)_3NMe_2H]$ (**10**).

Table 3 Selected distances (Å) and angles (deg) for **10** [a]

		Distances	
Yb(1)-O(1)	2.062(6)	Yb(1)-O(2)	2.074(6)
Yb(1)-O(3)	2.092(6)	Yb(1)-O(4)	2.077(6)
Si(1)-O(1)	1.594(6)	Si(2)-O(2)	1.593(6)
Si(3)-O(3)	1.597(6)	Si(4)-O(4)	1.600(7)
		Angles	
O(1)-Yb(1)-O(2)	107.5(2)	O(1)-Yb(1)-O(3)	110.1(2)
O(1)-Yb(1)-O(4)	107.8(2)	O(2)-Yb(1)-O(3)	111.2(2)
O(2)-Yb(1)-O(4)	109.0(2)	O(3)-Yb(1)-O(4)	111.2(2)
Yb(1)-O(1)-Si(1)	174.7(4)	Yb(1)-O(2)-Si(2)	176.5(4)
Yb(1)-O(3)-Si(3)	171.3(4)	Yb(1)-O(4)-Si(4)	165.6(4)

[a] estimated standard deviation in parentheses

The most unique structural feature of **10** is the location of the proton which has been removed from the fourth siloxide ligand. Initial refinement showed that two of the four dangling dimethylamino groups were in close proximity. The hydrogen atom was therefore placed between these two N atoms and refined isotropically in the final structure. Complex **10** is a zwitterion containing a discrete $Y(OR)_4^-$ core and a pendant, hydrogen-bonded ammonium counterion. One silanol ligand has therefore been deprotonated by an internal $RNMe_2$ base. To our knowledge this is the first example of self-deprotonation to form a zwitterionic complex for a lanthanide siloxide or alkoxide. Although the structural details are considerably different, **10** is reminiscent of the tetrakis(aryloxide) "ate" complex, $K[Nd(O\text{-}2,6\text{-}i\text{-}PrC_6H_4)_4]$[95], where H^+ is replaced by K^+. Indeed, reaction of **9** with Me_3SiCH_2Li produces an "ate" complex **11** as shown in eq 18.

$$\mathbf{8} + LiCH_2SiMe_3 \rightarrow \underset{\mathbf{11}}{Li^+\{Y[OSiBu^t_2(CH_2)_3NMe_2]_4\}^-} + SiMe_4 \qquad (18)$$

The deprotonation of a silanol by an amine has precedence in Al chemistry. Chisholm and coworkers have isolated and structurally characterized $[Me_2NH_2]^+[Al(OSiMe_3)_4]^-$ (**XIX**, eq 19)[96]. Complex **XIX** differs from **9** and **10** in that the $Me_2NH_2^+$ cation is hydrogen bonded

$$HNMe_2 + HOSiMe_3 + 1/2\ Al_2(OSiMe_3)_6 \rightleftharpoons \underset{\mathbf{XIX}}{[Me_2NH_2]^+[Al(OSiMe_3)_4]} \qquad (19)$$

to a siloxide oxygen rather than to another amine. No examples of zwitterionic alkoxide complexes have been reported, presumably reflecting the lower acidity of alcohols relative to silanols (pK_a in water: Et_3SiOH, 13.6[24a]; t-BuOH, 19[24b]). Caulton[89a] isolated **XVII** (section

2.3.2), which contains a coordinated silanol, in the absence of any deprotonating base and it seems likely that addition of an amine to this complex will produce a salt similar to **XIX**, **9** and **10**.

2.4.3 Solution behaviour of 9

The ^{1}H NMR spectrum of **9** shows the presence of free silanol **4**, tris(siloxide) **7** and a third component which is assumed to be intact **9**. Cooling the sample results in an increase in intensity of the resonances assigned to **9** and a corresponding decrease for those resonances due to **4** and **7**, consistent with the equilibrium illustrated schematically in eq 20. A plot of $\ln K_{eq}$ versus T^{-1} (Figure 10) for this equilibrium is a straight line giving $\Delta H° = 40 \pm 4$ kJ mol^{-1} and $\Delta S° = 124 \pm 10$ J mol^{-1} K^{-1}. The large positive value of $\Delta S°$ is consistent with dissociation of **9** into **4** and **7**. In comparison to **XIX**, **9** is more dissociated in solution which is further evidence for a high degree of steric crowding within the metal coordination sphere.

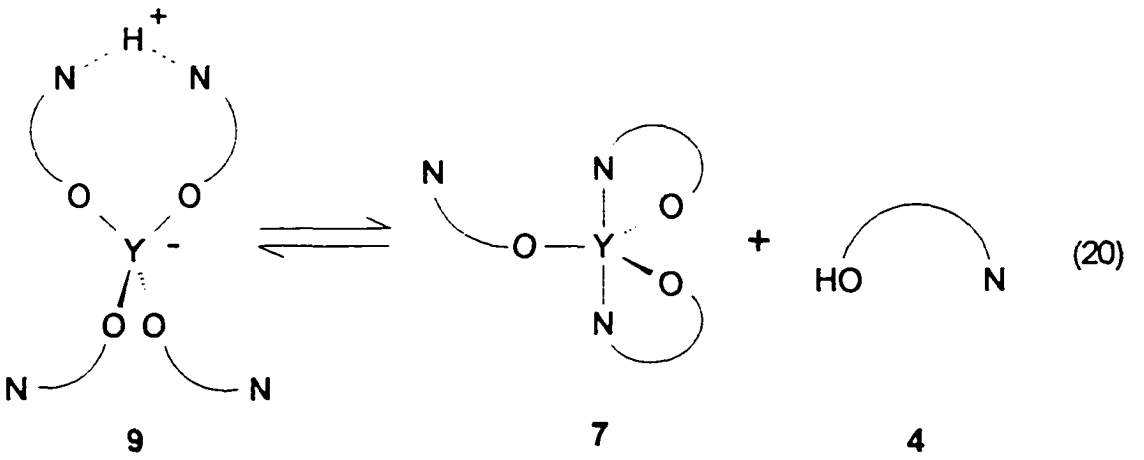

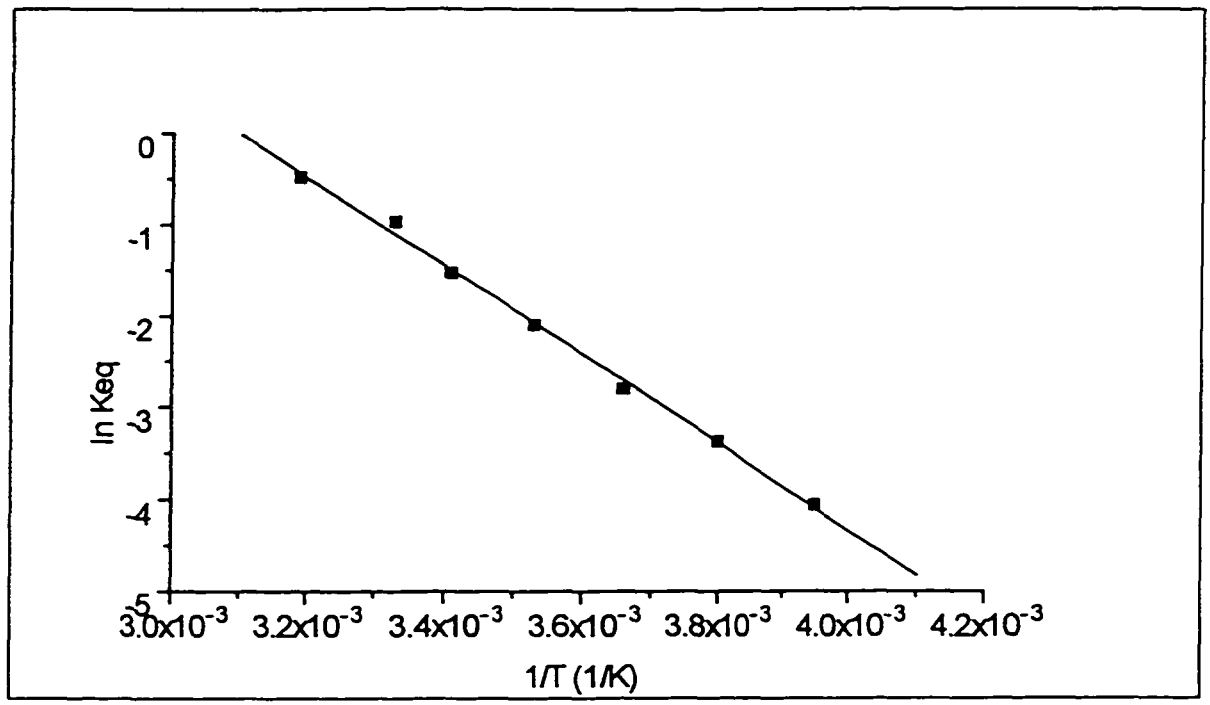

Figure 10 Plot of ln K_{eq} versus T^{-1} for the equilibrium **9** $\rightleftharpoons$ **4** + **6** (eq. 20)

The observation of all three components of the equilibrium shown in eq 20 requires slow exchange of free silanol and coordinated siloxide. This fact rules out exchange of trace free silanol with coordinated siloxide as a possible explanation for the rapid fluxional behavior of **7** at low temperature. Further, observation of a single set of siloxide resonances for **9** at low temperature indicates that proton migration between all four dangling dimethylamino groups is a low energy process. Paramagnetic line broadening precludes assignment of any ^{1}H NMR resonances for **10** but it is reasonable to assume that this compound exhibits solution behavior analogous to **9**.

2.5 Barium siloxide complexes

2.5.1 Synthesis of barium siloxide complexes

Reaction of $Ba[N(SiMe_3)_2]_2{\cdot}(THF)_2$ with 1 or 2 equiv of $HOSi(^tBu)_2((CH_2)_3NMe_2)$ proceeded smoothly in toluene to yield the mono- (**12a**) or bis(siloxide) (**13**) complexes (eqs 21 and 22). Complex **12a** was isolated as a crystalline, solvent-free dimer (*vide infra*) while **13** was obtained as an oil of extremely high hexane solubility. When the reaction of $Ba[N(SiMe_3)_2]_2{\cdot}(THF)_2$ and $HOSi(^tBu)_2((CH_2)_3NMe_2)$ was carried out in hexane in 1:1 ratio, and recrystallization of the crude product took place in hexane instead of toluene, crystals of THF adduct $\{Ba[OSi(^tBu)_2((CH_2)_3NMe_2)][N(SiMe_3)_2][THF]\}_2$ (**12b**) were isolated. However, THF can be removed to afford **12a** when **12b** was pumped under vacuum for a few hours.

$$2\ Ba[N(SiMe_3)_2]_2[THF]_2 + 2\ HOSi(^tBu)_2((CH_2)_3NMe_2) \rightarrow$$
$$\underset{\textbf{(12a)}}{\{Ba[OSi(^tBu)_2((CH_2)_3NMe_2)][N(SiMe_3)_2]\}_2} + 2\ HN(SiMe_3)_2 + 4\ THF \qquad (21)$$

$$Ba[N(SiMe_3)_2]_2[THF]_2 + 2\ HOSi(^tBu)_2((CH_2)_3NMe_2) \rightarrow$$
$$\underset{\textbf{(13)}}{Ba[OSi(^tBu)_2((CH_2)_3NMe_2)]_2} + 2\ HN(SiMe_3)_2 + 2\ THF \qquad (22)$$

2.5.2 Solid-structures of 12a and 12b

An X-ray diffraction study of **12a** was carried out in order to shed light on its molecular structure. The structure of **12a** is shown in Figure 11, atomic coordinates are given in Appendix Table IX, and selected bond lengths and angles are collected in Table 4. Complex **12a** crystallizes as a centrosymmetric dimer containing bridging siloxide ligands. The geometry at barium is distorted tetrahedral with one terminal silylamide and one dimethylamino group

completing the coordination sphere. As expected, the bridging Ba-O(siloxide) distances in **12a** (2.602(11) and 2.645(12) Å) are considerably longer than the terminal Y-O(siloxide) distances in $Y[OSi(^tBu)_2((CH_2)_3NMe_2)]_3$ **7** even after correction for metal ionic radius and coordination number (predicts ca. 2.53 Å)[91]. The Ba-N(amine) distance of 2.94(2) Å is significantly shorter than that in **7** (predicts ca. 3.03 Å) suggesting that **12a** is less sterically crowded than **7**.

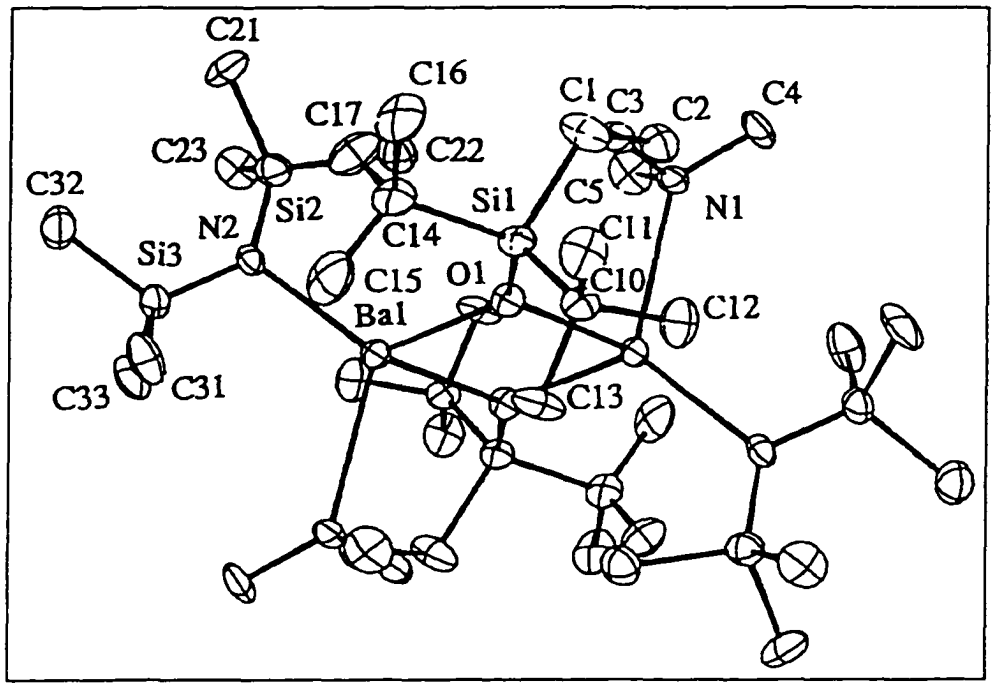

Figure 11 ORTEP diagram of **12a**

The crystal structure of **12b** is shown in Figure 12, while selected distances and angles are given in Table 4 and atomic coordinates are given in Appendix Table XI, respectively. The structure of **12b** is similar to that of **12a** with the important difference that one THF molecule has displaced the dimethylamino arm from each Ba center (the closest Ba···NMe_2 contact is 6.19 Å between Ba(1) and N(1)). The Ba(1)-O(2) (THF) distance of 2.78(2) Å is significantly shorter than the Ba(1)-N(1)' (amine) distance of 2.94(2) Å in **12a**. Nevertheless, the THF

ligands in **12b** are readily lost under vacuum, implying that THF is not a significantly better donor than the dimethylamino groups in these complexes.

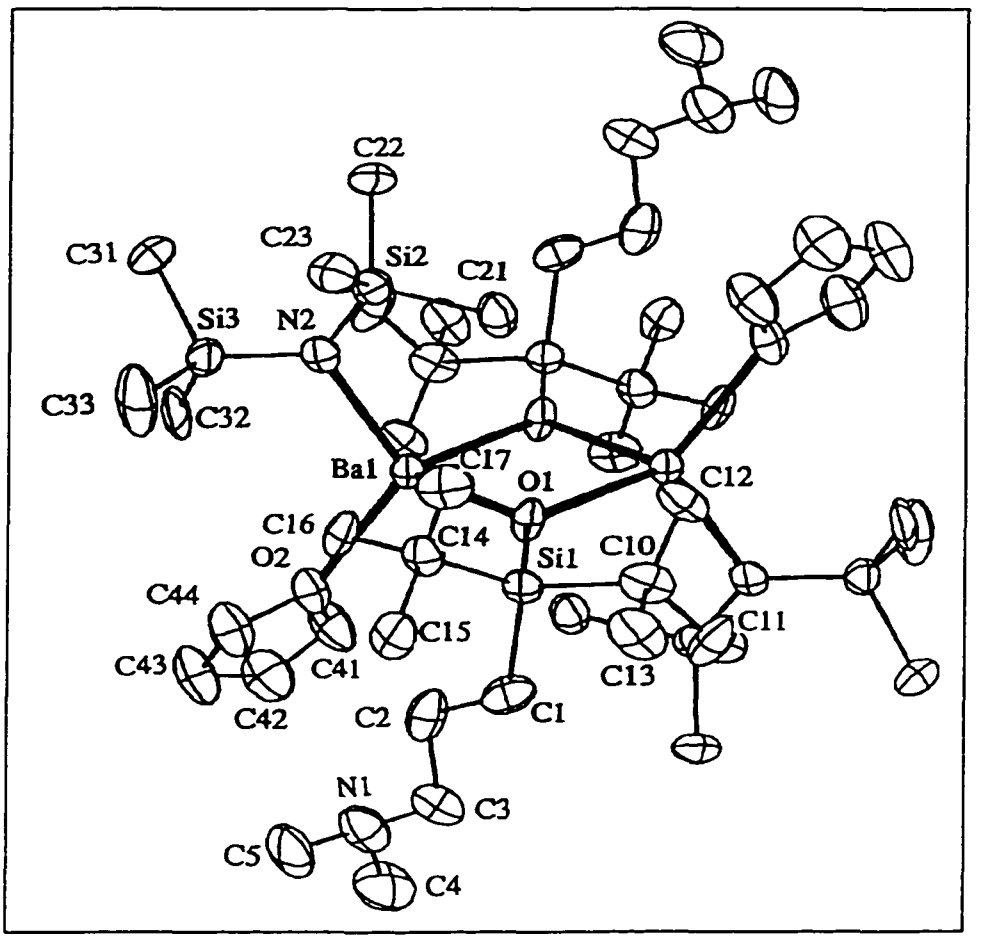

Figure 12 ORTEP diargram of **12b**

Table 4 Selected distances (Å) and angles (deg) for **12a** and **12b** [a,b]

12a		**12b**	
Distances			
Ba(1)-O(1)	2.602(11)	Ba(1)-O(1)	2.603(14)
Ba(1)-O(1)'	2.645(12)	Ba(1)-O(1)'	2.596(14)
Ba(1)-N(1)'	2.94(2)	Ba(1)-O(2)	2.78(2)
Ba(1)-N(2)	2.630(14)	Ba(1)-N(2)	2.58(2)
Si(1)-O(1)	1.618(11)	Si(1)-O(1)	1.637(14)
Si(2)-N(2)	1.662(15)	Si(2)-N(2)	1.65(2)
Si(3)-N(2)	1.672(14)	Si(3)-N(2)	1.71(2)
Angles			
O(1)-Ba(1)-O(1)'	82.0(3)	O(1)-Ba(1)-O(1)'	84.0(6)
O(1)-Ba(1)-N(1)'	107.5(3)	O(1)-Ba(1)-O(2)	109.8(7)
O(1)-Ba(1)-N(2)	125.3(4)	O(1)-Ba(1)-N(2)	113.5(5)
N(1)'-Ba(1)-O(1)'	94.5(3)	O(2)-Ba(1)-O(1)'	121.1(7)
N(1)'-Ba(1)-N(2)	117.1(4)	O(2)-Ba(1)-N(2)	115.6(9)
N(2)-Ba(1)-O(1)'	122.4(3)	N(2)-Ba(1)-O(1)'	109.7(7)
Ba(1)-N(2)-Si(2)	120.8(7)	Ba(1)-N(2)-Si(2)	116.9(10)
Ba(1)-N(2)-Si(3)	111.8(7)	Ba(1)-N(2)-Si(3)	117.0(10)
Ba(1)-O(1)-Si(1)	133.2(6)	Ba(1)-O(1)-Si(1)	130.8(8)
Ba(1)-O(1)'-Si(1)'	128.2(5)	Ba(1)-O(1)'-Si(1)'	130.8(8)
Ba(1)-O(1)-Ba(1)'	98.0(3)	Ba(1)-O(1)-Ba(1)'	96.0(7)
Si(2)-N(2)-Si(3)	127.4(9)	Si(2)-N(2)-Si(3)	126.0(12)

[a] estimated standard deviation in parentheses
[b] prime denotes symmetry (inversion) related atom.

While this work was in progress, Hanusa and coworkers reported the structural characterization of (clox)Ca[N(SiMe$_3$)$_2$][THF]$_3$ (clox = OCPh$_2$(CH$_2$C$_6$H$_4$-Cl-4)[97], which is, to our knowledge, the only other mixed alkoxide-amide complex of a group 2 metal. The Ca-N(SiMe$_3$)$_2$ distance of 2.353(5) Å is only marginally longer than those found in **12a** and **12b** (2.630(14) and 2.58(2) Å, respectively) after applying a correction of +0.33 Å to account for differences in metal ionic radius and coordination number.[91] Similarly the Ba(1)-O(2) (THF)

distance in **12b** (2.78(2) Å) falls within the range of Ca-O(THF) distances observed for (clox)Ca[N(SiMe$_3$)$_2$][THF]$_3$ (2.398(5) - 2.460(5) Å) after application of this correction factor.

2.5.3 Solution behavior of barium siloxide complexes

2.5.3.1 Monomer and dimer equilibrium of complex 13

Because it was not possible to obtain the crystal structure of the oily compound **13**, structural information for complex **13** relied on NMR data. The bis(siloxide) complex **13** gives a single set of ^{1}H NMR resonances for the OSi(^{t}Bu)$_2$((CH$_2$)$_3$NMe$_2$) ligands in d_8-THF solution between -80 and +80 °C (Table 5). However, in d_6-benzene two sets of resonances are observed in ca. 3:2 ratio at room temperature (Table 6). These observations are consistent with the existence of a monomer-dimer equilibrium in benzene solution and cleavage to a monomeric species in THF (Scheme 4). The variable temperature NMR data does not allow us to determine whether the predominant species at room temperature is the monomer or the dimer because the ratio changes little throughout the accessible temperature range. Furthermore, we cannot be certain whether or not the NMe$_2$ arms are coordinated or how many THF molecules bind to the monomer in d_8-THF solution. This is because the exchange of free and coordinated Lewis bases is generally rapid for barium compounds and as a result fluxional behaviour is usually observed even at -80 °C. The structures depicted in Scheme 4 are reasonable given the apparent tendency of barium to be 4-coordinate in complexes containing the OSi(^{t}Bu)$_2$((CH$_2$)$_3$NMe$_2$) ligand as evidenced by the solid state structures of **12a** and **12b**.

Scheme 4

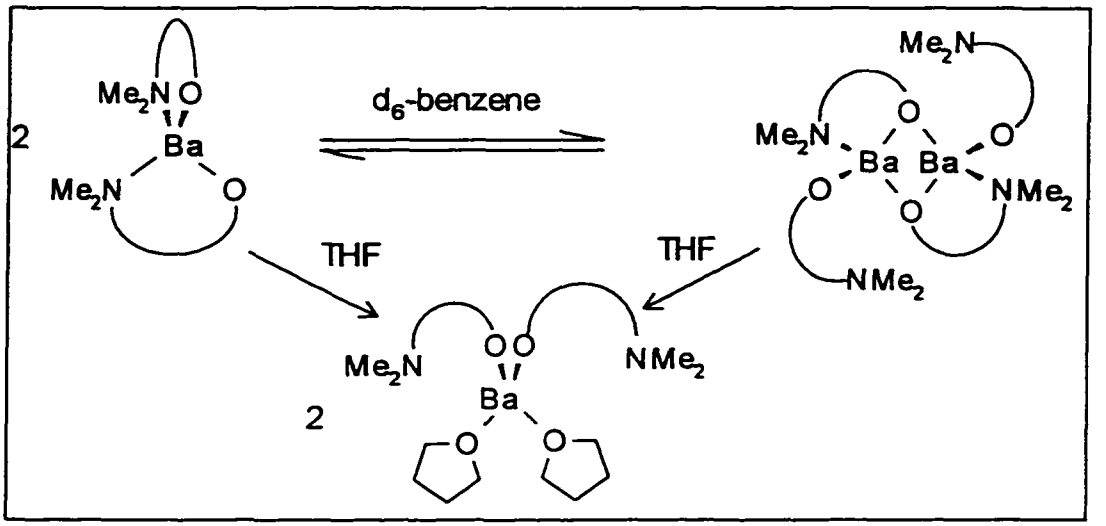

Table 5 NMR chemical shift data in d_8-THF

Assignment	**12a** or **12b**[a]	**13**	$Ba[N(SiMe_3)_2]_2[THF]_2$
		^{1}**H**	
CH_2N	2.11[b]	2.14[b]	
NMe_2	2.10	2.12	
$CH_2CH_2CH_2$	1.55	1.58	
CMe_3	0.91	0.95	
CH_2Si	0.36	0.40	
$SiMe_3$	-0.09		-0.05
		^{13}**C**{^{1}**H**}	
CH_2N	65.95	65.96	
NMe_2	46.04	46.07	
CMe_3	29.86	30.05	
$CH_2CH_2CH_2$	25.33[c]	[c]	
CMe_3	22.26	22.42	
CH_2Si	12.17	12.43	
$SiMe_3$	5.83		5.68

[a] contains ca. 10 % **13** and $Ba[N(SiMe_3)_2]_2$ as minor components
[b] partially obscured by NMe_2
[c] obscured by d_8-THF

Table 6 NMR chemical shift data in d_6-benzene

Assignment	**12a**	**13**[a]	**12b**[b]	$Ba[N(SiMe_3)_2]_2[THF]_2$
		^1H		
α-CH_2 THF			3.54	3.49
CH_2N	2.10	2.22, 2.39	2.15	
NMe_2	1.98	2.16, 2.27	1.98	
$CH_2CH_2CH_2$	1.41	1.74, 1.83	1.49	
β-CH_2 THF			1.35	1.32
CMe_3	1.10	1.20, 1.29	1.15	
CH_2Si	0.47	0.70[c]	0.57	
$SiMe_3$	0.30		0.36	0.33
		$^{13}C\{^1H\}$		
α-CH_2 THF			68.19	68.48
CH_2N	61.14	63.84, 65.75	61.69	
NMe_2	45.95	45.28, 46.10	45.81	
CMe_3	30.12	30.13, 30.01	30.20	
β-CH_2 THF			25.47	25.24
$CH_2CH_2CH_2$	24.10	23.96, 25.20	24.18	
CMe_3	21.81	21.84, 22.11	21.89	
CH_2Si	9.55	14.31, 12.79	10.61	
$SiMe_3$	6.20		6.14	5.50
		$^{29}Si\{^1H\}$		
SiO	-0.13	-1.95, -4.70	0.03	
$SiMe_3$	-18.01		-18.04	-18.99

[a] resonances due to the major component (60 %) are listed first and those of the minor component (40 %) are listed second.

[b] trace **13** and $Ba[N(SiMe_3)_2]_2[THF]_2$ are always present.

[c] obscured by the major component.

2.5.3.2 Solution behavior of complexes 12a and 12b

Complexes **12a** and **12b** exhibit the same NMR spectra as one another in d_8-THF solution but these spectra differ markedly from those obtained in d_6-benzene. In d_8-THF, the *same two sets* of silylamide and siloxide resonances are observed in the ^1H, ^{13}C and ^{29}Si NMR spectra of either **12a** or **12b** (Table 5) indicating that the *same species* is present in solution for both compounds. Close inspection of the ^{29}Si and ^1H NMR chemical shifts also indicated the presence of $Ba[N(SiMe_3)_2]_2[THF]_2$ and **13** as the minor components (ca. 10 %). This was confirmed by the disappearance of signals due to **13** upon addition of a five-fold excess of free $Ba[N(SiMe_2)_2]_2[THF]_2$ (Figure 13). Thus, in THF solution, ligand redistribution *is* occurring although the equilibrium lies well on the side of intact **12b** (eq. 23).

In d_6-benzene (or d_8-toluene) **12a** and **12b** exist as distinct compounds as is clearly evident from the observation of different NMR spectra (Table 6). Variable temperature NMR spectra of **12a** from -80 to +80°C show a single set of siloxide resonances which is consistent with either complete dissociation of dimeric **12a** into monomers *or* rapid exchange of free and coordinated NMe_2 arms in a dimeric structure similar to that observed in the solid state (Figure 11). We favour the latter explanation because rapid exchange of free and coordinated NMe_2 groups has been observed previously in $Y[OSi(^tBu)_2((CH_2)_3NMe_2)]_3$.

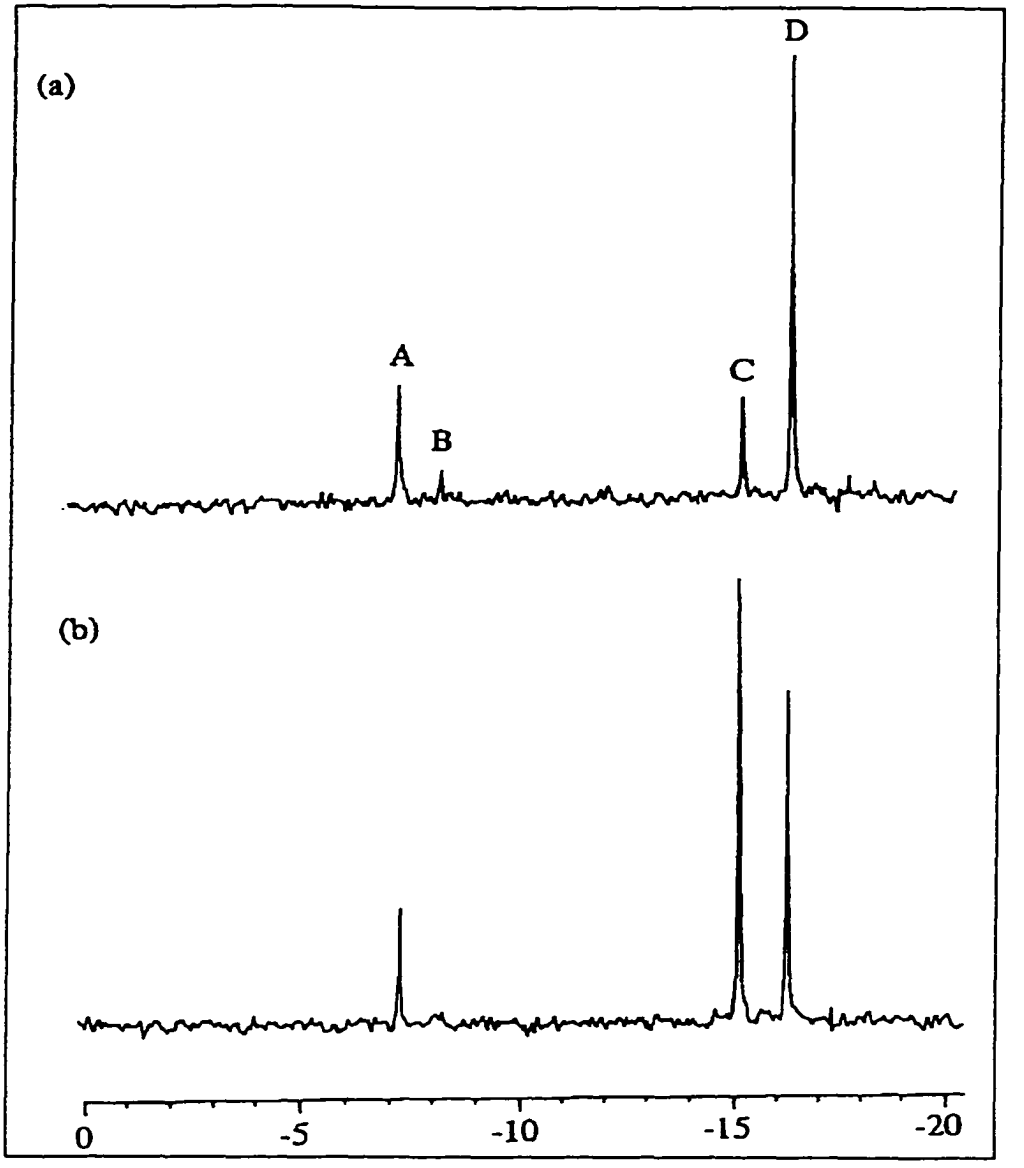

Figure 13 $^{29}Si\{^{1}H\}$ NMR Spectrum of (a) pure **12b** in d_8-THF (b) after addition of excess $Ba[N(SiMe_3)_2]_2[THF]_2$.
Assignments: A, $Ba[OSi(^{t}Bu)_2((CH_2)_3NMe_2)][N(SiMe_3)_2]$;
B, $Ba[OSi(^{t}Bu)_2((CH_2)_3NMe_2)]_2$; C, $Ba[N(SiMe_3)_2]_2$;
D, $Ba[OSi^{t}Bu_2(CH_2)_3NMe_2][N(SiMe_3)_2]$

Complexes **12a** and **12b** do not appear to undergo ligand redistribution as readily in benzene or toluene as they do in THF. There is no evidence for the presence of **13** or $Ba[N(SiMe_3)_2]_2$ in solutions of **12a** in toluene or benzene throughout the -80 to +80 °C range. Trace (< 5 %) amounts of **13** and $Ba[N(SiMe_3)_2]_2$ are just detectable in the NMR spectra of **12b**. The presence of some ligand redistribution in the case of **12b** is probably attributable to the presence of THF in this compound.

It is possible that ligand redistribution occurs more readily in d_8-THF solution because THF is required to stabilize $Ba[N(SiMe_3)_2]_2$ (ie. to favour the right hand side of eq. 23). The solution behaviour of **12a** is more reminiscent of $Cp^*CaI(THF)_2$[98] than $(clox)Ca[N(SiMe_3)_2][THF]_3$ since the former undergoes ligand redistribution in THF while the latter does so in toluene. It appears from these results that the susceptibility to ligand redistribution cannot be predicted reliably from the type of ancillary ligation (eg. Cp^* versus alkoxide) but depends, as might be expected, on the subtle interplay between steric and electronic factors for *all species* involved in the redistribution process (such as those in eq. 23).

$$\underset{\textbf{(12b)}}{\{Ba[OSi(^tBu)_2((CH_2)_3NMe_2)][N(SiMe_3)_2][THF]\}_2} \rightleftharpoons$$

$$Ba[N(SiMe_3)_2]_2[THF]_2 + \underset{\textbf{(13)}}{Ba[OSi(^tBu)_2((CH_2)_3NMe_2)]_2} \qquad (23)$$

2.6 Volatility of the barium and lanthanide complexes

Volatility is the most important property for MOCVD purposes. Lanthanide complexes **6 - 8** sublime at 115-135 °C ($5x10^{-4}$ torr) without decomposition. Sublimation at 10^{-2} torr did result in some decomposition due to the higher temperatures required. The volatility of **7** is

very similar to **IIIb-d** which were synthesized by the Herrmann group[87b], and somewhat higher than that of lanthanide complexes derived from less bulky monodentate ligands such as $OCMe_2Pr^i$, $OCMe(Et)Pr^i$, $OCEt_3$, $OCBu^t_3$, OAm^t, [99] $OCBu^t_2Pr^i$ [90f] and $OCHBu^t_2$ [90f] (135-240 °C at 10^{-3} Torr). Clearly, metal complexes with donor functionalized ligands show higher volatility than those with monodentate ligands.

Barium complexes **12a,b** and **13** are not volatile at 10^{-4} torr and undergo decomposition during prolonged heating at 130°C. Consistent with this observation, none of these complexes give molecular ions in the mass spectrum (EI or CI). Thus these barium complexes are not useful for MOCVD purposes, however they are extremely soluble in saturated hydrocarbon solvents and may be useful in sol-gel methods.

2.7 Tripod siloxide ligand and its yttrium complex

The crystal structure of yttrium complex 7 shows that only two of the three amino arms are coordinated. Although complex 7 has fairly high volatility, elimination of the third dangling donor arm should result in enhanced volatility. Binding the three coordinating arms in one, by use of a tripod ligand, should improve volatility even further (**XX**). Tris(alkoxide)[50a, 100] and tris(amide)[101] tripod ligands have been widely used for transition metal chemistry. However, the use of tris(siloxide) tripod ligands for preparation of MOCVD precursors has not been reported.

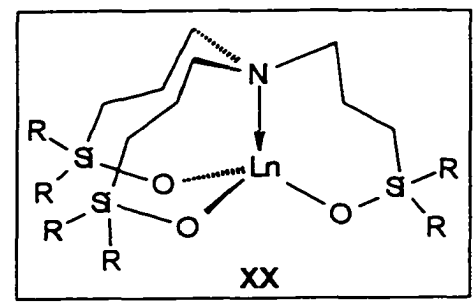

The synthetic strategy employed here (Scheme 5) was chosen, in part, because it involves $HSi^tBu_2CH_2CH_2CH_2I$ (**15**) as the key intermediate. This compound is a versatile

reagent for the preparation of new ligands. In addition to the direct reaction with amines described in this work, the Grignard reagent prepared from **15** can be used to prepare silanol-phosphines from PCl_3 and silanol-alcohols from ketones.

The initial step in this procedure involves preparation of allylsilane **14** from allylmagnesium bromide and HSi^tBu_2Cl. Conversion of **14** to $HSi^tBu_2CH_2CH_2CH_2I$ **15** is accomplished via hydroboration followed by treatment of the borane intermediate with I_2 and base in a one-pot procedure[102]. Hydroboration proceeded smoothly with both disiamylborane and 9-BBN. However, we found, as reported in the literature, that only the disiamylborane product could be cleaved selectively with I_2 and base[103]. Under the same conditions, all three B-C bonds of the 9-BBN product were cleaved leading to complex product mixtures. Even so, this step was the least satisfactory in this procedure since **18** was contaminated with ca. 10% boron-containing impurities even after vacuum distillation. Fortunately, these impurities did not interfere with subsequent steps.

A portion of **15** was converted to the primary amine $HSi^tBu_2CH_2CH_2CH_2NH_2$ **16** using Gabriel conditions[104]. Refluxing **15** and **16** (2:1 molar ratio) in acetonitrile with K_2CO_3 formed the tertiary amine $(HSi^tBu_2CH_2CH_2CH_2)_3N$ (**17**) as a hexane soluble oil. The reactions was conveniently followed by ^1H NMR (Figure 14). Hydrolysis of silane **17** does not proceed in water or cleanly in refluxing aqueous HCl. Conversion of **17** to $(HOSi^tBu_2CH_2CH_2CH_2)_3N$ (**18**, H_3amsilox) was eventually effected using a mixture of $CuCl_2$ and CuI in CH_3CN[105]. Cuprous iodide is necessary in catalytic amounts for the reaction to proceed. Crude H_3amsilox was recrystallized as its oxalate salt followed by liberation of the free base with KOH and vacuum distillation. Pure H_3amsilox **18** was

obtained as a viscous light yellow oil. The overall yield for the five step procedure was ca. 34 %.

Reaction of one equivalent of H_3amsilox **18** and $Y[N(SiMe_3)_2]_3$ proceeded smoothly in toluene / THF to produce the yttrium complex **19** as a hydrocarbon soluble viscous oil which slowly solidifies. Although we were not able to obtain single crystals for X-ray crystallographic studies, the structure of **19** is quite evident based on NMR data alone.

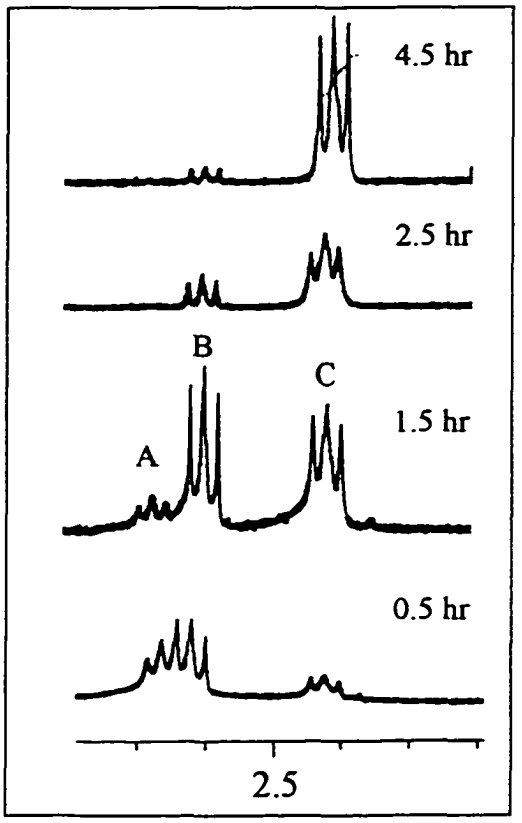

Figure 14 ^{1}H NMR spectra (CH_2N region) of the reaction mixture for the reaction between **15** and **16**: **A**, $HSi^tBu_2CH_2CH_2CH_2NH_2$ **(16)**; **B**, $(HSi^tBu_2CH_2CH_2CH_2)_2NH$; **C**, $(HSi^tBu_2CH_2CH_2CH_2)_3N$ **(17)**.

Scheme 5

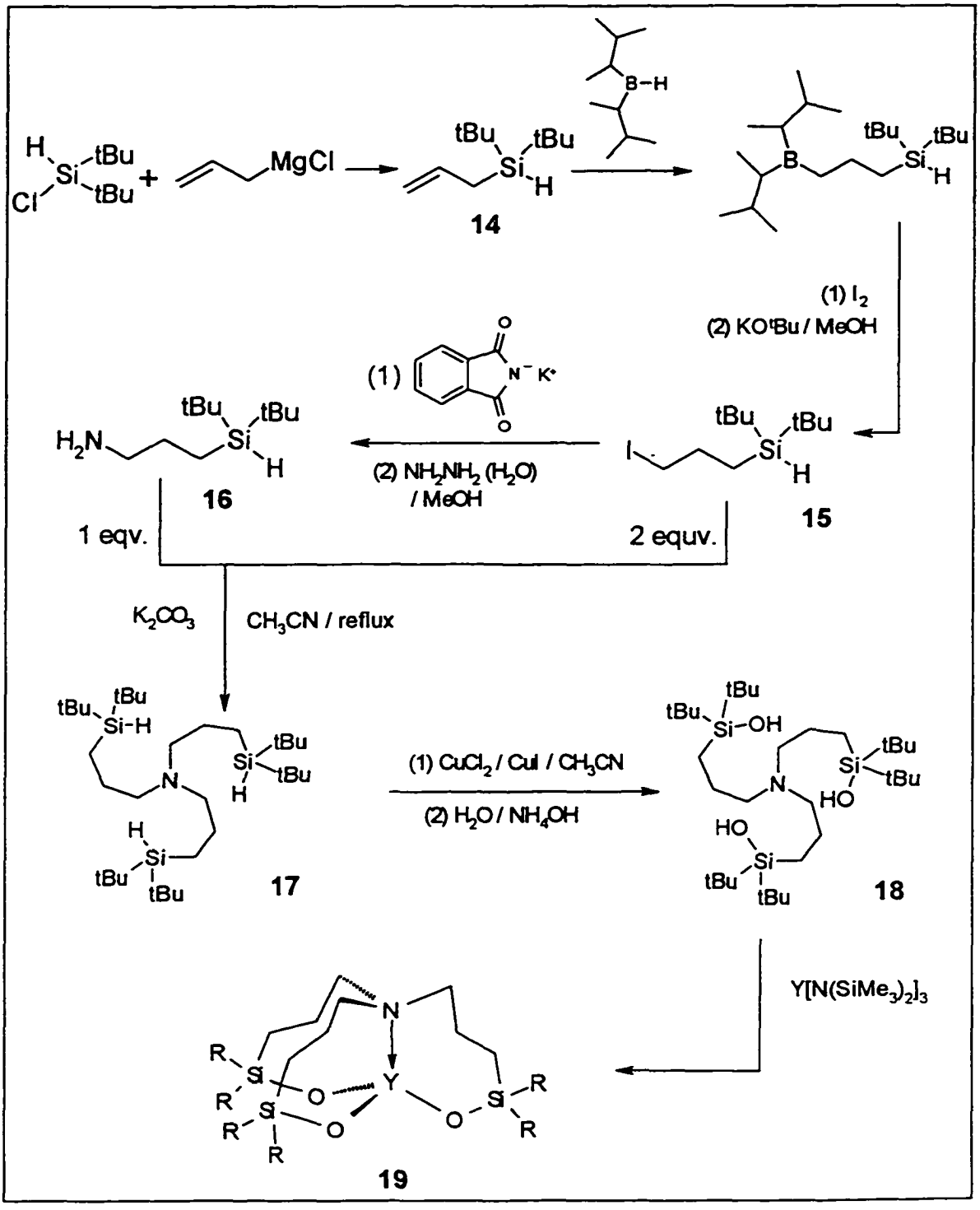
MgCl
14
(1) I_2
(2) KO^{t}Bu / MeOH
(1)
(2) NH_2NH_2 (H_2O) / MeOH
16
15
1 eqv.
2 equv.
K_2CO_3
CH_3CN / reflux
17
(1) $CuCl_2$ / CuI / CH_3CN
(2) H_2O / NH_4OH
18
$Y[N(SiMe_3)_2]_3$
19

The ^{1}H NMR spectrum of **19** shows two sharp singlets which correspond to the two *tert*-butyl groups, and six different resonances due to ligand backbone protons which indicates that all three sets of geminal $NCH_2CH_2CH_2Si$ proton pairs are inequivalent. Although ligand **18** itself possesses C_{3v} symmetry, the observed NMR resonance pattern is consistent with C_3 symmetry which is very similar to the zirconium complex **38** bearing tripod ligand **27** (Chapter 3). One THF molecule coordinates to the complex strongly as indicated by the large chemical shift change from the free THF (3.7 ppm for free THF CH_2O, 4.2 ppm for coordinated THF CH_2O). Because complex **19** possesses high symmetry and the metal is well encapsulated, **19** is expected to have high volatility. Indeed, the strongest peak observed in the mass spectrum is due to the fragment corresponding to loss of one *tert*-butyl group from the molecular ion (Figure 15).

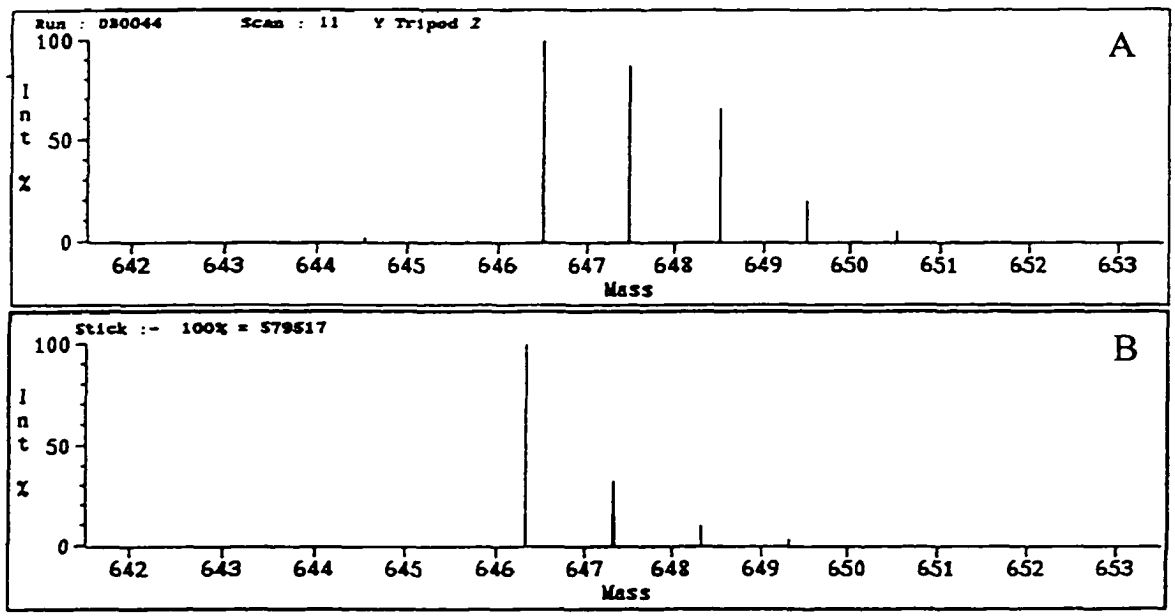

Figure 15 Isotopic distributions for fragment M^+ - ^{t}Bu of complex **19**. (A): experimental distribution; (B): theoretical distribution

2.8 Organolanthanide chemistry with arylsiloxide ligands

2.8.1 Introduction

Organometallic chemistry of the lanthanides has a unique character that is quite different from that of transition metal chemistry. In lanthanide chemistry, electrostatic and steric factors, rather than metal-ligand orbital interactions, govern the structure and chemical reactivity. Because the 4f valence orbitals of the lanthanides are highly contracted and efficiently shielded by filled 5s and 5p orbitals, overlap of these orbitals with ligand orbitals is extremely small and π-backbonding effects are virtually absent. Thus both the Ln^{2+} and Ln^{3+} ions form complexes which are mainly ionic in character and which most resemble the alkali and alkaline earth ions. Additionally, the lanthanide ions are highly oxophilic and organolanthanide complexes are extremely air- and moisture sensitive[106].

Organolanthanide complexes have revealed fascinating reactivities and catalytic activities. For example, the neutral lutetium complex $Cp^*_2LuCH_3$ shows high catalytic activity towards Ziegler-Natta ethylene polymerization; and it also activates unreactive alkanes such as tetramethylsilane and methane (Scheme 6)[69].

The bulky anionic cyclopentadienyl ligand (Cp) and its derivatives (especially Cp*, pentamethylcyclopentadienyl) are ideally suited for stabilizing highly reactive lanthanide alkyl and hydride complexes, and organolanthanide chemistry has been dominated by Cp* as ancillary ligation[46,107]. However, alternative ligands, such as bulky σ-alkyl and allyl ligands, neutral arenes, anionic macrocycles, η^8-cyclooctatetraene ligands, bulky amides and alkoxide (aryloxide) ligands, have also been increasingly used in organolanthanide chemistry[46].

Scheme 6

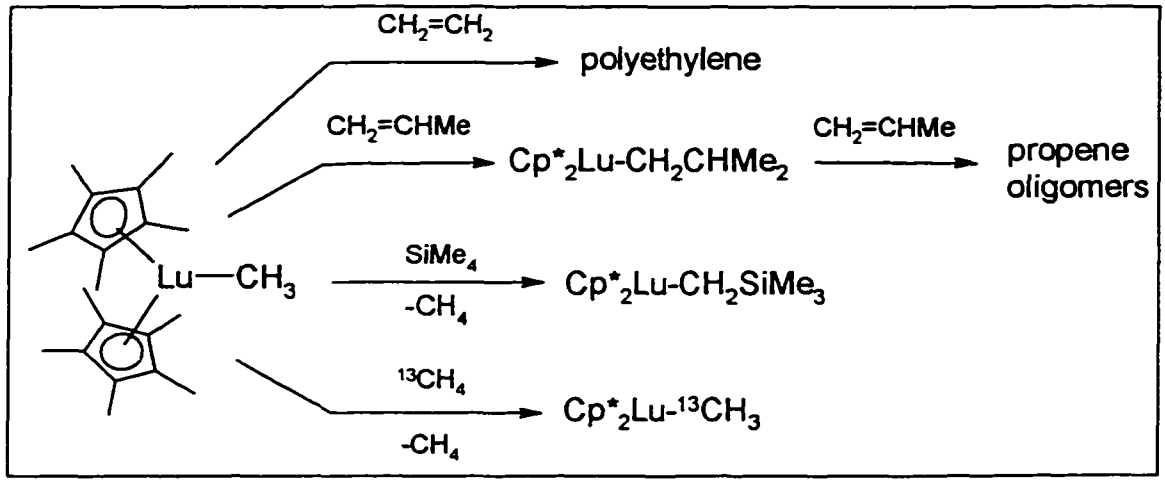

Alkoxide (aryloxide) ligands have been used in lanthanide chemistry for a long time. Bulky phenoxides such as $Ln(2,4,6\text{-}^{t}Bu_3C_6H_2O)_3$ have served as excellent starting materials for the preparation of lanthanide alkyl complexes because the byproduct lithium phenoxide is insoluble and can be easily separated from the highly hydrocarbon soluble lanthanide alkyls by filtration[108]. The first monomeric alkyllanthanide alkoxide complex was prepared by Schaverien employing the sterically demanding chelating biphenyl diolate as shown in eq. 24[109]. Alkyllanthanide alkoxide complexes are of great interest in the

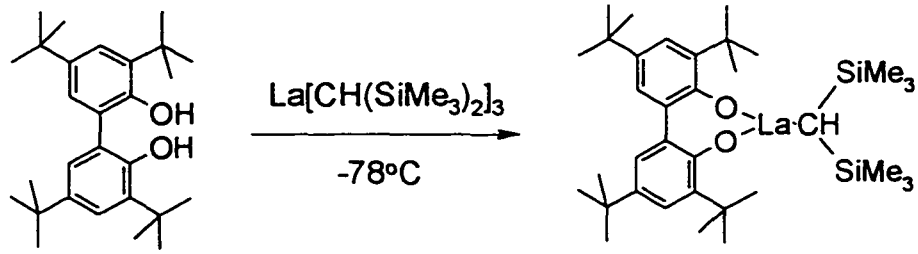

(24)

catalytic polymerization of 1,3-dienes. One commercial system uses a $Nd(OiPr)_3/AlEt_3/Et_2AlCl$ mixture, and a catalytically active heterobimetallic

alkyllanthanide alkoxide $[Nd_6Al_3(\mu\text{-}Cl)_6(\mu\text{-}Et)_9Et_5(O^iPr)]_2$ has been isolated from this system and structurally characterized[110].

Arylsiloxide ligand **5** is an attractive ancillary ligand because of the ease of preparation, the high crystallinity and the presence of ^{29}Si as a NMR probe. Arylsiloxide ligands are well suited to organolanthanide chemistry because the siloxide anion serves as a robust unit due to the fact that both Ln-O and Si-O bonds are very strong, so cleavage reactions typically observed for the C-O bonds of alkoxides are unlikely to occur. Additionally, the bulky *tert*-butyl group on silicon provides steric shielding and the amino groups contribute extra steric shielding and electronic saturation. Donor functionalization has been successfully employed by Herrmann in the synthesis of volatile lanthanide alkoxides for MOCVD[10] and by Takats[54], in the successful synthesis of solvent-free, divalent lanthanide alkyls and trivalent lanthanide dialkyls using tris(pyrazolyl)borate ligands. The possibility that **5** might also provide access to simple $LLnR_2$ and LLnR complexes led to an investigation of this ligand as an ancillary in organolanthanide chemistry.

2.8.2 Synthesis of yttrium alkyl complex 22

Reaction of one equivalent of **5** with $Y[N(SiMe_3)_2]_3$ proceeded smoothly at toluene reflux to produce the mono(siloxide) **20** in good yield (Scheme 7). Complex **20** showed no tendency towards ligand redistribution and reacted very sluggishly (toluene reflux, several days) with excess **5** to yield impure bis- and tris(siloxide) products. However, replacement of the remaining silylamide ligands was achieved cleanly using 2,6-di-*tert*-butylphenol ($HOC_6H_3{}^tBu_2$) producing the bis(phenoxide) complex **21**. Protonolysis of the arylsiloxide

ligand by $HOC_6H_3{}^tBu_2$ to give the known $Y(OC_6H_3{}^tBu_2)_3$ was not observed provided only two equivalents of the phenol were used[111].

Scheme 7

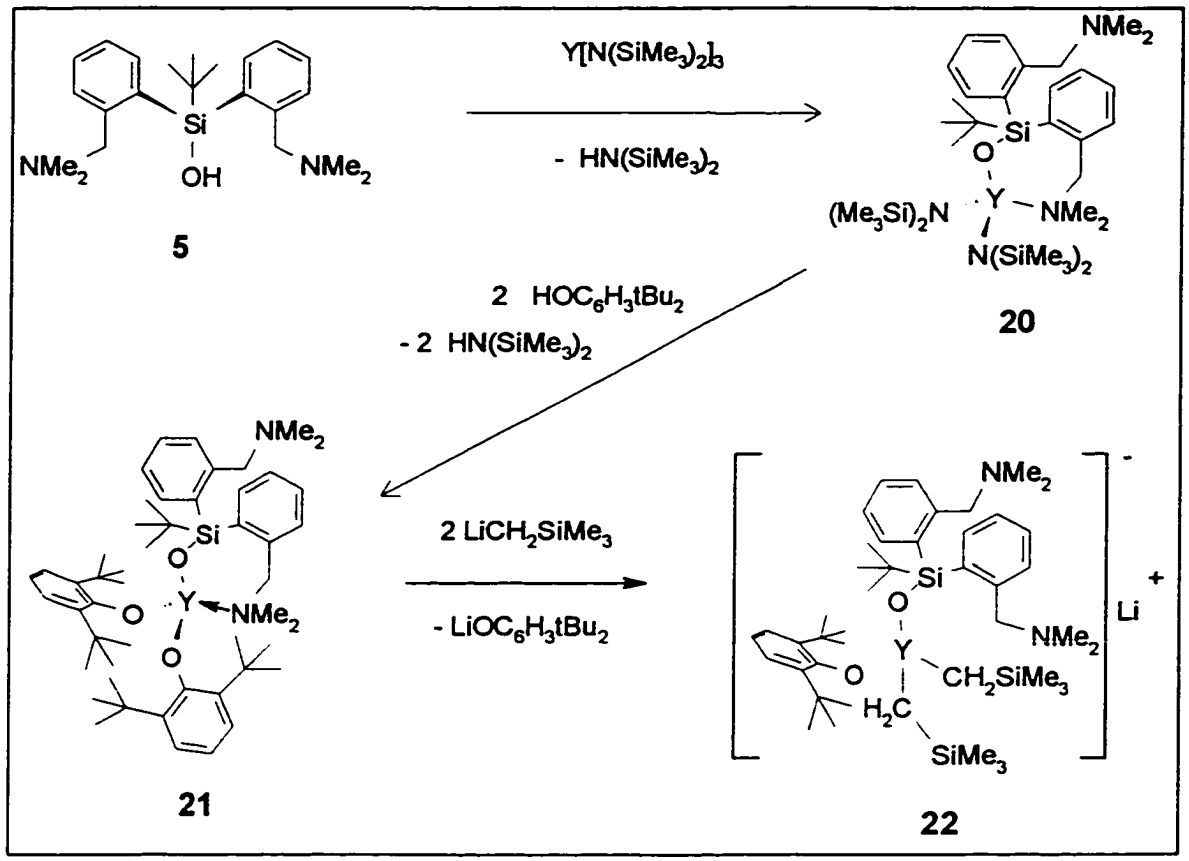

Phenoxides often serve as a good starting material for preparation of lanthanide alkyls because the byproduct lithium phenoxides are insoluble in hydrocarbon solvent. Reaction of **21** with two equivalents of $LiCH_2SiMe_3$ proceeded smoothly in toluene with elimination of $LiOC_6H_3{}^tBu_2$ to yield colorless crystals of **22**, as shown in Scheme 7. Elemental analysis and NMR spectra confirmed that only one equivalent of $LiOC_6H_3{}^tBu_2$ was eliminated. Effort to synthesize neutral dialkyl complex $Y[OSi^tBuAr_2][CH_2SiMe_3]_2$ by repeating recrystallization from hexane only led to unchanged complex **22**. Complex **22**, while crystalline, loses hexane

very readily and a crystal structure could not be obtained. The high toluene solubility and steric bulk of the ligands suggest that a monomeric structure is likely. Complex **22** is highly reactive, and decomposes rapidly in solution at temperatures above 40 °C. Attempts to prepare neutral $Y[OSi^tBuAr_2][OC_6H_3{}^tBu_2][CH_2SiMe_3]$ by reaction of one equivalent of $LiCH_2SiMe_3$ with **21** produced complex mixtures of products containing **22** as a major component.

2.8.3 Solid-state structure of complex 20 and 21

The complex NMR behavior of **20** and **21** prevented unambiguous structural assignments to be made by this technique alone. Therefore, **20** was subject to an X-ray crystallographic investigation. The structure of **20** is shown in Figure 16. Fractional atomic coordinates are given in Appendix Table XIV, and selected bond distances and angles are collected in Table 7. The X-ray structure reveals that **20** is monomeric and contains a four-coordinate yttrium center. One of the 2-(N,N-dimethylaminomethyl)phenyl arms of the siloxide ligand is not coordinated to the yttrium center. As might be expected, the geometry at yttrium is severely distorted from the ideal tetrahedral configuration due to the narrow siloxide angle (N(1)-Y(1)-O(1) 82.7(3)°) and the larger size of the silylamide ligands. A close nonbonded contact between Si(4) and Y(1) of 3.322(4) Å is observed. However, none of the three methyl carbons on Si(4) approach within 3.5 Å of Y(1) and this close approach is therefore probably necessitated by unfavourable steric interactions between the two silylamide ligands, rather than a reflection of any agostic interaction with the metal center. Indeed, observation of hindered silylamide rotation supports this explanation (*vide infra*).

Complex **21** was also subjected to an X-ray crystallographic investigation. There were 4 molecules of **21** and 4 molecules of hexane in the unit cell. The gross structural features of **21**

are very similar to **20** with only one arm of the siloxide ligand coordinated to the yttrium center. However, the hexane molecules are highly disordered and accurate structural parameters were not obtained.

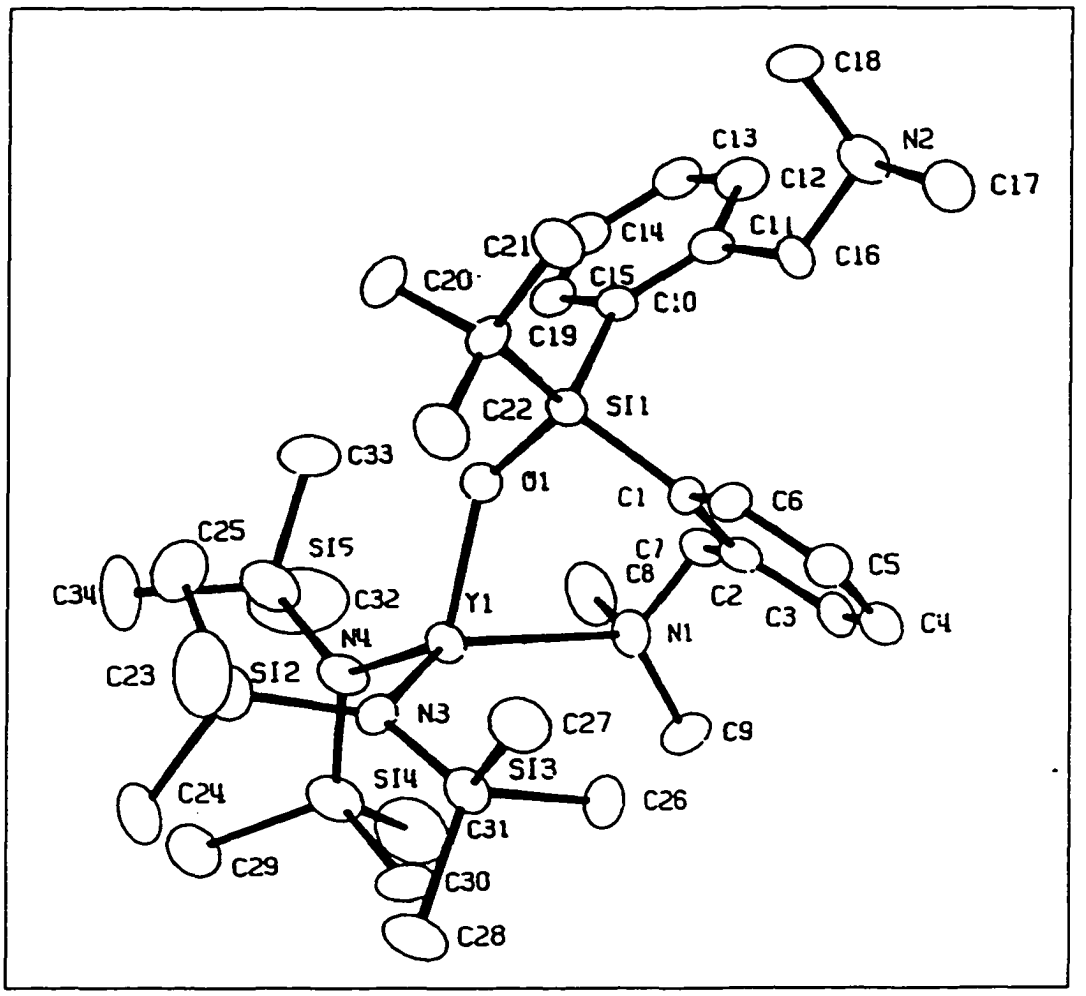

Figure 16 ORTEP diagram of **20**

Table 7 Selected distances (Å) and angles (deg) for **20** [a]

		Distances	
Y(1)-O(1)	2.093(7)	N(3)-Si(2)	1.733(10)
Y(1)-N(1)	2.611(9)	N(3)-Si(3)	1.679(10)
Y(1)-N(3)	2.237(9)	N(4)-Si(4)	1.705(11)
Y(1)-N(4)	2.221(9)	N(4)-Si(5)	1.744(12)
O(1)-Si(1)	1.606(7)		
		Angles	
Y(1)-O(1)-Si(1)	141.2(4)	O(1)-Y(1)-N(1)	82.7(3)
Y(1)-N(1)-C(7)	114.9(7)	O(1)-Y(1)-N(3)	106.7(3)
Y(1)-N(3)-Si(2)	119.7(5)	O(1)-Y(1)-N(4)	117.2(3)
Y(1)-N(3)-Si(3)	117.0(5)	O(1)-Si(1)-C(1)	106.4(5)
Y(1)-N(4)-Si(4)	114.9(6)	O(1)-Si(1)-C(10)	107.9(5)
Y(1)-N(4)-Si(5)	126.6(5)	O(1)-Si(1)-C(19)	108.1(5)
N(1)-Y(1)-N(3)	136.8(3)	Si(1)-C(1)-C(2)	121.7(9)
N(1)-Y(1)-N(4)	98.2(3)	C(1)-C(2)-C(7)	119.0(11)
N(3)-Y(1)-N(4)	112.9(3)	C(2)-C(7)-N(1)	114.1(9)

[a] estimated standard deviation in parentheses

The Y(1)-O(1) distance of 2.093(7) Å is long in comparison to structurally characterized lanthanide triphenylsiloxides (OR = $OSiPh_3$; $[Ce(OR)_2(\mu\text{-}OR)]_2$[112a] ; $[Ln(OR)_3(THF)_3]\bullet THF$ Ln = La[112b], Ce[112c], Y[112b,112d] ; $Ce(OR)_4(DME)\bullet toluene$[112e] ; $Y(OR)_3(O{=}PBu_3)_2$[112b] ; $[Y(OR)_4(DME)]^-[K(DME)_4]^+$ [112b]). After correction for differences in ionic radii due to coordination number and oxidation state,[91] these compounds predict a Y-O bond length range of 1.95-2.08 Å. Restricting the comparison to Y (2.00-2.08 Å) or four-coordinate (2.03-2.08 Å) complexes leads to the same conclusion. Similarly, the complexes $[Y(OR)_2(HOR)(\mu\text{-}OR)_2]Y(OR)_2$ (OR = OSi^tBuMe_2)[112b] and $Y[OSi^tBu_2(CH_2)_3NMe_2]_3$ 7 predict Y-O bond lengths in the range 2.01-2.06 Å. The latter complex, which is trigonal bipyramidal with two axially coordinated NMe_2 groups, also predicts a Y-N distance of 2.57(1) Å. The observed Y(1)-N(1) distance of 2.611(9) Å provides further support for the high

degree of steric crowding in **20**. Only $Yb[OSi^tBu_2(CH_2)_3NMe_2]_3[OSi^tBu_2(CH_2)_3NMe_2H]$ **10**, which we have previously shown to be very crowded, has Ln-O bonds of comparable length (predicts 2.09-2.12 Å). The Y(1)-O(1)-Si(1) angle of 141.2(4)° is considerably more bent than those found in other lanthanide siloxides (157.8-179.7°),[112] perhaps reflecting a requirement for chelation.

2.8.4 Fluxional behavior of 20 and 21

The variable temperature ^1H NMR behavior of **20** is shown in Figure 17 for the temperature range -40 to +110 °C. At -40 °C four silylamide $SiMe_3$ groups are clearly visible (δ -0.40 to +0.65 ppm). The siloxide 2-(N,N-dimethylaminomethyl)phenyl arms are also inequivalent. The NMe_2 groups of the coordinated arm are inequivalent from each other (1.79 and 2.16 ppm) while those of the noncoordinated arm are equivalent (1.73 ppm). The low temperature spectrum is consistent with the solid state structure (Figure 16). The silicon center is chiral rendering the CH_2 groups of both chelate arms diastereotopic. Upon warming from -10 to +50 °C, the $SiMe_3$ resonances pass through coalescence and reappear as two sharp singlets of equal intensity while the chelate arms of the siloxide ligand *remain* inequivalent. This process can therefore only be due to free rotation about the Y-$N(SiMe_3)_2$ bonds rendering the A/B and C/D $SiMe_3$ pairs equivalent. The free energy of activation for Y-N(silylamide) rotation was estimated from the coalescence temperatures as $\Delta G^{\ddagger}_{rotation} = 53 \pm 1$ kJ/mol.[113] Continued heating from +85 to 110 °C results in further collapse of the two $SiMe_3$ signals to a single resonance. This process also results in collapse of the inequivalent 2-(N,N-dimethylaminomethyl)phenyl arms to a single set of resonances and is consistent with exchange

of free and coordinated NMe_2 groups (an "arm on - arm off" process). The free energy of activation for this process is $\Delta G^{\ddagger}_{\text{arm exchange}} = 72 \pm 1$ kJ / mol.

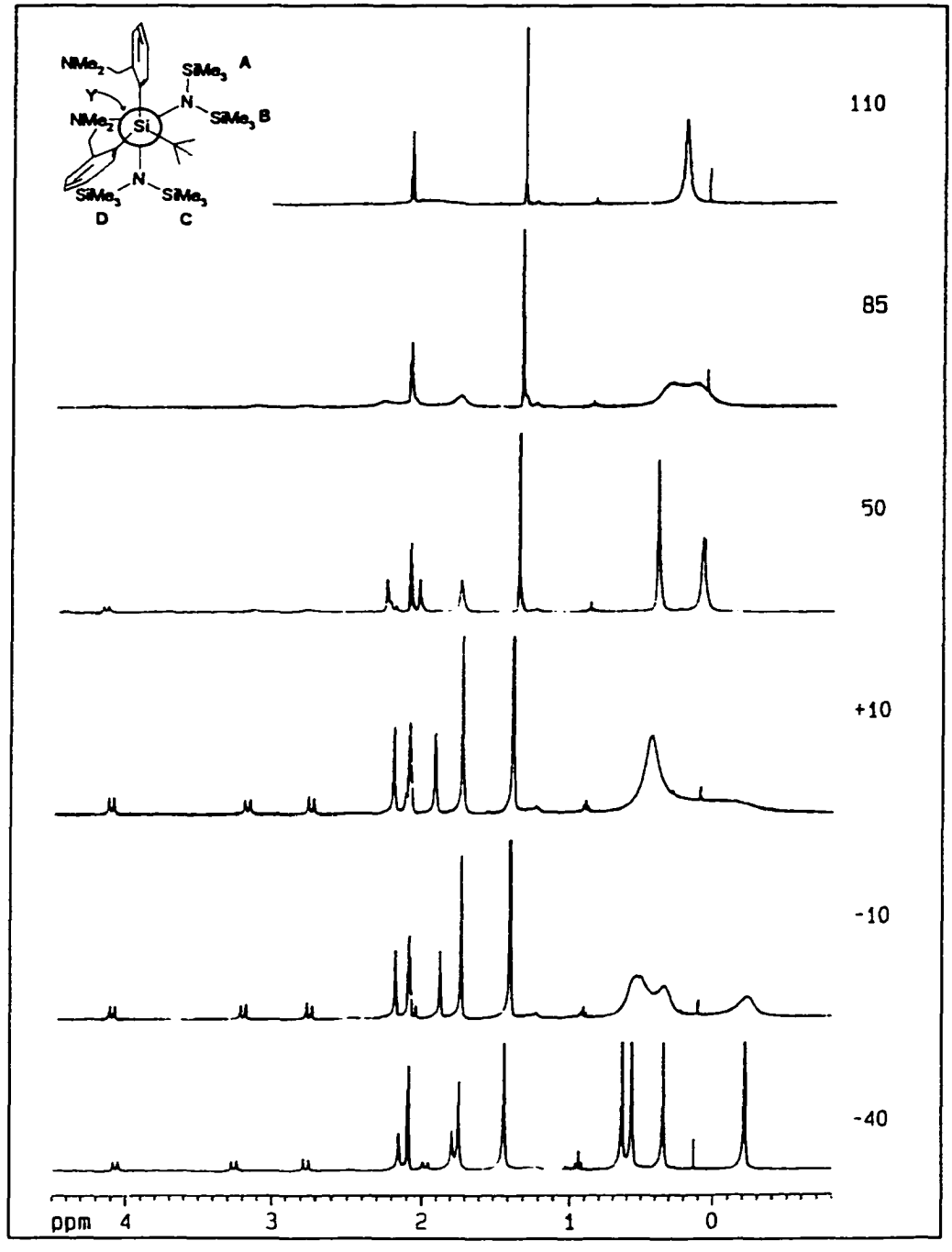

Figure 17 Variable temperature ^1H NMR spectra of **20**

The high value of $\Delta G^{\ddagger}_{rotation}$ is not surprising given the evidence presented earlier for steric crowding in the solid-state structure. On the other hand, the remarkably high value of $\Delta G^{\ddagger}_{arm\ exchange}$ requires further comment. In the relatively uncrowded complex, $Y[OSi^tBu_2(CH_2)_3NMe_2]_3$, exchange of free and coordinated N,N-dimethylaminopropyl arms is extremely facile, occurring rapidly on the NMR time scale even at -80 °C. This is consistent with the well-known lability of lanthanide-Lewis base adducts.[93] Thus, it seems likely to us that the large value of $\Delta G^{\ddagger}_{arm\ exchange}$ derives from a large energy barrier to reorientation of the siloxide ligand such that the free 2-(N,N-dimethylaminomethyl)phenyl arm can coordinate. This explanation is reasonable given the steric congestion at yttrium noted earlier.

Complex **21** exhibits very similar NMR behavior to **20**. This is not surprising given the similarity in solid-state structure (*vide supra*). Values of $\Delta G^{\ddagger}_{rotation}$ = 57 ± 1 kJ/mol for the phenoxide rotation processes and $\Delta G^{\ddagger}_{arm\ exchange}$ = 75 ± 1 kJ/mol for the NMe_2 exchange process were derived from variable temperature ^1H NMR. The similarity between the $\Delta G^{\ddagger}_{rotation}$ and $\Delta G^{\ddagger}_{arm\ exchange}$ values observed for **21**, compared with those observed for **20**, is reasonable given the similar steric bulk of the $N(SiMe_3)_2$ and $OC_6H_3{}^tBu_2$ ligands.[114]

The ^{29}Si variable temperature NMR of **20** is consistent with the ^1H NMR behavior. Four silylamide resonances are observed at low temperature but no silylamide signals were observed at temperatures above +30 °C. The ^{29}Si resonance of the siloxide ligands in **20** and **21** appear ca. 8 ppm upfield of the signal in **5** and show coupling to ^{89}Y of 5 Hz. Very similar values were obtained for $Y[OSi^tBu_2(CH_2)_3NMe_2]_3$ **7** (10 ppm upfield; $^2J(^{29}Si\text{-}^{89}Y)$ = 6 Hz).

2.8.5 Solution behavior of 22

Complex **22** shows very complicated ^{1}H NMR behavior which is not due to impurities since repeated recrystallization and preparation of fresh samples does not alter the appearance or relative intensity of the resonances observed (Figure 18). It is clear that at +40 °C the complex is undergoing a rapid fluxional process (or processes) which renders both 2-(N,N-dimethylaminomethyl)phenyl arms of the siloxide and both CH_2SiMe_3 groups equivalent. Cooling to -20 °C results in several significant spectral changes. The CH_2SiMe_3 ligand environments become inequivalent as evidenced by the observation of two $SiMe_3$ resonances (δ 0.45 and 0.30 ppm). Further, all methyl groups of the NMe_2 donors become inequivalent (δ 2.42, 1.90, 1.55, and 1.40 ppm). The observation of 4 methyl resonances of equal intensity in both the ^{1}H and ^{13}C NMR spectrum is consistent with coordination of both NMe_2 arms, in contrast to the 1:1:2 pattern observed in the limiting low temperature spectra of **20** and **21**. This data alone does not allow us to determine which metal center, yttrium or lithium, is involved in this interaction.

As the temperature is lowered further to -70 °C, the ^{1}H NMR spectrum becomes more complex. At this temperature, the phenoxide *tert*-butyl (ca. δ 1.8 to 2.0 ppm) and siloxide *tert*-butyl (δ 1.15 ppm) resonances become extremely broad. However, the two major $SiMe_3$ resonances sharpen once more and several new resonances appear in this region.[22] The CH_2SiMe_3 resonances sharpen into two distinct sets of doublets (Figure 19). Coupling to ^{89}Y is not observed but this is not surprising since $^2J_{YH}$ is generally 2-3 Hz and the line widths observed here are about 5 Hz[71] (the doublet patterns in Figure 19 are due to geminal coupling between the CH_2SiMe_3 protons: $^2J_{HH}$ = 8 to 12 Hz). We were able to locate two doublets in the ^{13}C NMR spectrum corresponding to the 4 major CH_2SiMe_3 signals by using a ^{13}C-^{1}H

COSY experiment at -60 °C. The chemical shifts and coupling constants (δ 36.1 , $^1J_{YC}$ = 40 Hz and δ 24.5, $^1J_{YC}$ = 36 Hz) for these carbons are very similar to those observed for other yttrium alkyls[115] which indicates clearly that the CH_2SiMe_3 groups are still attached to the yttrium center. The presence of two sets of resonances of unequal intensity for the CH_2SiMe_3 protons is consistent with the observation of an equilibrium between two yttrium alkyls, such as the one shown in eq. 25. However, we did not have enough data to propose a definitive explanation for the observed low temperature behavior of complex **22**.

$$\underset{\mathbf{22}}{\{Y[OSi^tBuAr_2][OC_6H_3{}^tBu_2][CH_2SiMe_3]_2\}^-Li^+} \rightleftharpoons Y[OSi^tBuAr_2][CH_2SiMe_3]_2 + Li\,OC_6H_3{}^tBu_2 \qquad (25)$$

Schaverien has recently reported replacement of only one phenoxide during reaction of $Cp^*Y(OC_6H_3{}^tBu_2)_2$ with $KCH(SiMe_3)_2$ although MeLi reportedly leads to replacement of both phenoxides ligands.[71] In the present case, reaction of **22** with one or two equivalents of MeLi failed to produce clean products. It is possible that the dangling NMe_2 arm *promotes* formation of an anionic "ate" complex by stabilizing the Li^+ counterion.

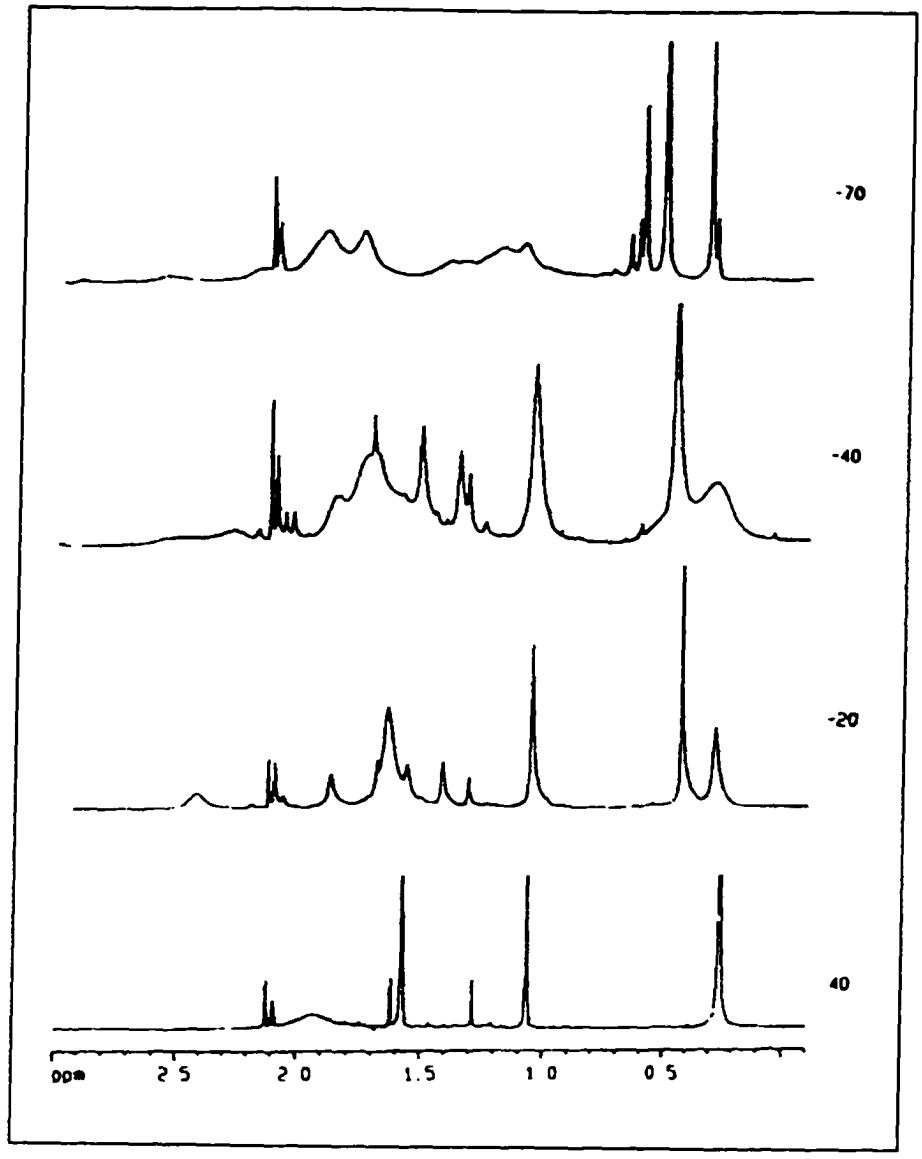

Figure 18 Variable temperature ^{1}H NMR spectra of **22**

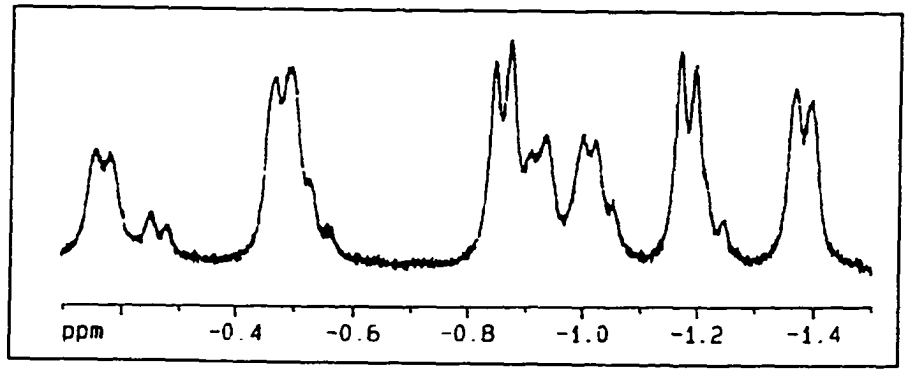

Figure 19 ^{1}H NMR spectrum (-70 °C) showing the CH_2SiMe_3 region of **22**

CHAPTER 3

SYNTHESIS AND CHARACTERIZATION OF ZIRCONIUM COMPLEXES BEARING AMINODIOLATE AND TRIOLATE LIGANDS

3.1 Introduction

Despite the dominance of Cp and its derivatives as ancillary ligands for group 4 organometallic chemistry, alkoxide (siloxide and aryloxide as well) ligands have also been intensively used[100b]. Organometallic chemistry of group 4 metals with bulky monodentate alkoxide (such as $^tBu_3CO^-$ and $^tBu_3SiO^-$)[11c] and aryloxide ligands (2,6-di-*iso*-propyl, *tert*-butyl, cyclohexyl and phenyl phenoxides)[23] has been well studied. Application of chelating biphenols and binaphthols in transition metal chemistry has also been explored[69]. Group 4 metal complexes bearing binaphthol ligands are especially important in asymmetric catalysis due to their intrinsic C_2 chirality[116]. Tripod ligands, such as triethanolamine, $[N(CH_2CH_2CH_2OH)_3]$ have been used for early transition metal chemistry, particularly by Verkade, who has synthesized and structurally characterized a series of monomeric and dimeric titanium complexes bearing triethanolamine as a ligand[110]. These complexes showed remarkable stability towards ligand redistribution and hydrolysis (alcoholysis). For example, alcoholysis of cyclopentadienyl titanatrane* only results in displacement of Cp, and the triethanolamine remains attached (eq. 26). However, triethanolamine is not sterically demanding enough to allow isolation of stable zirconium complexes because zirconium is substantially larger than titanium. In our own work, we have been investigating alternative ligand systems to Cp based on donor-functionalized alkoxide ligands. By adding bulky groups to the alcohol carbon, sterically demanding tripodal amino alkoxide ligands such as **21** (Chapter 2) and **27** can be prepared which are better suited to zirconium chemistry. However for group 4 metals, tripodal ligands of this type will only allow synthesis of monoalkyl complexes; dialkyl, alkylidene, amido, oxo and

cationic alkyl complexes are not accessible with such a ligand set. Thus we turned our attention to amino diol ligands **28-32** to overcome these limitations. Furthermore, by using the amino diol ligand framework, it allows us to investigate the effect and contribution of the amine donor to the stability and reactivity of the complexes by conveniently varying the steric bulk of the amino group (*vide infra*). While this work was in progress, Nugent reported elegant work on application of homochiral tripodal amino triol ligands (**XXII**) to early transition metal chemistry. These enantio-pure tripodal ligands were conveniently synthesized by the epoxide ring opening reaction (eq.27), and a number of titanium, vanadium, niobium and tantalum complexes bearing these ligands have been synthesized and structurally characterized[50a]. Zirconium complexes bearing these ligands show high enantioselectivity in catalyzing the cleavage reaction of meso epoxide with azidotrialkylsilanes[52]. However, these zirconium complexes are structurally complicated oligomers and are not yet well characterized.

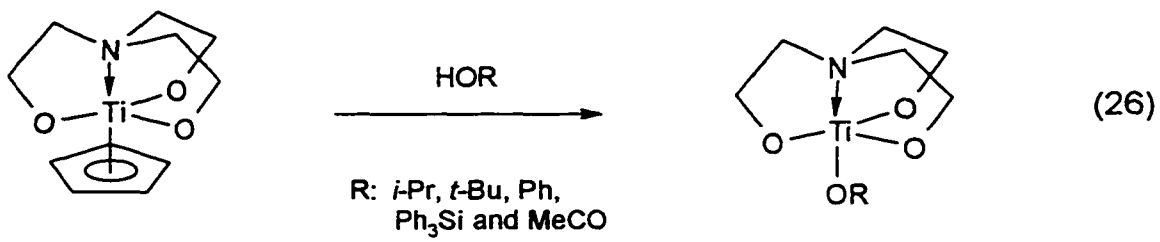

(26)

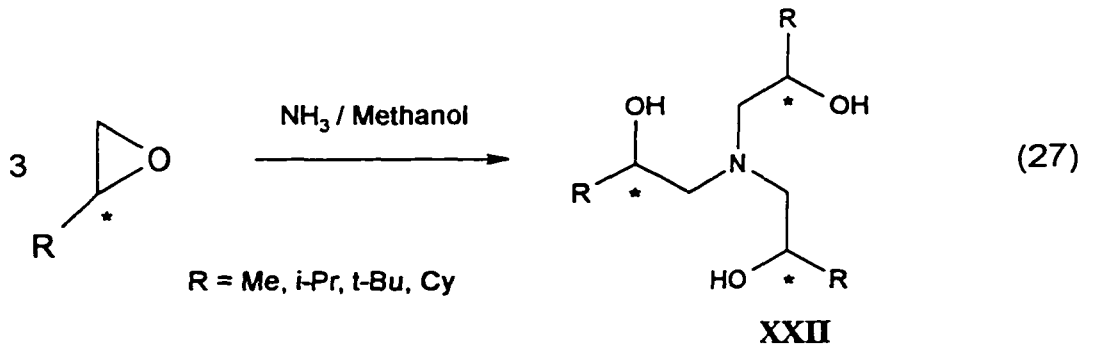

(27)

XXII

---

* "atranes" are the complexes derived from deprotonated triethanolamine.

3.2 Ligand synthesis and characterization

The amino diol or triol ligands **27-32** were synthesized in two steps from readily available starting materials. (Scheme 8). Michael addition[117] proceeds smoothly in excellent yield when the starting amine is not sterically hindered (**23** and **24**). With bulky amines, Michael addition proceeds very slowly, and in the case of *tert*-butyl amine, gives a mixture of monoester and diester even after one week of refluxing in methanol. Ligand precursors **23-26** were all colorless oils which distilled under vacuum. They were characterized by NMR (Table 8 and 9) and mass spectroscopy.

Scheme 8

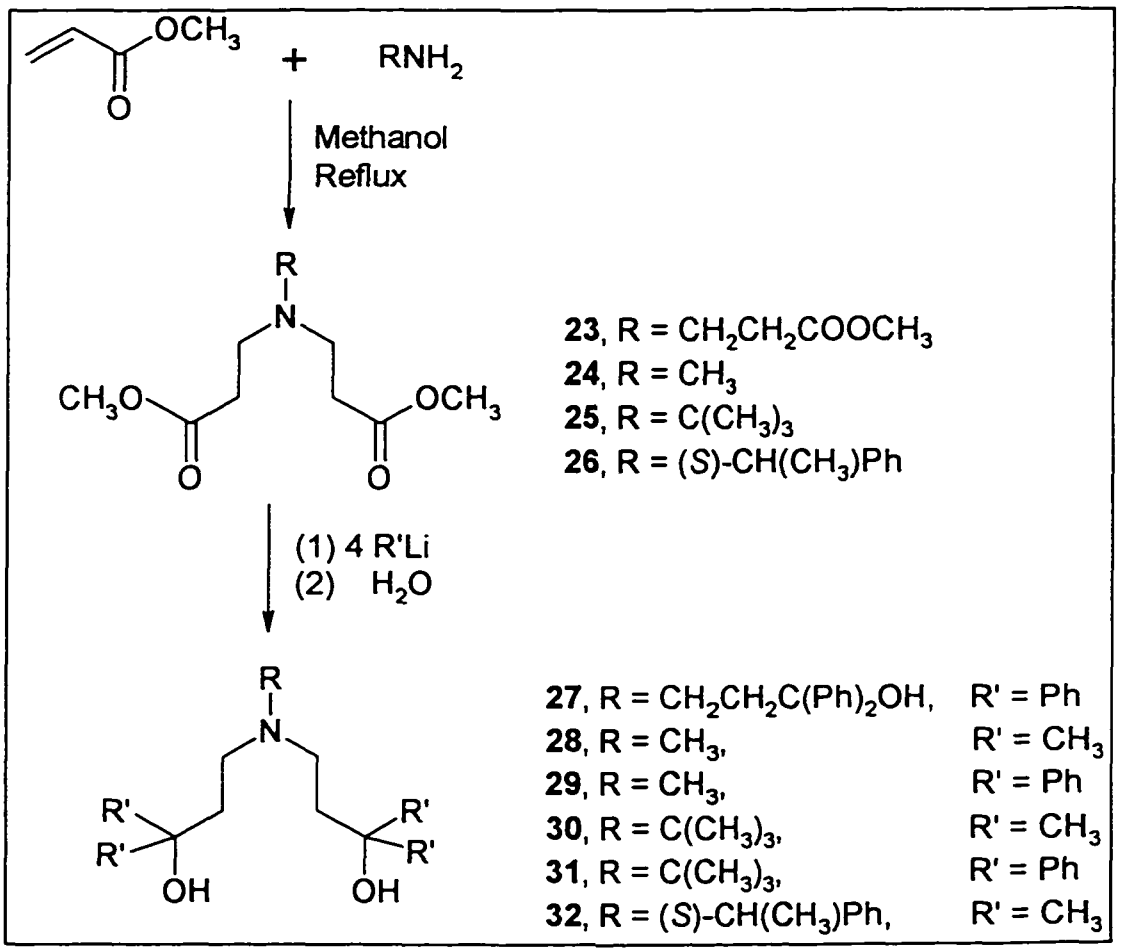

Table 8 ^{1}H NMR chemical shift and coupling constant data in $CDCl_3$

Assignment	23	24	25	26	
CH_3N		s, 2.19			
$NCMe_3$			s, 1.01		
aryl*CH*				m, 7.27, 7.20	
Ph*CH*N				q, 3.81, $^{3}J_{HH}$ = 6.8 Hz	
*Me*CHN				d, 1.33, $^{3}J_{HH}$ = 6.8 Hz	
NCH_2	t, 2.74, $^{3}J_{HH}$ = 7.1 Hz	t, 2.65, $^{3}J_{HH}$ = 7.2 Hz	t, 2.78 $^{3}J_{HH}$ = 7.6 Hz	t, 2.82, $^{3}J_{HH}$ = 6.8 Hz	t, 2.70, $^{3}J_{HH}$ = 7.0 Hz
CH_2CO	t, 2.41, $^{3}J_{HH}$ = 7.1 Hz	t, 2.41,	t, 2.40, $^{3}J_{HH}$ = 7.6 Hz	t, 2.40, $^{3}J_{HH}$ = 7.0 Hz	
OCH_3	s, 3.63	s, 3.61	s, 3.62	s, 3.61	

Table 9 $^{13}C\{^{1}H\}$ NMR chemical shift data in $CDCl_3$

Assignment	23	24	25	26
CH_3N		41.7		
$NCMe_3$			27.1	
$NCMe_3$			55.1	
arylCH				143.4, 128.1, 127.6, 126.8
PhCHN				58.9
*Me*CHN				16.2
NCH_2	49.2	52.4	46.1	45.8
CH_2CO	32.6	32.3	36.5	33.4
OCH_3	51.5	51.5	51.4	51.4
C=O	172.8	172.8	173.1	172.9

The desired ligands **27-32** were synthesized by nucleophilic addition of methyl or phenyllithium to the amino di- or triesters (**23-26**). Although the α-protons of the esters are relatively acidic, deprotonation at this site did not occur, and direct nucleophilic attack proceeded smoothly. In the case of **32**, a side reaction involving metallation at the acidic site resulted in formation of a secondary amine as shown in Scheme 9. It was

separated from **32** as a colorless liquid by vacuum distillation and was identified by NMR and mass spectroscopy. Ligand **28** was isolated as a colorless oil and was purified by vacuum distillation, while ligands **27** and **29-31** were obtained as colorless crystals by recrystallization from a toluene / hexane mixture. Crude **32** was isolated as a viscous oil and was purified by column chromatography (silica gel, 95 % ethyl acetate / 5 % methanol).

Scheme 9

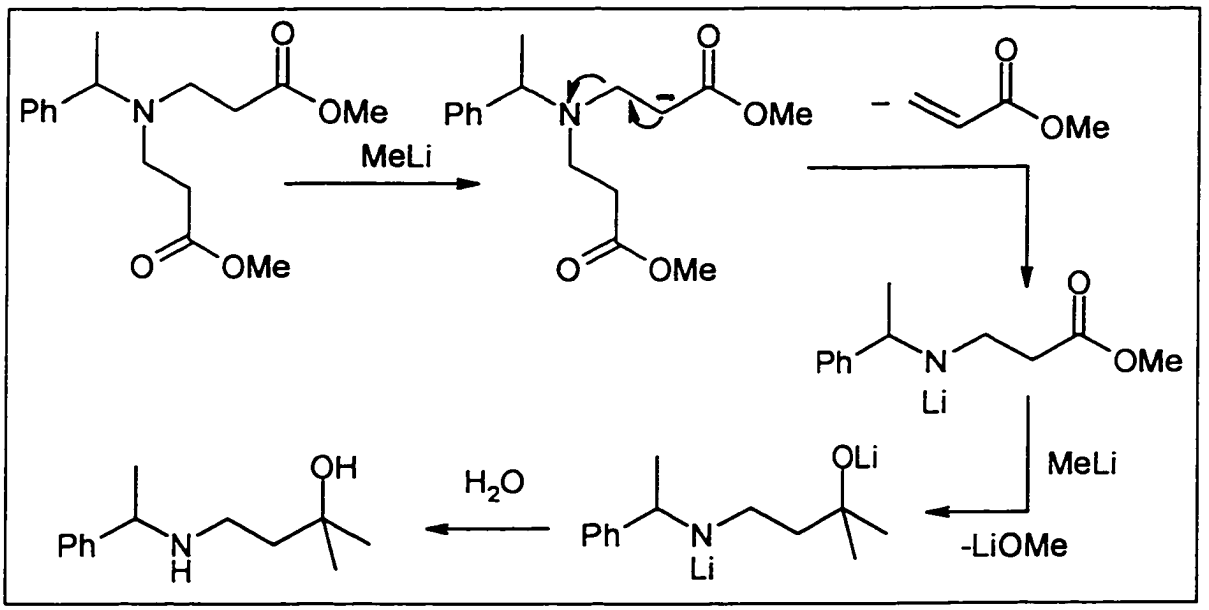

Ligands **27-32** were characterized by NMR (Table 10 and 11), mass spectroscopy and elemental analysis. The high symmetry of ligands **27-31** results in simple NMR spectra as illustrated for **30** in Figure 20. The chiral group attached to nitrogen in **32** breaks the symmetry and makes the geminal NCH_2 protons inequivalent as shown by the AB pattern in the ^1H NMR spectrum of this ligand. (Figure 22 and 23). The mass spectrum shows the molecular ion and fragment ions due to sequential loss of alcohol arms. A typical mass spectral fragmentation pattern is shown for **28** in Figure 21.

Table 10 ^{1}H NMR chemical shift data in $CDCl_3$

Assignment	27	28	29	30	31	32
C*H*$_3$N		2.22	2.22			
NC*Me*$_3$				0.95	0.69	
aryl*CH*						7.3
PhC*H*N						3.93
*Me*CHN						1.36
NC*H*$_2$	2.33	2.25	2.36	2.58	2.51	2.68,2.57
C*H*$_2$CO	2.13	1.60	2.36	1.67	2.47	1.60,
C*H*$_3$CO		1.17		1.22		1.10,1.00
*Ph*CO	7.43,7.14 7.02		7.38,7.27 7.18		7.58,7.13 7.00	
CO*H*	4.20	4.05	5.22	4.54	5.23	4.19

Table 11 $^{13}C\{^{1}H\}$ NMR chemical shift data in $CDCl_3$

Assignment	27	28	29	30	31	32
C*H*$_3$N		41.9	42.3			
NCMe$_3$				55.8	56.1	
NC*Me*$_3$				26.9	26.6	
aryl*C*H						141.5,128.4 128.1,127.2
PhCHN						58.2
*Me*CHN						14.7
NCH$_2$	50.4	53.9	53.7	46.5	47.2	45.0
*C*H$_2$CO	38.2	38.8	37.5	42.4	40.0	38.6
*C*OH	78.0	70.6	78.2	70.6	78.6	70.5
*C*H$_3$CO		29.7		30.2		29.6, 29.3
*Ph*CO	147.9,128.3 126.8,126.4		147.2,128.1 126.6,125.8		147.5,128.1 126.5,125.9	

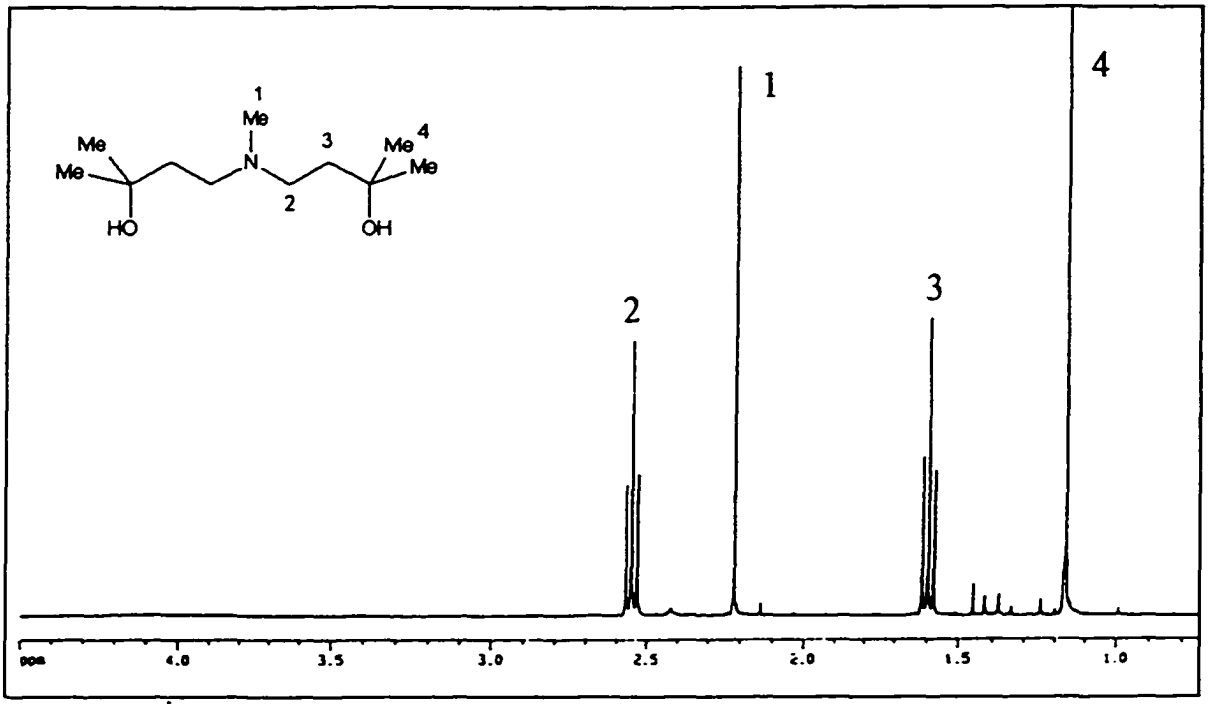

Figure 20 ^{1}H NMR spectrum of $MeN(CH_2CH_2CMe_2OH)_2$ (**28**) in $CDCl_3$ (300MHz)

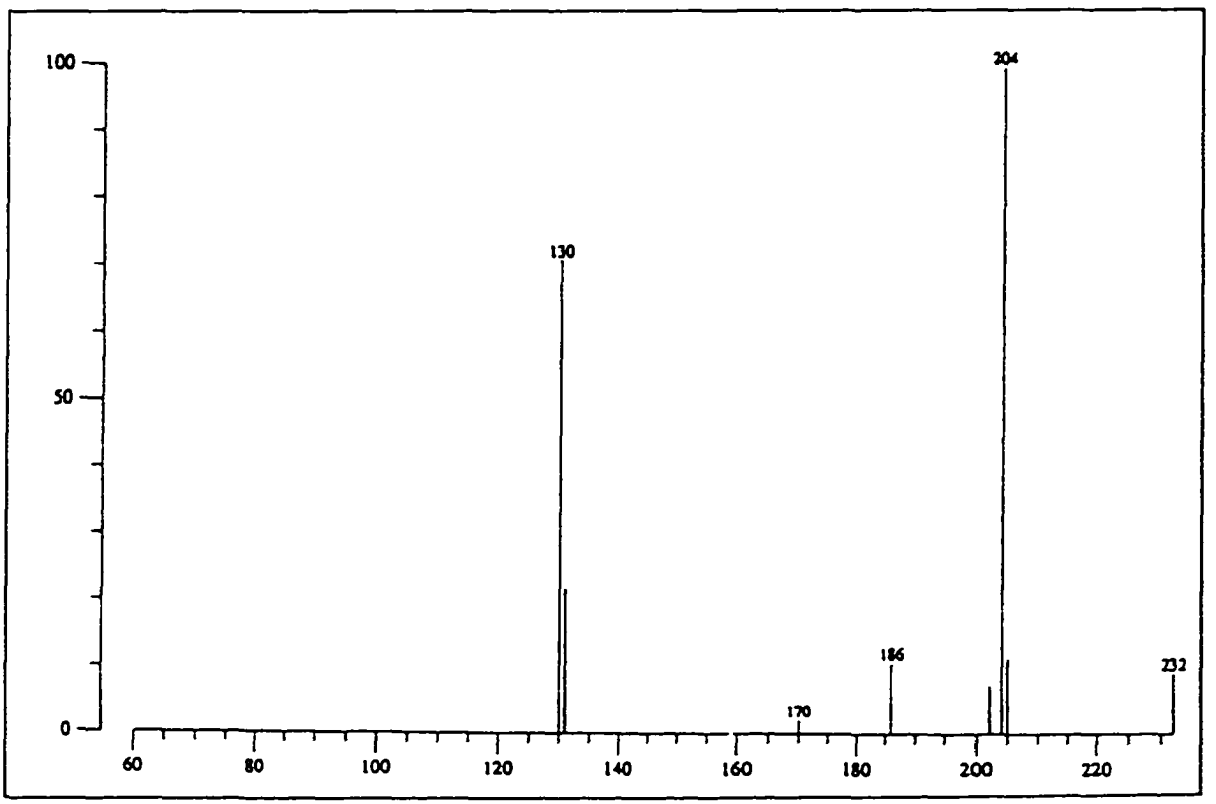

Figure 21 Mass spectrum (CI) of $MeN(CH_2CH_2CMe_2OH)_2$ (**28**)

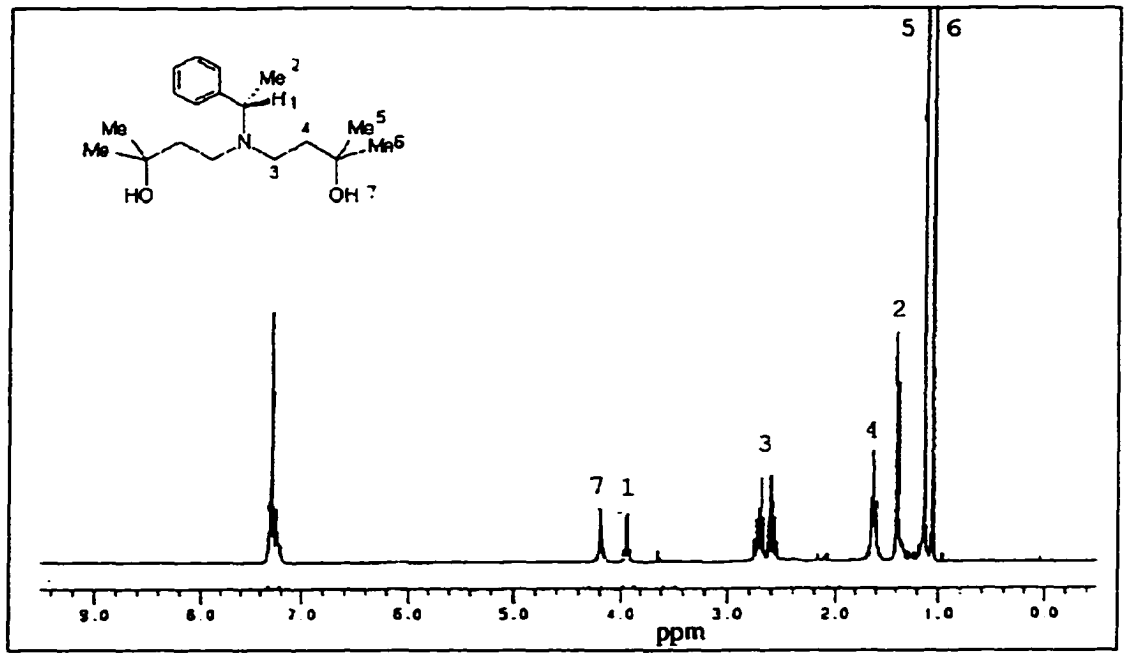

Figure 22 ^{1}H NMR of (*S*)-$Ph(CH_3)CHN(CH_2CH_2CMe_2OH)_2$ (**32**) in $CDCl_3$ (300 MHz)

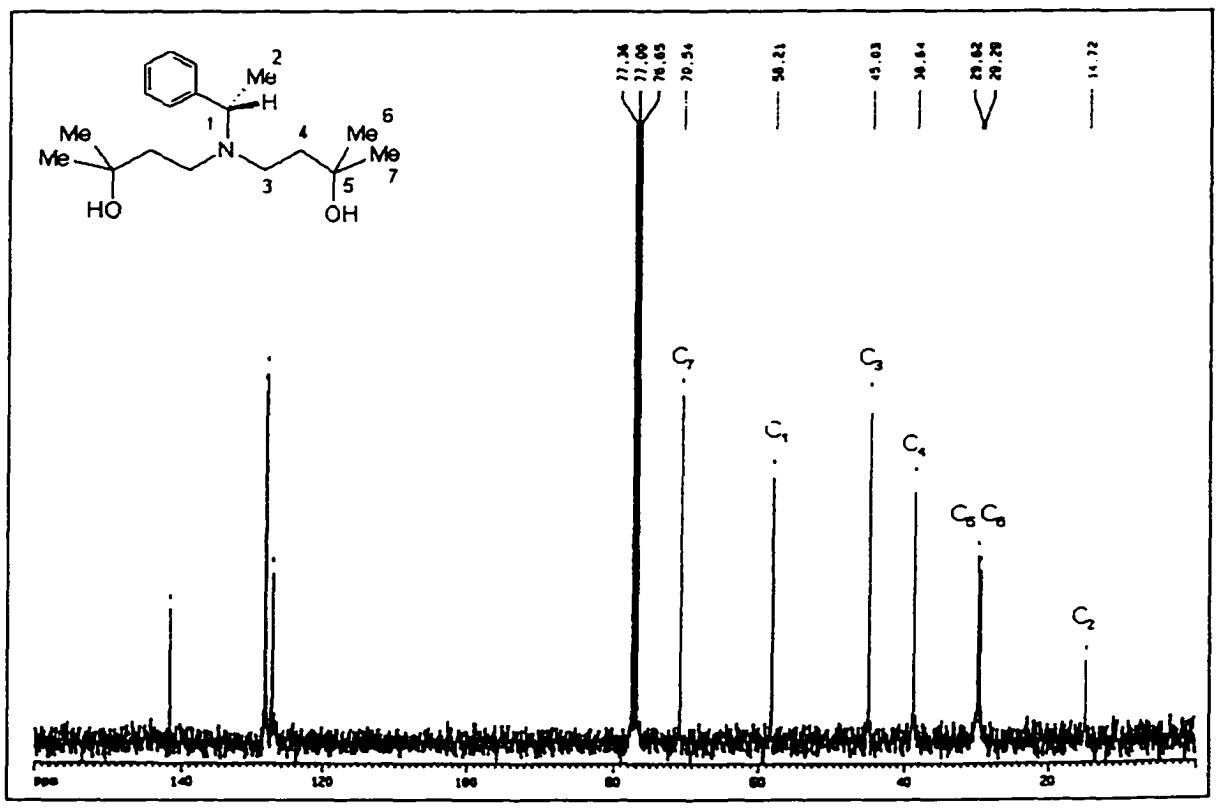

Figure 23 $^{13}C\{^{1}H\}$ spectrum of (*S*)-$Ph(CH_3)CHN(CH_2CH_2CMe_2OH)_2$ (**32**) in $CDCl_3$

3.3 Zirconium bis(ligand) complexes

3.3.1 Synthesis of zirconium bis(ligand) complexes

Addition of two equivalents of amino diol ligands **28-32** to tetrabenzyl zirconium resulted in formation of the corresponding zirconium bis(ligand) complexes **33-37.** (eq. 28). Phenyl substituents on the alkoxide carbons significantly improve the crystallinity: **34** and **36** were isolated as crystalline solids while **33, 35** and **37** are so soluble in hexane that purification by recrystallization was not possible. However, even without further purification, the complexes isolated were of high purity as indicated by NMR and elemental analysis. In all cases, molecular ions were observed in mass spectrum. (Figure 24).

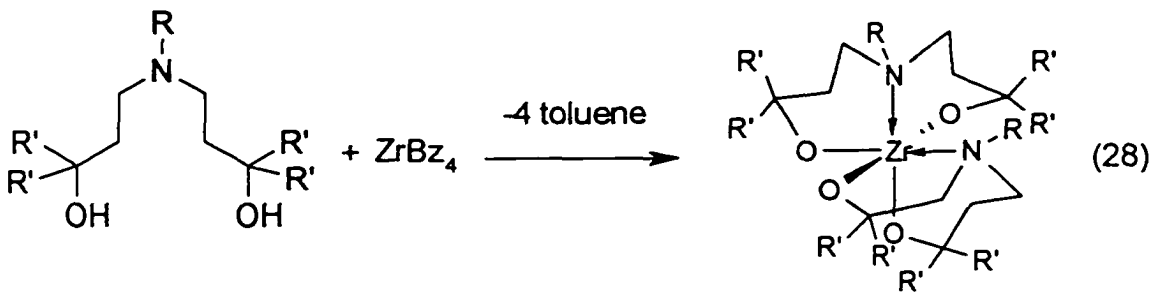

33, R = CH_3, R' = CH_3
34, R = CH_3, R' = Ph
35, R = $C(CH_3)_3$, R' = CH_3
36, R = $C(CH_3)_3$, R' = Ph
37, R = (*S*)-$CH(CH_3)Ph$, R' = CH_3

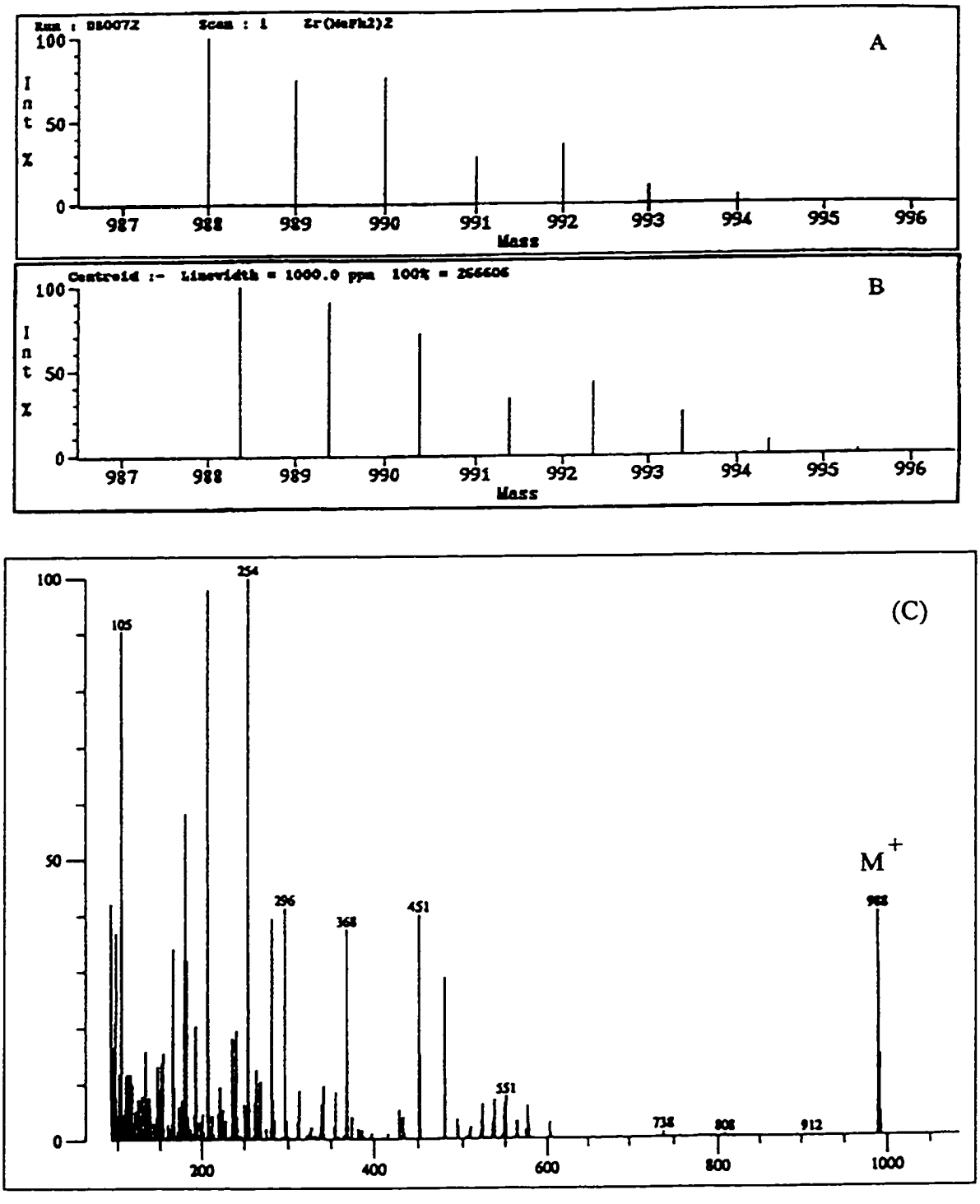

Figure 24 Mass spectrum of **34** (C) and isotopic distribution for molecular ion M^+ (A): experimental distribution; (B): theoretical distribution

3.3.2 Structure of zirconium bis(ligand) complexes

Dimeric and oligomeric solution structures are very common for zirconium alkoxide complexes[6, 118]. However, cryoscopic solution molecular weight determinations for complexes **33-37** indicated that they are all monomeric. The low tendency of these complexes to form aggregates suggests that the coordination sphere of the zirconium ion is sufficiently saturated with two of these bulky ligands. The monomeric structure greatly simplifies the interpretation of the solution structure by NMR spectroscopic methods.

Proton NMR evidence points to a *cis*-octahedral (C_2) geometry (**XXIV**, Figure 25) for both **33** and **34** since eight resonances are observed for the CH_2 backbone protons. The *trans*-octahedral structure (**XXIII**, Figure 25) can be excluded since it would have C_{2h} symmetry and should only display four resonances due to the ligand backbone CH_2 protons. A preliminary X-ray crystallographic study also revealed a *cis*-octahedral geometry for **34**. The ORTEP diagram of **34** is shown in Figure 26. However, disorder problems prevented satisfactory refinement of this structures and an accurate determination of bond lengths and angles was not possible. It is interesting to note that the chemical shift difference between the geminal backbone CH_2 protons is unusually large; for example in complex **34**, the chemical shift of one geminal proton (NCH_a) appears at 3.1 ppm while the other (NCH_b) appears at 1.0 ppm, so that the chemical shift difference between these geminal protons is over 2.0 ppm (Figure 27 and 28).

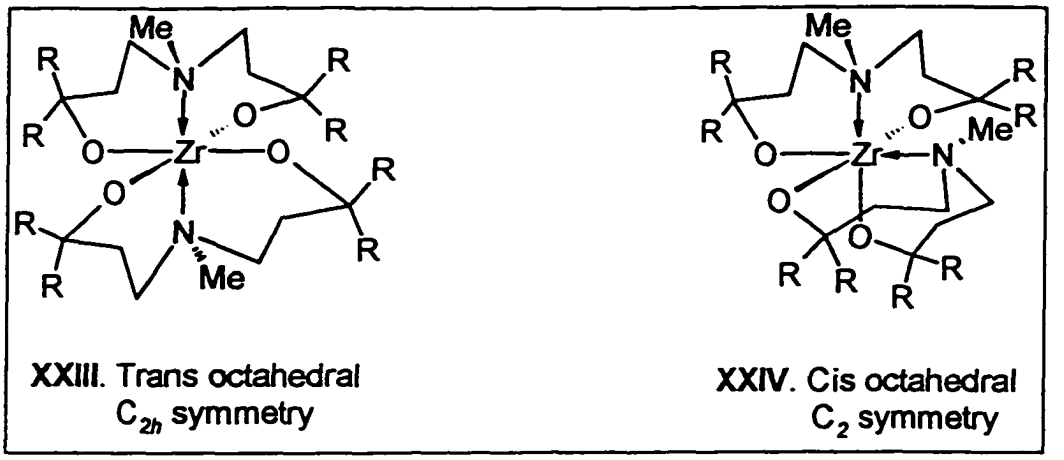

Figure 25 Two possible octahedral geometries for **33** and **34**

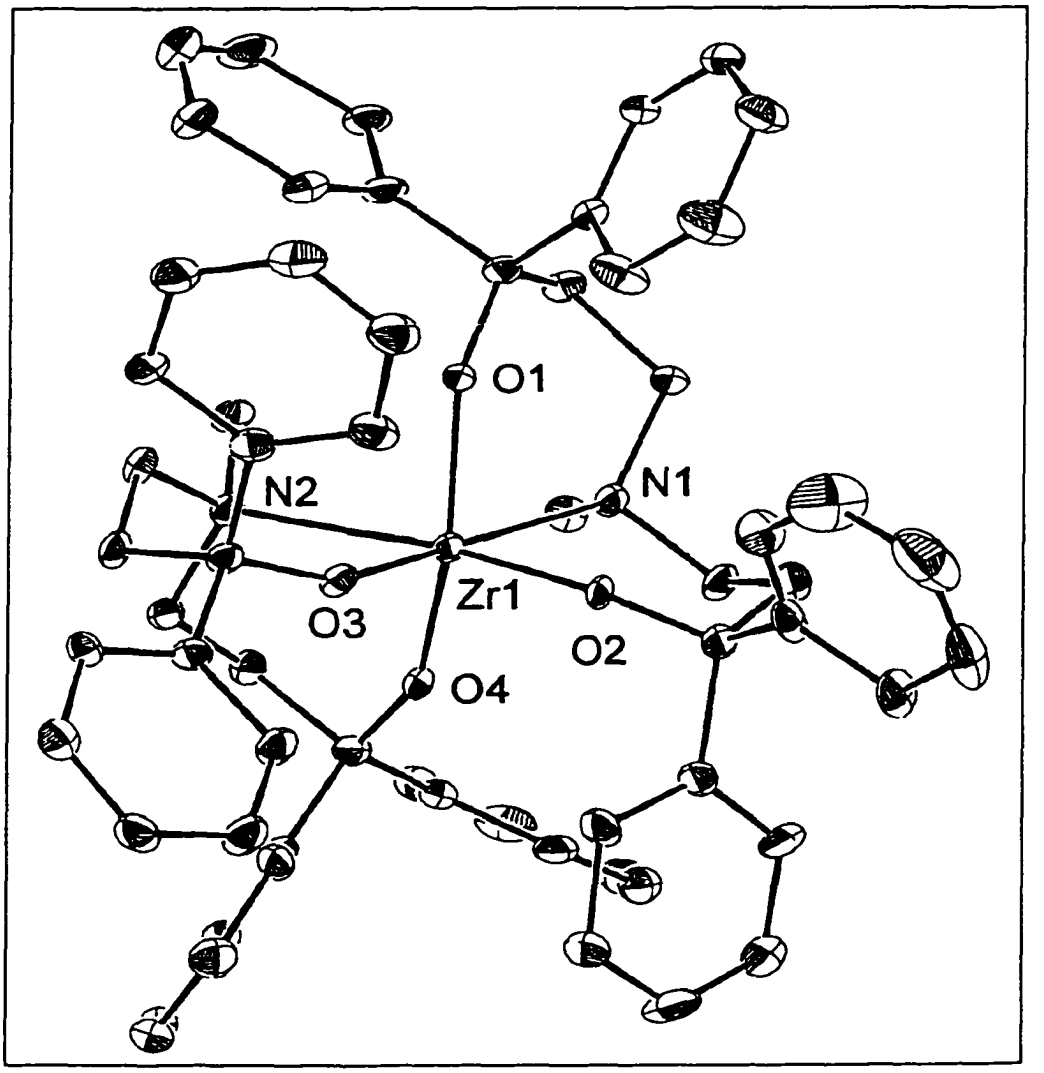

Figure 26 ORTEP diagram of **34**

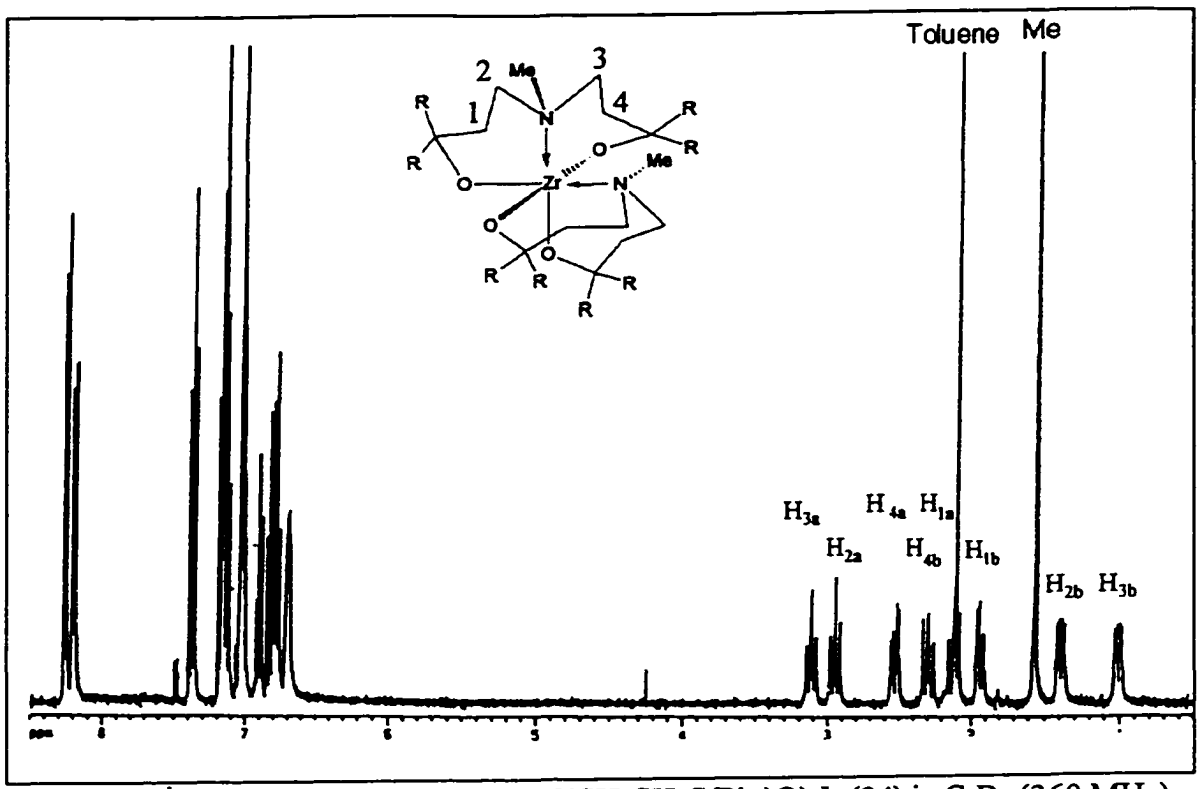

Figure 27 ^{1}H NMR spectrum of $Zr[MeN(CH_2CH_2C(Ph_2)O)_2]_2$ (34) in C_6D_6 (360 MHz)

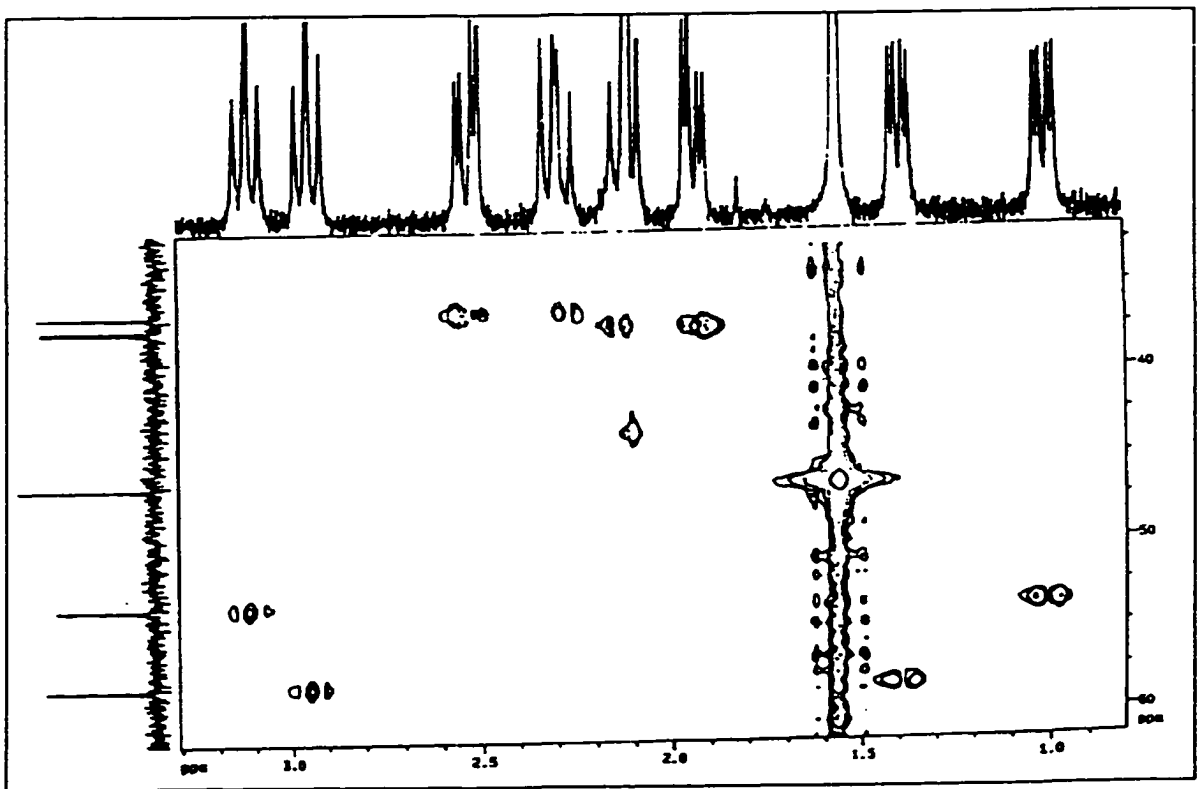

Figure 28 ^{1}H-^{13}C coorelated spectrum of $Zr[MeN(CH_2CH_2C(Ph_2)O)_2]_2$ (34) in C_6D_6

Verkade also observed a similar preference for the *cis*-octahedral geometry in the dimeric dimethylamino titanatranes **XXV** and **XXVI**: the amide group prefers the equatorial position in order to avoid being trans to the tertiary amino group; in contrast, the *iso*-propoxy group takes the position trans to the amino group[110]. Verkade rationalized the difference in geometry in terms of electronic effects: the more strongly electron donating amido group prefers to be *trans* to the more electronegative alkoxide group rather than another strongly electron donating tertiary amine group. Similar reasoning may be valid in our case as well.

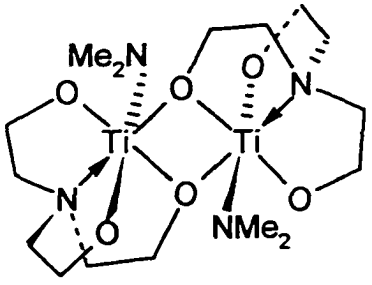

XXV

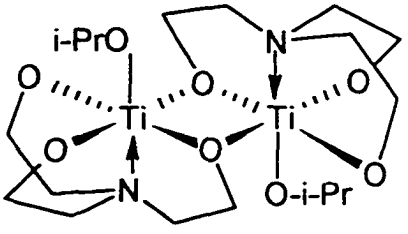

XXVI

The NMR signals of **33** are not as sharp as those for **34** at room temperature, so that a dynamic process is expected for **33**. Indeed, when an NMR sample of **33** is heated, the signals broaden and the ligand backbone proton resonances collapse. From the coalescence temperature for the four alkoxide methyl peaks of 42 °C, a free energy of activation for this dynamic process was calculated as $\Delta G^* = 66.7 \pm 0.5$ kJ/mol[•]. At 80 °C,

---

[•] The free energy of activation was calculated from the coalescence temperature (T_c) using the equal population, two-site exchange equation: $\Delta G^* = (1.912 \times 10^{-2})(T_c)[9.972 + \log(T_c/\delta v)]$ in kJ/mol where δv is the separation of the resonances in Hz at coalescence and T_c is in K (Sandstrom, J. *Dynamic NMR Spectroscopy*, Pergamon: London, 1982; pp 77-91). The error in ΔG^* of ± 0.5 kJ/mol was estimated assuming a liberal error of ± 2°C in estimation of T_c.

a single sharp peak for the eight alkoxide methyl groups are observed. (Figure 30). The possible process which explains the dynamic behavior of **33** is shown in Figure 29. First, one of the amino groups dissociates to form a five-coordinate trigonal bipyramidal intermediate. It can reassociate to form **33** or it can undergo inversion at nitrogen followed by coordination trans to O_4 to form **33a**, the mirror image of **33**. This process only requires that one amine dissociates and inverts and is therefore expected to have a low activation barrier. A similar dynamic process also occurs for **34** as indicated by broadening of the ligand backbone proton resonances at 80 °C, but in this case the coalescence temperature is beyond the boiling range of common NMR solvents. The presence of the bulky phenyl groups in **34** rather than methyl groups as in **33** can have two effects: (1) because the phenyl groups are bulkier than the methyl groups, complex **34** is more sterically congested which makes the amino groups more labile, and thus lowers the activation energy; (2) more energy is required to rearrange the bulky phenyl groups which results in a higher activation energy barrier. The much higher activation energy barrier for **34** shows that the second effect is more significant.

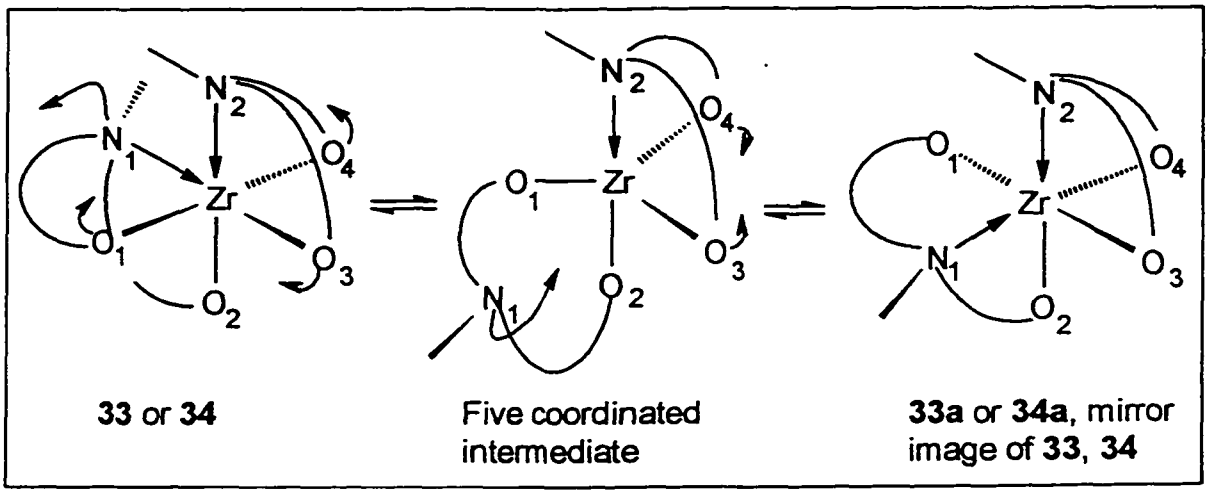

Figure 29 A possible mechanism for the dynamic process observed for **33** and **34**

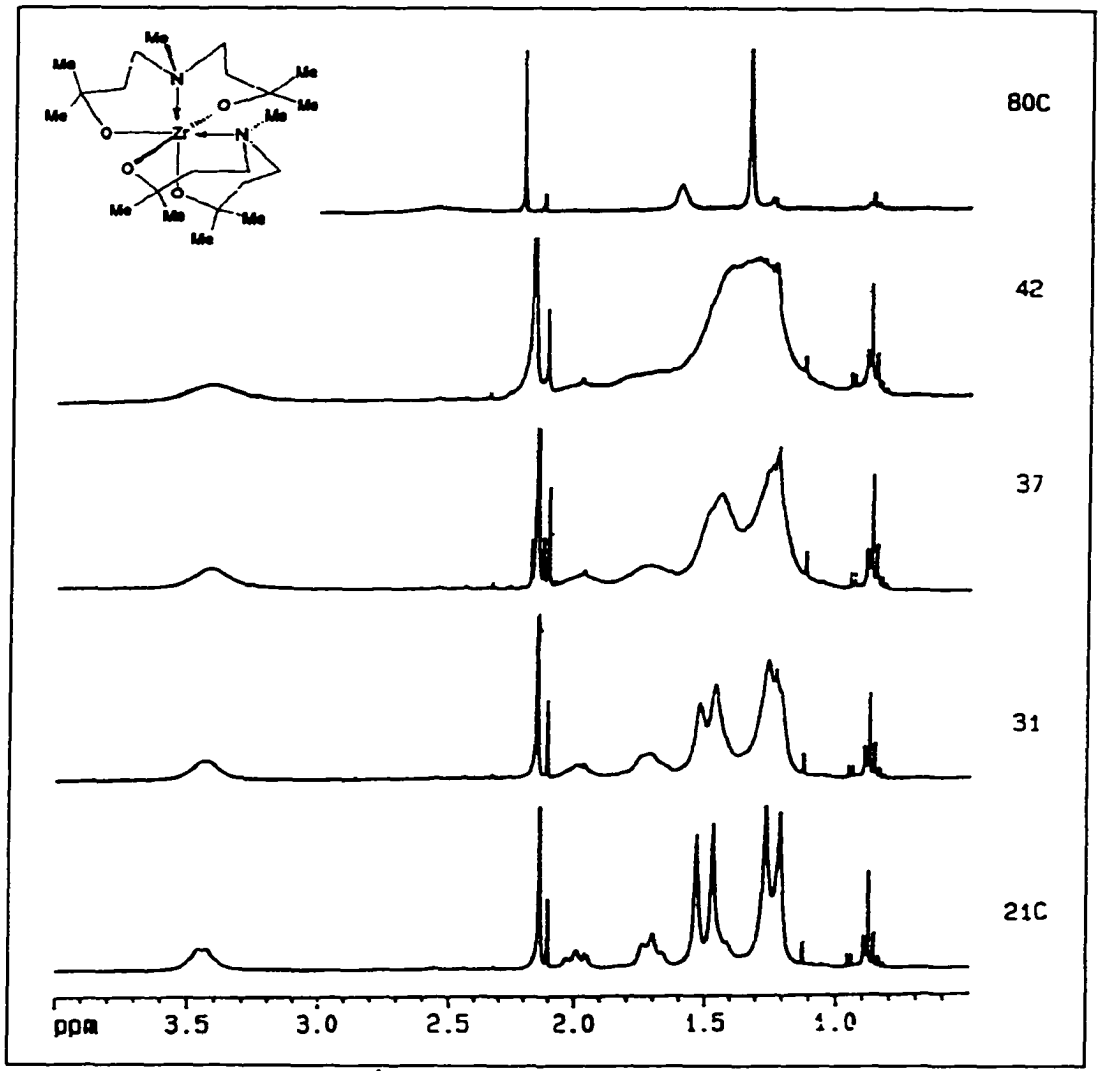

Figure 30 Variable temperature ^{1}H NMR spectra of **34**

The NMR spectra of **35-37** at room temperature are very simple and show only one set of resonances for the ligand backbone which are similar to the high temperature NMR spectra of **33** and **34**. At low temperature, the NMR resonances of **35** and **37** do show broadening, but even at -80 °C the resonances failed to resolve into two sets of resonances. Low temperature NMR experiments were not attempted for **36** due to its low solubility. Although no definitive NMR evidence can be obtained to deduce the solution structure for **35-37**, the spectral similarities between these complexes and **33** and **34** suggest that these complexes also adopt a *cis*-octahedral geometry. The low activation barrier is reasonable since the bulky α-methylbenzyl or *tert*-butyl groups on nitrogen weaken the Zr-N bond making the amino groups more labile.

3.4 Zirconium mono(ligand) dichloride and dialkyl complexes

3.4.1 Synthesis of $LZrCl_2$

When ligand **29** and $Cl_2Zr[N(SiMe_3)_2]_2$ [82] were dissolved in toluene in a 1:1 ratio at room temperature, the solution turned cloudy immediately. After heating at 70 °C for 30 minutes, a white precipitate of **40** formed. Complex **40** was isolated as a hydrocarbon insoluble white powder (eq. 29). The ^1H NMR spectrum recorded in d_8-THF shows only broad and weak peaks, while the ^{13}C NMR spectrum could not be obtained because of low solubility. Complex **40** is assumed to possess an oligomeric structure judging from its low solubility even in coordinating solvents. Although the exact nature of **40** was not fully established, this material proved to be a useful precursor for the synthesis of various dialkyl complexes.

$$n\ MeN[CH_2CH_2C(Ph)_2OH]_2 + n\ Cl_2Zr[N(SiMe_3)_2]_2 \rightarrow$$

$$\{Cl_2Zr[MeN(CH_2CH_2(Ph)_2O)_2]\}_n + 2\ n\ HN(SiMe_3)_2 \qquad (29)$$

Cloke reported closely related work on the synthesis of titanium and zirconium dichloride complexes utilizing the tridentate amino diamido ligand **XXVII** (eq. 30)[64, 119]. The dichloride complexes with diamido ligand **XXVII** are much more soluble in hydrocarbon solvent than **40**. A dimeric structure was confirmed by NMR and mass spectroscopy for the zirconium dichloride complex (eq. 30). It appears that the tridentate diamido ligand **VI** is bulkier than the amino diol ligands used in this project.

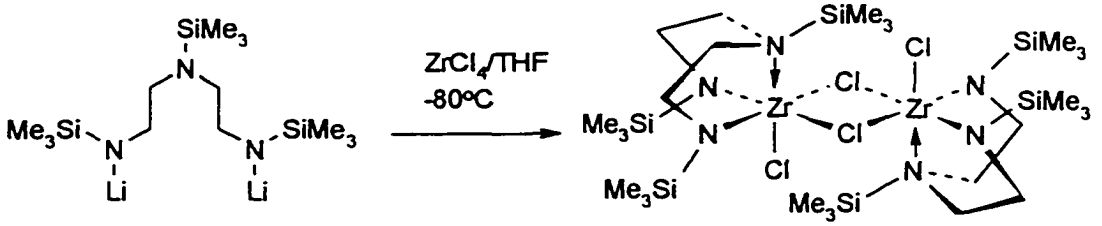

XXVII (30)

3.4.2 Synthesis of zirconium alkyl complexes

Three methods were applied to the synthesis of zirconium alkyl complexes as outlined in Scheme 10. Zirconium alkyl complexes **38** (Figure 33), **41c** and **42-44** can be conveniently synthesized by reacting tetrabenzyl zirconium with one equivalent of the corresponding ligands. No side reactions were observed for **38** and **42-44** and the yields obtained were quantitative. However, in the case of **41c**, the reaction conditions were found to be critical. Slow addition of the dilute ligand solution to tetrabenzyl zirconium solution at low temperature (-78°C) must be employed in order to eliminate the side

reaction leading to bis(ligand) complex **34**. Complex **39** may also be synthesized by this method, however the reaction product always contains a mixture of **33** and **39**, since the side reaction forming bis(ligand) complex **33** cannot be suppressed under these conditions. Complex **39** was therefore only identified by NMR, and efforts to isolate pure **39** by recrystallization were not successful due to the similarity in solubility of **33** and **39**.

The ligand redistribution reaction between appropriate bis(ligand) complexes and tetrabenzyl zirconium is another convenient way to prepare **42-44**. When **35** or **36** were mixed with tetrabenzyl zirconium in toluene, a rapid ligand redistribution reaction takes place to form the dibenzyl complexes **42** or **43**. Neither the starting material nor any intermediate was observed by NMR. Complex **37** also reacted with tetrabenzyl zirconium to form dibenzyl complex **44** but at a lower rate, and both the starting material and the intermediate were observable by NMR. Because the NMR signal of NC*H*(CH_3)Ph is very diagnostic, the signal of this proton was carefully monitored during the reaction. Ten minutes after the two starting materials were dissolved in C_6D_6, three resonances were observed between 4.3 to 3.9 ppm which can be attributed to NC*H*(CH_3)Ph protons from three different compounds. A broad resonance at 4.14 ppm was identified as the starting bis(ligand) complex **37**, while a sharp well resolved quartet at 3.96 ppm was assigned to the product dibenzyl complex **44**. A third well-resolved resonance at 4.28 appears to correspond to an intermediate, which is shown in Figure 31. The resonance due to the starting bis(ligand) complex decreased rapidly (vanished within one hour), while the dibenzyl complex signal grew steadily. The resonance due to the intermediate increased to a maximum after 30 minutes then slowly disappeared over a period of 3 hours (Figure 32).

Scheme 10

Method I. Hydrocarbon elimination

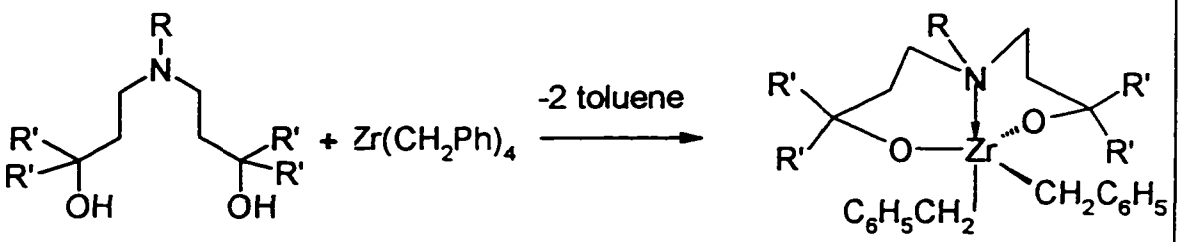

39a, R = Me, R' = Me
41c, R = Me, R' = Ph
42, R = *t*-Bu, R' = Me
43, R = *t*-Bu, R' = Ph
44, R = *S*-CH(CH_3)Ph R' = Me

Method II. Ligand redistribution

L_2Zr + $Zr(CH_2Ph)_4$ ⟶ $LZr(CH_2Ph)_2$

42, L = $(CH_3)_3CN[CH_2CH_2C(CH_3)_2O]_2$
43, L = $(CH_3)_3CN[CH_2CH_2C(Ph)_2O]_2$
44, L = *S*-$Ph(CH_3)CHN[CH_2CH_2C(CH_3)_2O]_2$

Method III. Metathesis

$[LZrCl_2]_n$ + 2 n MR ⟶ n $LZrR_2$ + 2 n MCl

L = $CH_3N[CH_2CH_2C(CH_3)_2O]_2$
39, MR = KCH_2Ph
L = $CH_3N[CH_2CH_2C(Ph)_2O]_2$
41a, MR = $LiCH_2SiMe_3$
41b, MR = LiMe
41c, MR = KCH_2Ph

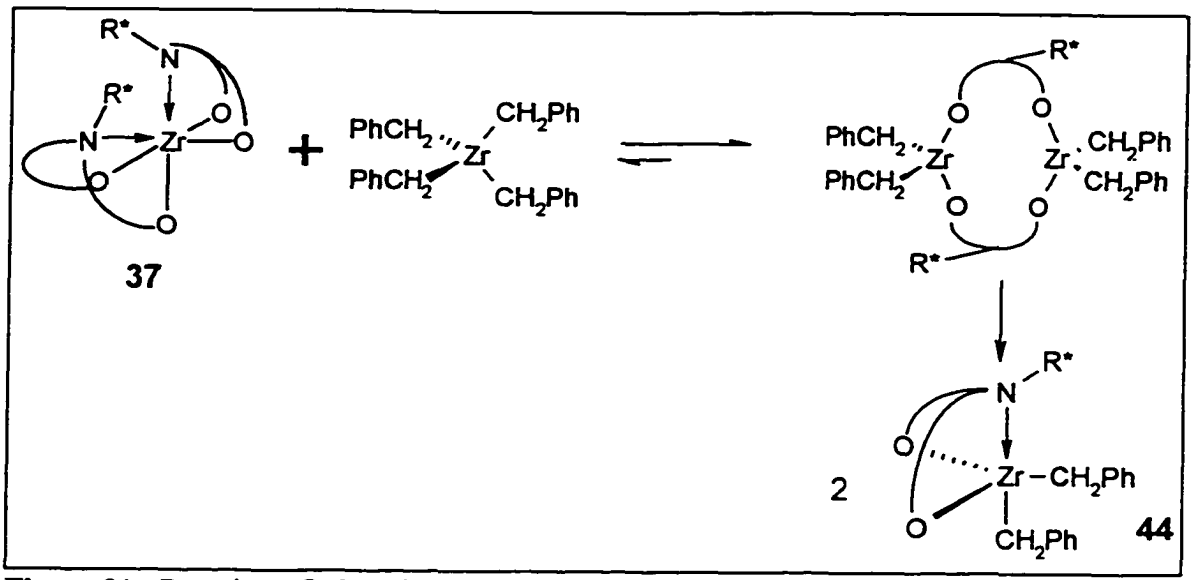

Figure 31 Reaction of **37** and tetrabenzyl zirconium

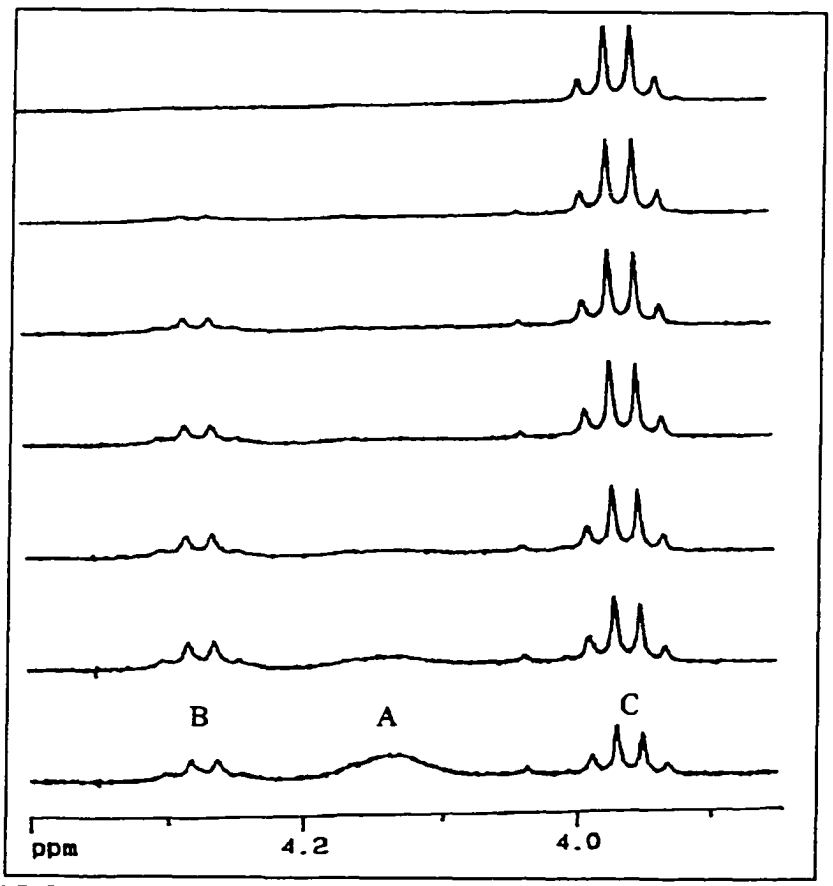

Figure 32 ^{1}H NMR spectra (Ph(CH$_3$)C*H*N region) of the reaction mixture for the reaction between **37** and tetrabenzyl zirconium: (A) **37**; (B) intermediate; (C) **44**.

In contrast to **35-37**, bisligand complexes **33** and **34** do not undergo ligand redistribution with tetrabenzyl zirconium even when heated at 70 °C in C_6D_6 solution. This difference can be attributed to the size difference of the amino substituents. Thus **33** and **34** have a methyl group on nitrogen which allows the strongest coordination to the metal. With the amino group firmly coordinated, the six coordinated octahedral structure provides no free coordination sites for bridging groups which are essential if ligand redistribution is to occur. In the case of complex **37**, the bulky $Ph(CH_3)CH$ group reduces the coordination strength of the amine and makes it dissociate easily to open a free coordination site which can accommodate an incoming group, so that ligand redistribution can occur. Following this trend, with the even bulkier *tert*-butyl group, the ligand redistribution occurs so rapidly that no intermediate can be observed. This trend also matches very well with the fluxional behavior of bis(ligand) complexes **33-37**. The amino donor substituents have such a significant effect on complex stability that they must be carefully considered in future ligand design.

The first two synthetic methods are not general because they can be used only when the starting tetraalkyl zirconium complexes are available (i.e., tetrabenzyl or tetraneopentyl zirconium). The third method is a general route which would allow us to synthesize a wide range of zirconium alkyl complexes by metathesis reactions between the monoligand zirconium dichloride and an appropriate alkali metal alkyl. The reaction was very clean when $LiCH_2SiMe_3$ or KCH_2Ph were used, but in the case of LiMe, low temperatures were necessary since the product (**41a**) proved to be unstable at room temperature. It is also interesting to note that although KCH_2Ph and **40** are both

considered insoluble in toluene, the reaction went smoothly and finished after the toluene suspension of **40** and KCH_2Ph was stirred overnight.

3.4.3 Solution structure of zirconium alkyl complexes

The solution structure of **38** was determined unambiguously by NMR spectroscopy. It is clear that **38** possesses C_3 instead of C_{3v} molecular symmetry at room temperature in C_6D_6 solution since the ligand backbone and $PhCH_2Zr$ geminal protons are inequivalent (resembling complex **22**). Group 4 metal complexes with tripod ligands that possess C_3 symmetry have also been observed by other authors; however in these cases, the ligands themselves are C_3 symmetrical.[50a] With C_{3v} symmetric tripodal ligands, the metal complexes usually also have C_{3v} symmetry[110]. One possible reason for **38** to adopt C_3 symmetry is that it is impossible to arrange the six phenyl groups symmetrically in a plane which would result in C_{3v} symmetry. To minimize steric interaction, one of the geminal phenyl groups on each alkoxide carbons must tip over to avoid the eclipsed conformation, and this distortion destroys the C_{3v} symmetry. (Figure 33.) When the

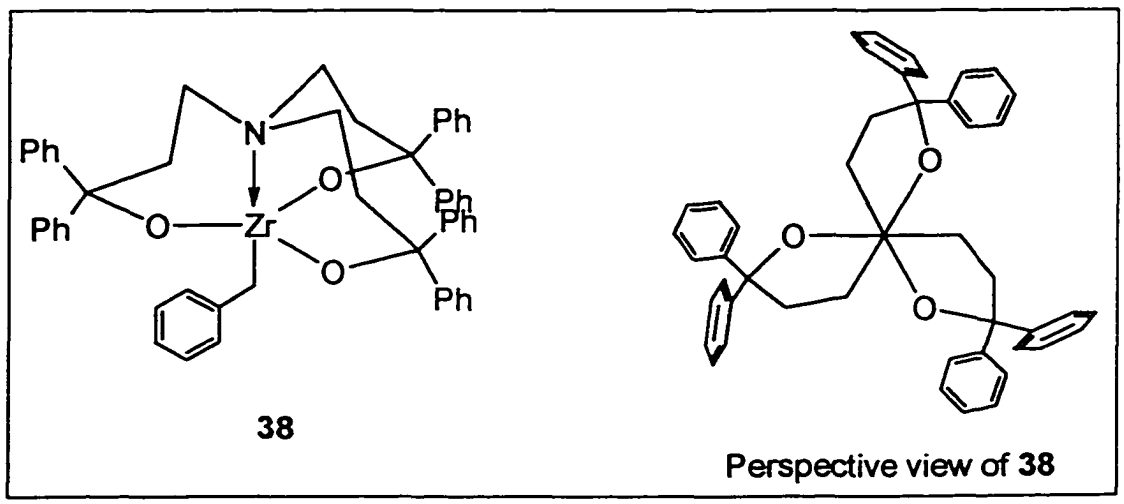

Figure 33 C_3 symmetry of complex **38**

temperature is increased, interconversion of the Λ and Δ enantiomers takes place which renders the molecule C_{3v} symmetric and the ligand backbone geminal protons, as well $PhCH_2Zr$ protons, become equivalent.

NMR spectra of **39**, **41a**, **41b**, and **41c** show that these molecules are conformationally rigid in C_6D_6 at room temperature. For each of these compounds, resonances due to two inequivalent sets of benzyl groups and one set of alkoxide arms are observed, however the geminal protons of the alkoxide arm are inequivalent indicating that the two alkoxide arms are related by mirror plane symmetry. This observation is consistent with C_s molecular symmetry. Although there are three possible conformations with C_s symmetry (**XXVIII**, **XXIX**, **XXX**), the *pseudo-fac* trigonal bipyramid (**XXVIII**, Figure 34), which is the same as the solid state structure as shown by the preliminary X-ray crystallographic studies, is the most likely one.

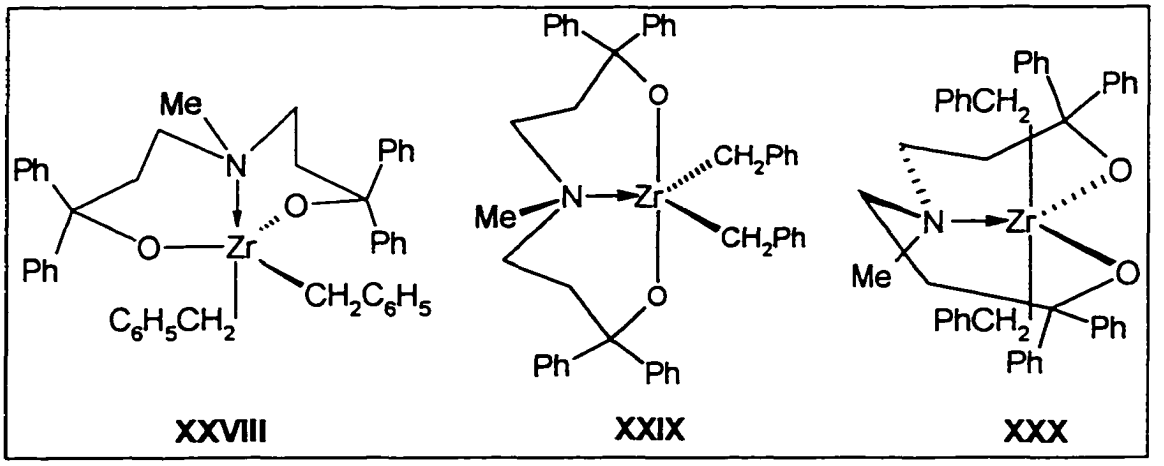

XXVIII **XXIX** **XXX**

Figure 34 Three possible C_s structures for **41c**

In contrast, **42-44** are fluxional at room temperature and exhibit only one type of benzyl group and a single set of signals for both alkoxide arms. This observation cannot be attributed to simple pseudorotation since this would not render the exo and endo CH_2 or

$C(O)R_2$ (R = Me or Ph) groups equivalent. Based on the reasoning discussed in section **3.3.2**, **42-44** may have similar structures to **41c**, however, the bulky substituents on the amino group prevent strong coordination to zirconium, and a process involving amino group dissociation, inversion at nitrogen, and recoordination can take place more easily than **41c**. A low temperature NMR experiment was carried out to freeze this dynamic process. Indeed, when the NMR sample of **42** was cooled to -60 °C, the CH_2 and $C(O)R_2$ resonances split into two sets of resonances consistent with C_s symmetry. However, in this case, the two benzyl groups remained equivalent to -80 °C suggesting that pseudorotation remains rapid even at low temperatures. The variable temperature NMR experiments have not been done on **43** and **44** due to the low solubility of **43** and thermal instability of **44**.

A similar dynamic process was observed by Cloke[64a, 119] and Horton[64b] on the titanium dimethyl complex, and zirconium dimethyl and dibenzyl complexes respectively with the tridentate diamido ligand **XXVII**. In the case of the zirconium dibenzyl complex of **XXVII**, the coalescence temperature of the two benzyl methylene proton resonances was 20 °C, which is much lower than that of **41c** (the resonances remain sharp at 70 °C) and higher than those of **42-44**.

3.5 Decomposition of zirconium dibenzyl complexes

3.5.1 Kinetic studies of the decomposition reactions of 42 and 43

The thermal decomposition reaction of dibenzyl complexes **41c** and **42-44** were studied by NMR and found to show a marked dependence on the substituents at nitrogen. The methyl-substituted complex **41c** shows the highest thermal stability and remains unchanged after heating at 80 °C overnight. However, after heating for one week at 100

°C in d_8-toluene, it decomposes completely. The decomposition reaction presumably involves metallation of the ligand backbone, however, the decomposition products were not clean and could not be identified.

In contrast, the *tert*-butyl derivatives **42** and **43** decompose by elimination of isobutene and toluene. The decomposition reaction was carefully monitored by NMR and was found to be first order in the starting dibenzyl complex. The thermodynamic parameters obtained for **43** showed $\Delta H^{\ddagger}$ and $\Delta S^{\ddagger}$ of 107 ± 8 kJ mol^{-1} and - 44 ± 5 J mol^{-1} K^{-1}, respectively (Figure 35). In the case of **42**, the decomposition reaction was too slow to allow accurate kinetic studies over a range of temperatures; however, it was estimated

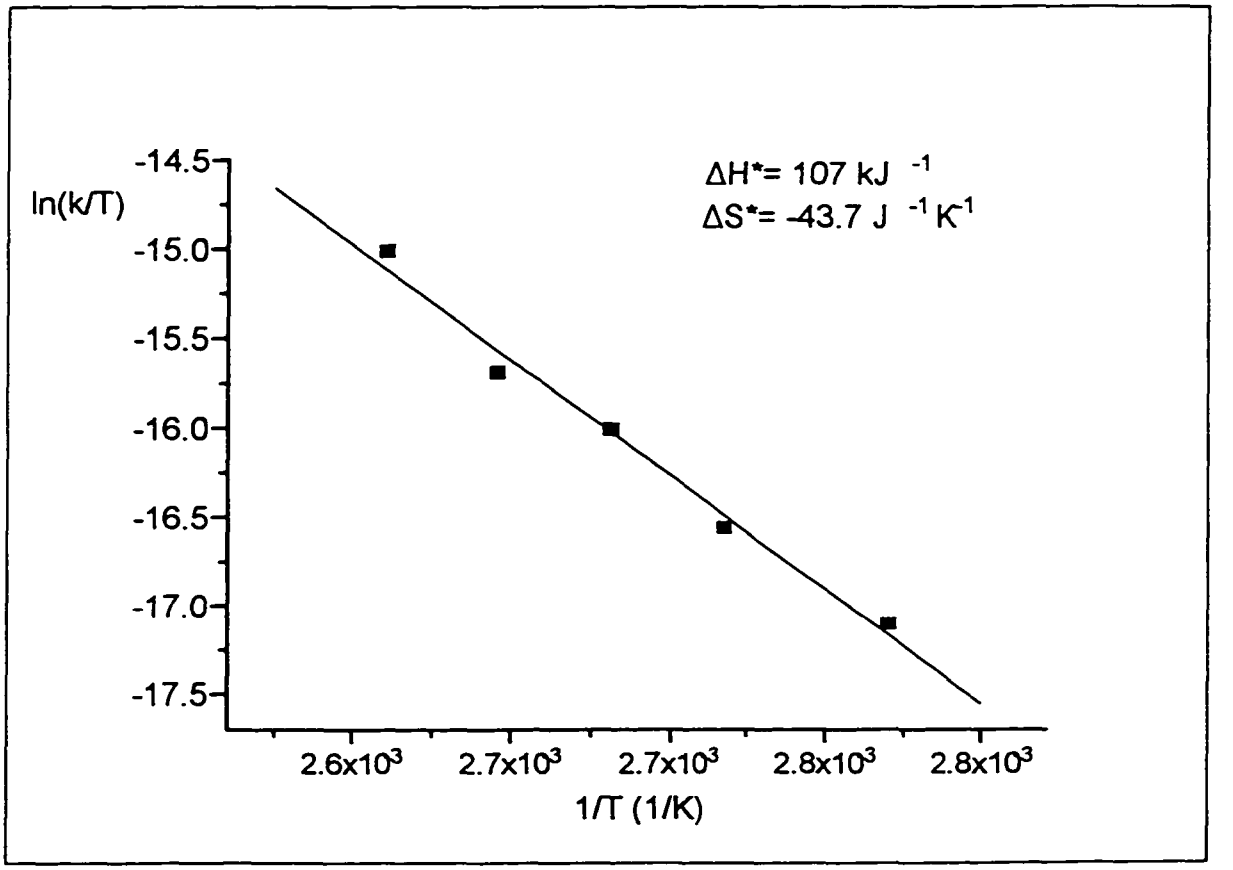

Figure 35 Eyring plot of decomposition of complex **43**

that **42** decomposes about 5 times slower than **43** under the same reaction conditions based on preliminary kinetic data.

Elimination of *iso*-butene from the *tert*-butyl group of a *t*-butylamine has been reported in the literature with both ionic and radical mechanisms being proposed[120]. In the present case, a concerted process such as that outlined in Scheme 11 seems most likely because this reaction displays a large negative activation entropy (see discussion in Section **3.5.3**). The more sterically crowded complex **43** reacts more rapidly than **42** suggesting that steric pressure plays a role in favoring this decomposition route. The ^{1}H NMR spectrum of the final decomposition products is very complex, and the expected

Scheme 11

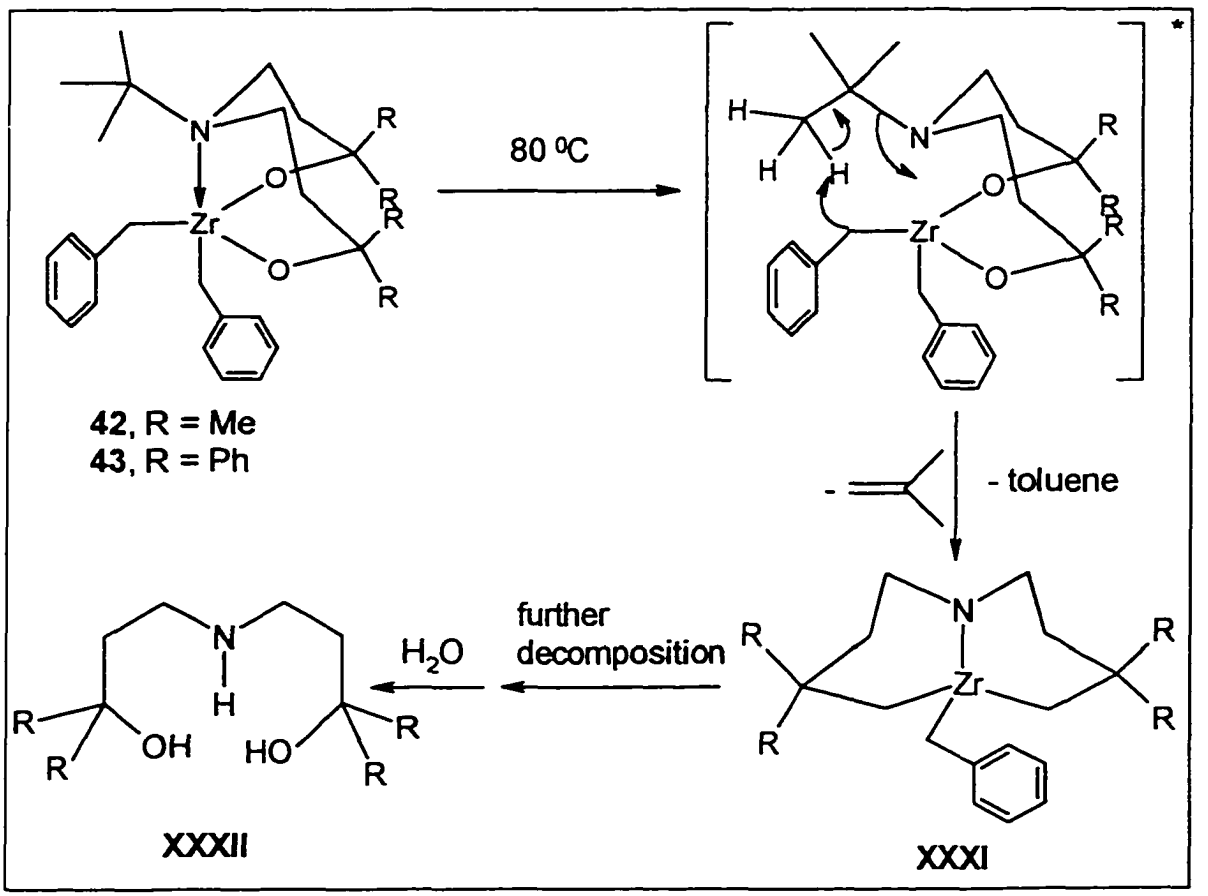

decomposition product **XXXI** could not be identified. However after aqueous work up, amino diol **XXXII** was identified as the main component and was characterized by ^{1}H NMR and mass spectroscopy.

3.5.2 Synthesis and structural characterization of 45

3.5.2.1 Solution structure of 45

Chiral complex **44** decomposes cleanly during mild heating (70 °C, 4 hours) in toluene to afford **45** in 75 % isolated yield. Based on NMR (^{1}H, ^{13}C, ^{1}H-COSY, ^{1}H-^{13}C COSY and NOESY) information, it was not possible to choose between structures **XXXII** or **XXXIII** (Figure 36), since both structures matched well with the NMR data. The structure was shown to be **XXXII** by subsequent X-ray crystallographic studies (*vide infra*). All the ligand backbone protons and ZrOC*Me*$_2$ methyl groups are inequivalent due to the chiral nature of **45**. The downfield shift to 4.6 ppm of the Ph(CH_3)C*H*N proton appears to be characteristic of complexes with the *Ph*(CH_3)CHN phenyl group involved in a macrocyclic structure, while chemical shifts to fields higher than 4.2 ppm are characteristic of simple *Ph*(CH_3)CHN groups (Figure 37 and 38). The ^{13}C NMR spectrum also shows a characteristic downfield resonance at 183 ppm for the metallated aromatic carbon.

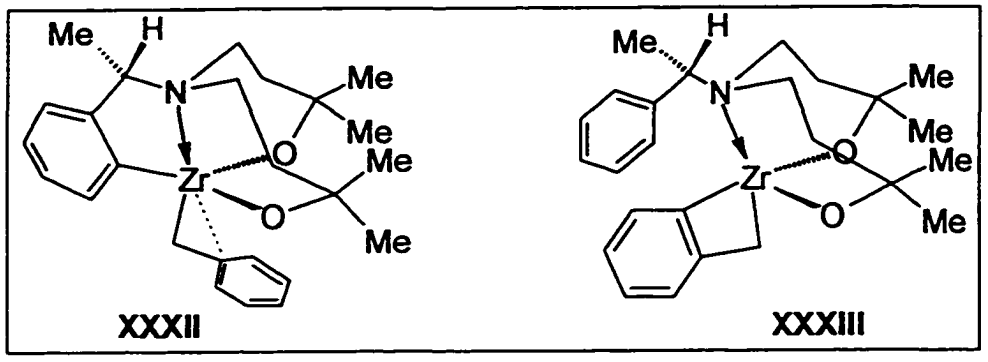

Figure 36 The two possible structures for complex **45**

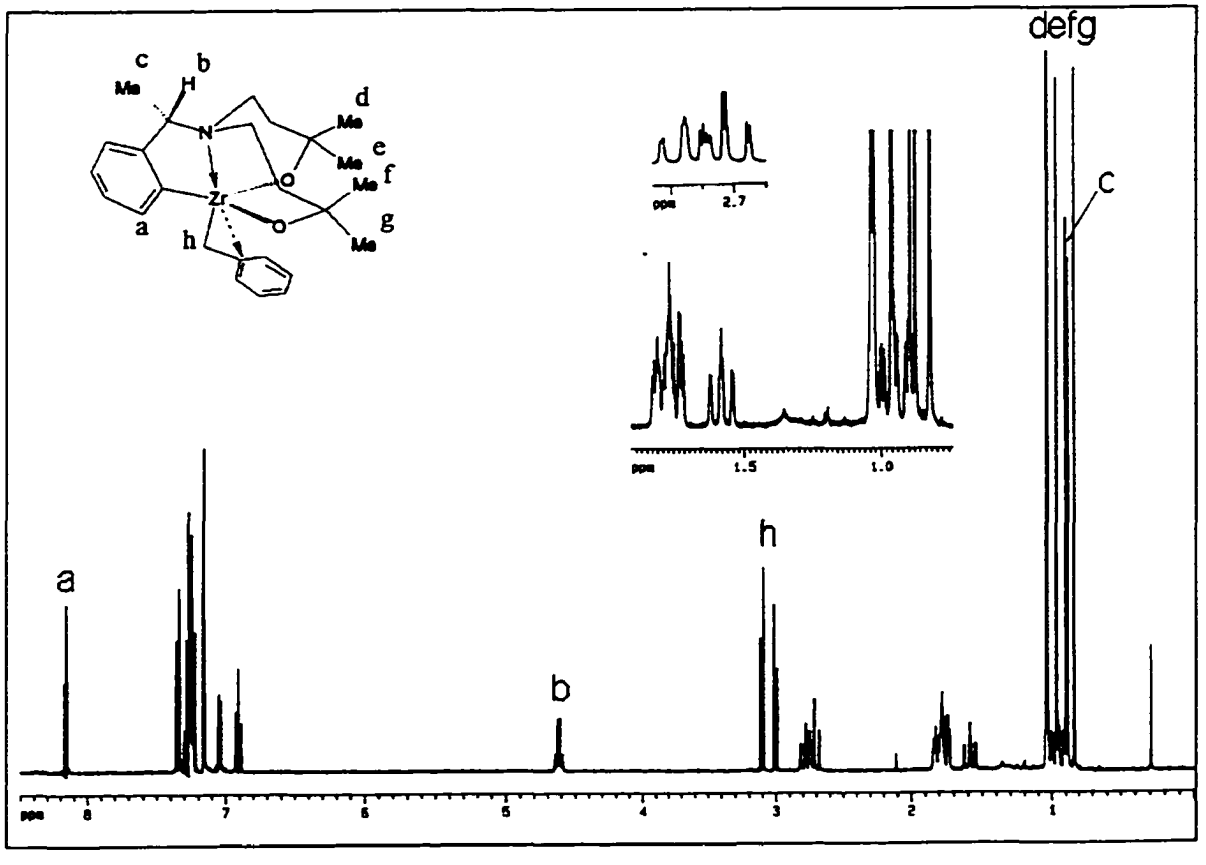

Figure 37 ^{1}H NMR spectrum of **45** in C_6D_6 (360 MHz)

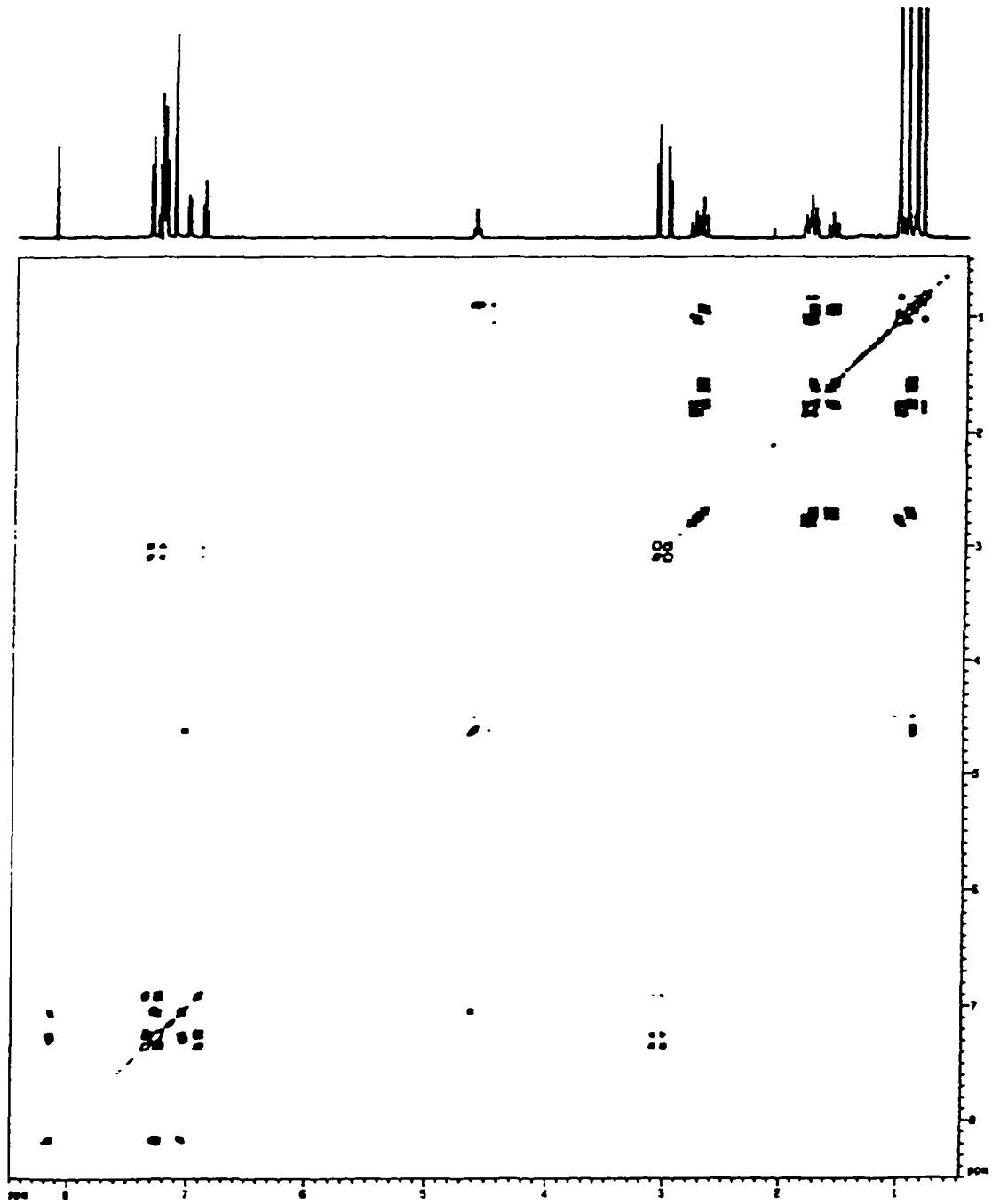

Figure 38 ^{1}H COSY of **45** in C_6D_6

3.5.2.2 X-ray crystallographic structure of 45

The structure of **45** is shown in Figure 39. Fractional atomic coordinates are given in Appendix Table XVII, and selected bond lengths and angles are collected in Table 12. The X-ray crystal structure reveals that **45** possesses a pseudo-trigonal bipyramidal geometry at the central zirconium atom with the coordinated amino donor and the benzyl group occupying the axial positions (N-Zr-C angle 159.1(6)°) and the two alkoxide groups and the *ortho*-metallated phenyl group occupying the equatorial sites (average of the three bond angles is 116°).

The benzyl group is clearly η^2-bound to the zirconium center as indicated by an acute bond angle for Zr(1)-C(8)-C(81) of 93.4(11)°. η^2-Bonding is very common for electron deficient early transition metal benzyl complexes. Rothwell has shown that one of the three benzyl groups in $Zr(OAr)(CH_2Ph)_3$ (OAr = 2,6-di-*tert*-butyl phenoxide) is η^2-bound to zirconium. The Zr-C-Ph angle is 84° for this benzyl group compared to 98° and 115° for the remaining two benzyl groups[23a]. The π-interaction appears to be stronger in $Zr(OAr)(CH_2Ph)_3$ than in **45** since the benzyl group is bent more towards zirconium, and the distance between zirconium and the *ipso*-carbon is shorter in the former (2.64 Å versus 2.82 Å).

The difference between the two Zr-O bond distances is very small (1.938(10) Å versus 1.927(9) Å) and they are similar to that found in $Zr(OAr)(CH_2Ph)_3$ (1.94 Å) and those of the terminal Zr-alkoxides (average Zr-O^{i}Pr: 1.94 Å), but significantly longer than the bridging Zr-alkoxides (average Zr-O^{i}Pr: 2.17 Å), in $\{[(^iPrO)_3(^iPrOH)]Zr(\mu\text{-}O^iPr)\}_2$. The average Zr-O-C angle in **45** is 142° which is smaller than that in $Zr(OAr)(CH_2Ph)_3$

(165.7(9)°), or for the terminal alkoxides of $\{[(^{i}PrO)_3(^{i}PrOH)]Zr(\mu\text{-}O^{i}Pr)\}_2$ (average bond angle of Zr-O-C: 172°)[121]. The Zr-N distance is 2.42 Å which is much shorter than those found in zirconium complexes bearing tridentate amino-diamido ligands[64a,119]. The short distance may be enforced by formation of the five-membered ring involving the *ortho*-metallated phenyl group which forces the amino nitrogen close to the zirconium. Short Ti-N distances were also observed in the titanium complexes bearing amino-triol ligands (the titanatranes)[50a].

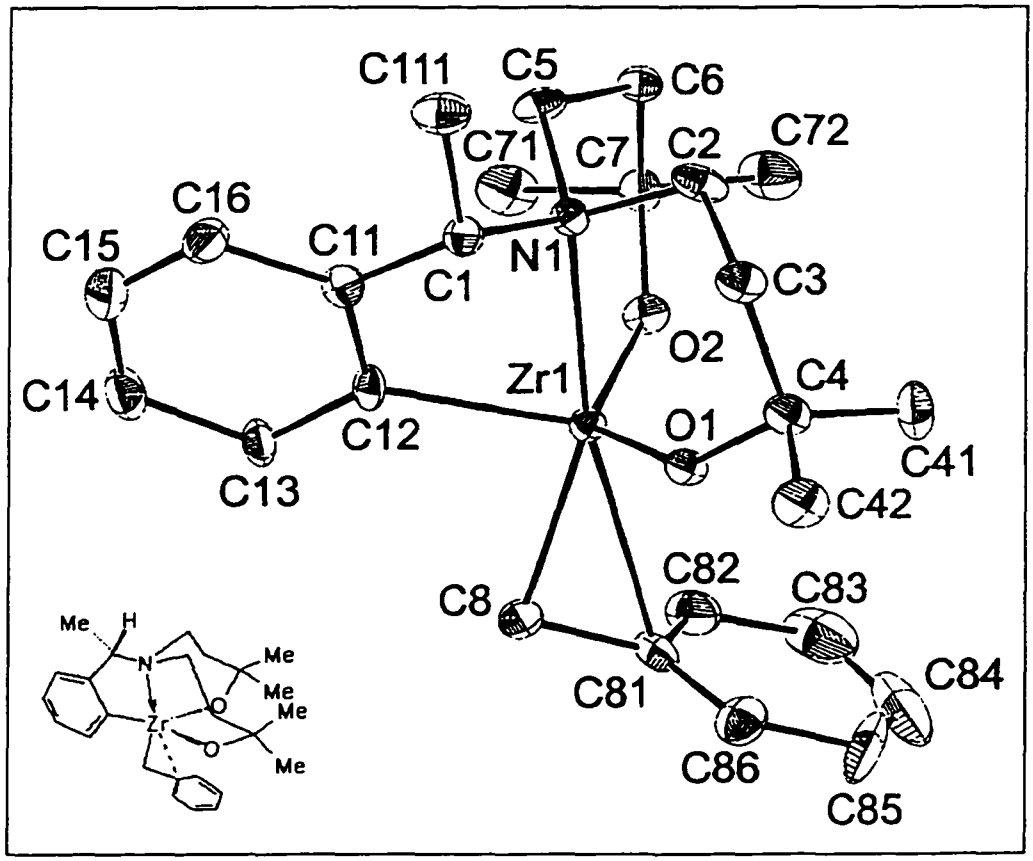

Figure 39 ORTEP diagram of **45**

Table 12 Selected bond distances and angles for **45**

		Distances	
N(1) -Zr(1)	2.419(12)	C(8) -Zr(1)	2.313(16)
O(1) -Zr(1)	1.938(9)	C(12) -Zr(1)	2.275(14)
O(2) -Zr(1)	1.927(10)	C(81) -Zr(1)	2.817(19)
		Angles	
O(1) -Zr(1) -N(1)	81.0(5)	C(12) -Zr(1) -O(1)	112.8(5)
O(2) -Zr(1) -N(1)	82.8(5)	C(12) -Zr(1) -O(2)	110.7(5)
O(2) -Zr(1) -O(1)	125.4(4)	C(12) -Zr(1) -C(8)	87.4(6)
C(8) -Zr(1) -N(1)	159.1(6)	C(4) -O(1) -Zr(1)	140.4(10)
C(8) -Zr(1) -O(1)	107.5(8)	C(7) -O(2) -Zr(1)	145.2(10)
C(8) -Zr(1) -O(2)	105.9(8)	C(81) -C(8) -Zr(1)	93.4(11)
C(12) -Zr(1) -N(1)	71.7(5)		

Estimated standard deviation in parentheses.

3.5.3 Mechanistic studies on the decomposition reaction of 44

The decomposition of **44** was studied by ^{1}H NMR and was found to follow first order kinetics consistent with an intramolecular process and an Eyring plot (Figure 40) yielded values for $\Delta H^{\ddagger}$ and $\Delta S^{\ddagger}$ of 99 ± 2 kJ mol^{-1} and 20 ± 1 J mol^{-1} K^{-1}, respectively. The two most likely pathways for this intramolecular metallation are by direct sigma-bond metathesis (A) or via a benzylidene intermediate (B). (Figure 41). Generally, the first pathway will show a larger negative entropy of activation (ΔS^* ~ -80 J mol^{-1} K^{-1}) because the intermediate involves a highly-ordered four center intermediate[122]. On the other hand, the second pathway often shows a low entropy of activation (ΔS^* ~ 0 J mol^{-1} K^{-1})[123] because the rate determining step is formation of a benzylidene intermediate, and the subsequent step, abstraction of a proton by the benzylidene, is generally very fast due to the highly reactive zirconium-carbon double bond. However, there are some cases which

conflict with this general observation. Earlier studies by Fryzuk showed that the thermal decomposition of $Y[N(SiMe_2CH_2PMe_2)_2]_2(CH_2C_6H_5)$ occurs exclusively at the CH_2 site adjacent to P with elimination of toluene by sigma-bond metathesis. This process also has an unusually low entropy of activation ($\Delta S^{\ddagger}$ = -12 ± 10 J mol^{-1} K^{-1})[124]. The authors postulated that phosphine dissociation occurs in the transition state to provide a positive contribution to $\Delta S^{\ddagger}$, so that the overall $\Delta S^{\ddagger}$ is close to zero. By analogy, in the present case, the intermediate value of activation entropy seems to imply a sigma-bond metathesis pathway because a positive contribution to the activation entropy from amine dissociation could likewise occur in the transition state. However, the alkylidene pathway could not be ruled out convincingly based on these kinetic arguments, so in order to establish the decomposition mechanism unequivocally, isotope labeling studies were deemed necessary.

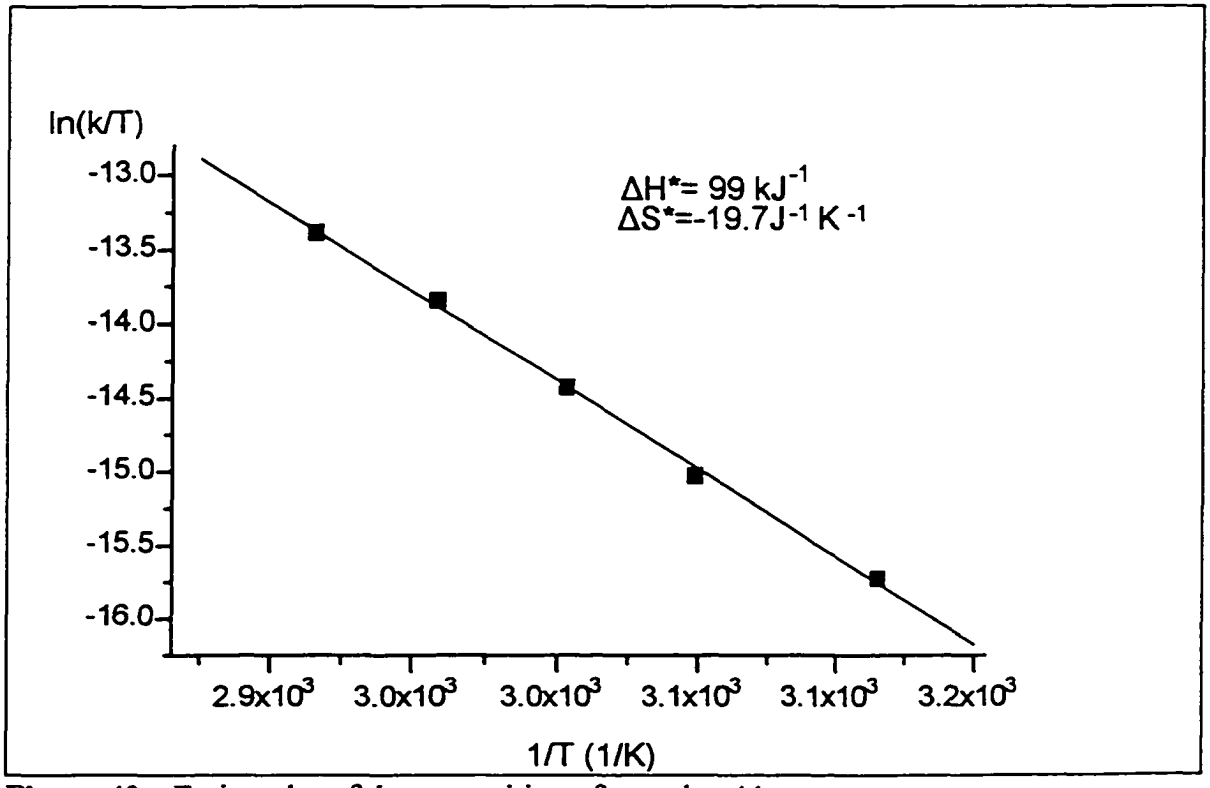

Figure 40 Eyring plot of decomposition of complex **44**

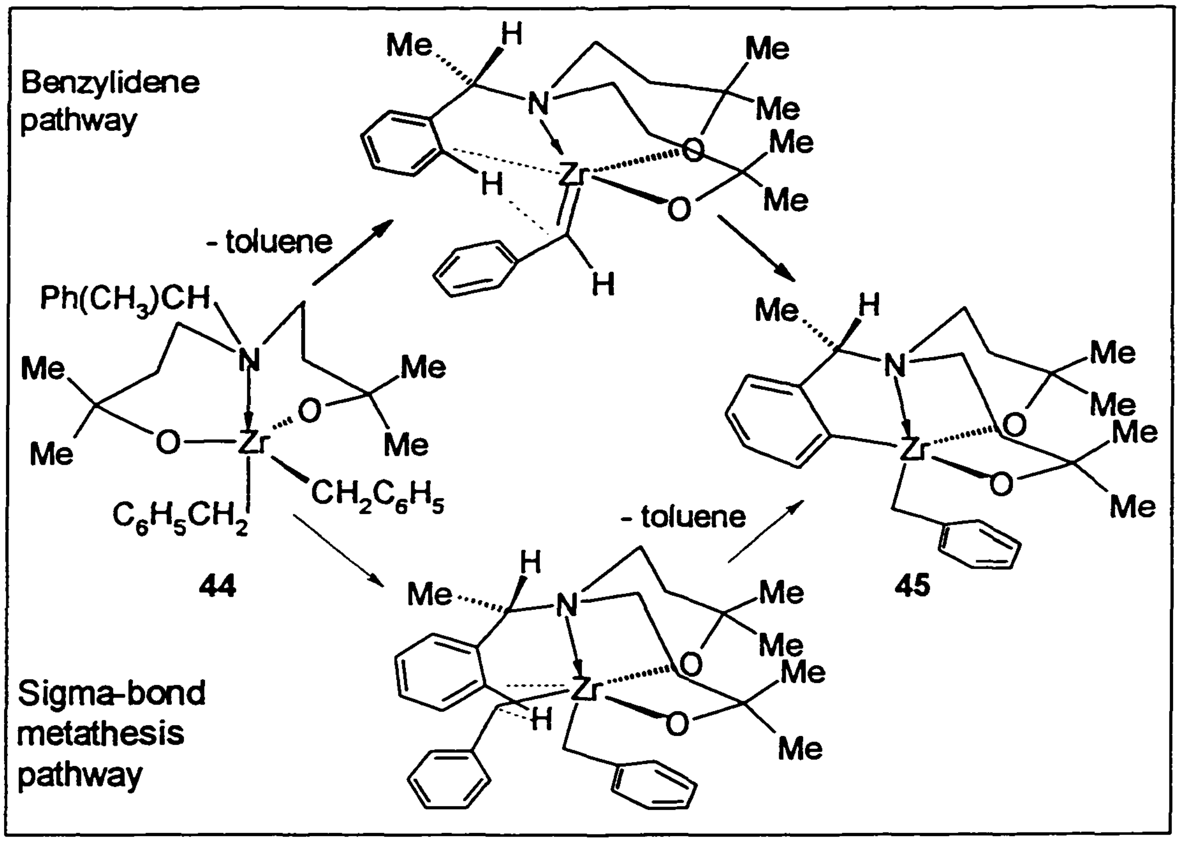

Figure 41 The two possible mechanisms for the decomposition of 44

Figure 42 shows two approaches to the labeling experiment: prepare deuterated complex **44** with deuterium on the two benzyl groups, **44a**, <u>or</u> on the *ortho* positions of the ligand phenyl ring, **44b**. Complex **44a** was synthesized by reaction of **32** and deuterated tetrabenzyl zirconium, and **44b** was prepared by repeated quenching of **44** with D_2O (due to isotopic effects, repeating this procedure three times gave > 90 % deuterium in the *ortho* position). Either method was expected to give the product with hydrogen and deuterium scrambled in the benzyl CH_2 position if the decomposition pathway involved a benzylidene intermediate. On the other hand, sigma-bond metathesis should show no hydrogen-deuterium scrambling. Both experiments clearly supported the sigma-bond

metathesis pathway since there was no hydrogen-deuterium scrambling observed in either case.

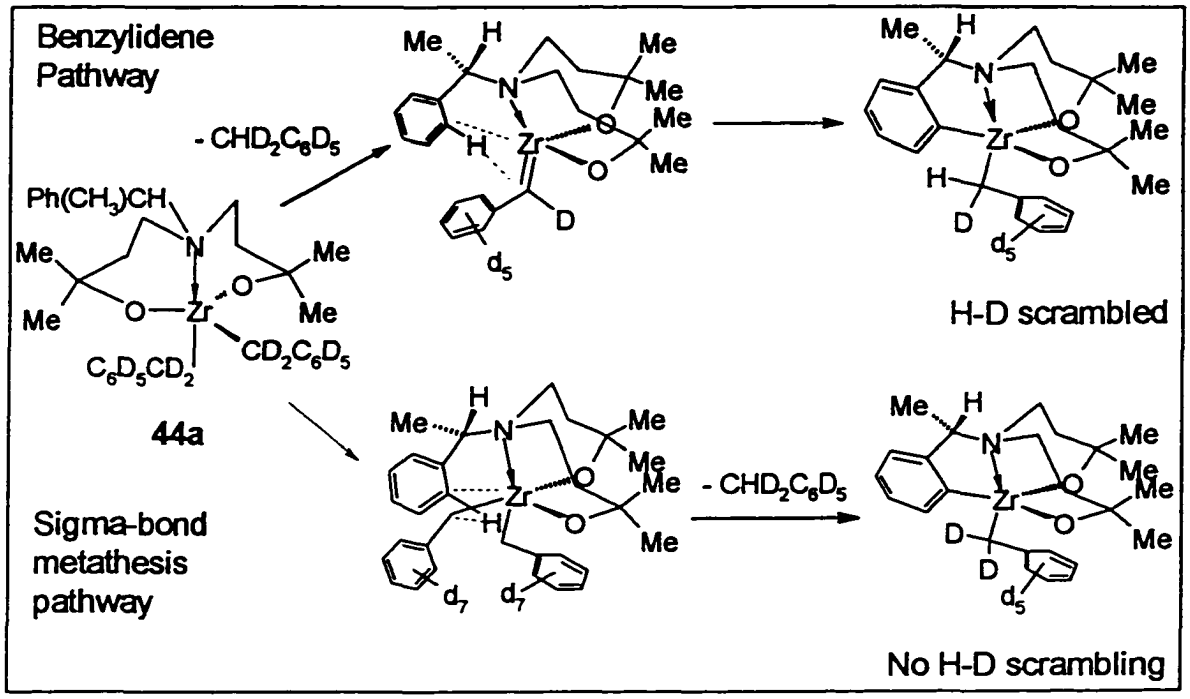

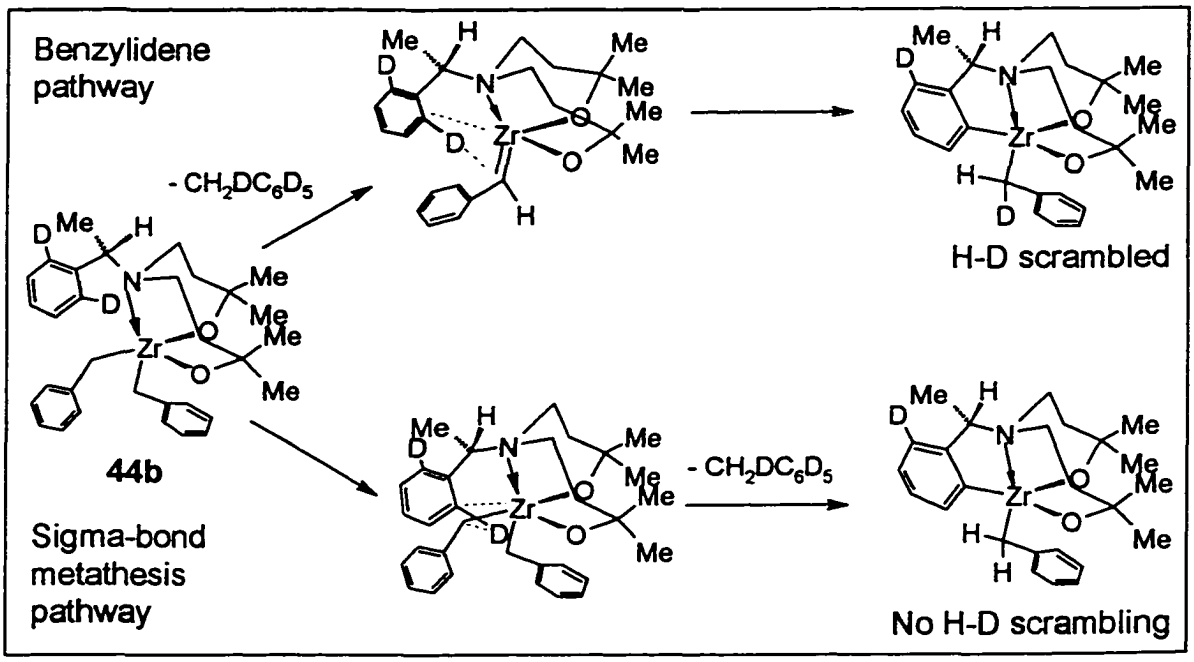

Figure 42 Deuterium labeling studies of the decomposition mechanism of **44**

CHAPTER 4

REACTIVITY STUDIES OF ZIRCONIUM ALKYL COMPLEXES BEARING AMINODIOLATE LIGANDS

Group 4 organometallic complexes have exhibited extremely versatile reaction chemistry and have been extensively used in organic and polymer synthesis[100, 116a]. The most important of these reactions include: hydrozirconation[125], bicyclization of enynes (dienes and diynes)[126], Sharpless epoxidation[51,116a], zirconium-stabilized benzyne reactions[127], catalytic hydrogenation[128] of alkenes, imines and esters and Ziegler-Natta olefin polymerization[61]. In this chapter, synthesis of zirconium imido complexes, insertion reactions of carbonyl groups, alkyne cyclotrimerization and synthesis of zirconium cationic complexes and their application in olefin polymerization are presented.

4.1 Zirconium imido chemistry

4.1.1 Introduction

Imido complexes are species containing metal-nitrogen double bonds of general formula $L_nM{=}NR$[129]. Since the first organoimido transition metal complex, t-butylimidotrioxo osmium(VIII)[130], was prepared in 1956, a large number of such complexes have been synthesized, especially for the group 5-8 metals. Despite the presence of an unsaturated metal-nitrogen double bond, these imido complexes are generally not very reactive and are easily handled. Transition metal imido complexes have many applications in organic synthesis, and particularly, Schrock has used group 6 imido complexes as efficient olefin metathesis and ROMP (Ring Opening Metathesis Polymerization) catalysts[131]. Compared to other transition metals, group 4 imido complexes are much more reactive and less common, and before 1988, there were no structurally characterized terminal group 4 imido complexes known[132]. Imido zirconocene complexes exhibit rich reaction chemistry which includes the activation of benzene and [2

+ 2] cycloadditions with unsaturated substrates such as alkenes, alkynes and imines (Scheme 12)[132]. Bergman has successfully constructed a catalytic cycle for preparation of enamines by addition of primary amines across alkynes (hydroamination). However, these catalysts failed to catalyze hydroamination of alkenes[132]. Other ancillary ligand systems such as macrocycles[133] and bulky amido ligands[134] have also been employed to explore zirconium imide chemistry. As part of this project, we have investigated zirconium imide chemistry supported by amino diol ligation in order to compare this chemistry with that of the Cp ligand system.

Scheme 12

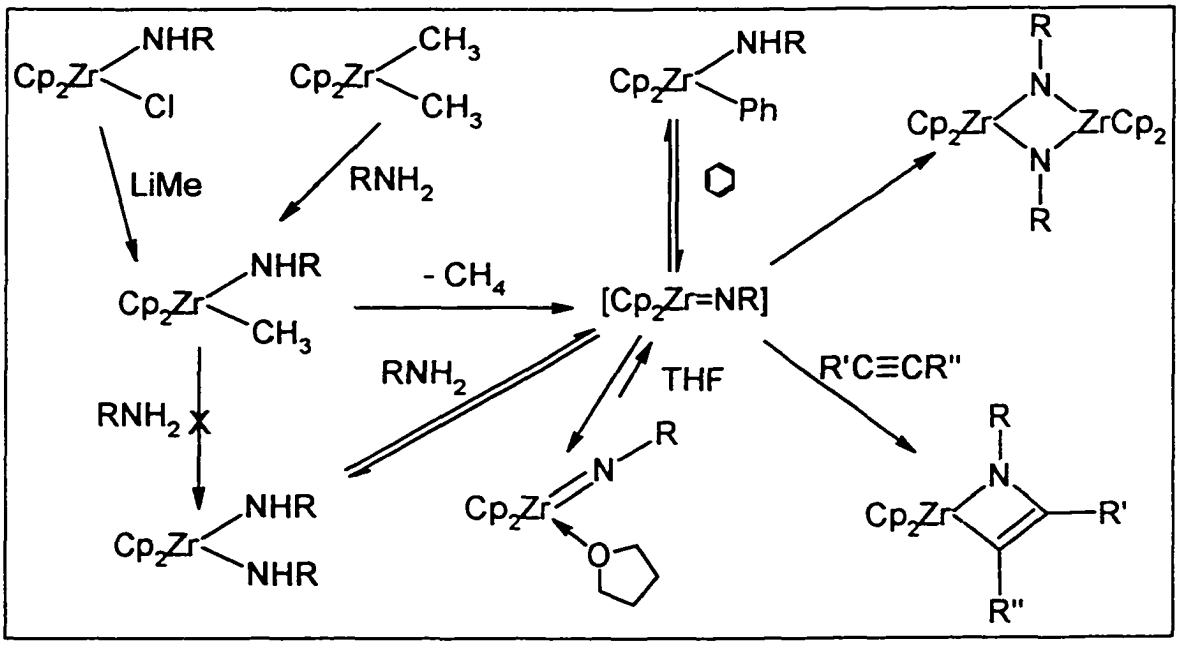

4.1.2 Reaction of metallacycle 45 and amines

The reactions between **45** and *tert*-butyl amine or 2,6-dimethyl aniline are outlined in Scheme 13 and 14. Addition of one equivalent of *tert*-butyl amine or 2,6-dimethyl aniline to **45** at room temperature results in clean formation of **46** or **47**, respectively. Both complexes were isolated as light yellow solids and were characterized by NMR spectroscopy. The NMR spectra show that **46** and **47** have similar structures to **45** with one benzyl group substituted by *tert*-butyl amide or 2,6-dimethyl aniline amide, respectively. The deprotonation reaction takes place exclusively at the benzylic position and leaves the phenyl-zirconium bond untouched.

Scheme 13

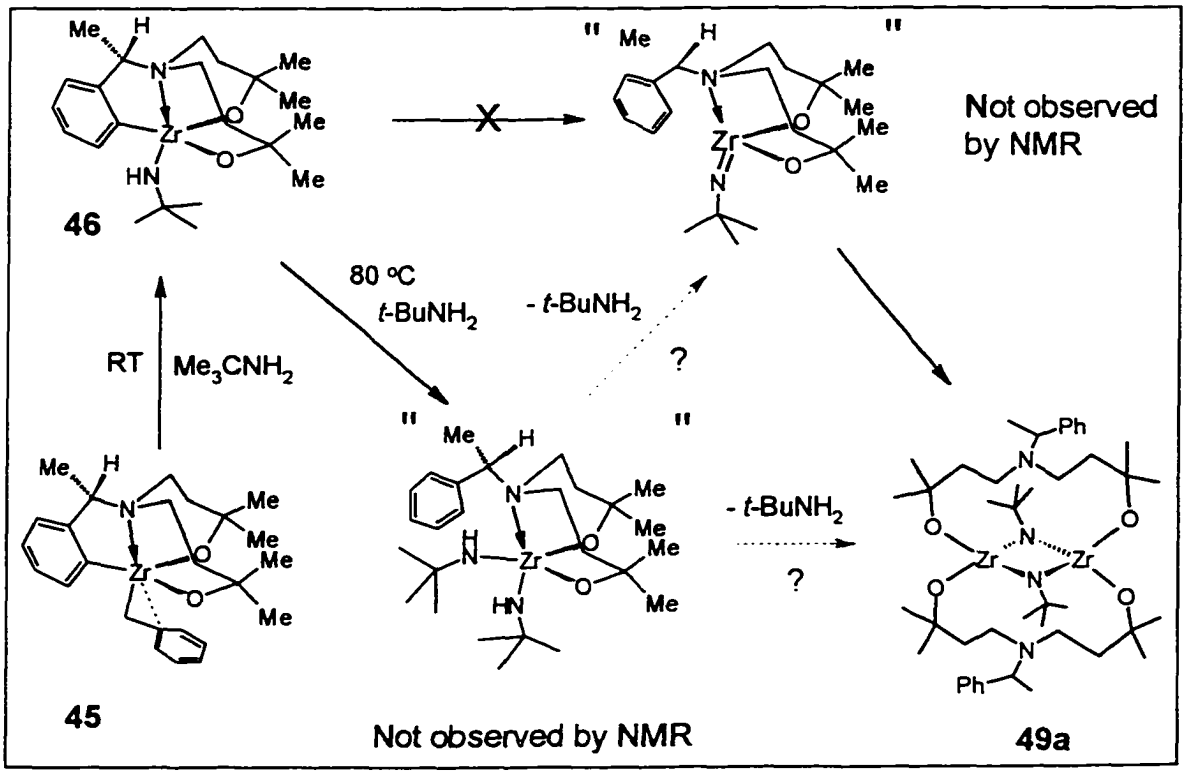

Scheme 14

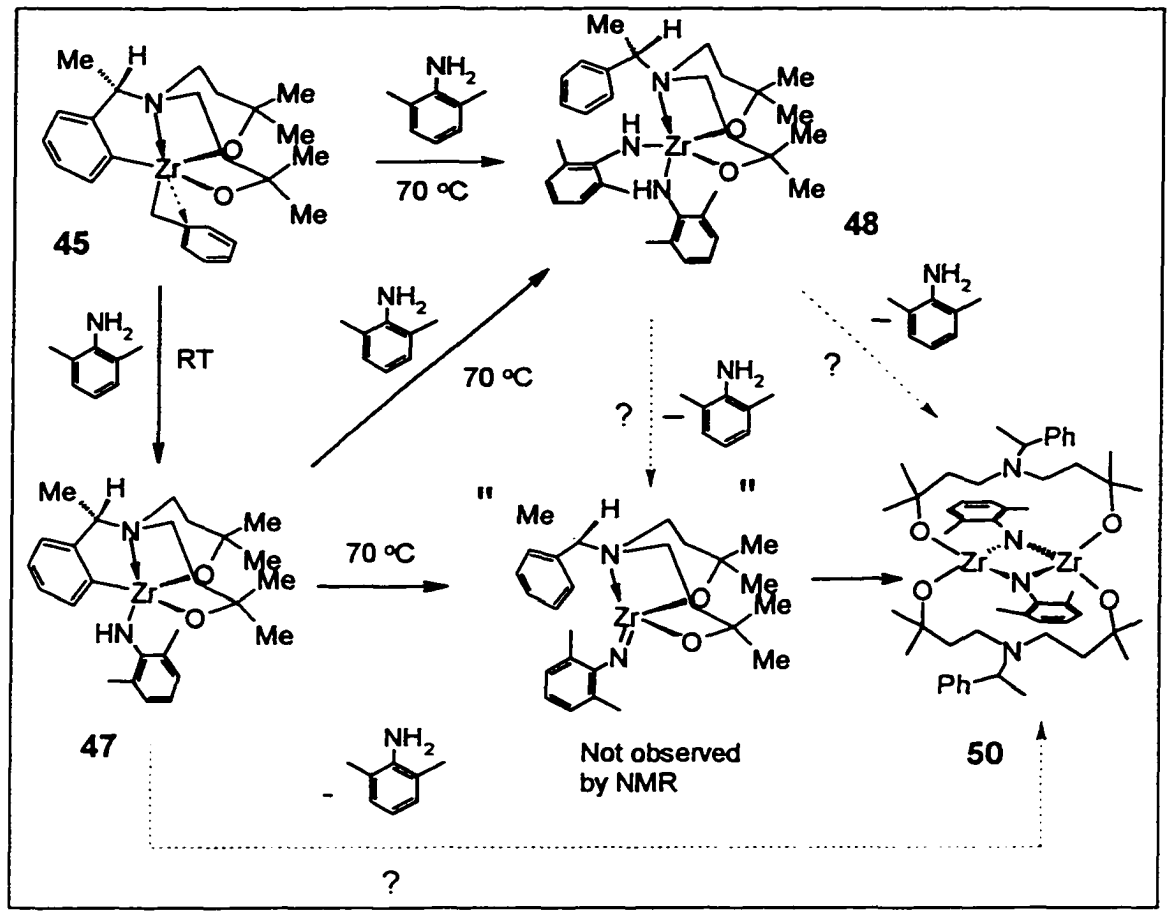

Complex **46** is very stable: when a NMR sample of **46** was heated at 80 °C for two days, there was no noticeable change. However, in the presence of trace *tert*-butyl amine impurity, **46** decomposed to form the zirconium bridging imide dimer **49a** in 60 % yield under the same reaction conditions. Bergman was able to trap terminal zirconium imido complexes by stabilization with coordinating THF or by addition of unsaturated substrates such as alkynes or imines to generate zirconocyclobutene complexes (Scheme 12)[132]. His group also characterized the THF adduct by X-ray crystallography. Wolczanski has also isolated terminal zirconium imido complexes, and these complexes did not undergo dimerization due to the extremely bulky *t*-Bu_3SiNH^- ligand[134]. We were unable to trap the

zirconium imide, and efforts to break bridging dimer **49a** by addition of Lewis bases such as THF and PMe_3 were not successful, although NMR shows that PMe_3 coordinates to **49a** to form an adduct of the intact dimer, **49b**. Due to the difficulty in determining the concentration of *tert*-butyl amine and **46**, accurate kinetic studies were not carried out. Kinetic studies by Bergman showed that formation of $Cp_2Zr(NHR)_2$ proceeded through the reaction of zirconium imido intermediate [Cp_2Zr=NR] and amine exclusively and did not involve protonolysis of $Cp_2Zr(NHR)(Me)$. (Scheme 12)[132]. In our case, L*Zr(*t*-BuNH)$_2$ (L* = *S*-Ph(Me)HCN($CH_2CH_2CMe_2O^-$)$_2$) must have been generated from the reaction of **46** and *tert*-butyl amine directly since **46** itself does not decompose to form [*t*-BuN=ZrL*] or **49a**. L*Zr(*t*-BuNH)$_2$ then decomposes directly to bridging dimer **49a** through a bimetallic pathway or, by forming [*t*-BuN=ZrL*] first, which then dimerizes rapidly to give **49a**. Presumably, L*Zr(*t*-BuNH)$_2$ is present in the reaction mixture in such low concentration that it is not detected by NMR spectroscopy. During the reaction, *tert*-butylamine acts as a catalyst, and increasing the concentration of *tert*-butylamine results in an increase in the rate of formation of **49a**. However, the bridging imido complex **49a** is very inert and does not display the typical reactivities found for zirconium imido complexes. [132,134]

Compared to **46**, **47** is more reactive: when a NMR sample of **47** was heated at 70 °C, it decomposed cleanly to **50**. In presence of excess 2,6-dimethylaniline, **47** reacts to form **48** which eliminates aniline to form **50**. (Scheme 14). In both cases, the reactions were monitored by ^{1}H NMR. The quartets at 4.65, 4.38 and 3.90 ppm correspond to the CH_3(Ph)*H*CN proton resonances for **47**, **48** and **50** respectively (Figure 43 and 44). Complex **48** appears to be much more stable than L*Zr(t-BuNH)$_2$ and can be identified by

NMR. The reactivity difference between *tert*-butyl amine and 2,6-dimethyl aniline complexes can be attributed to steric and electronic effects: *tert*-butyl amide ($ZrNH^tBu$) is less acidic and bulkier than 2,6-dimethyl aniline amide. Thus, the lower tendency of **46** to decompose is likely due to the lower acidity of the *tert*-butyl amide proton ($ZrNH^tBu$). For the more sterically congested molecule, $L^*Zr(t\text{-}BuNH)_2$, the driving force is elimination of *tert*-butyl amine which releases steric pressure.

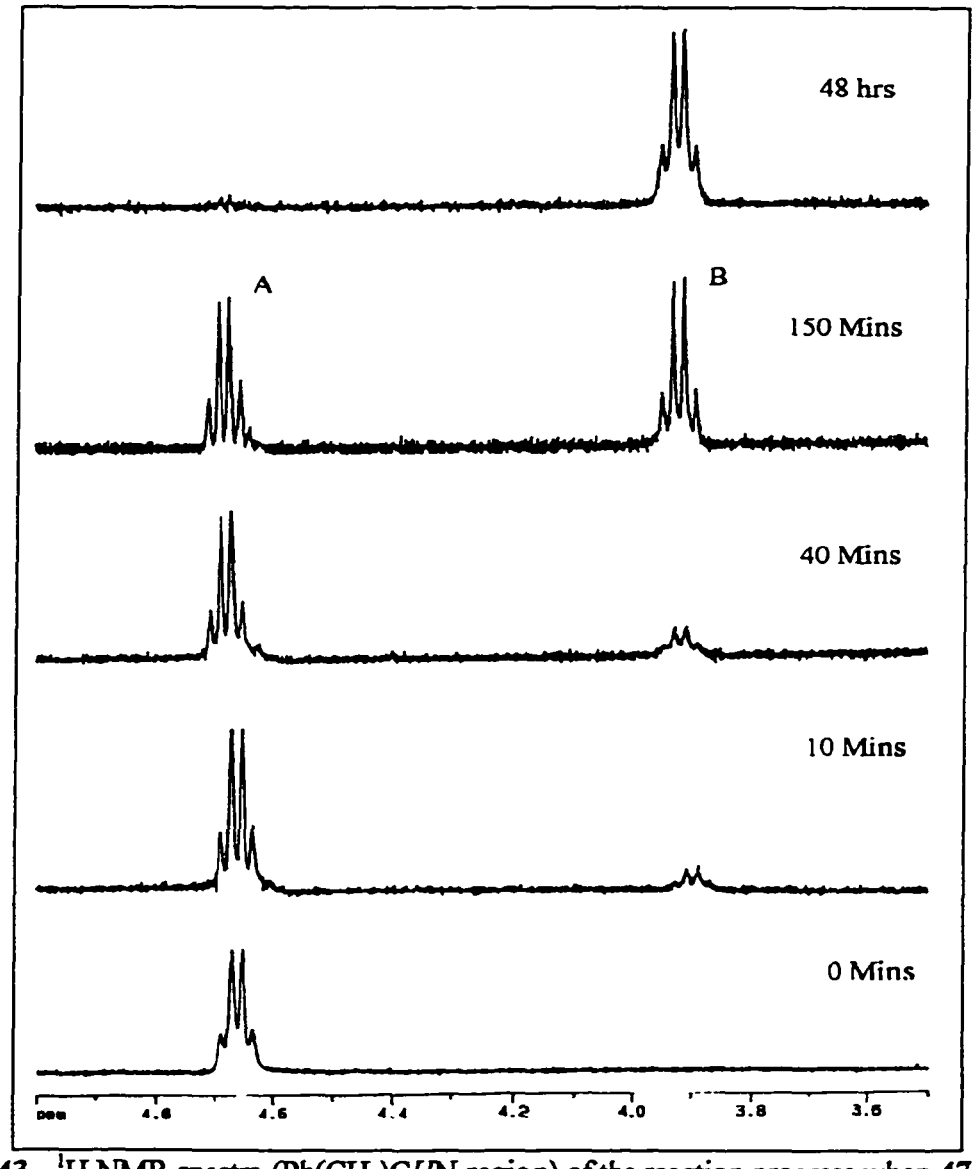

Figure 43 ^1H NMR spectra ($Ph(CH_3)CHN$ region) of the reaction progress when **47** is heated at 70 °C. A: **47**, B: **50**.

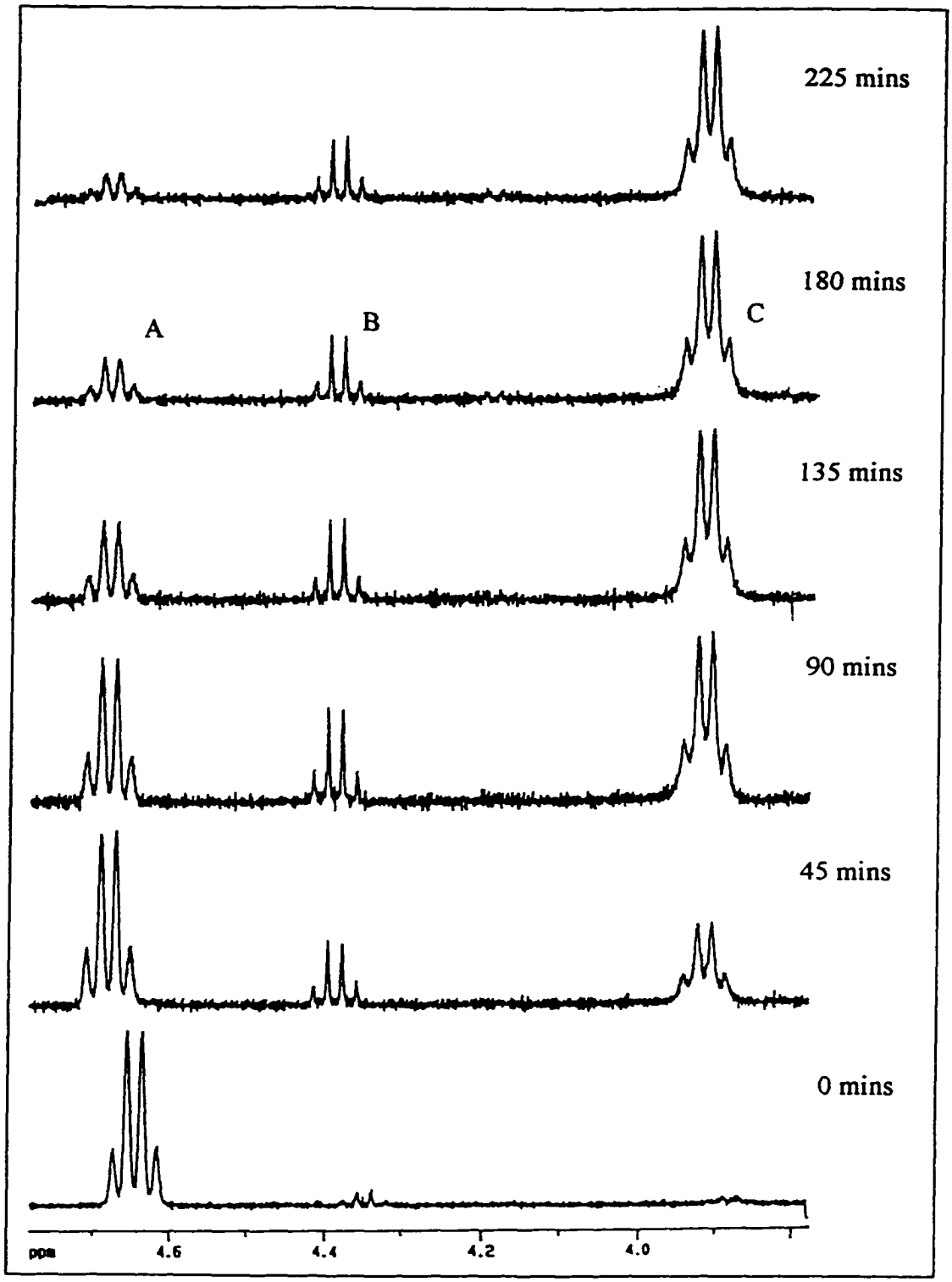

Figure 44 ^{1}H NMR spectra (Ph(CH$_3$)C*H*N region) of the reaction mixture for the reaction between **47** and 2,6-dimethyl aniline. A: **47**, B: **48**, C: **50**.

4.1.3 Structure of bridging imido complexes

The ^{1}H NMR signals of **49a** are sharp and well resolved with only one resonance for the *tert*-butyl group and one set of resonances for the ligand arms, which implies C_2 symmetry if the molecule is a dimer. (Figure 45 and 46). Because it is C_2 symmetric, the amino group $Ph(CH_3)CHNR_2$ must be coordinated to both zirconium nuclei or not coordinated at all. It is unlikely that the amino group can coordinate to both zirconium nuclei due to the steric pressure around the zirconium center. Thus **49a** should be a bridging imido dimer with both zirconium centers possessing pseudo-tetrahedral geometry (both of the amino groups are dangling in the space). This structure was confirmed in a preliminary X-ray crystallographic study but better crystals are needed to carry out a complete structural determination. Complex **50** is likely to have a similar structure to **49a** because the ^{1}H NMR spectrum of **50** at 80 °C shows the same features as that of **49a**. However, at room temperature, the ^{1}H NMR resonances are very broad which is likely due to restricted rotation of the 2,6-dimethyl phenyl groups. The ^{1}H NMR resonances of the PMe_3 coordinated bridging imido complex **49b** also resemble those of **49a** except that the ligand backbone CH_2 proton signals are broader. Since C_2 symmetry is retained, symmetrical coordination of PMe_3 to both zirconium centers is likely. The large ^{31}P shift change (δ 47.21 ppm in **49b**, δ = -62 ppm for free PMe_3)[135] supports strong phosphine coordination. Complex **49a** exhibited luminescent property under UV light. This is interesting because luminescence is fairly rare for a d^0-metal complex, and an collaborative study is currently pursuing.

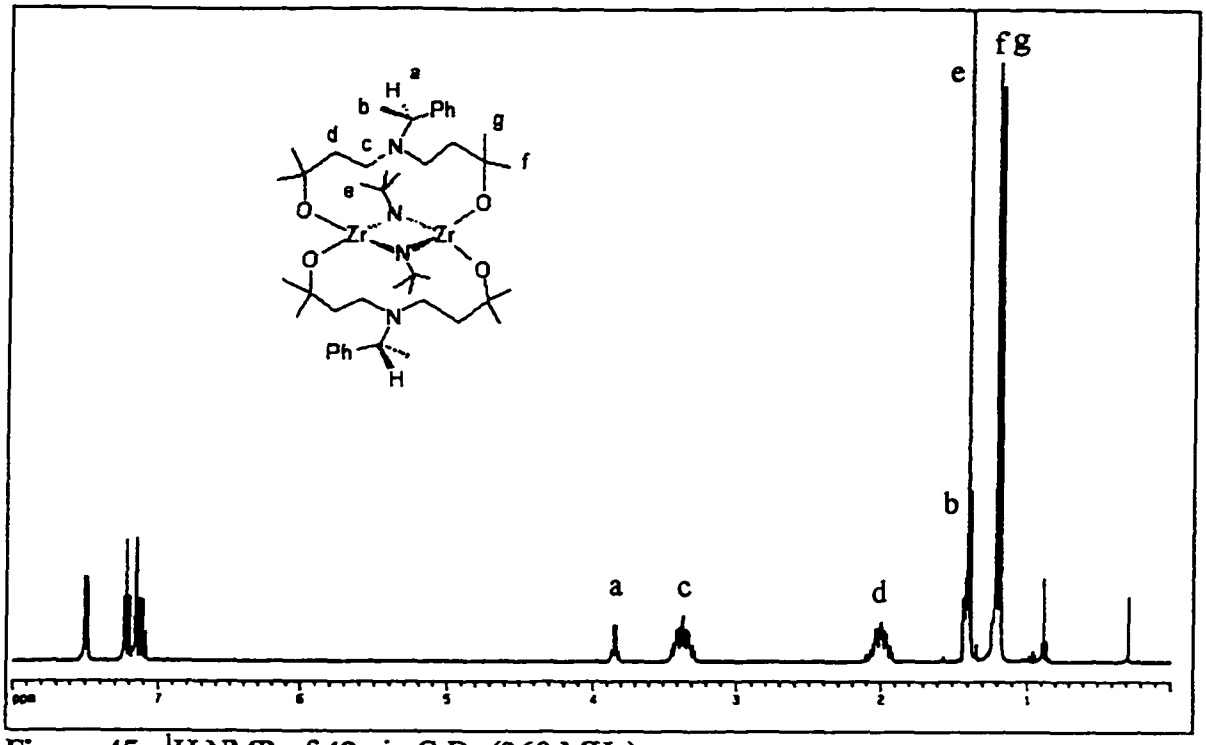

Figure 45 ^{1}H NMR of **49a** in C_6D_6 (360 MHz)

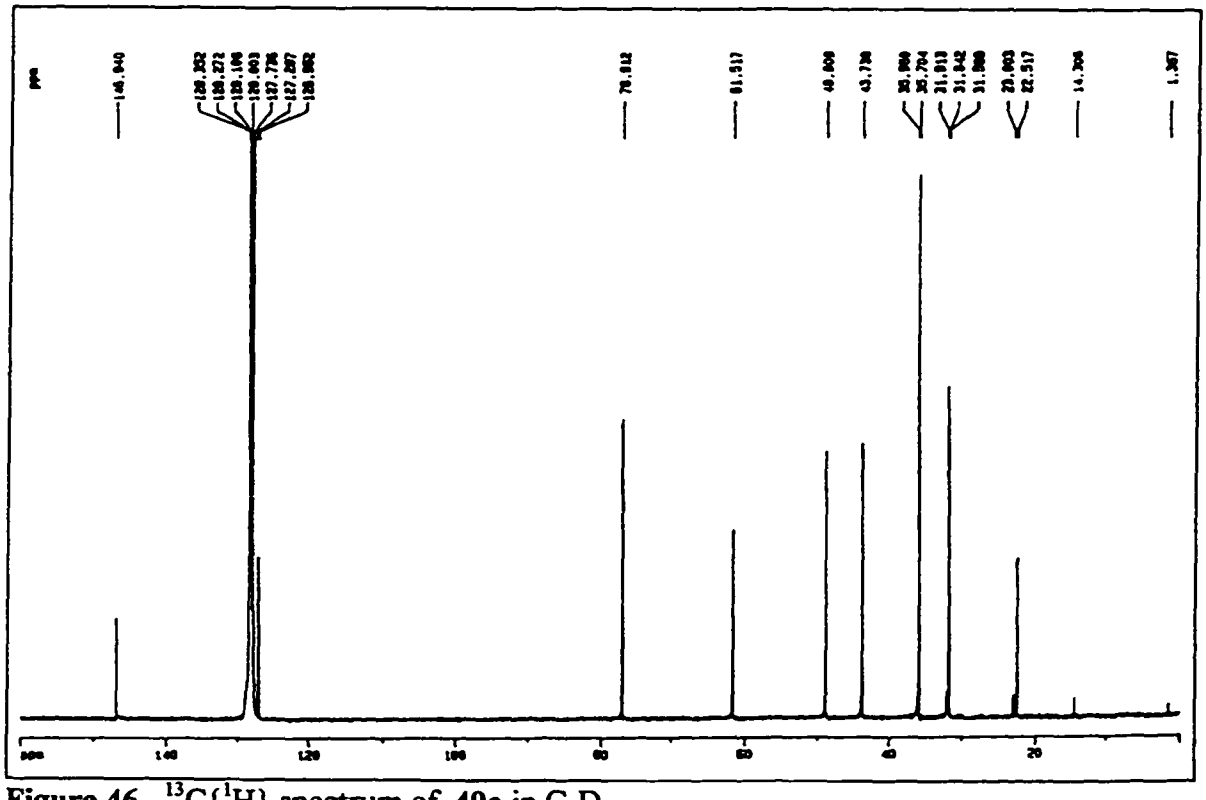

Figure 46 $^{13}C\{^{1}H\}$ spectrum of **49a** in C_6D_6

4.1.4 Reaction of 41c and amines

At room temperature, **41c** does not react with *tert*-butylamine or 2,6-dimethyl aniline. However, when a 1:1 mixture of **41c** and *tert*-butylamine was sealed in a NMR tube and heated at 70 °C overnight, a very complicated mixture was obtained as indicated by NMR. Efforts to isolate pure product were not successful. In contrast, the reaction between **41c** and 2,6-dimethyl aniline under the same reaction conditions yields **53** as a crystalline solid in 70 % yield. (Scheme 15). Although the mass spectrum showed the molecular ion for the dimer (Figure 47), **53** is likely to be oligomeric in the solid state structure because it is insoluble in hydrocarbon solvents and THF. Although **53** precipitated from the reaction solution as a crystalline materials, single crystals were not obtained. Due to the low solubility, it was not possible to recrystallize this compound for an X-ray diffraction study. The insoluble nature of **53** also excluded the possibility of structural studies using NMR spectroscopic techniques. Both elemental analysis and H_2O quenching showed that it contains the [LZrN(2,6-$C_6H_3Me_2$)] unit, and considering the similarity between **53** and **49a**, it is reasonable to assign **53** as an oligomeric bridging imide.

When a toluene solution containing **41c** and 2,6-dimethylaniline in 1:2.5 ratio was heated at 70 °C for 2 hours, the main product was **52**, although the isolated yield was only 28 %. The reaction mechanism may involve LZr(CH_2Ph)(NHR) as an intermediate, which is too reactive to be observed by NMR techniques (Scheme 15). LZr(CH_2Ph)(NHR) may react with another equivalent of 2,6-dimethylaniline to form **52** or decompose rapidly to produce oligomer **53**. With a large excess of 2,6-dimethylaniline and short reaction times (< 2 hours), **52** may be isolated as the major product. Complex **52** also decomposes to

form **53** when heated, but at much lower rate compared to the decomposition of $LZr(CH_2Ph)(NHR)$ itself. This is consistent with the lower Bronsted basicity of the amide nitrogen compared with the benzylic carbanion (pK_a of the parent acids are: toluene, pK_a = 40; 2,6-dimethylaniline, pKa = 29)[136].

The ^1H and ^{13}C NMR spectra of **52** show the same features as those of **41c**. It is reasonable to assume that **52** possesses the same structure as **41c** which is a *pseudo-fac*-trigonal bipyramidal geometry with one anilide group occupying an equatorial site and the other taking an axial position.

Scheme 15

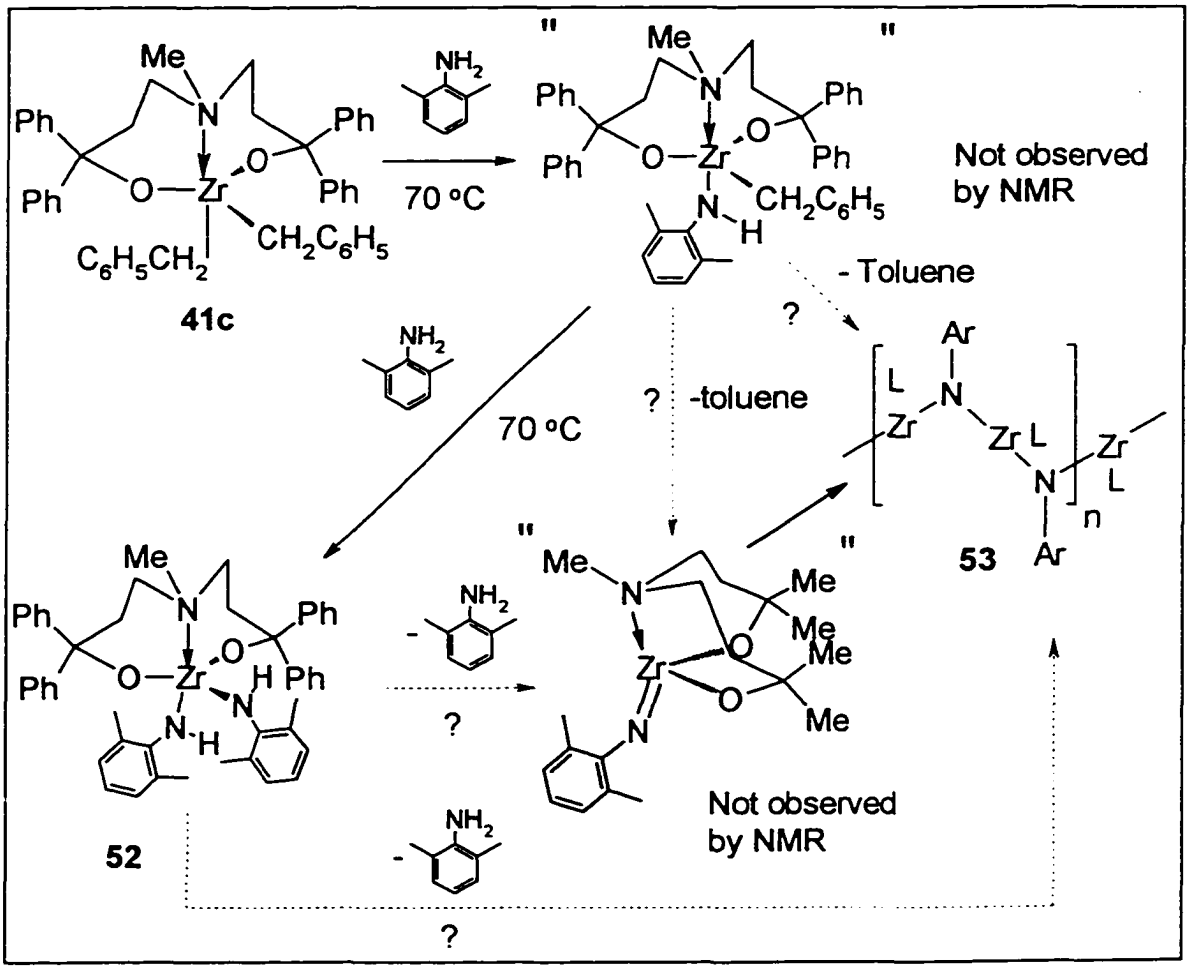

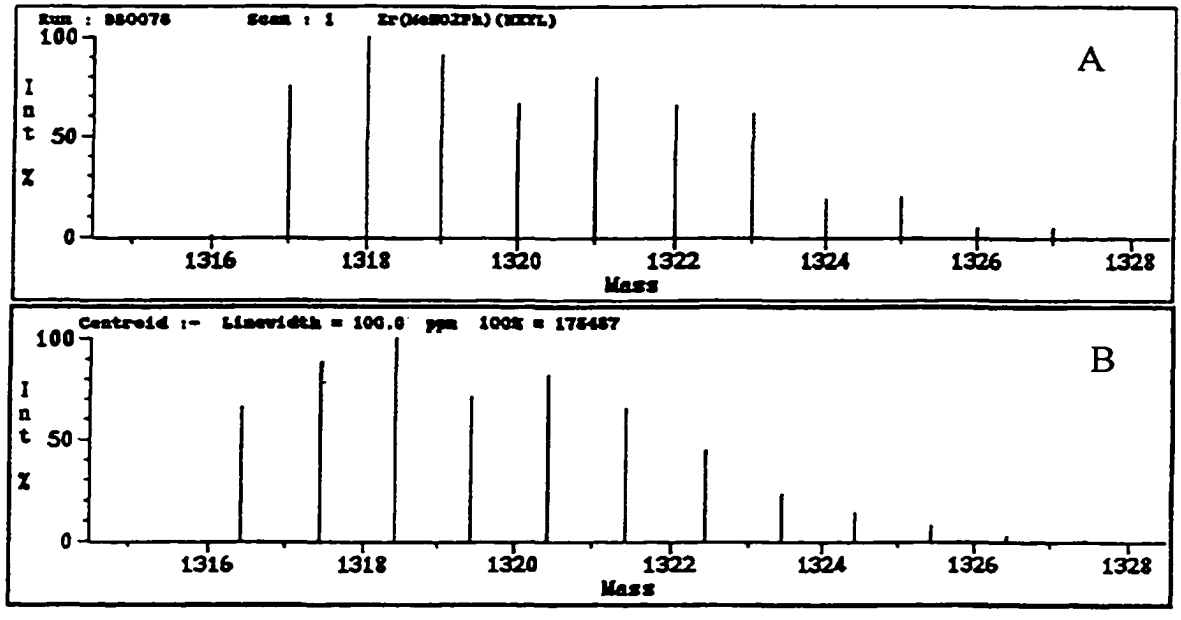

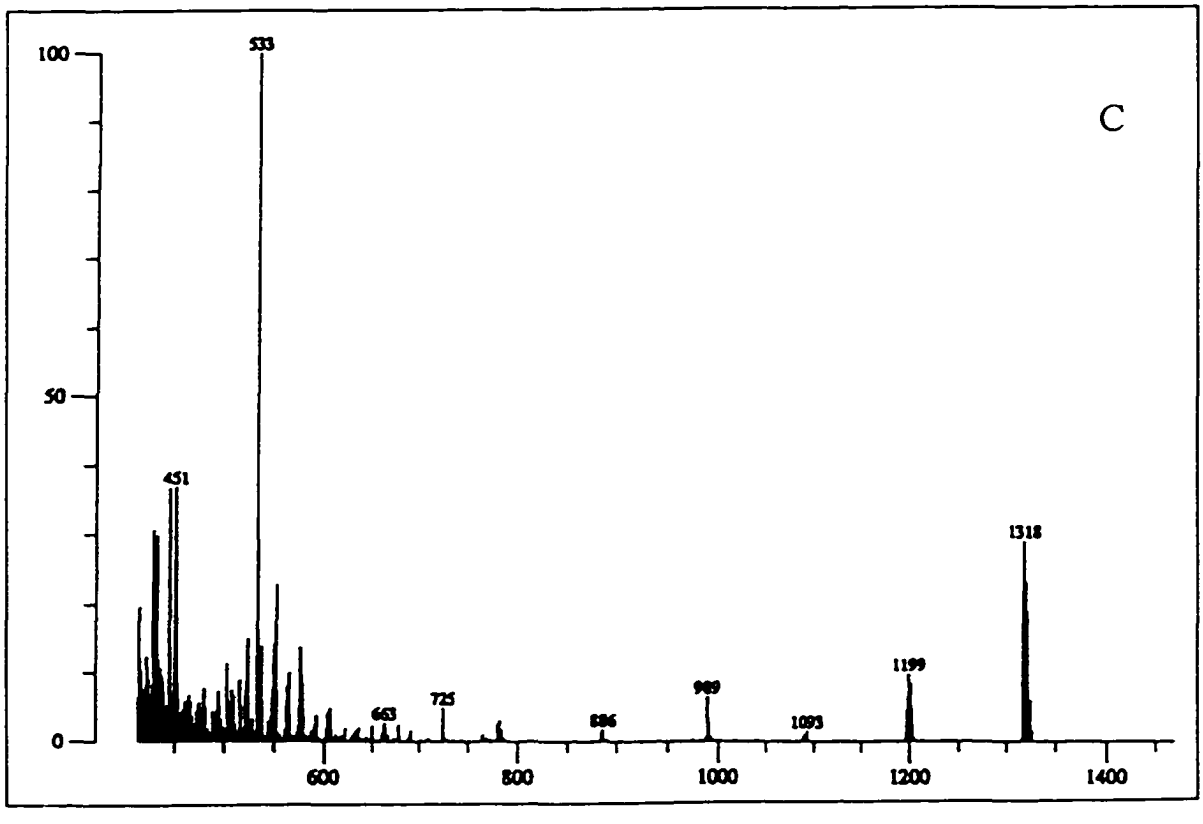

Figure 47 Mass spectrum of **53** (C) and isotopic distribution for molecular ion M^+ (A): experimental distribution; (B): theoretical distribution

4.1.5 Synthesis and structural characterization of Zr-Al bimetallic complexes 51a and 51b

Since the amide proton in complex **46** is acidic and can be deprotonated intramolecularly to form imido complexes as outlined above, intermolecular deprotonation by a metal alkyl can give a bimetallic complex. Addition of one equivalent of $AlMe_3$ to a toluene solution of **46** results in clean formation of diastereomers **51a** and **51b** in 6:1 ratio (eq. 31). It is interesting to note that although the chiral center [$Ph(CH_3)CHN$] is far from both oxygen and aluminum, the coordination of oxygen to aluminum is still stereoselective. Single crystals of **51a** were isolated by recrystallization from a toluene / hexane mixture and an X-ray crystallographic study was carried out.

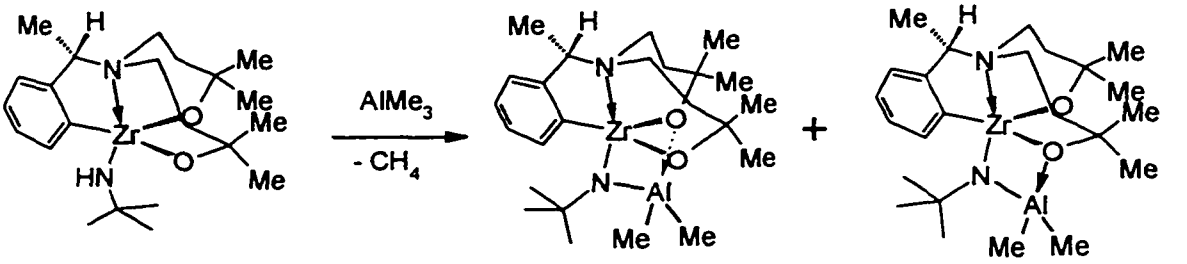

The structure of **51a** is shown in Figure 48, atomic coordinates are given in Appendix Table XX, and the selected bond lengths and angles are collected in Table 13. The Zr-Al distance of 2.93 Å is too long to consider any direct bonding interaction. The bridging imido Zr-N bond distance (2.00 Å) is shorter than those found in other bridging imides[131,132,137]. The terminal alkoxide Zr-O distance is significantly shorter than that of the bridging alkoxide (1.956(8) Å versus 2.083(8) Å) and is marginally longer than those for the terminal alkoxides in **45** (average 1.93 Å). The bridging alkoxide Al-O distance (1.92

Å) is much longer than Al-O bonds in typical 4-coordinate aluminum alkoxides (1.71 Å and 1.79 Å for the terminal and bridging aluminum alkoxide Al-O distances respectively in $Al_4(O^iPr)_{12}$)[138] and is significantly longer than the Zr-O (2.08 Å) distance after applying a correction of -0.27 Å to account for differences in metal ionic radius and coordination number. Thus, O(1) can be viewed as mainly bonded to Zr and weakly coordinated to Al.

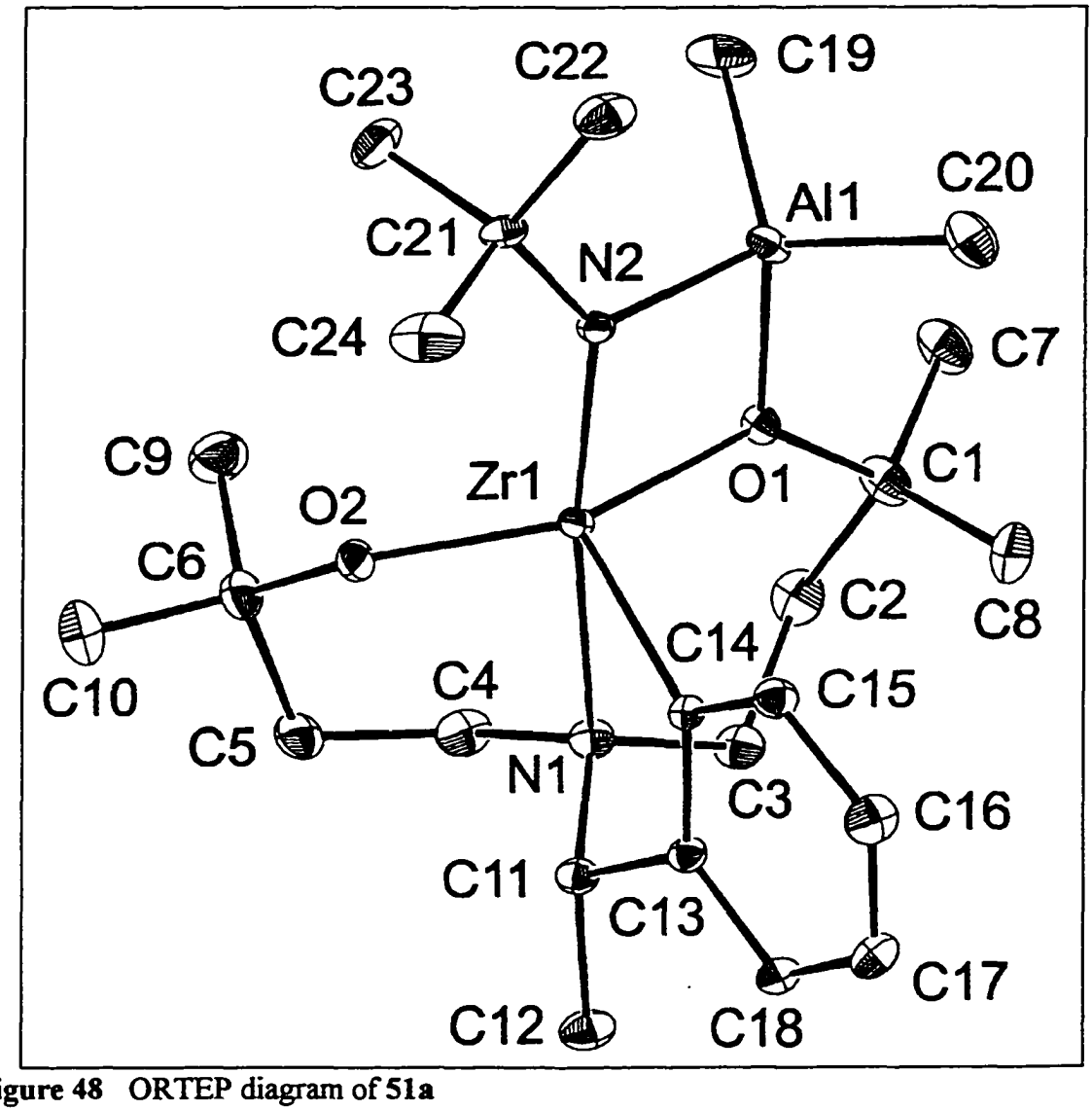

Figure 48 ORTEP diagram of **51a**

Table 13 Selected bond distances and angles for complexes **51a**

		Distances	
Zr(1)-Al(1)	2.933(4)	Zr(1)-O(1)	2.083(8)
Zr(1)-O(2)	1.956(8)	Zr(1)-N(1)	2.457(9)
Zr(1)-N(2)	2.001(9)	Zr(1)-C(14)	2.279(10)
Al(1)-O(1)	1.919(9)	Al(1)-N(2)	1.921(11)
Al(1)-C(19)	2.020(15)	Al(1)-C(20)	1.983(16)
		Angles	
O(1)-Zr(1)-O(2)	138.8(4)	O(1)-Zr(1)-N(1)	86.8(3)
O(1)-Zr(1)-N(2)	81.3(4)	O(1)-Zr(1)-C(14)	103.3(3)
O(2)-Zr(1)-N(1)	80.5(3)	O(2)-Zr(1)-N(2)	107.5(4)
N(2)-Zr(1)-C(14)	107.1(4)	N(1)-Zr(1)-C(14)	77.1(3)
O(1)-Al(1)-N(2)	87.7(4)	O(1)-Al(1)-C(19)	110.0(7)
O(1)-Al(1)-C(20)	109.1(6)	N(2)-Al(1)-C(19)	114.1(7)
N(2)-Al(1)-C(20)	115.5(6)	C(19)-Al(1)-C(20)	116.4(8)
Zr(1)-O(1)-Al(1)	94.2(4)	Zr(1)-N(2)-Al(1)	96.8(5)
Zr(1)-O(1)-C(1)	135.8(8)	Zr(1)-O(2)-C(6)	143.9(9)
Zr(1)-C(14)-C(13)	110.9(7)	Al(1)-O(1)-C(1)	126.9(8)
Zr(1)-C(14)-C(15)	128.8(8)		

Estimated standard deviation in parentheses.

4.2 Insertion of carbonyl groups

High selectivity in carbanion chemistry can be achieved if the counterion, traditionally a main group element (especially, lithium, magnesium and zinc) is replaced by a transition metal[21, 139]. Being mild and tolerant to many organic function groups, group 4 metal complexes have attracted great interest in this area.

Group 4 alkoxide complexes generally possess higher Lewis acidity, and often exhibit higher reactivity as alkyl transfer catalysts, than metallocene complexes. Thus, with the titanium alkoxide complex **XXXV**, high enantioselectivity has been achieved in the

reaction between methyl lithium and benzylaldehyde[140]; whereas, the cyclopentadienyl dialkoxide methyl titanium complex **XXXVI** does not react with benzylaldehyde[141]. However, the zirconium analog **XXXVII** showed excellent enantioselectivity (Scheme 16)[141]. In a more closely related case, Nugent has reported using an oxo bridging dimeric

Scheme 16

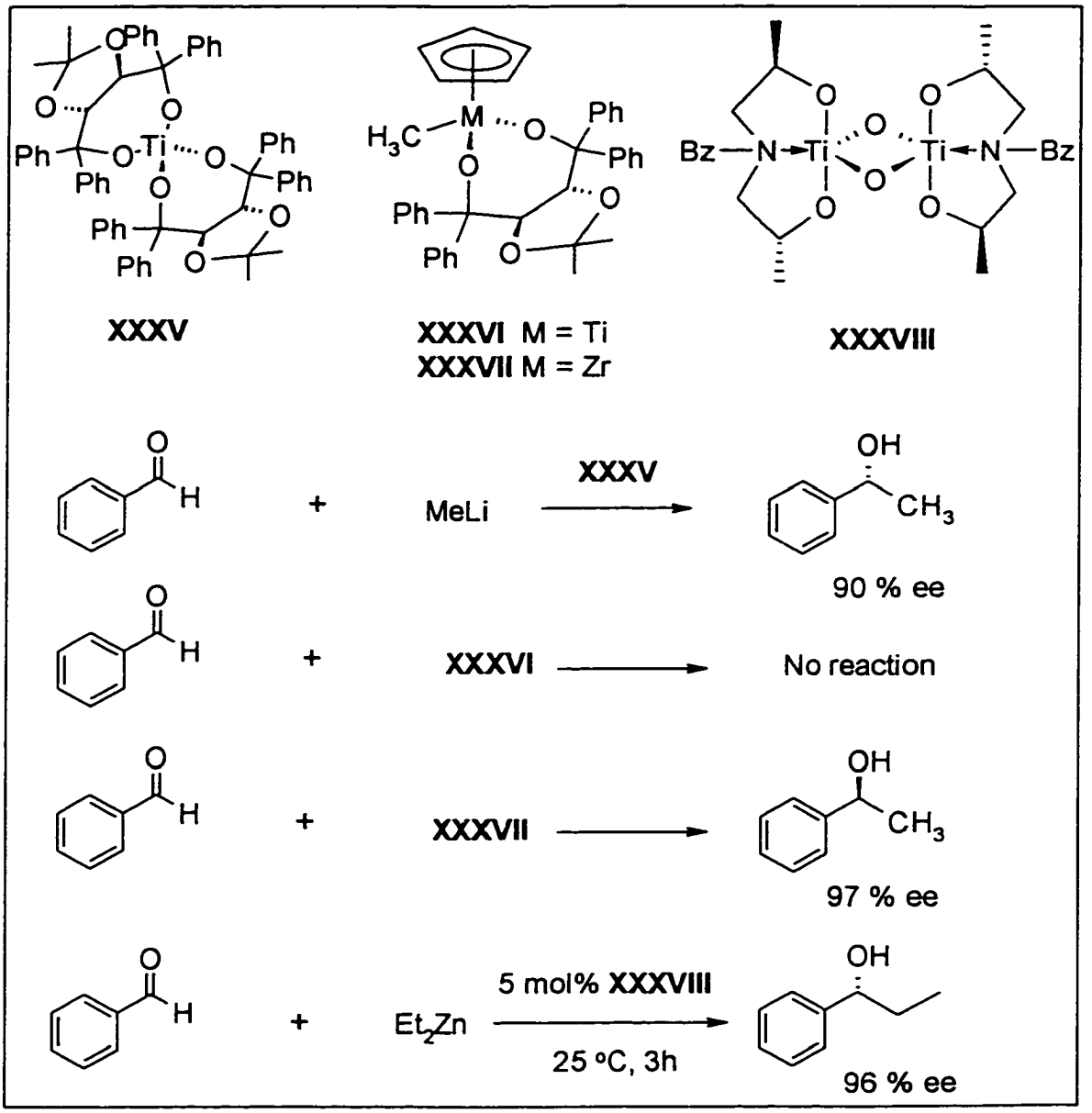

titanium complex bearing chiral amino diol ligands **XXXVIII** for alkyl transfer. Even with only 5 mol % catalyst and very mild reaction conditions, excellent enantioselectivity (96 % ee) was obtained. (Scheme 16)[21]. Because the amino diol ligands used in this project can be easily modified to include chirality, we have explored the possibility of utilizing the resulting chiral zirconium complexes for enantioselective alkyl transfer. Since complex **45** is chiral, and the chiral center is remote to the zirconium center, it should be interesting to see whether this chiral center has any effect on the enantioselectivity of carbonyl insertion. This kind of information is invaluable for future ligand design.

4.2.1 Insertion of carbonyl groups into metallacycle 45

Benzaldehyde, acetophenone, β-naphthaldehyde and α-naphthaldehyde react with **45** at -30 °C, and the first insertion occurs exclusively into the phenyl-zirconium bond. Quenching this reaction mixture with H_2O followed by aqueous work-up and silica gel chromatography, allows isolation of **56-59** as pure oils. Because the configuration of the $CH_3CH(Ph)NR_2$ chiral center was known to be pure *S* from the starting material (*S*)-α-methylbenzyl amine, only two diastereomers *SR* and *SS* are possible for each of **56-59**. Examination of **56-59** by ^1H NMR spectroscopy reveals a diastereomeric excess (*de*) of greater than 85 % for **56-58** and a 50 % *de* for α-naphthaldehyde insertion (**59**). (Scheme 17). The low *ee* obtained with α-naphthaldehyde is unexpected and may be due to steric effects.

Scheme 17

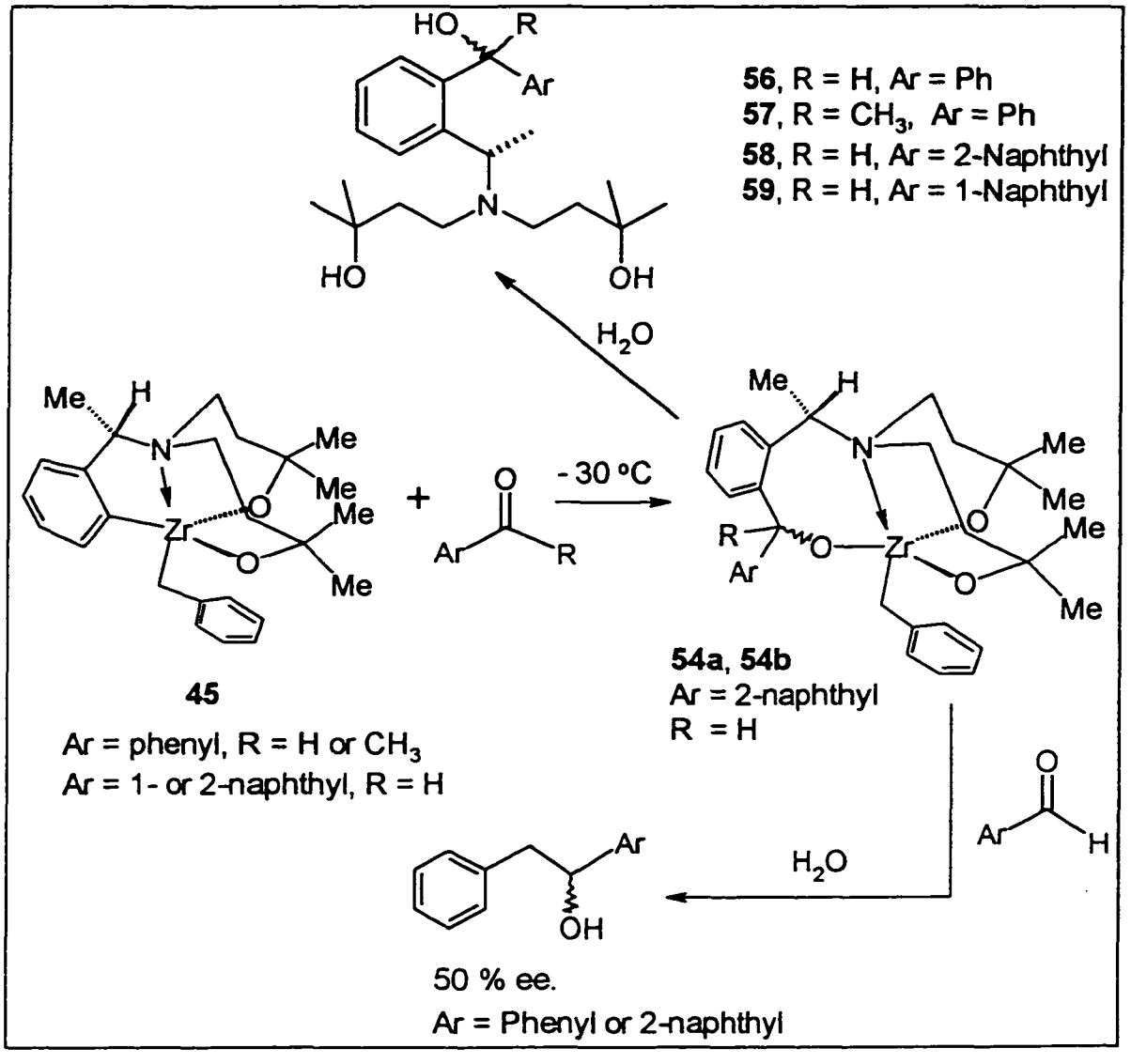

The absolute configuration of the two diastereomers of **56**, **58** and **59** may be determined by NOE difference experiments[142] and computational molecular modeling*. From molecular modeling, the distance between H_a to H_b of the *RS* isomer (2.147 Å) of **56** is shorter than that of the *SS* isomer (2.294 Å) (Figure 49). Since nuclear overhauser enhancement is dependent on the through-space distance of the two coupled protons[142],

* CASHe Scientific molecular modeling program.

enhancement of H_a to H_b for the *SS* isomer should be larger than that for the *SR* isomer. Indeed, when the C*H*(OH)Ph(Ph') ^{1}H NMR signal at 6.16 ppm of the minor isomer of **58** was irradiated, the NOE effect of irradiation of the $CH_3CH(Ph)NR_2$ signal at 4.57 ppm was 8.8 %, whereas upon irradiation of the signal at 5.56 ppm, the Nuclear Overhauser enhancement of the signal at 3.91 ppm was only 2.5 %. (Figure 50). Thus we can conclude that the main isomer of the insertion products is the *SR* isomer and the minor isomer is *SS*. This assignment was confirmed by X-ray crystallography (*vide infra*). The main isomers of **58** and **59** were also determined as *SR* by the same methodology.

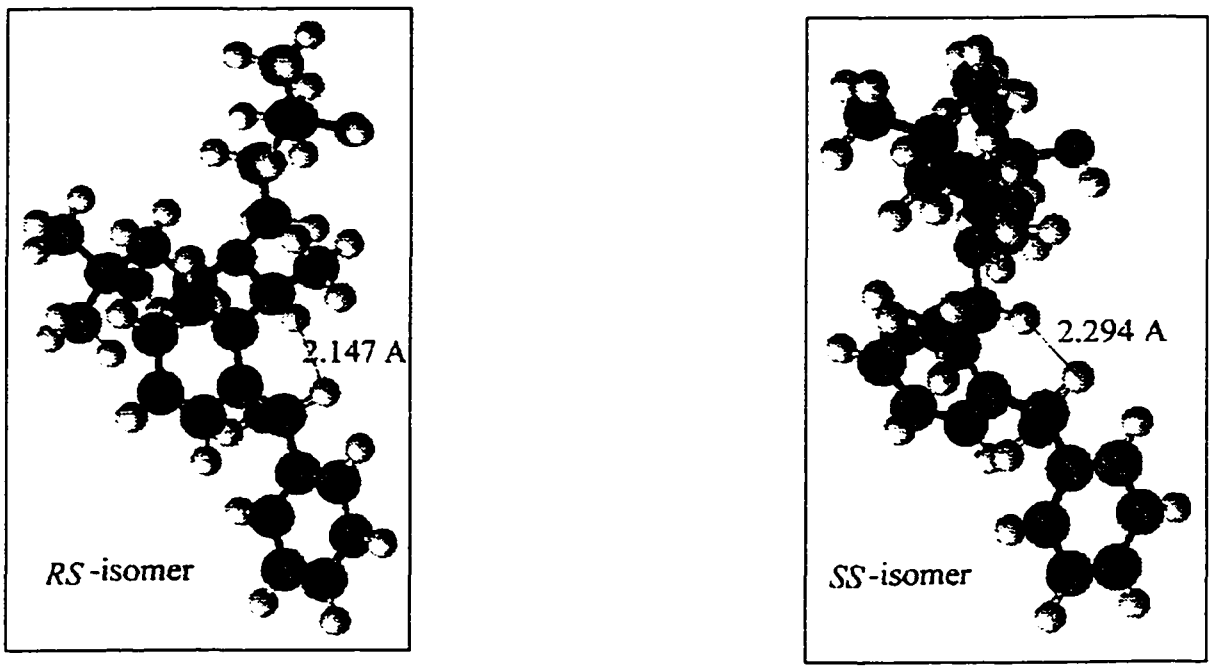

Figure 49 Minimum energy conformation of the two isomers of **56** by molecular modeling

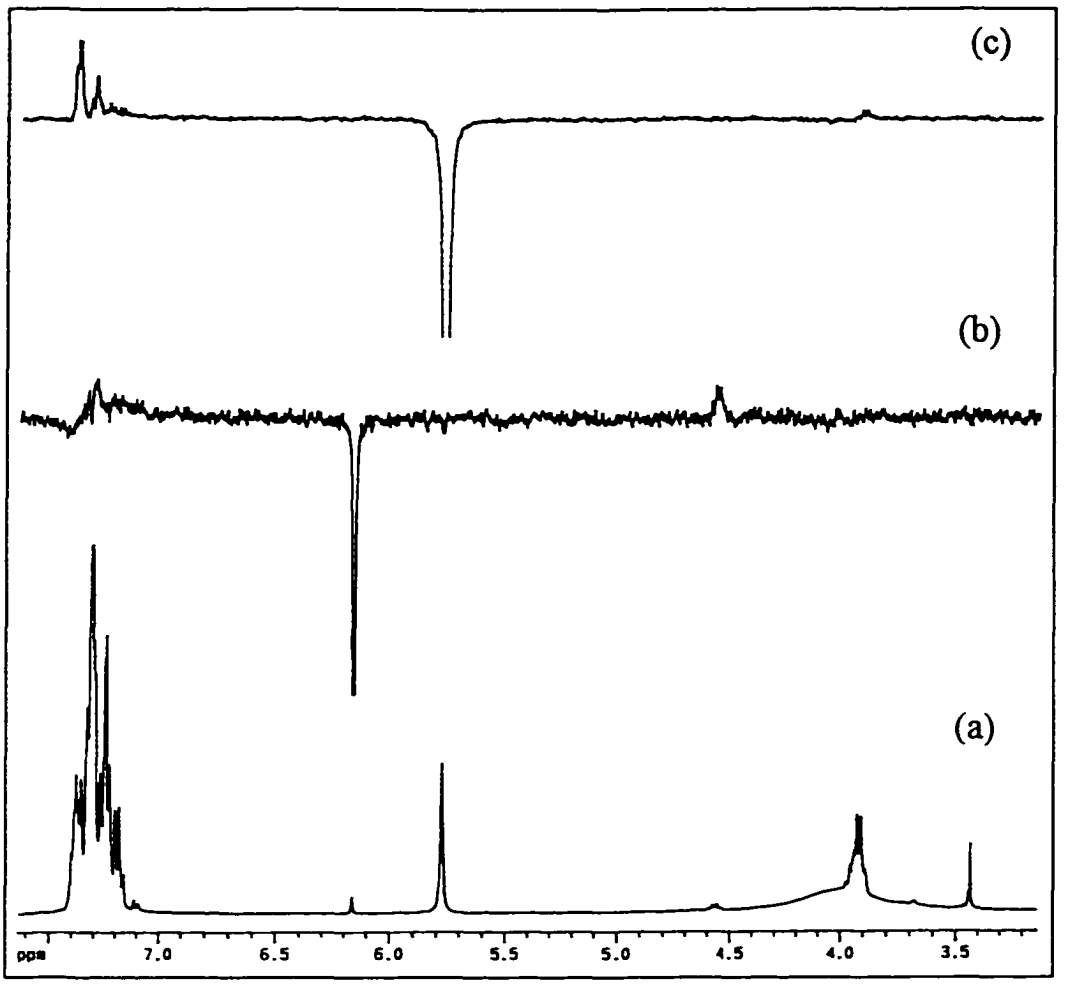

Figure 50 NOE difference spectra of **56** in $CDCl_3$: (a) off-resonance irradiation spectrum; (b) irradiated at δ 6.16 ppm; (c) irradiated at δ 4.56 ppm.

The addition of two equivalents of benzaldehyde or β-naphthaldehyde to **45** gave a second insertion into the benzyl-zirconium bond when the reaction mixture was slowly warmed to room temperature. The *ee* for the benzyl insertion product, 1,2-diphenyl ethanol or 1-β-naphthyl-2-phenyl ethanol, was only 43 % as determined by NMR experiments using a chiral NMR shift reagent. The absolute configuration of these two products was not determined.

In the case of acetophenone, the second insertion did not proceed cleanly and the expected product, 1,2-diphenyl propanol, could not be isolated. ^{1}H NMR showed a complicated series of resonances between 6.4-5.5 ppm which indicate the presence of alkene products. In the case of α-naphthaldehyde, the second insertion was also not clean. There were at least three products present in the reaction mixture: 1-α-naphthyl-2-phenyl ethanol, 1-naphthalenemethanol and 1-naphthoic acid. Apparently, besides the expected insertion reaction, a self redox reaction also occurred to α-naphthaldehyde (Scheme 18).

Scheme 18

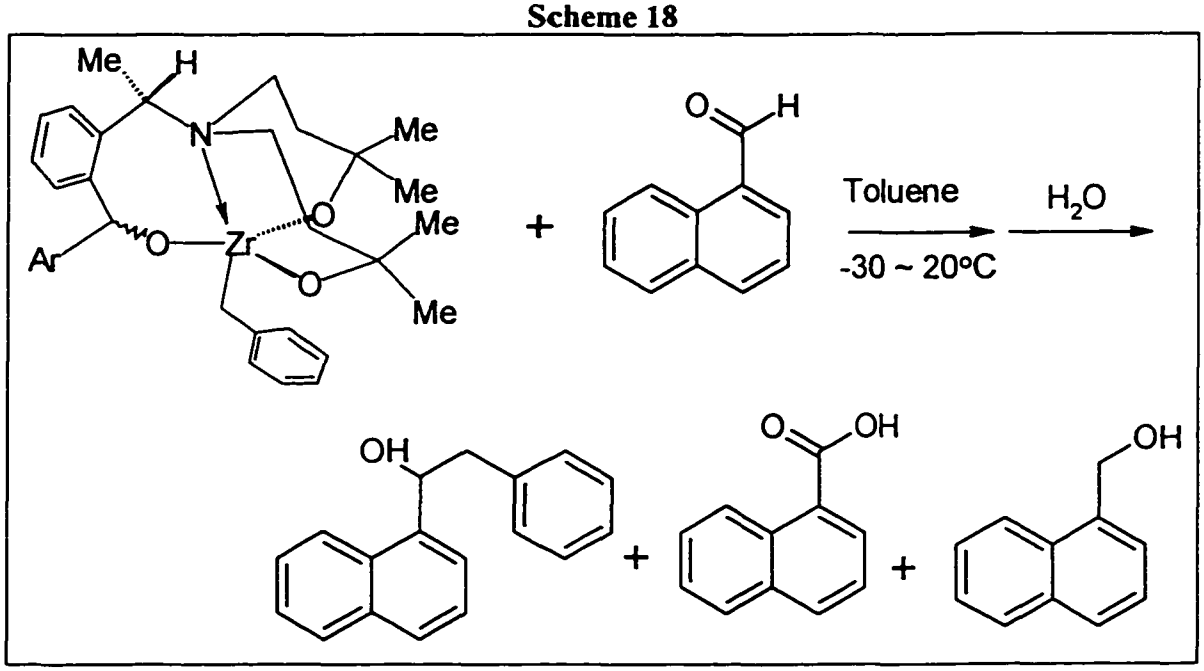

It is interesting to note that when **45** reacts with amines versus carbonyl groups, the site of initial reaction is reversed. It appears that the sp^3 benzylic carbon has greater basicity (reaction with amines) while the sp^2 phenyl carbon exhibits greater nucleophilicity. Generally, sp^3 carbon-metal bonds are more reactive thermodynamically. However in the case of **45**, nucleophilic attack at a carbonyl group by the sp^2 phenyl carbon is kinetically favored. During nucleophilic addition, it is likely that the carbonyl group first coordinates

to zirconium to form an octahedral intermediate. To minimize steric interactions, the benzaldehyde plane must align parallel to the N-Zr-C (benzyl) axis. This is the correct coordination geometry to engage in a four-center transition state with the phenyl-zirconium bond. (Figure 51, **XXXIX**). On the other hand, to form an analogous transition state with the benzyl-zirconium bond, benzaldehyde would have to coordinate to zirconium such that the benzaldehyde plane aligns perpendicular to the N-Zr-C (benzyl) axis causing severe steric interactions with the ligand (Figure 51, **XXXX**). Thus transition

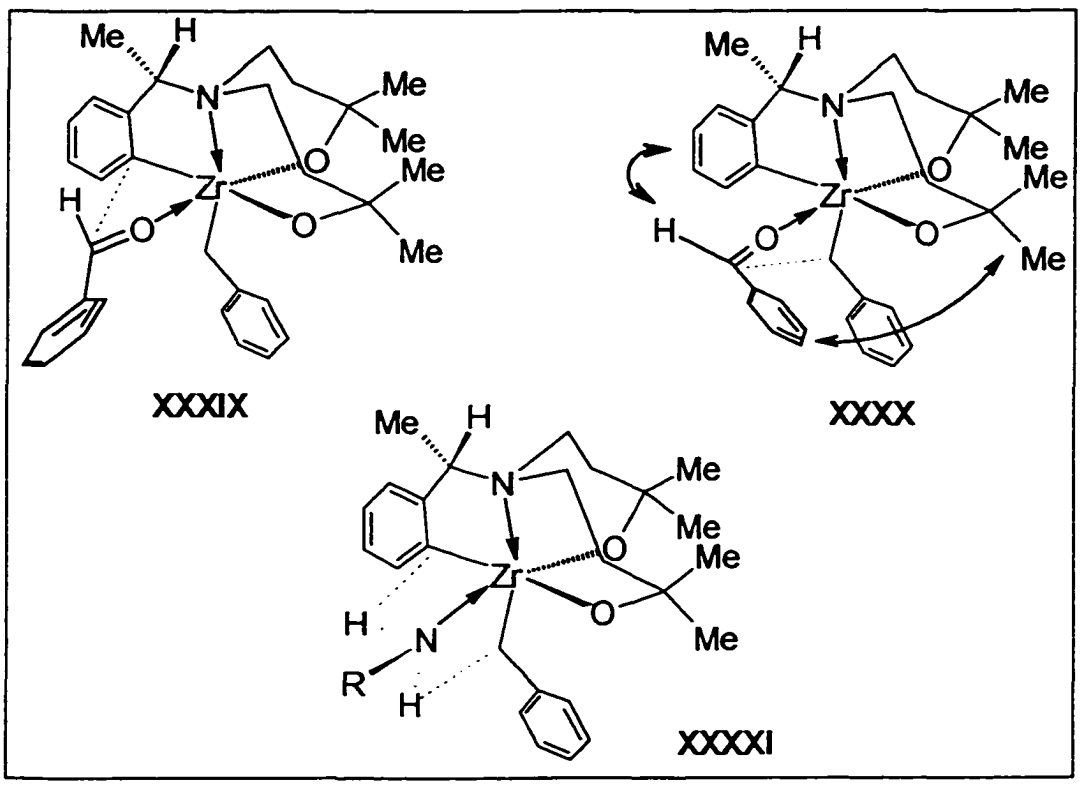

Figure 51 Schematic drawing of the transition states for reaction between **45** and aldehydes or amines

state **XXXIX** is well favored which leads to insertion into the phenyl-zirconium bond. In the case of amines, they are tetrahedral themselves and have no trouble forming a four-center transition state with either the phenyl-zirconium or benzyl-zirconium bonds. As a

result, thermodynamic considerations should take precedence and the more reactive sp^3 benzyl-zirconium bond reacts (Figure 51, **XXXXI**).

4.2.2 Structure of 54a and 54b

With β-naphthaldehyde, the initial insertion product, diastereomers **54a** and **54b**, are solids which can be isolated as pale yellow needles by recrystallization from toluene. The ^{1}H NMR resonances for the ligand backbone of the major diastereomer **54a** are broad at room temperature but become sharp and well resolved at 50 °C. This may be explained by a fluxional process involving dissociation and reassociation of the amino group. The chemical shift difference between the two geminal benzyl protons is very small ($\Delta\delta$ = 0.034 ppm), but they are clearly inequivalent and form an AB pattern. (Figure 52).

Complex **54a** reacts with O_2 to form **55a** quantitatively by NMR spectroscopy. The ^{1}H NMR spectrum of **55a** shows that it has a very similar structure to **54a** with oxygen inserted into the zirconium-benzyl bond (eq. 32). The ^{1}H NMR resonances of **55a** are also broad at room temperature and become sharp at 80 °C. The two germinal protons of the phenylmethoxide are also inequivalent and show a clear AB pattern with chemical shifts of 5.4 and 4.6 ppm respectively.

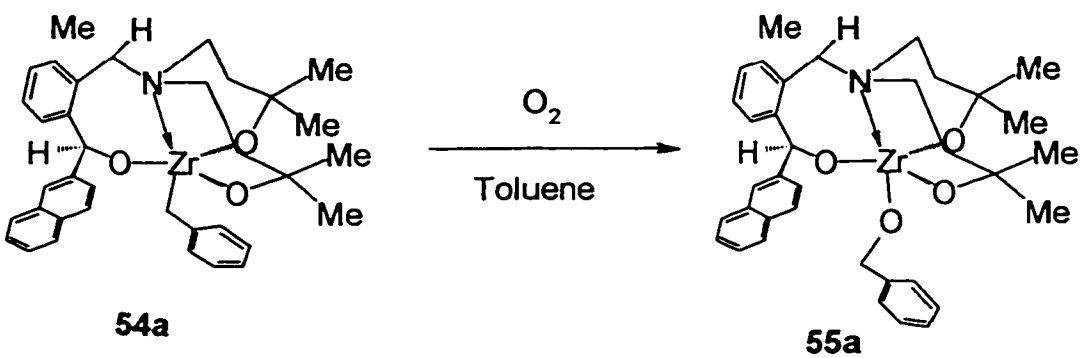

54a **55a** (32)

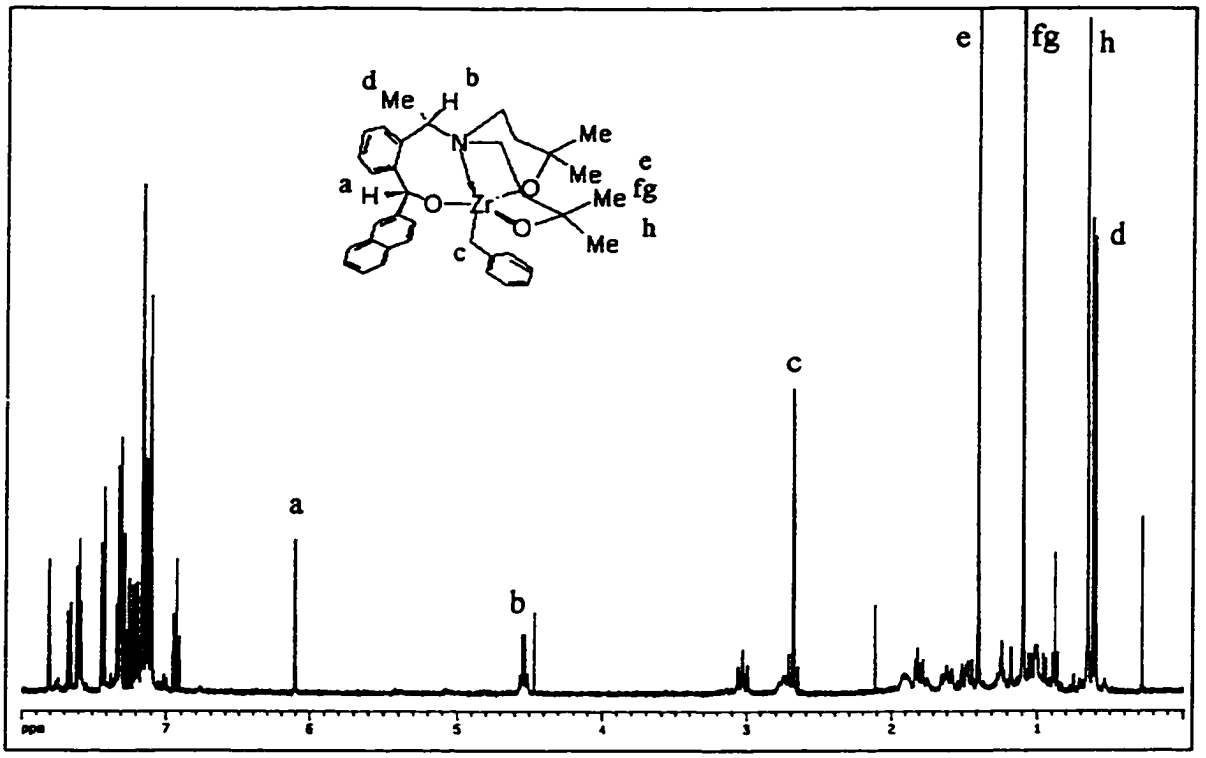

Figure 52 ^{1}H NMR spectrum of **54a** in C_6D_6 solution (360 MHz)

The structure of **54a** is shown in Figure 53. Fractional atomic coordinates are given in Appendix Table XXIII, and selected bond distances and angles are collected in Table 14. The X-ray structure reveals that **54a** possesses pseudo-trigonal bipyramidal geometry at the central zirconium atom with the three alkoxide groups occupying the equatorial positions (mean O-Zr-O angle 118°) and the coordinated amino group and the benzyl group occupying the axial sites.

In contrast to **45**, whose benzyl group is bent toward the zirconium center (Zr-C-Ph angle: 93.4°), the C(31)-C(30)-Zr angle in **54a** is 110.1°, which indicates this benzyl group is purely σ-bound to the zirconium. The Zr-O distances (average distance: 1.93 Å) are similar to those found in **45**. The Zr-O-C angles (mean angle: 149.4°) are larger than

those found in **45** (mean angle: 142.8°). Both bond distance and angle data indicate that these Zr-O bonds contain multibonding character.

Because of the bulky naphthyl substituent on the third alkoxide group, the other two alkoxide oxygens in **54a** are pushed towards one another as indicated by the smaller O(1)-Zr(1)-O(2) angle (119.8(4)°) compared to that in **45** (138.8(4)°). The steric pressure around the zirconium center may also be the reason that the benzyl group is η^2-bound to zirconium.

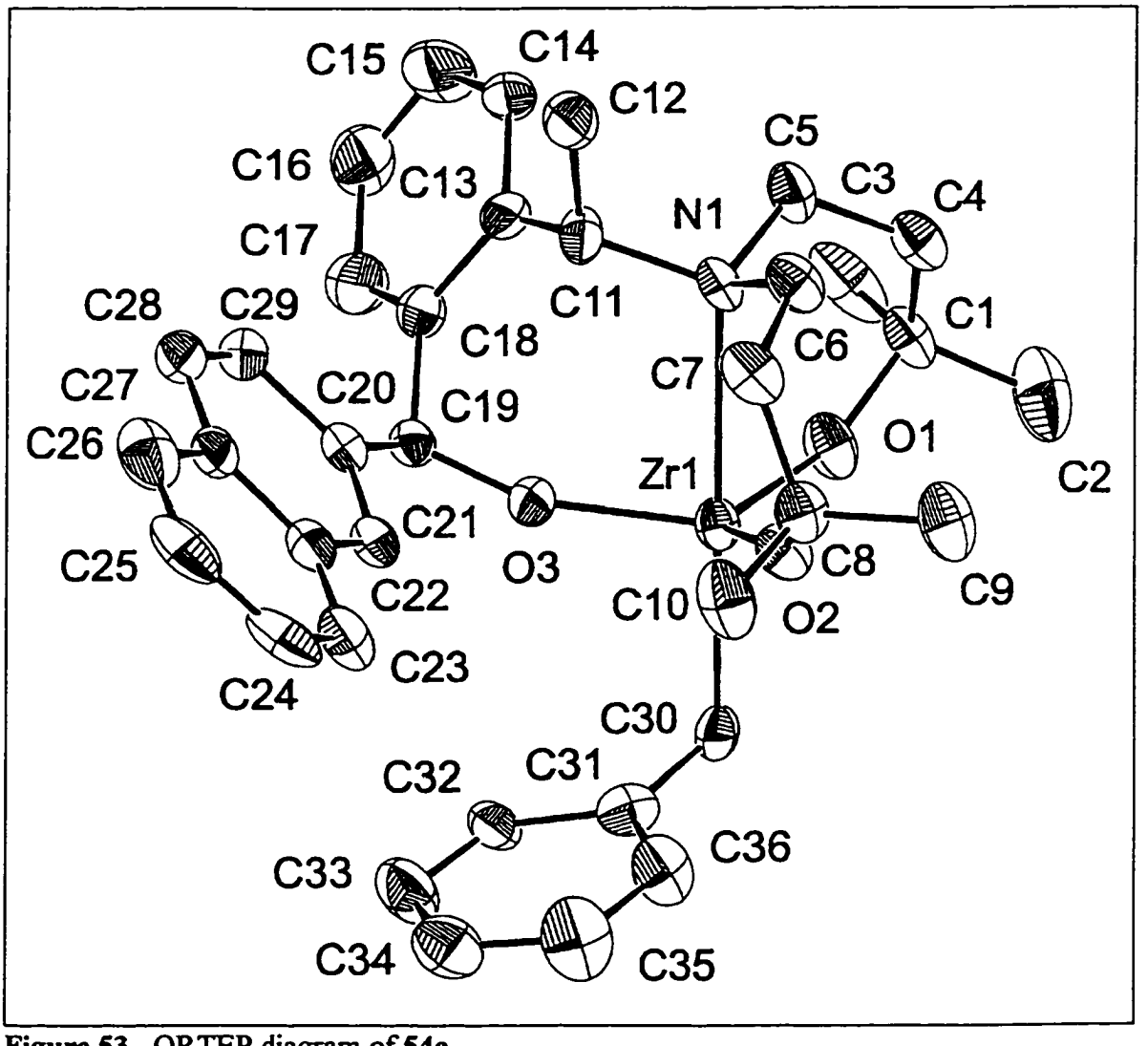

Figure 53 ORTEP diagram of **54a**

Table 14 Bond distances and bond angles of **54a**

		Distances	
Zr(1)-O(1)	1.928(9)	Zr(1)-O(2)	1.917(9)
Zr(1)-O(3)	1.945(10)	Zr(1)-C(30)	2.284(15)
		Angles	
O(1)-Zr(1)-O(2)	119.8(4)	O(1)-Zr(1)-O(3)	119.8(4)
O(1)-Zr(1)-C(30)	99.4(6)	O(2)-Zr(1)-O(3)	114.5(4)
O(2)-Zr(1)-C(30)	98.9(5)	O(3)-Zr(1)-C(30)	95.8(5)
Zr(1)-O(1)-C(1)	147.4(10)	Zr(1)-O(2)-C(8)	151.4(10)
Zr(1)-O(3)-C(19)	161.1(9)	Zr(1)-C(30)-C(31)	110.2(11)

Estimated standard deviation in parentheses

4.3 Alkyne cyclotrimerization

The cyclotrimerization of alkynes into aromatic products is one of the most ubiquitous catalytic reactions in organometallic chemistry[110, 143]. The commonly employed catalysts involve late transition metals such as cobalt[144]. Catalysis of alkyne cyclotrimerization by group 4 complexes is much less common[68, 145] . This is because the organometallic chemistry of group 4 metals is largely based on Cp and its derivatives as ancillary ligation, and these complexes appear to be inactive towards alkyne cyclotrimerization, although large numbers of metallacyclopentediene compounds containing the group 4 metallocene unit are known. It appears that, once a metallacyclopentediene is formed, further reaction with alkynes does not readily occur[146]. On the other hand, titanium and zirconium complexes containing aryloxide ligands show high catalytic activity towards alkyne cyclotrimerization. Rothwell has shown that titanium (IV) bis(aryloxide) dichlorides must be reduced to titanium (II) in order to function as

catalysts[68]; in contrast, Schaverien has found that zirconium dialkyl complexes supported by binaphtholates (biphenolates) are highly active catalysts without preactivation[69]. This is the only example in the open literature where group 4 organometallic complexes show catalytic cyclotrimerization activity without preactivation.

4.3.1 Cyclotrimerization of alkynes with metallacycle 45

Dissolution of complex **45** and 20 equivalents of phenyl acetylene in C_6D_6 at room temperature, gave no reaction by ^1H NMR spectroscopy. However, when the NMR sample was heated at 70 °C, a reaction took place as indicated by the growth of the resonance due to toluene. After 24 hours, the reaction was complete by NMR and the reaction mixture was quenched with water followed by aqueous work-up and silica gel chromatography. The product mixture was found to contain 1,3,5-triphenyl benzene and 1,2,4-triphenyl benzene in 4:1 ratio along with a small amount of phenyl acetylene oligmers by NMR and GC-Mass spectroscopy (Scheme 19).

Internal alkynes failed to react with **45** directly even at elevated temperatures. However, in presence of 2 equivalents of a terminal alkyne, internal alkynes were found to cyclotrimerize. Thus, with catalytic amounts of phenyl acetylene and **45** (2:1 ratio) 2-butyne cyclotrimerizes to form hexamethyl benzene. (Scheme 19).

Scheme 19

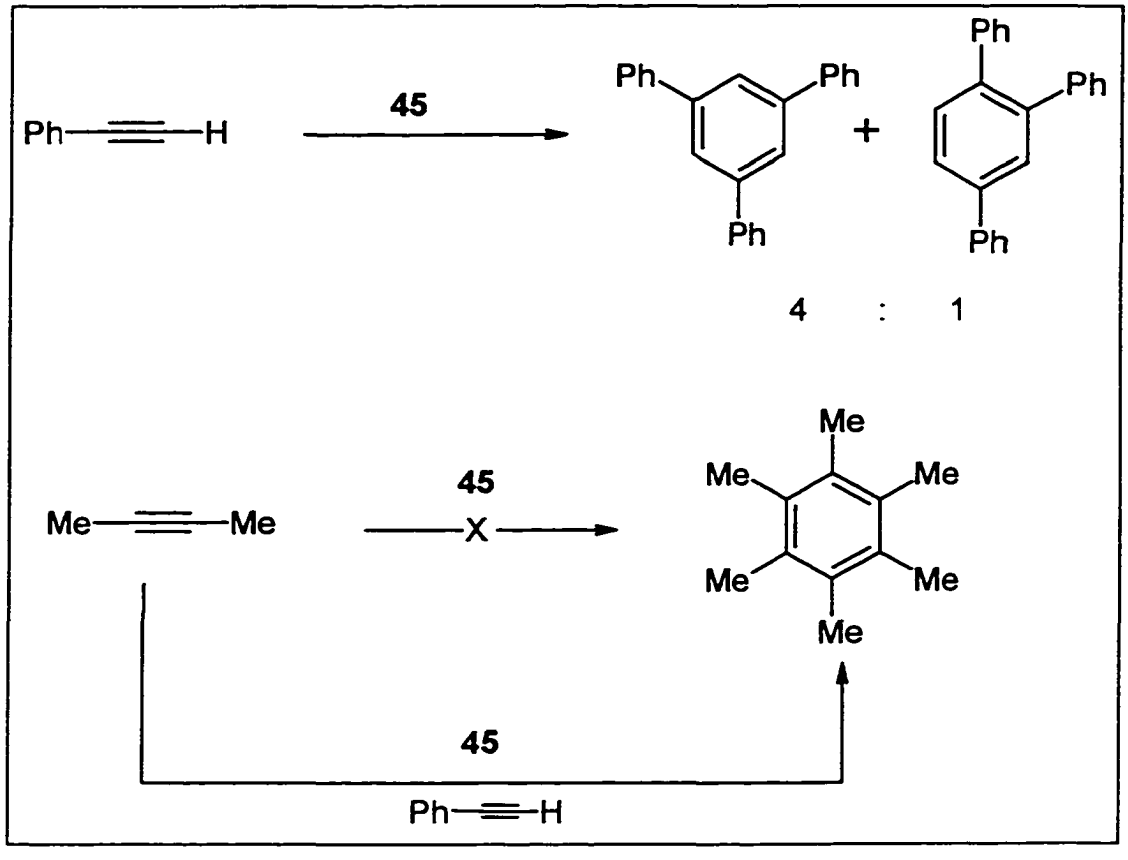

The mechanism of transition metal catalyzed alkyne cyclotrimerization has been a controversial issue in the literature. Reaction via a metallacycloheptatriene intermediate (stepwise mechanism) or a metallanorbornadiene intermediate (concerted 4 + 2 reaction, analogous to a Diels-Alder reaction) have been proposed[145]. Wigley et al. have isolated and structurally characterized both tantalacyclopentadiene and tantalanorbornadiene complexes supported by aryloxide ligation which appears to support the concerted mechanism[147]. Although Rothwell showed that an olefin may insert into a titanacyclopentene to form a titanacycloheptene complex, it undergoes β-hydrogen elimination followed by reductive elimination to give a 1,4-hexadiene product instead of

undergoing direct reductive elimination to generate a cyclohexene product[145] (eq. 33). Thus, Rothwell's study also seems to favor the concerted mechanism. Furthermore, the fact that Cp supported group 4 organometallic complexes rarely catalyze alkyne cyclotrimerization also supports the concerted mechanism, since formation of the metallanorbornadiene intermediate is sterically prohibited by the bis-Cp ligation, while formation of the metallacycloheptatriene intermediate has no obvious steric problems.

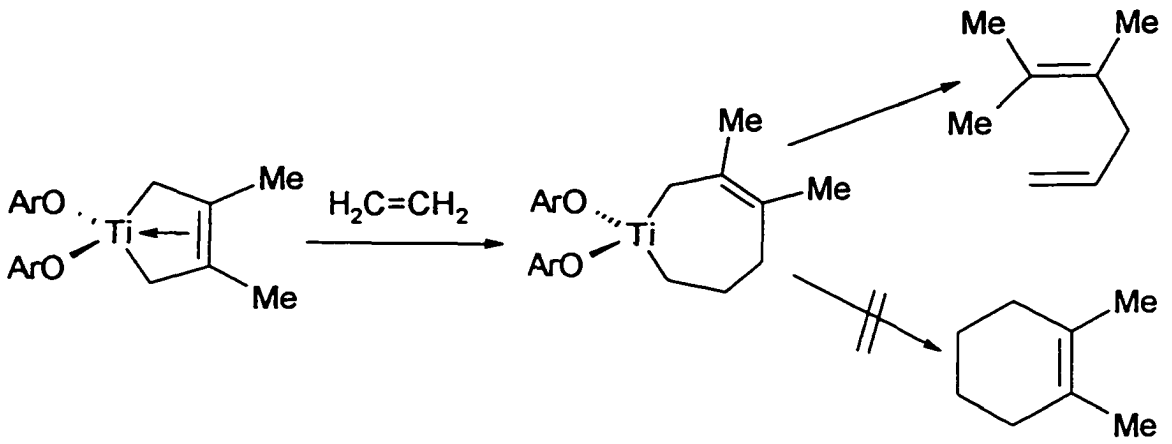

(33)

The mechanism of cyclotrimerization in the present case has not been proven, but a likely catalytic cycle can be constructed as shown in Figure 54. Since liberation of toluene was observed in the initial stage of this reaction, it is likely that protonlysis of **45** takes place first to form a diacetylide species L*Zr(C≡CPh)$_2$ which undergoes reductive elimination to generate a Zr(II) species, the true catalyst involved in the cyclotrimerization reaction. Once this species has formed, a catalytic cycle similar to that proposed by Rothwell[145] seems reasonable: coordination of one equivalent of alkyne to the Zr(II) species produces a zirconacyclopropene intermediate, which undergoes insertion of

another equivalent of alkyne to generate a zirconacyclopentadiene. This species may undergo a further insertion to generate a zirconacycloheptatriene or, more likely, may enter into a [4 + 2] cycloaddition (Diels-Alder) with another equivalent of alkyne to generate a zirconanorbornene. Either species then undergoes reductive elimination to generate arene products and the active Zr(II) catalyst.

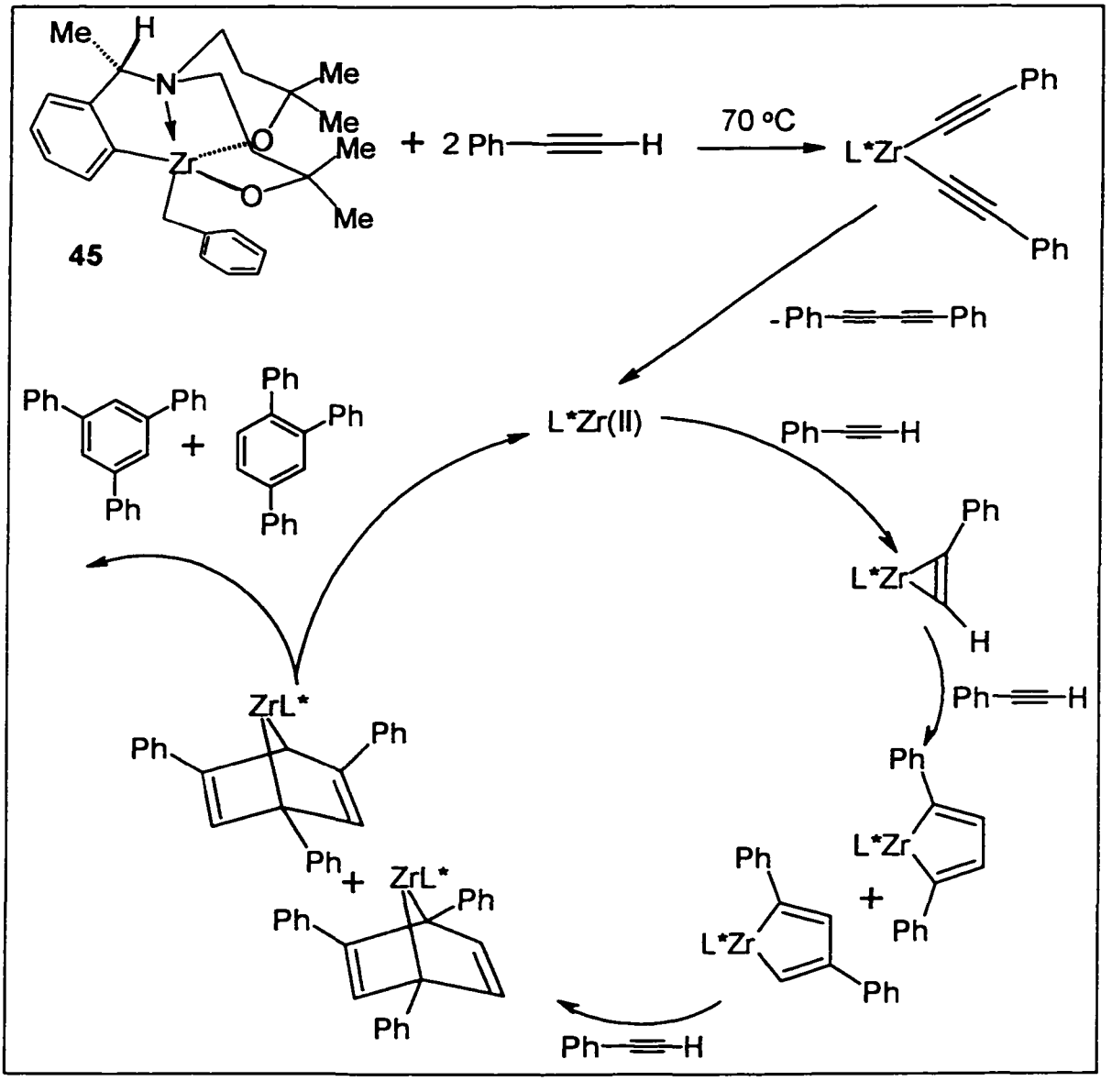

Figure 54 A possible catalysis cycle of alkyne cyclotrimerization catalyzed by 45

4.4 Zirconium cationic complexes and olefin polymerization

Since the mid-1980's the chemistry of group 4 cationic complexes has developed rapidly and attracted tremendous interest due to their important role in Ziegler-Natta olefin polymerization[61]. For neutral metallocene complexes, the low-lying metal centered LUMO is localized in the "equatorial" plane between the Cp ligands, while the cationic complexes have two low-lying metal-centered empty orbitals and are isolobal with AlR_2^+ and L_2LnR (Ln = group 3 and lanthanide) as illustrated in Figure 55[148]. The cationic complexes possess much higher Lewis acidity compared with the neutral parent complexes.

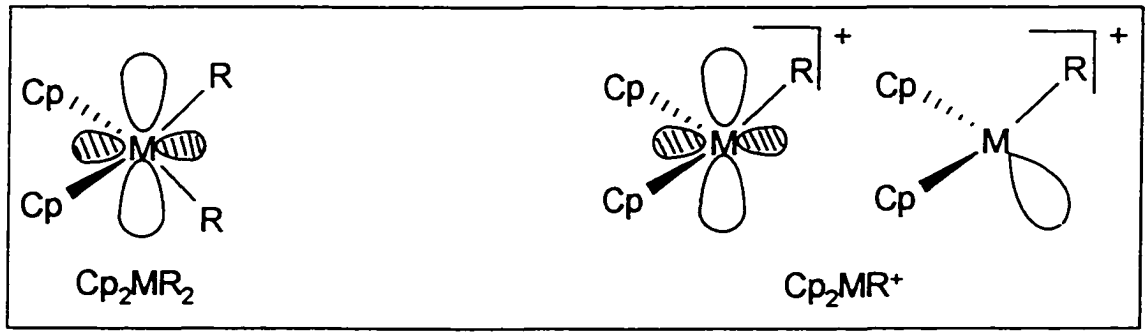

Figure 55 Schematic drawing of low-lying empty orbitals of d^0 Cp_2MR_2 and Cp_2ZrR^+ complexes

Several general methods[60] have been used to prepare group 4 cations from their parent neutral dialkyl complexes including oxidative cleavage of M-R bonds, protonolysis of $L_2M(R)_2$ and alkyl abstraction by strong Lewis acids. Typical examples of these methods are shown in Scheme 20. MAO (methylaluminoxane) abstraction is the most widely used method in industry although it often requires a large excess of MAO (Al:Zr ratios of > 1000:1). $B(C_6F_5)_3$ abstraction is one of the simplest methods for generation of

cationic complexes[149]. It generally requires only stoichiometric amount of $B(C_6F_5)_3$, and the catalytic activity is usually comparable to that of cations generated by MAO.

In this project, stable zirconium cationic complexes were easily generated by $B(C_6F_5)_3$ abstraction from the parent dialkyl complexes. Although it is well accepted that the cationic species is the true active catalyst, it is still unclear what factors govern catalytic activity. The fact that the electron donating ability and steric bulk of the amino diol ligands used in this project can be easily modified by changing the substituent groups (Chapter 3) provides us an opportunity to explore the electronic and steric effects of ancillary ligands on the catalytic activity of cationic complexes.

Scheme 20

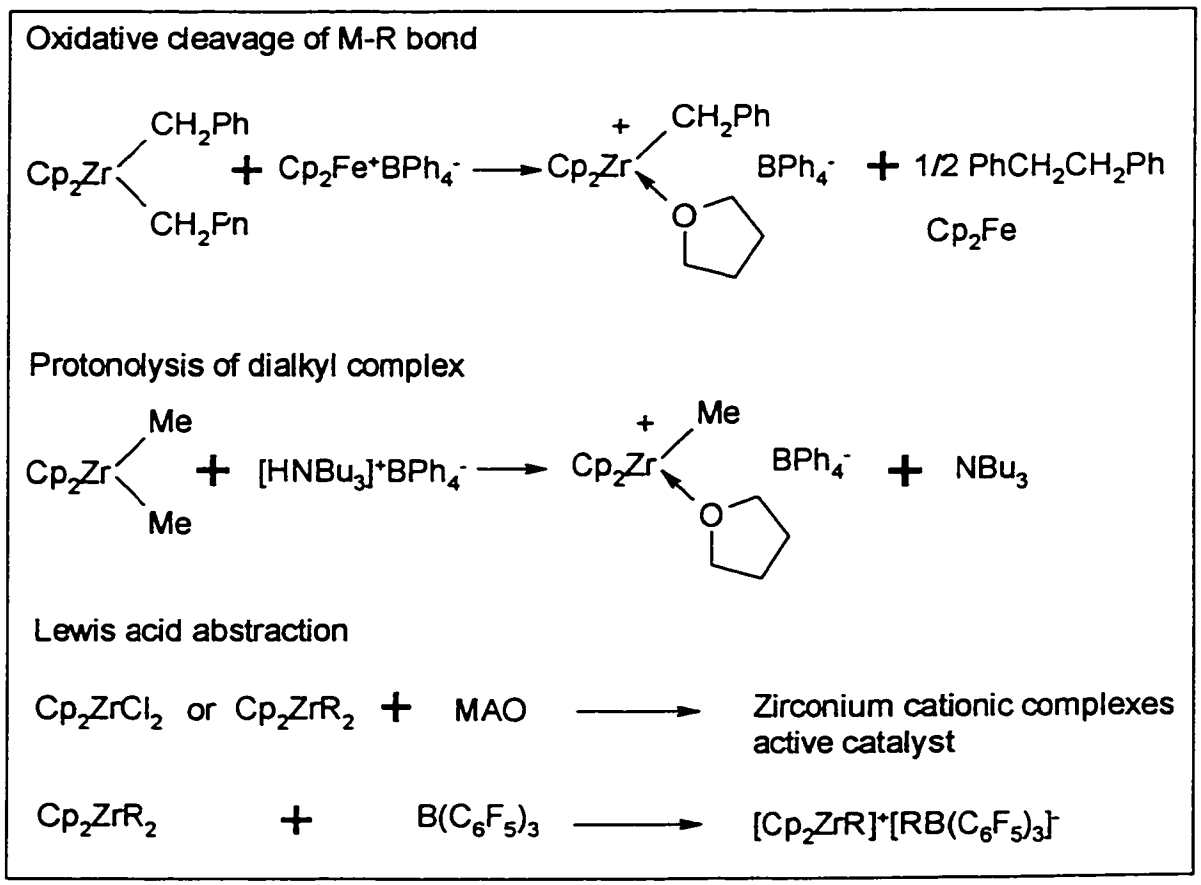

4.4.1 Synthesis and characterization of zirconium cationic complexes

The simplest way to generate zirconium cationic complexes is to react a zirconium dialkyl complex with $B(C_6F_5)_3$, an extremely strong Lewis acid that is capable of abstracting one of the alkyl groups from the parent zirconium dialkyl complex. $B(C_6F_5)_3$ rapidly abstracts a benzyl group from **41c**, **42** or **45** in C_6D_6 solution to generate cationic complexes **60**, **61** and **62**, respectively (Scheme 21), as indicated by a rapid change from pale to bright yellow upon mixing. The cationic complexes have very low solubility in C_6D_6 and precipitate out as orange oils. Efforts to grow crystals were not successful. Despite this, NMR spectroscopy provides a great deal of information about the structure of these complexes. The ^1H NMR resonances of these complexes in C_6D_6 are broad and complex, but notable signals around 6 ppm may signify an η^2-benzyl group[69]. The ^{19}F NMR spectrum of **62** shows three peaks at 130.7, 164.0 and 166.9 ppm which can be assigned as meta, para and ortho fluorine resonances, however, all three peaks are broad and poorly resolved. In the case of **60** and **61**, the ^{19}F spectra are very complex. There are two main signals at 130.4 and 130.9 ppm for the meta fluorines and at least 10 signals at 160.0-167 ppm for *para* and *ortho* fluorines. Usually, a chemical shift difference ($\Delta\delta$) of over 3 ppm between the *para* and *ortho* fluorine resonances is an indication that the benzyl groups abstracted by $B(C_6F_5)_3$ is still strongly associated with zirconium[64b]. In the case of **60-62**, the chemical shift difference of *para* and *ortho* fluorine is close to 3 ppm, which is indicative of strong association of $PhCH_2B(C_6F_5)_3^-$. In a mixed solvent of C_6D_6 and d_8-THF, these cationic complexes dissolve to give simple NMR spectra (Figure 56). Presumably, this is because the THF displaces $B(C_6F_5)_3(CH_2Ph)^-$ from the zirconium coordination sphere to generate the free anion. A single resonance at 3.4 ppm is assigned

to the BCH_2Ph protons, and it is broad because of quadrupolar coupling to ^{11}B. The ^{19}F resonances in C_6D_6 / d_8-THF mixture also become sharp and well-resolved. The chemical shift difference between the *para* and ortho fluorine reduces to 2.7 ppm which indicates that the anion is free.

Scheme 21

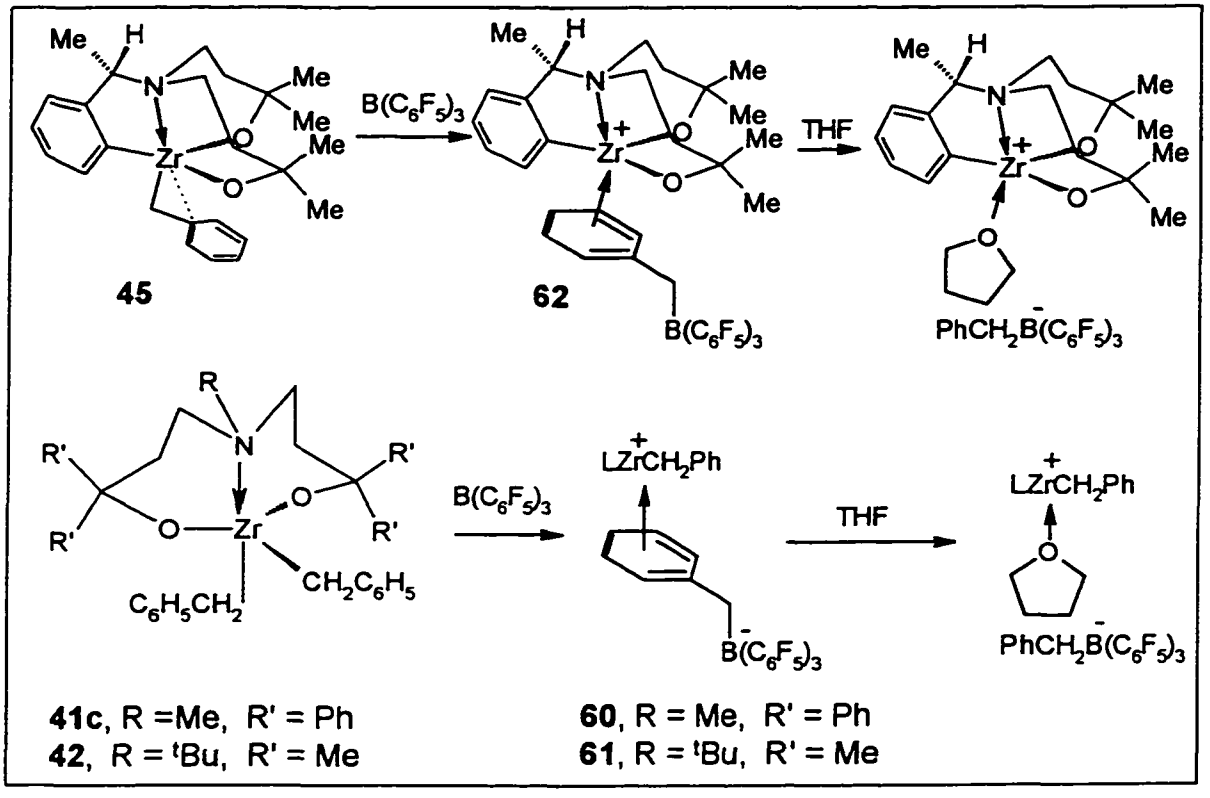

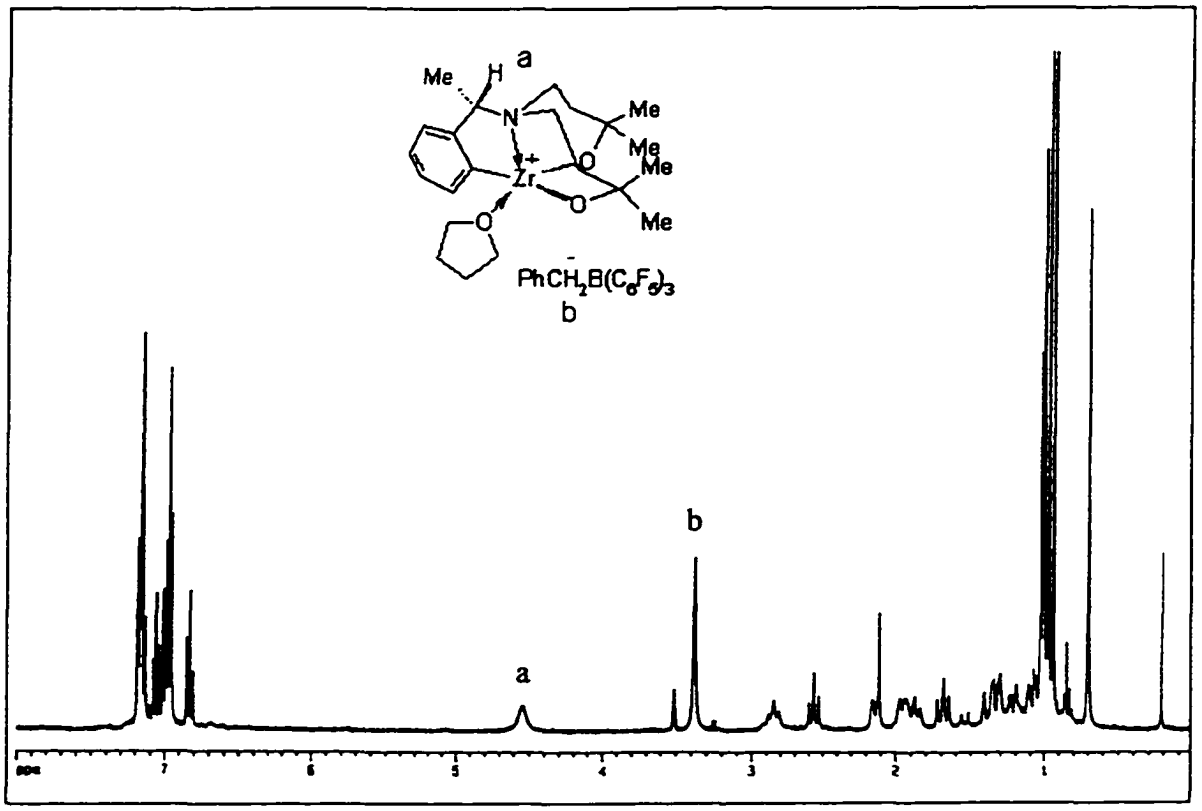

Figure 56 ^{1}H NMR spectrum of **62** in C_6D_6/d_8-THF solvent mixture (360 MHz)

4.4.2 Olefin polymerization

Complex **60** and **62** showed catalytic activity towards olefin (ethylene and 1-hexene) polymerization (eq.34 and 35). In the case of ethylene polymerization, 35 mg **60** (0.028 mmol) produced 300 mg polyethylene as a white solid in two hours (experimental section). Because it is hard to estimate the amount of ethylene used in the reaction, percentage conversion cannot be calculated.

Complexes **60** and **61** are also active catalysts for 1-hexene oligomerization. When **60** and 30 equivalents of 1-hexene are mixed in C_6D_6 solvent at room temperature, the ^{1}H NMR indicates 80 % conversion of 1-hexene in 30 minutes. Because the NMR sample becomes very viscous, the remaining 20 % takes much longer to react (overnight). In

another trial, 37 mg (0.028 mmol) of **60** and 2.2 g 1-hexene (26.2 mmol, 935 equivalent) were stirred at room temperature overnight, and 1.5 g of polyhexene was obtained (68 % conversion) as a sticky gel-like material. The average molecular weight of this polyhexene product was determined to be about 2016 (24 units per polyhexene chain) by comparing the integration of terminal alkene protons (4.7 ppm) with the alkyl protons. Molecular ions with molecular masses over 2000 were also observed in the mass spectrum which showed a pattern of consecutive loss of hexene units. The low molecular weight can be attributed to relatively fast β-hydrogen elimination or chain transfer processes. It appears that higher molecular weight polyhexene can be synthesized by using **61** as catalyst since the polyhexene product obtained in this case was an elastic semi-solid; however, the molecular weight for this polymer has not been determined.

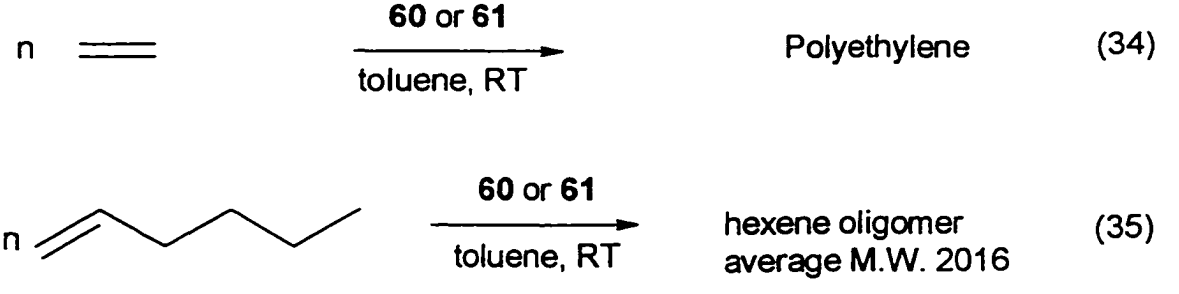

The chiral cationic complex **62** could be interesting if it can catalyze the olefin polymerization. Unfortunately, it appears inactive towards 1-hexene oligomerization based on preliminary results.

Although cationic complexes **60** and **61** showed some catalytic activity towards olefin polymerization, reactivity and molecular weight of the polymers produced are not satisfying. It is difficult to quantify the factors that govern the catalytic activity, however

some clues about the effects of metal Lewis acidity and ligand basicity may be drawn from this work and the literature. It appears that alkoxide (aryloxide and siloxide) cationic complexes generally show low catalytic activity[69]. So far as we know, there are no oxygen based ligand systems which can rival Cp and its derivatives as catalysts. Alkoxide ligands can be viewed as similar to Cp when the two lone pair electrons are considered (Chapter 1). However, because the electronegativity of oxygen is much higher than carbon, the alkoxide complexes often possess significantly higher Lewis acidity. The fact that neutral group 4 metal alkyl complexes do not catalyze olefin polymerization has led some to believe that higher Lewis acidity leads to higher catalytic activity. However, this effect could be over-emphasized. Although a highly Lewis acidic metal center should increase the strength of olefin binding, it may also result in strong ion pairing with the anion which would prevent olefin coordination. It has been observed that having electron withdrawing substituents on Cp resulted in a catalytic activity decrease for cationic zirconocene complexes[150]. Compared to metallocene complexes, alkoxides are also sterically more flexible, which facilitates strong association of the counter anion. These arguments may explain the generally low activity of the alkoxide complexes as α-olefin polymerization catalysts.

Although Lewis base donors often contribute to the stability of metal complexes, increasing the number of Lewis base donors usually results in decreased catalytic activity. Group 4 cationic complexes with macrocyclic ligands are generally poor catalysts because of the high number of donors[65,66]. That bidentate cationic diamide complexes (tri-coordinated) are also more active than the tridentate aminodiamide analogues (tetra-coordinated), provides further proof that Lewis base donors exert a generally negative

effect on activity. In the present case, it is clear that the pendant amino donors contribute to the stability of the metal complexes; however, they may be partially responsible for the low olefin polymerization activity.

In future ligand design, it will be important to balance the Lewis acidity and steric bulk of the cationic complexes to the point where coordination of olefins is facilitated but association of counter anion is prevented. Furthermore, such ligand systems should be rigid with a minimum number of Lewis base donors.

CHAPTER 5

SYNTHESIS AND CHARACTERIZATION OF A CYCLOPENTADIENYL LIGAND BEARING A PENDANT FLUORINATED ALKOXIDE ARM AND ITS ZIRCONIUM COMPLEXES

5.1 Introduction

The electron donating and accepting ability of a ligand can be shifted dramatically by fluorination. For example, trialkyl phosphines are excellent σ-donors but weak π-acceptors; however, fluorinated trialkyl phosphines are poor σ-donors and excellent π-acceptors (comparable to CO)[151]. The electron donating ability of fluorinated alkoxide ligands is also much lower than that of non-fluorinated analogs. Thus, metal complexes bearing fluorinated ligands often show enhanced Lewis acidity and reactivity. Schrock has observed that fluorination of OR groups in the olefin metathesis catalysts $W(CHR')(NAr)(OR)_2$ (Ar = 2,6-diisopropylphenyl) results in great enhancement of catalytic activity compared to their non-fluorinated counterparts[152]. Thus, when OR = $OCMe(CF_3)_2$, the catalysts react rapidly with ordinary internal olefins, while a very slow reaction has been observed when OR = $OCMe_3$. Dramatic enhancement of the catalytic activity of lanthanide β-diketonate complexes towards the hetero Diels-Alder reaction (eq. 36 and 37) has been observed by Danishefsky when the ordinary β-diketones are replaced with fluorinated analogues[153]. Efforts of design fluorinated tripodal chiral β-diketone ligands for the inverse-demand hetero Diels-Alder reaction is currently ongoing in this group[154].

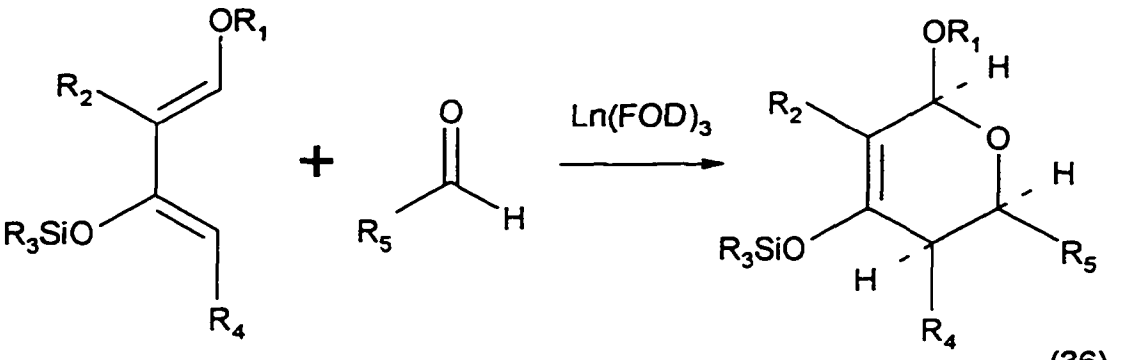

(36)

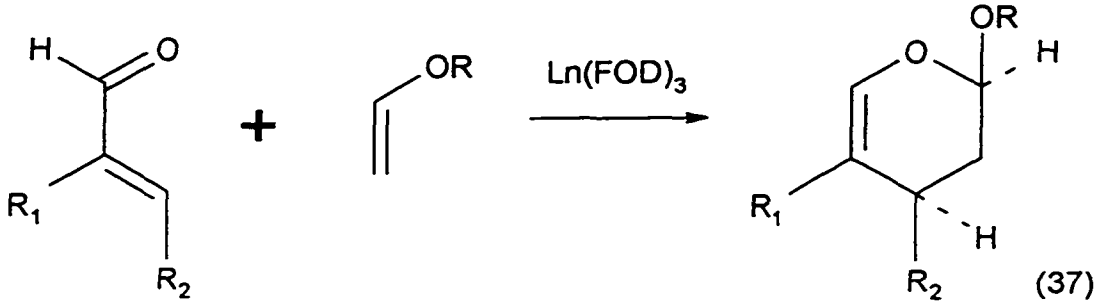

(37)

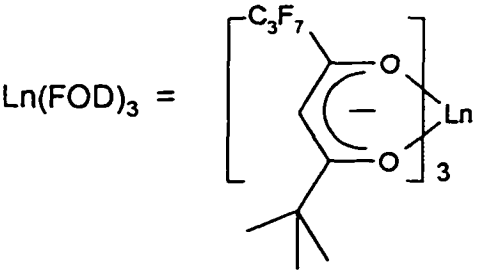

Introducing fluorinated groups into the amino diol ligand system used in this project should result in interesting changes in the reactivity and stability of their metal complexes. However, because of the strongly electron withdrawing nature of fluorine, unexpected difficulties were encountered in preparing these fluorinated amino diol ligands (*vide infra*). In contrast, synthesis of a cyclopentadienyl fluorinated alkoxide ligand by epoxide ring-opening has been proven much more straightforward, and the combination of a cyclopentadienyl group and a fluorinated alkoxide group could result in unique ligation

properties especially considering the great success of cyclopentadienyl ligands bearing pendent amido groups in olefin polymerization[59].

Very recently, Grubbs's group has successfully synthesized an enantiopure fluorinated chelating diol ligand (**XXXXII**) and its molybdenum complex (**XXXXIII**) for enatioselective olefin metathesis[155]. Some enantioselectivity has been observed in the ring-closing metathesis (RCM) reaction catalyzed by this catalyst (Scheme 22).

Scheme 22

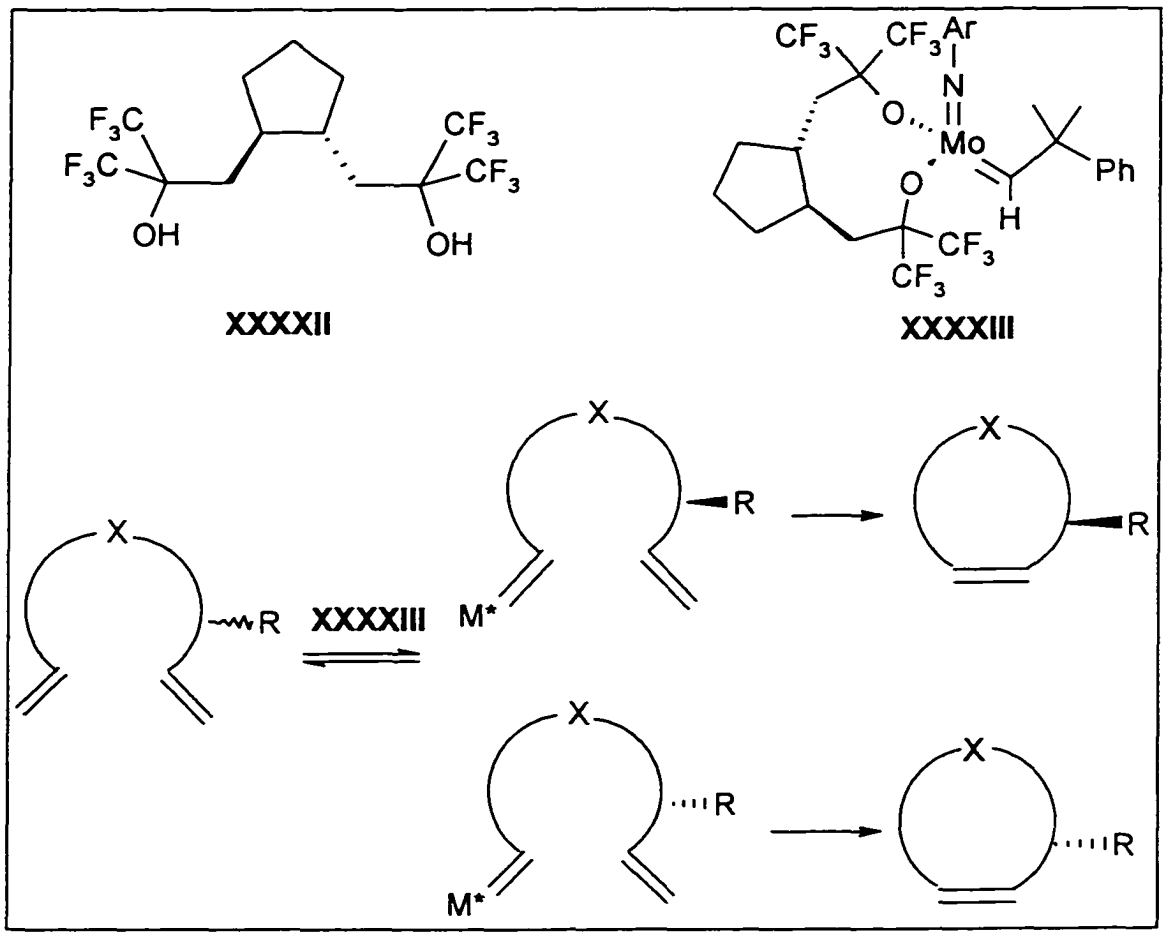

5.2 Synthesis of fluorine substituted ligands

5.2.1 Reaction of amino diesters with fluorinated aryl or alkyl lithium reagents

Reaction of the amino diester **24** with fluorinated aryl or alkyl lithium reagents resulted in formation of six-membered ring products **63a-c** by intramolecular nucleophilic addition rather than the expected amino diol products. (Scheme 23). When lithium reagents were reacted with the amino diester, the intermediate amino ketone was initially formed. However, the strong electron withdrawing nature of the R_f groups makes the α-protons much more acidic than those of nonfluorinated analogues. These α-protons are easily deprotonated by a second equivalent of the lithium reagent, and the resulting carbanions undergo intramolecular nucleophilic attack on the carbonyl group of the other arm forming the new ring products **63a**, **b** and **c**. The ^{1}H NMR spectra of these compounds show complicated coupling of the ring protons due to the chiral nature of these molecules (Figure 57). Although there are two pairs of possible diastereomers (*RR*, *SS* and *RS*, *SR*), only one pair of diastereomers was observed by NMR spectroscopy.

In contrast to the reaction of the amino diester **24** with methyl or phenyl lithium which gives a high yield of amino diol products (Chapter 3), addition of two equivalents of 3,5-bis(trifluoromethyl)phenyl lithium to **XXXXIV** resulted in formation of the six-membered ring product **63d** as the main product. In order to avoid deprotonation of the α-proton, the less basic zinc aryls were employed. Unfortunately, formation of the ring products is also catalyzed by Lewis acids. Thus, in presence of the strongly Lewis acidic, fluorinated aryl zinc reagents, formation of ring product **63d** was quantitative.

Reaction of the amino diester **24** with the fluorinated aryl Grignard reagents takes place in a more controllable manner. Thus, one hour after addition of two equivalents of

$BrMg(C_6F_5)$ to amino diester **24** at -15 °C, the main product was the amino ester ketone **64**. However, when the reaction mixture was warmed to room temperature, the ring product **63b** again formed as the major product over a period of 8 hours. (Scheme 23).

Scheme 23

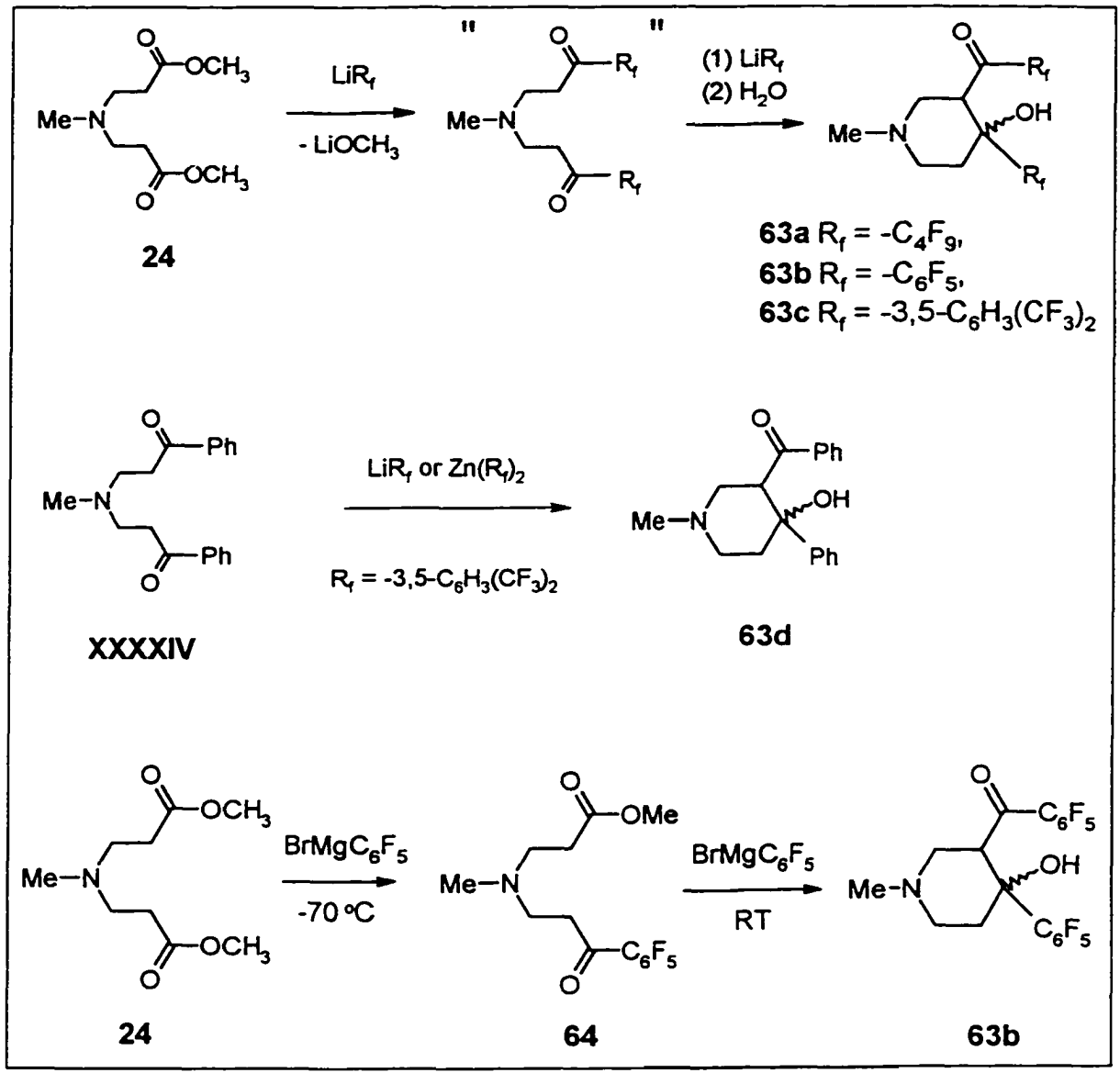

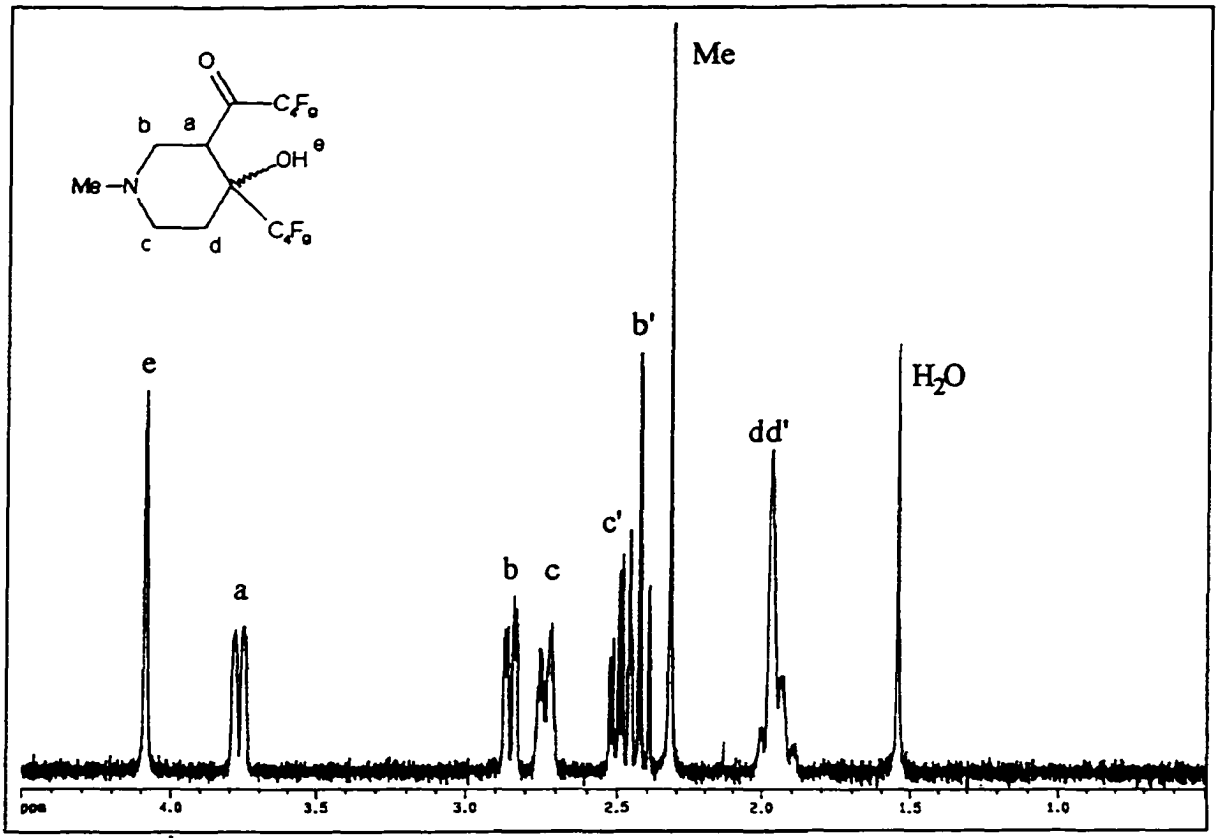

Figure 57 ^{1}H NMR spectrum of **63a** in $CDCl_3$ (360 MHz)

5.2.2 Synthesis of fluorinated ligands by epoxide ring opening

Addition of one equivalent of $Na^+(CH_2)^-SO(CH_3)_2$[156] to bis-(3,5-bis(trifluoromethyl)phenyl) ketone at -10 °C in DMF / THF resulted in quantitative formation of the desired epoxide product **65** (Scheme 24). **65** was isolated as colorless crystals by recrystallization of the crude product from a toluene / hexane mixture and was characterized by NMR and mass spectroscopy. The ^{1}H NMR resonance of the epoxide ring CH_2 protons showed an unusual dependency of the chemical shift on solvents. It appears at 2.22 ppm in C_6D_6 solution but moves to 3.36 ppm in $CDCl_3$.

Nucleophilic epoxide ring opening by cyclopentadienyl anion was studied by Fujisawa[157]. Normally, elevated temperatures are necessary because of the low

nucleophilicity of the cyclopentadienyl anion, and as a result, unwanted cyclopentadiene dimerization is a common problem for this reaction. However, in the present case, the enhanced electrophilicity of epoxide **65** due to the electron withdrawing trifluoromethyl groups, results in smooth nucleophilic attack at room temperature. Thus, addition of 1.5 equivalents of CpNa to **65** in THF gave the desired product **66** in 70 % yield. Ligand **66** was isolated as a pale yellow crystalline solid that contains two isomers **66a** and **66b** in an initial 2:1 ratio (Figure 58). Isomerization takes place slowly between these two isomers and reaches equilibrium (1:1 ratio) after two days in $CDCl_3$ at room temperature (Scheme 24). It is interesting to note that **66c** could not be detected; it is unclear however, whether this isomer is simply not formed or if it is formed initially and isomerizes rapidly to **66a** and **b**.

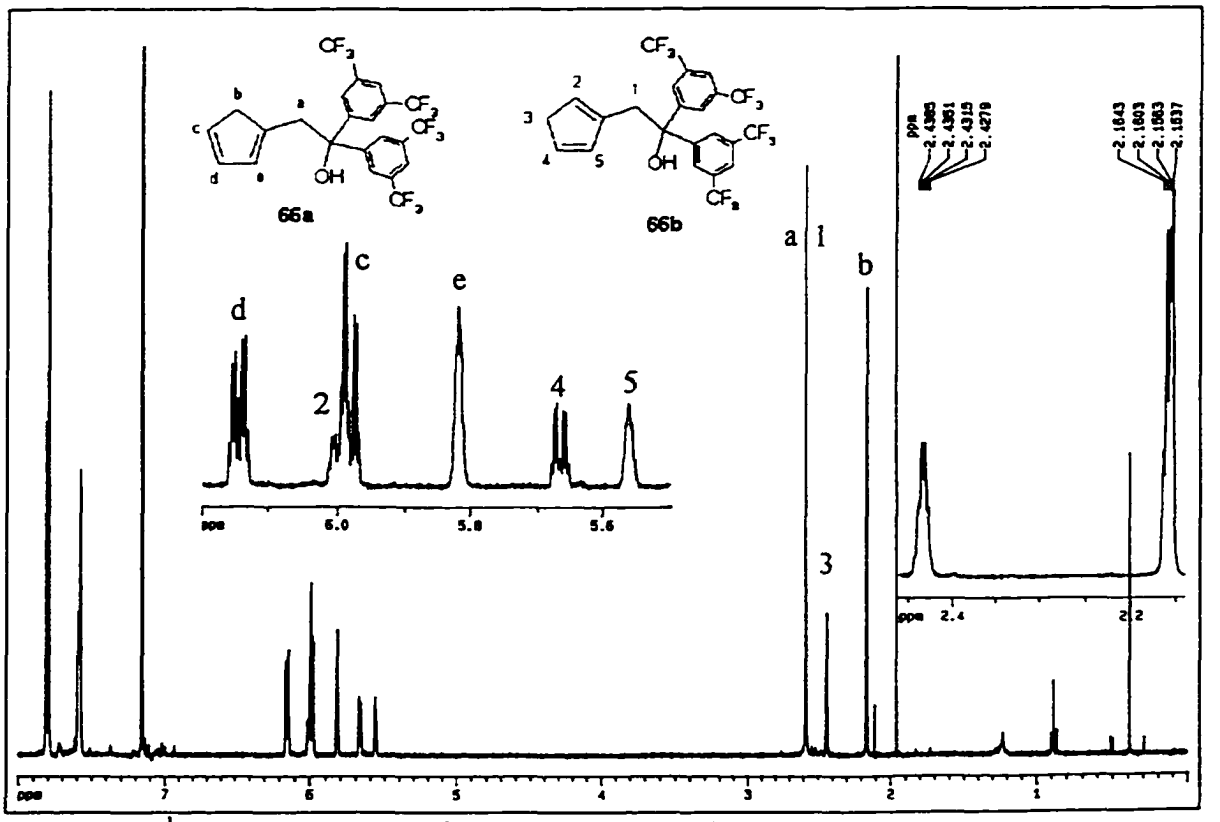

Figure 58 ^{1}H NMR spectrum of **66a** and **b** in C_6D_6 (360 MHz)

In contrast to the cyclopentadienyl anion, nucleophilic addition of tetramethyl cyclopentadienyl or fluorenyl anions to **65** led only to complex mixtures of unidentifiable products. The desired products **XXXXV** or **XXXXVI** did not form, presumably due to the bulkiness of these nucleophiles. (Scheme 24)

Scheme 24

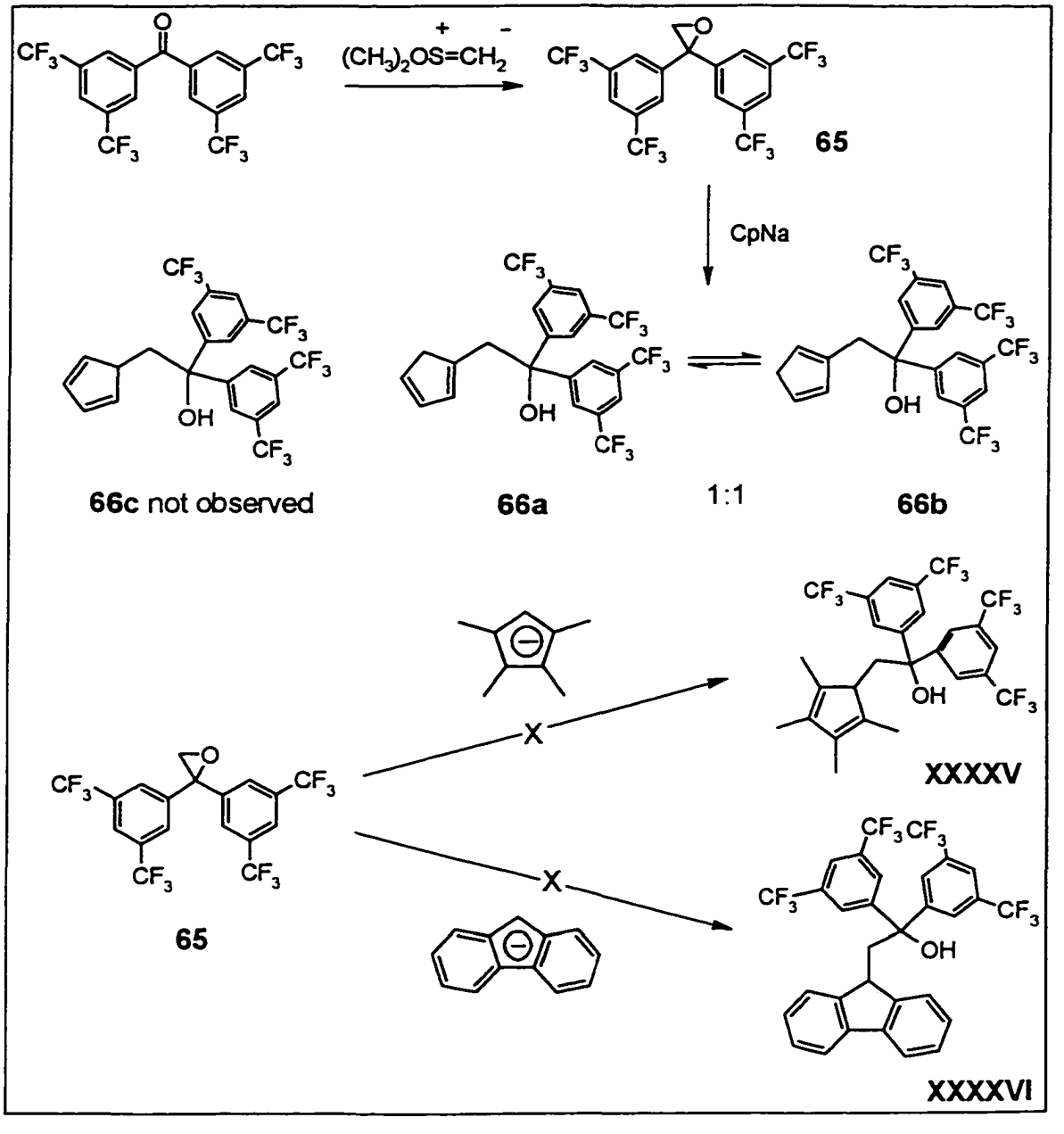

5.3 Zirconium complexes with cyclopentadienyl-alkoxide ligand 66

Reaction of tetrabenzyl zirconium with **66a** or **b** resulted in formation of the expected dibenzyl complexes as indicated by ^{1}H NMR spectroscopy. However, the reaction was not clean, and it was not possible to isolate the pure dibenzyl complex **68** from the reaction mixture.

In contrast to the amino diol ligands **28** and **29**, reaction of $Cl_2Zr[N(SiMe_3)_2]_2$ with **66a** and **b** did not result in formation of desired zirconium dichloride complex **67** (Scheme 25). This may be due to the large pK_a difference between the cyclopentadiene and the alcohol which results in a large difference in reaction rate. As a result, the reaction products were a complex mixture of mono(ligand) and bis(ligand) complexes.

Heating one equivalent of $Cl_2Zr(CH_2C_6H_5)_2$·ether and **66** at 70 °C for 20 minutes in toluene cleanly produced $LZrCl_2$·ether **67** which precipitated out as a light brown solid upon addition of hexane (Scheme 25). Unlike the corresponding dichloride complex **40** which is insoluble in C_6D_6 and only slightly soluble in coordinating solvents like THF, **67** is soluble in C_6D_6. The ^{1}H NMR resonances of **67** in C_6D_6 are broad at room temperature indicating some degree of aggregation. Addition of d_8-THF to this NMR sample results in a sharp and well-resolved ^{1}H NMR spectrum indicative of a monomeric structure (Figure 59). Reaction of **67** with two equivalents of $KCH_2C_6H_5$ in toluene results in clean formation of zirconium dibenzyl complex **68**. Complex **68** was isolated as a light yellow crystalline solid by recrystallization from a hexane / toluene mixture and was characterized by NMR spectroscopy. The ^{1}H NMR spectrum of **68** is consistent with C_s molecular symmetry. The two benzyl groups are equivalent but the geminal CH_2 proton of each benzyl group are inequivalent and show an AB pattern. The upfield shift of the two benzyl

ortho protons (6.53 ppm) is consistent with an η^2-bonding mode for the benzyl groups. Although **68** is expected to be a very strong Lewis acid, addition of $B(C_6F_5)_3$ still results in formation of cationic complex **69** as indicated by ^{19}F NMR. Cationic complex **69** does not show any catalytic activity towards olefin polymerization. This may be due to strong association of the counter anion with the highly electrophilic zirconium center such that olefin coordination is diminished.

Scheme 25

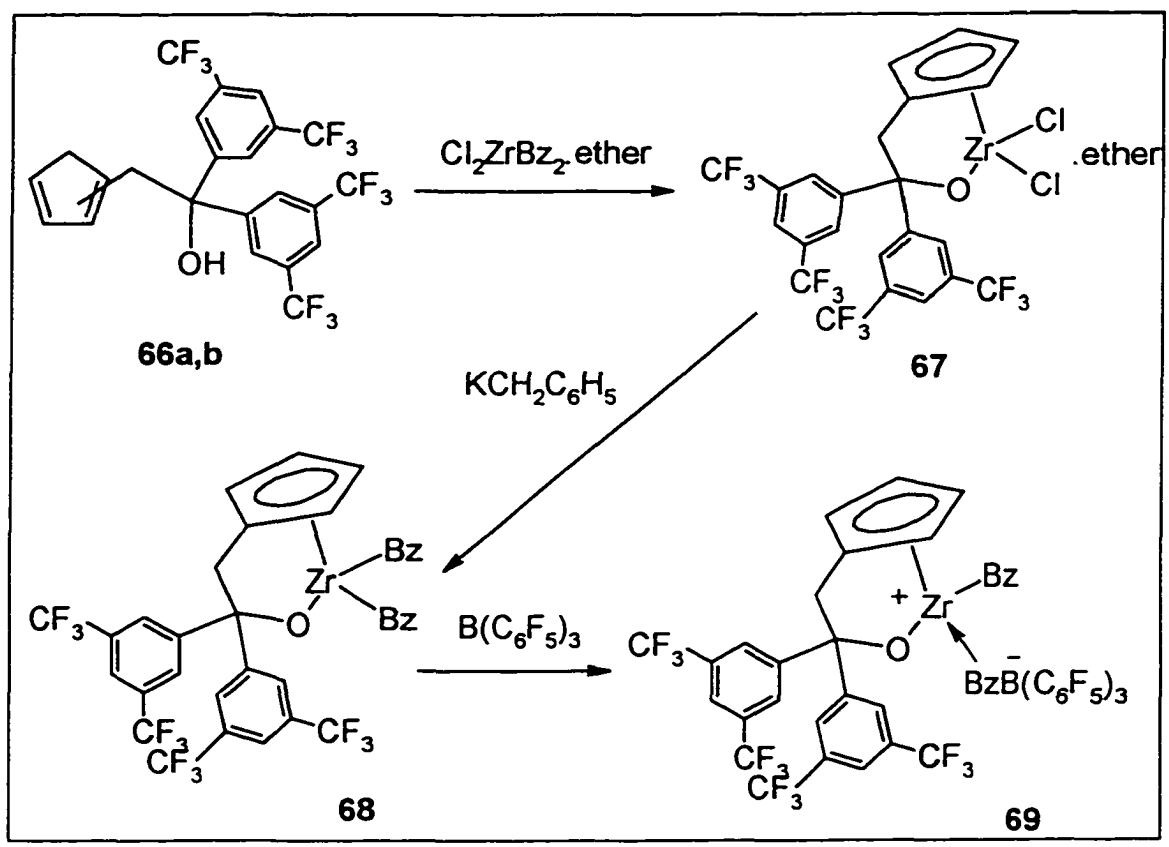

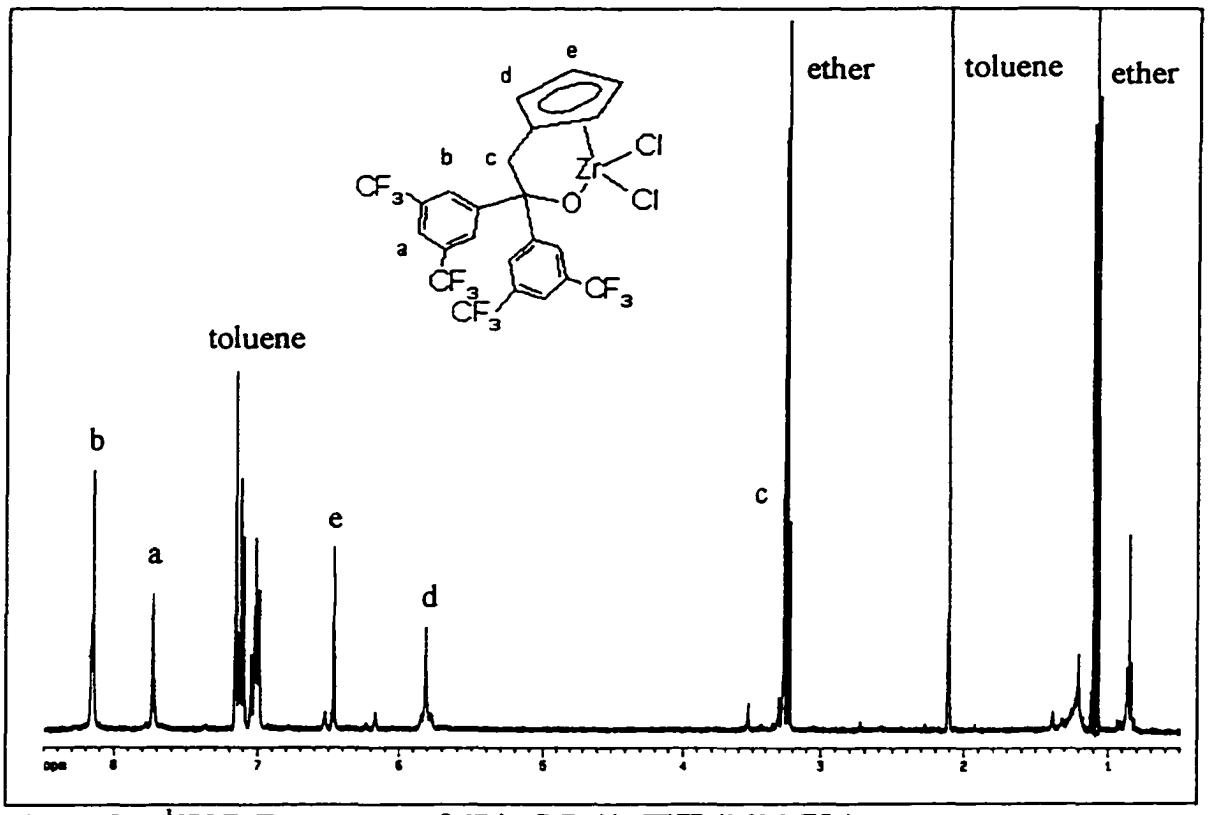

Figure 59 ^{1}H NMR spectrum of **67** in C_6D_6/d_8-THF (360 MHz)

Complex **67** itself exhibits extremely high Lewis acidity. Figure 60 shows that when the NMR sample of **67** is heated at 70 °C overnight, two new resonances appear at 2.8 and 1.0 ppm corresponding to -CH_2CH_3 fragments generated by cleavage of diethyl ether. After the reaction mixture was quenched by D_2O, these two resonances remained unchanged. Ether is well known to be cleaved in the presence of strong Lewis acids[158]. The actual decomposition product was not identified.

Complex **67** also catalyzed the polymerization of ethyl vinyl ether (eq. 38). In contrast, Cp_2ZrCl_2 and complex **40** do not under the same reaction conditions. Lewis acids such as BF_3·ether are well known to catalyze the polymerization of vinyl ether, and the real catalyst is believed to be trace Et^+ [159] generated from cleavage of ether by BF_3. In the

present case, Et^+ may also be the active catalyst as well, since cleavage of ether was observed.

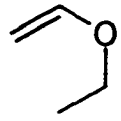

$$\xrightarrow[CDCl_3]{\mathbf{67}} \quad \text{Polyvinylether} \qquad (38)$$

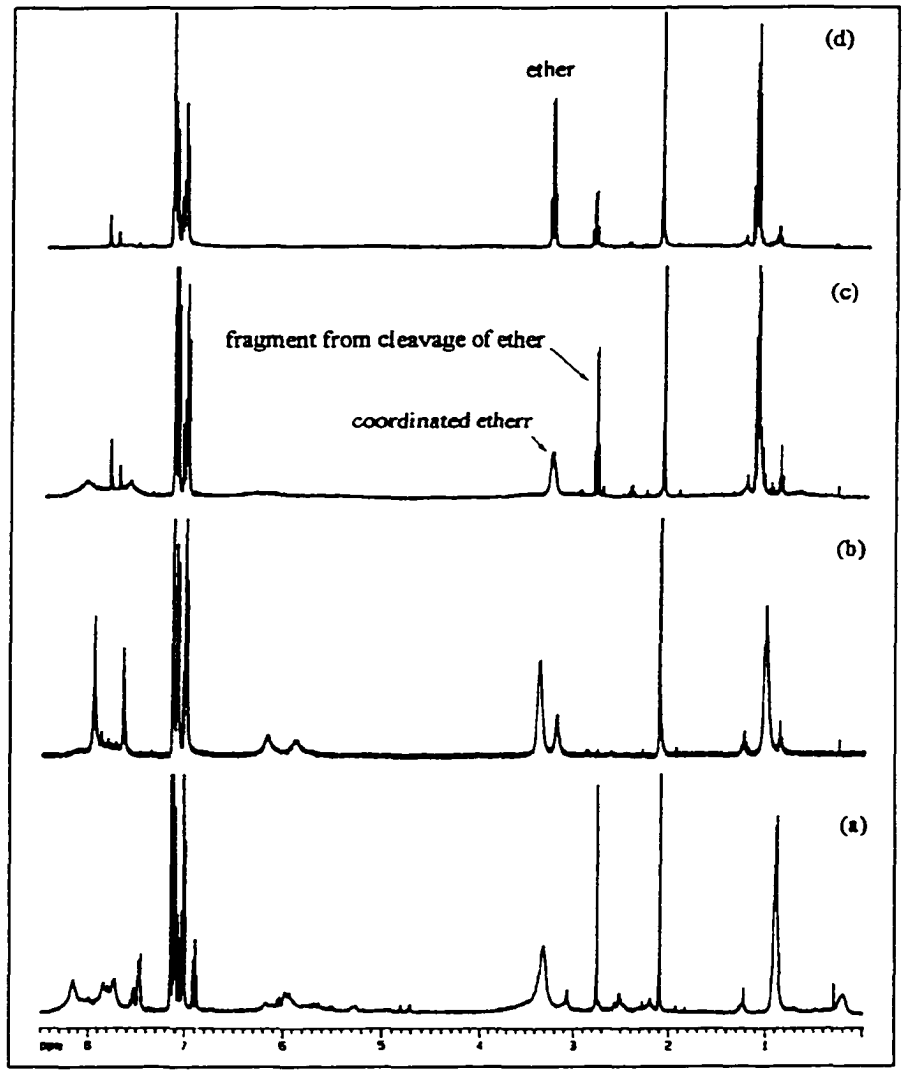

Figure 60 ^1H NMR spectra of the reaction progress when **67** heated at 70 °C in C_6D_6 (360 MHz): (a) at room temperature; (b) at 70 °C; (c) room temperature after the sample was heated at 70 °C overnight; (d) D_2O quenched

CHAPTER 6

CONCLUSIONS AND FUTURE DIRECTION

A series of new amino siloxide and alkoxide ligands were synthesized. These oxygen-based ligands combine steric bulk and donor functionalization and are useful alternative ancillary ligands to the Cp system for organometallic chemistry of group 3 and 4 metals. In addition, these ligands allow preparation of volatile or hydrocarbon soluble group 2 and 3 metal complexes which serve as precursors to metal oxides by MOCVD or sol-gel methods.

The bulky amino siloxide ligand (**4**) allowed isolation of monomeric lanthanide tris(siloxide) complexes. However, the metal centers in these complexes are highly congested due to the bulky *tert*-butyl groups on silicon which leads to one noncoordinated dimethylamino group. In the future work, changing these *tert*-butyl substituents to less bulky *iso*-propyl groups may result in coordination of all the three dimethylamino arms to form highly symmetric octahedral complexes which possess higher volatility.

Amino trialkoxide and trisiloxide ligands are promising for the preparation of highly volatile group 3 metal complexes since such a complex will be highly symmetrical and the metal ion will be completely encapsulated. In terms of organometallic chemistry, these tripodal ligands might be more useful for group 5 and 6 metals since they could allow preparation of metal complexes with metal-ligand multiple bonds (alkylidene, imide, alkylidyne and nitrido complexes).

Group 3 organometallic chemistry with amino siloxide and alkoxide ligands is plagued by ease of formation of anionic 'ate'-complexes. The extra Lewis base donors (in case of ligand **5**) or the flexibility of the ligand framework may be the cause of this problem. If the former is the problem, it should be easily resolved by eliminating the extra

Lewis base donor (in the case of ligand **5**, replacing one of the coordinating arms with a bulky group).

Aminodiol ligands have been used to isolate stable zirconium dialkyl complexes. This ligand system provided a unique environment to study the effects of Lewis base coordination to the metal: small methyl substituents at nitrogen allow strong coordination of the amino group which renders the complex conformationally stable and helps suppress ligand redistribution; in contrast, bulky substituents such as tert-butyl or α-methylbenzyl groups prevent strong coordination by the amino groups and results in fluxional behavior and increased ligand redistribution.

Synthesis of the metallacycle **45** is a special case and has no value to the general synthetic methodology. However, it should be interesting to study the use of **45** (or **54**) as chiral alkyl transfer reagents which can be generated by a one-pot procedure from easily available starting materials. The cationic complex derived from **45** is not active towards ethylene polymerization. However, it may be useful in catalyzing polymerization of more reactive substrates such as styrene and butadiene. Application of cationic complex **62** (or the cationic complex derived from **54**) as Lewis acid catalyst in asymmetric synthesis is also worth further investigation.

Although stable zirconium cationic complexes were easily generated from zirconium dialkyls through alkyl abstraction by $B(C_6F_5)_3$, these cation complexes showed low catalytic activity towards ethylene and 1-hexene polymerization. This result is consistent with the literature that the oxygen based zirconium cationic complexes generally possess low activity for Ziegler-Natta polymerization. Therefore, further work on this area is not expected to generate exciting results.

A cyclopentadienyl ligand with pendant fluorinated alkoxide was synthesized. From preliminary study, the zirconium dichloride complex (**67**) derived from this ligand showed interesting reactivity such as cleaving ether and polymerizing vinylether. Synthesis of other fluorinated alkoxide ligands and an investigation of their applications in organometallic chemistry should be the main focus of future work, and promising results are expected in this area.

CHAPTER 7

EXPERIMENTAL

General Procedures

All manipulations were carried out under an argon atmosphere, with the rigorous exclusion of oxygen and water, using standard glovebox (Braun MB150-GII) or Schlenk techniques, except as noted. Tetrahydrofuran (THF), diethyl ether, hexane and toluene were dried by distillation from sodium benzophenone ketyl under argon immediately prior to use. Anhydrous metal chlorides (Ce, Yb and Y) were prepared from the hydrated salts by prolonged reflux in neat $SOCl_2$ followed by vacuum distillation and drying at 150 °C (10^{-2} torr) for 16 to 20 h. Lanthanide silylamides, $Ln[N(SiMe_3)_2]_3$ (Ln = Ce, Yb, Y), barium silylamide, $Ba[N(SiMe_3)_2]_2 \cdot 2THF$, zirconium bis(silyamide) dichloride, $Cl_2Zr[N(SiMe_3)_2]_2$, zirconium dibenzyl dichloride, $Cl_2Zr(CH_2C_6H_5)_2$, and zirconium tetrabenzyl, $Zr(CH_2C_6H_5)_4$, were prepared as reported in the literature [79-82].

^1H, ^{13}C, ^{29}Si and ^{89}Y NMR spectra were recorded on a Bruker WM-250 MHz or a Bruker AMX-360 MHz spectrometer. Spectra were recorded in C_6D_6 or C_7D_8 solvent, previously distilled from sodium under argon, using 5 mm tubes fitted with a teflon valve (Brunfeldt). All two-dimensional spectra (e.g., ^1H-COSY, ^1H-^{13}C correlated spectra, NOE difference and NOESY spectra) were recorded on the Bruker AMX-360 MHz spectrometer. ^{29}Si spectra were recorded using DEPT or INEPT pulse sequences as appropriate. ^1H and ^{13}C NMR spectra were referenced to residual solvent resonances; ^{29}Si and ^{89}Y NMR were referenced to external TMS and 3M YCl_3 in D_2O, respectively. Mass spectra were recorded on a Finnegan 3300 or a Kratos Concept H spectrometer using chemical ionization and electron impact (70eV) sources, respectively. Melting points were recorded using a Reichert hot stage and are not corrected. Infrared spectra were recorded on a Bruker IFS 25 FT instrument as nujol mull or neat oils on KBr disks. X-ray crystallographic details are given in

Appendix. Elemental analyses were performed by Canadian Microanalytical, Delta, B.C or Atlantic Microanalytical, Atlanta, Ga.

tert-Butylbis(N,N-dimethylaminopropyl)silane, $HSiBu^t[(CH_2)_3NMe_2]_2$. (1) A 10% solution of KOH in water (250 mL) was added dropwise to a solution of 25.0 g (157 mmol) $ClCH_2CH_2CH_2NMe_2H^+Cl^-$ cooled to 0 °C, over a period of 20 min. The aqueous layer was extracted with 2 x 250 mL Et_2O and the combined ether phases dried over anhydrous $MgSO_4$. The free-base was isolated as a colorless oil after removal of ether by rotary evaporation (water aspirator).

The Grignard reagent, $ClMgCH_2CH_2CH_2NMe_2$, was prepared by dropwise addition of 15.6 g (127 mmol) of the free amine to 3.50 g (146 mmol) Mg turnings in 300 mL THF. The green-gray Grignard solution was then added rapidly by canula to a stirred solution of 8.30 g (52.9 mmol) t-$BuSiHCl_2$ in 100 mL THF cooled to 0 °C with an ice bath. After addition was complete, the bath was removed and the reaction mixture heated at reflux for 24 h. The reaction mixture was quenched with $Na_2SO_4 \bullet 10H_2O$ and the THF removed under reduced pressure. The residue was extracted with 750 mL Et_2O and the extract dried over anhydrous $MgSO_4$. Filtration and removal of Et_2O from the filtrate afforded **1** as a colorless oil. Yield: 9.3 g (36 mmol, 68 %). b.p. 59 °C (10^{-2} Torr). ^1H NMR (C_6D_6): δ 3.65 (t, 1H, Si*H*, $^3J_{HH}$ = 3.2 Hz), 2.14 (t, 4H, CH_2N, $^3J_{HH}$ = 7.1 Hz), 2.07 (s, 12H, NMe_2), 1.52 (m, 4H, $CH_2CH_2CH_2$), 0.92 (s, 9H, CMe_3), 0.59 (m, 4H, SiCH_2). $^{13}C\{^1H\}$ NMR (C_6D_6): δ 63.22 (CH_2N), 45.61 (NMe_2), 27.94 (CMe_3), 23.79 ($CH_2CH_2CH_2$), 16.93 (CMe_3), 7.43 (SiCH_2). $^{29}Si\{^1H\}$ NMR (C_6D_6): δ 5.5 ppm. IR: 2095 cm^{-1} (vs, υ Si-H). MS (CI): m/z 258 (M^+), 201 (M^+ - t-Bu), 172 (M^+ - $CH_2CH_2CH_2NMe_2$). Anal. Calcd. for $C_{14}H_{34}N_2Si$: C, 65.04; H, 13.26; N, 10.84. Found: C, 64.96; H, 13.21; N, 10.53.

Bis(tert-butyl)(N,N-dimethylaminopropyl)silane, $HSiBu^t_2(CH_2)_3NMe_2$ (2) This compound was prepared from t-Bu_2SiHCl by the procedure detailed above for 1 except that the reaction mixture was refluxed for 48 h following addition of the Grignard reagent. The product was isolated as a colorless air stable liquid. Yield: 58%. b.p. 41 °C (10^{-2} torr) ^1H NMR (C_6D_6): δ 3.24 (t, 1H, Si-*H*, $^3J_{HH}$ = 2.6 Hz), 2.18 (t, 2H, CH_2N, $^3J_{HH}$ = 7.6 Hz), 2.14 (s, 6H, NMe_2), 1.54 (m, 2H, $CH_2CH_2CH_2$), 0.93 (s, 18H, CMe_3), 0.53 (m, 2H, $SiCH_2$). $^{13}C\{^1H\}$ NMR (C_6D_6): δ 63.41 (CH_2N), 45.55 (NMe_2), 28.87 (CMe_3), 25.07 ($CH_2CH_2CH_2$), 18.90 (CMe_3), 6.54 ($SiCH_2$). $^{29}Si\{^1H\}$ NMR (C_6D_6): δ 14.4 ppm. IR: 2092 cm^{-1} (vs, υ Si-H). MS (CI): m/z 230 (M^+ +1), 171 (M^+ - t-Bu). Anal. Calcd for $C_{13}H_{31}NSi$: C, 68.04; H, 13.62; N, 6.10. Found: C, 68.11; H, 13.40; N, 6.07.

tert-Butylbis(N,N-dimethylaminopropyl)silanol, $HOSiBu^t[(CH_2)_3NMe_2]_2$ (3) A 500 mL flask was charged with 1 (9.0 g , 35 mmol) and 100 mL water and cooled to 0 °C with an ice bath. A solution of 10% aqueous HCl (100 mL) was added and the now homogeneous mixture refluxed 40 h exposed to air. The reaction mixture was then neutralized with aqueous KOH and the oily product which separated was extracted with diethyl ether. After removal of Et_2O, the residue was purified by sublimation to afford colorless crystals of silanol 3. Yield: 8.2 g (30 mmol , 86 %). m.p. 43-44 °C. ^1H NMR (C_6D_6): δ 2.55 (m, 4H, CH_2N), 2.02 (s, 12H, NMe_2), 1.67 (m, 4H, $CH_2CH_2CH_2$), 1.12 (s, 9H, CMe_3), 0.70 (m, 4H, $SiCH_2$). $^{13}C\{^1H\}$ NMR (C_6D_6): δ 63.09 (CH_2N), 45.24 (NMe_2), 26.74 (CMe_3), 22.21 ($CH_2CH_2CH_2$), 18.81 (CMe_3), 11.61 ($SiCH_2$). $^{29}Si\{^1H\}$ NMR (C_6D_6): δ 10.5 ppm. IR: 3349 cm^{-1} (br w, υ SiO-H). MS (CI): m/z 275 (M^+ + 1), 259 (M^+ - CH_3), 217 (M^+ - t-Bu), 188 (M^+ - $CH_2CH_2CH_2NMe_2$). Anal. Calcd for $C_{14}H_{34}N_2OSi$: C, 61.25; H, 12.48; N, 10.21. Found: C, 60.93; H, 12.06; N, 9.99.

Bis(tert-butyl)(N,N-dimethylaminopropyl)silanol, $HOSiBu^t_2(CH_2)_3NMe_2$ (4)

This silanol was prepared by the procedure outlined above for **3** except the acidic solution was refluxed for 72 h prior to basic workup. Yield: 93 %. b.p. 58-60 °C (10^{-2} torr) ^{1}H NMR (C_6D_6): δ 1.93 (m, 2H, CH_2N), 1.85 (s, 6H, NMe_2), 1.53 (m, 2H, $CH_2CH_2CH_2$), 1.16 (s, 18H, CMe_3), 0.65 (m, 2H, SiCH_2). ^{13}C{^{1}H} NMR (C_6D_6): δ 62.56 (CH_2N), 45.01 (NMe_2), 27.98 (CMe_3), 22.46 ($CH_2CH_2CH_2$), 20.89 (CMe_3), 10.85 (SiCH_2). ^{29}Si{^{1}H} NMR (C_6D_6): δ 8.0 ppm. IR: 3362 cm^{-1} (br m, υ SiO-H). MS (CI): m/z 246 (M^+ + 1), 230 (M^+ - CH_3), 188 (M^+ - t-Bu). Anal. Calcd for $C_{13}H_{31}NOSi$: C, 63.60; H, 12.73; N, 5.71. Found: C, 62.45; H, 12.47; N, 5.80.

$HOSi^tBu[o\text{-}C_6H_4(CH_2NMe_2)]_2$ (5) A solution of Li[*o*-$C_6H_4(CH_2NMe_2)$][88] (10.1 g, 71.5 mmol) in 80 mL of THF was added rapidly by canula to a 250 mL flask containing t-$BuSiCl_3$ (6.45 g, 33.7 mmol) in 50 mL of THF precooled to 0 °C. The reaction mixture was stirred overnight at room temperature and then quenched with $Na_2SO_4 \cdot 10H_2O$. The solids were filtered off and the filtrate was evaporated to an oily residue under reduced pressure. The oil was washed with a 100 mL portion of 10% aqueous KOH at 0 °C and extracted with 500 mL of diethyl ether. The ether extract was dried over anhydrous $MgSO_4$, filtered, and the solvent was removed from the filtrate by rotary evaporation. The yellow oil was recrystallized from toluene to afford slightly yellow crystals of the silanol. Yield: 10.3 g (27.8 mmol, 82.5%). Mp: 63 - 65 °C. ^{1}H NMR (C_6D_6): δ 8.75 (s, 1H, *H*OSi), 7.17-8.10 (m, 8H, arylC*H*), 3.42 (d, 2H, $CH_aH_bNMe_2$, $^2J_{HH}$ = 12.8 Hz), 3.05 (d, 2H, $CH_aH_bNMe_2$, $^2J_{HH}$ = 12.8 Hz), 1.85 (s, 12H, NMe_2), 1.40 (s, 9H, CMe_3). ^{13}C{^{1}H} NMR (C_6D_6): δ 145.0, 139.0, 136.3, 130.8, 129.4, 126.4 (aryl*C*), 64.3 (CH_2N), 44.5 (NMe_2), 27.7 (CMe_3), 20.1 (CMe_3). ^{29}Si{^{1}H} NMR (C_6D_6): δ -6.86. MS(CI): *m/z* 371 (M^+ + 1), 355 (M^+ - Me), 313 (M^+ - ^{t}Bu), 236 (M^+ -

$C_6H_4(CH_2NMe_2)$). Anal. Calcd for $C_{22}H_{34}N_2OSi$: C, 71.30; H, 9.25; N, 7.56. Found: C, 71.95; H, 9.15; N, 7.56.

Lanthanide Complexes The lanthanide complexes described below were all prepared in an argon-filled glove box by dropwise addition (30 min) of the appropriate number of equivalents of silanol in toluene solution to $Ln[(N(SiMe_3)_2]_3$ in toluene. After stirring for 1 h, the solvent was removed in vacuo and the residue recrystallized from toluene-hexane mixtures at -30 °C.

$Y[OSiBu^t((CH_2)_3NMe_2)_2]_3$ (6) The complex was isolated as a viscous, hexane soluble oil which slowly crystallized on standing. Yield: 65 % m.p. 72-75 °C ^1H NMR (C_6D_6): δ 2.32 (m, 12H, CH_2N), 2.27 (s, 36H, NMe_2), 1.76 (m, 12H, $CH_2CH_2CH_2$), 1.11 (s, 27H, CMe_3), 0.69 (m, 12H, $SiCH_2$). $^{13}C\{^1H\}$ NMR (C_6D_6): δ 64.32 (CH_2N), 46.36 (NMe_2), 27.52 (CMe_3), 23.24 ($CH_2CH_2CH_2$), 19.43 (CMe_3), 12.52 ($SiCH_2$). $^{29}Si\{^1H\}$ NMR (C_6D_6): δ -1.7 ($^2J_{Si-Y}$ = 5.8 Hz). MS (CI): m/z 909 (M^+), 852 (M^+ - t-Bu), 823 (M^+ - $CH_2CH_2CH_2NMe_2$). Anal. Calcd for $C_{42}H_{99}N_6O_3Si_3Y$: C, 55.47; H, 10.97; N, 9.24. Found: C, 55.56; H, 10.51; N, 8.76.

$Y[OSiBu^t_2(CH_2)_3NMe_2]_3$ (7) Yield: 84 %. m.p. 117-119 °C. ^1H NMR (C_6D_6): δ 2.36 (s, 18H, NMe_2), 2.30 (t, 6H, CH_2N, $^3J_{HH}$ = 6.5 Hz), 1.79 (m, 6H, $CH_2CH_2CH_2$), 1.17 (s, 54H, CMe_3), 0.65 (t, 6H, $SiCH_2$, $^3J_{HH}$ = 7.1 Hz). $^{13}C\{^1H\}$ NMR (C_6D_6): δ 64.03 (CH_2N), 47.54 (NMe_2), 29.36 (CMe_3), 23.62 ($CH_2CH_2CH_2$), 21.34 (CMe_3), 10.84 ($SiCH_2$). $^{29}Si\{^1H\}$ NMR (C_6D_6): δ -2.7 ($^2J_{Si-Y}$ = 6.0 Hz). MS (CI): m/z 821 (M^+), 764 (M^+ - t-Bu). Anal. Calcd for $C_{39}H_{90}N_3O_3Si_3Y$: C, 56.96; H, 11.03; N, 5.11. Found: C, 56.31; H, 10.93; N, 5.06.

$Ce[OSiBu^t_2(CH_2)_3NMe_2]_3$ (8) Yield: 71 %. m.p. 142-144 °C. ^1H NMR (C_6D_6, 30 °C): δ 3.04 (54H, CMe_3, f.w.h.m. = 5 Hz), 2.18 (6H, $CH_2CH_2CH_2$, 31 Hz), 1.48 (6H, $SiCH_2$,

12 Hz), -4.31 (6H, C*H*$_2$N, 49 Hz), -4.8 (18H, N*Me*$_2$, 39 Hz). (-60 °C): δ 6.2 (18H, 120 Hz), 3.0 (9H, 65 Hz), 2.4 (9H, 200 Hz), 0.4 (9H, 140Hz), -1.1 (9H, 110 Hz). MS (CI): m/z 873 (M^+), 816 (M^+ - t-Bu), 787 (M^+ - $CH_2CH_2CH_2NMe_2$), 760 (M^+ - 2 t-Bu). Anal. Calcd for $C_{39}H_{90}CeN_3O_3Si_3$: C, 53.62; H, 10.38; N, 4.81. Found: C, 53.26; H, 10.30; N, 4.79.

Y[OSiBu$^t_2$(CH$_2$)$_3$NMe$_2$]$_3$[OSiBu$^t_2$(CH$_2$)$_3$NMe$_2$H] (9) Yield: 73 %. m.p. 144 - 147 °C. ^{1}H NMR (C_6D_6): δ 1.88 (s, 24H, N*Me*$_2$), 1.32 (s, 72H, C*Me*$_3$). ^{13}C{^{1}H} NMR (C_6D_6, -10 °C): δ 68.97 (*C*H$_2$N), 52.71 (N*Me*$_2$), 34.42 (C*Me*$_3$), 15.57 (Si*C*H$_2$). Other peaks in the ^{1}H and ^{13}C{^{1}H} NMR were obscured by equilibrium concentrations of Y[OSi(t-Bu)$_2$(CH$_2$CH$_2$CH$_2$NMe$_2$)]$_3$ and HOSi(t-Bu)$_2$(CH$_2$CH$_2$CH$_2$NMe$_2$). ^{29}Si{^{1}H} NMR (C_6D_6): δ -6.7 ($^2J_{Si-Y}$ = 6.8 Hz). MS (CI): m/z 952 (M^+ - 2 t-Bu), 821 (M^+ - HOSi(t-Bu)$_2$CH$_2$CH$_2$CH$_2$NMe$_2$)). Anal. Calcd for $C_{52}H_{121}N_4O_4Si_4Y$: C, 58.49; H, 11.42; N, 5.25. Found: C, 58.09; H, 11.20; N, 5.23.

Yb[OSiBu$^t_2$(CH$_2$)$_3$NMe$_2$]$_3$[OSiBu$^t_2$(CH$_2$)$_3$NMe$_2$H] (10) Yield: 76 %. m.p. 140 - 141 °C. No signals were observable in the ^{1}H NMR spectrum of this paramagnetic complex. The highest mass fragment observed in the mass spectrum was m/z 892 (possibly M^+ - 3 $CH_2CH_2CH_2NMe_2$). Anal. Calcd for $C_{52}H_{121}N_4O_4Si_4Yb$: C, 54.22; H, 10.59; N, 4.86. Found: C, 54.22: H, 10.41; N, 4.87.

Li$^+${Y[OSiBu$^t_2$(CH$_2$)$_3$NMe$_2$]$_4$}$^-$ (11) Reaction of equimolar quantities of **9** and $LiCH_2SiMe_3$ in toluene-hexane mixtures afforded **11** as colorless crystals after concentration of the reaction mixture and cooling at -30 °C. Yield: 85 %. m.p. 107-109 °C. ^{1}H NMR (C_7D_8): δ 2.29 (t, 8H, C*H*$_2$N, $^3J_{HH}$ = 6.9 Hz), 2.15 (s, 24H, N*Me*$_2$), 1.73 (m, 8H, CH$_2$C*H*$_2$CH$_2$), 1.21 (s, 72H, C*Me*$_3$), 0.72 (m, 8H, SiC*H*$_2$). ^{13}C{^{1}H} NMR (C_7D_8): δ 64.1 (*C*H$_2$N), 45.8 (N*Me*$_2$), 29.9 (C*Me*$_3$), 23.9 (CH$_2$*C*H$_2$CH$_2$), 21.6 (*C*Me$_3$), 12.6 (Si*C*H$_2$). ^{29}Si{^{1}H} NMR (C_7D_8): δ 1.2

($^2J_{Si-Y}$ = 4.9 Hz). Anal. calcd for $C_{52}H_{120}LiN_4O_4Si_4Y$: C, 58.17; H, 11.26; N, 5.22. Found: C, 57.65; H, 11.03; N, 4.95.

{Ba[OSi(^{t}Bu)$_2$((CH$_2$)$_3$NMe$_2$)][N(SiMe$_3$)$_2$]}$_2$ (12a) A solution of HOSi(^{t}Bu)$_2$((CH$_2$)$_3$NMe$_2$) (0.514 g, 2.09 mmol) in 25 mL of toluene was added dropwise over 15 minutes to a stirred solution of Ba[N(SiMe$_3$)$_2$]$_2$[THF]$_2$ (1.259 g, 2.09 mmol) in 25 mL of toluene in the glovebox. After an additional 30 minutes of stirring, the solvent was removed by rotary evaporation and the white powder redissolved in a minimum of hexane. Cooling at -30 °C afforded colourless crystals of **12a**. Yield: 0.74 g (66 %). M.p. 143-145 °C. NMR data are collected in Tables 5 and 6 in Chapter 2. Anal. Calcd for $C_{38}H_{96}Ba_2N_4O_2Si_6$: C, 42.09; H, 8.92; N, 5.17 %. Found: C, 41.32; H, 8.61; N, 4.98 %.

{Ba[OSi(^{t}Bu)$_2$((CH$_2$)$_3$NMe$_2$)][N(SiMe$_3$)$_2$][THF]}$_2$ (12b) Compound **12b** was isolated directly from the reaction mother liquors using the same procedure as given for **12b** but using hexane rather than toluene as solvent. Yield: 82 %. M.p. 94-95 °C. NMR data are collected in Tables 5 and 6 in Chapter 2. A satisfactory elemental analysis could not be obtained due to the tendency of **12b** to lose THF. Despite prolonged vacuum drying, the analytical data was consistently low in carbon and hydrogen and high in nitrogen, consistent with loss of weakly coordinated THF. A typical analysis is as follows: Calcd. for $C_{46}H_{112}Ba_2N_4O_4Si_6$: C, 44.97; H, 9.19; N, 4.56 %. Found: C, 42.86; H, 8.36; N, 4.65 %.

Ba[OSi(^{t}Bu)$_2$((CH$_2$)$_3$NMe$_2$)]$_2$ (13) Compound **13** was prepared using a procedure analogous to that described for **12a** above except that a 2:1 ratio of silanol to silylamide was employed. The product **13** was isolated as a colourless oil of extremely high hexane solubility. We were unable to obtain satisfactory elemental data on this compound, presumably because of presence of trace impurities. The low volatility of this compound did not allow purification by

distillation because significant decomposition occurred during heating. Similarly, attempts to obtain mass spectroscopic data for **13** led to extensive fragmentation under chemical ionization conditions and the compound is not compatible with other techniques due to reaction with the common matrix solvents employed. Despite these difficulties, the extremely clean NMR spectra obtained in d_8-THF indicate that **13** is of reasonably high purity and that the impurities which affect the elemental data are minor in nature. NMR data are collected in Tables 5 and 6 in Chapter 2.

$HSi^tBu_2CH_2CH{=}CH_2$ (14) The Grignard reagent, $BrMgCH_2CH{=}CH_2$, was prepared by dropwise addition of allyl bromide (8.4 g, 0.069 mol) in 50 mL of THF to Mg turnings (2.4 g, 0.10 mol) in 100 mL of THF at 0°C. The green-gray Grignard solution was then added rapidly by canula to a stirred solution of 9.2 g (0.052 mol) HSi^tBu_2Cl in 100 mL of THF cooled with an ice bath. After addition was complete, the reaction mixture was refluxed overnight. The reaction mixture was then quenched with $Na_2SO_4{\bullet}10H_2O$. The precipitate which formed was removed by filtration and the THF was removed from the filtrate under reduced pressure. The residue was extracted with 200 mL of hexane and the extract dried over anhydrous $MgSO_4$. Filtration and removal of hexane from the filtrate afforded **14** as a colorless oil. Yield 8.8 g (0.048 mol, 92 %). ^1H NMR ($CDCl_3$): δ 5.9 (m, 1H, C*H*=), 4.9 (m, 2H, CH_2=), 3.34 (t, 1H, *H*Si, $^3J_{HH}$ = 2.8 Hz), 1.67 (m, 2H, CH_2), 1.01 (s, 18H, CMe_3). $^{13}C\{^1H\}$ NMR ($CDCl_3$): δ 137.0 (HC=), 113.14 (H_2C=), 28.81 (CMe_3), 19.26 (*C*Me_3), 16.91 (CH_2Si). $^{29}Si\{^1H\}$ NMR ($CDCl_3$) δ 12.10. IR: 2089 cm^{-1}(vs, υ Si-H). MS (CI): *m/z* (relative intensity) 183(45) [M^+ - H], 127(31) [M^+ - ^{t}Bu], 101(100) [M^+ - ^{t}Bu - C_2H_3], 73(75) [possibly $C_5H_{13}^+$].

$HSi^tBu_2CH_2CH_2CH_2I$ (15) A solution of disiamylborane (0.054 mol) in 100 mL of THF was added rapidly by canula to a solution of **14** (8.8 g, 0.048 mol) in 100 mL of THF

precooled to -78 °C. The reaction mixture was stirred for 4 h. At the end of this period, 1 mL of methanol was added to quench the excess borane, followed by addition of I_2 (14.0 g, 0.055 mol). A solution of KO^{t}Bu (6.72 g, 0.060 mol) in 20ml of methanol was added dropwise at 0°C to the reaction mixture. After the addition was complete, a 10 % solution of $Na_2S_2O_3$ in water (20 mL) was added to destroy any excess I_2. The solvent was removed from the reaction mixture under reduced pressure and the residue extracted with 250 mL of diethyl ether. Removal of ether by rotary evaporation afforded an oil. Vacuum distillation (10^{-2} Torr) produced **15** as the major component (ca. 90 %) of the 64-92 °C fraction. Yield: 14.5 g (ca. 88 %) ^{1}H NMR ($CDCl_3$): δ 3.31 (t, 1H, *H*Si, $^3J_{HH}$ = 2.6 Hz), 3.19 (t, 2H, C*H*$_2$I, $^3J_{HH}$ = 7.0 Hz), 1.95 (m, 2H, CH$_2$*CH*$_2$CH$_2$), 0.99 (s, 18H, C*Me*$_3$), 0.69 (m, 2H, C*H*$_2$Si). ^{13}C{^{1}H} NMR ($CDCl_3$): δ 31.4 (*C*H$_2$I), 28.7 (C*Me*$_3$), 18.9 (*C*Me$_3$), 11.3 (CH$_2$*C*H$_2$CH$_2$), 10.8 (*C*H$_2$Si). ^{29}Si{^{1}H} NMR ($CDCl_3$): δ 13.1. MS (CI): *m/z* (relative intensity) 311(8) [M$^+$ - H], 255(8) [M$^+$ - ^{t}Bu], 185(17) [M$^+$ - I], 73(100) [$C_5H_{13}^+$].

HSi^{t}Bu$_2$CH$_2$CH$_2$CH$_2$NH$_2$ (16) Potassium phthalamide (2.5 g, 0.014 mol) and **18** (2.8 g, 0.091 mol) were weighed into a round bottom flask and dissolved in 20 mL DMF. The mixture was refluxed for an hour followed by removal of the DMF solvent under reduced pressure. The residue was extracted with 200 mL of hexane and the extract stripped to dryness under vacuum to produce a yellow oil. The yellow oil was dissolved in 50 mL of methanol, $NH_2NH_2 \bullet H_2O$ (5 mL) was added and the mixture refluxed for 1 h.. The white precipitate which formed was filtered off and the solvent removed from the filtrate to afford crude **16**. The crude amine was washed with water and extracted into hexane. Removal of hexane afforded pure **16**. Yield: 1.33 g (73 %). ^{1}H NMR ($CDCl_3$): δ 3.29 (t, 1H, *H*Si, $^3J_{HH}$= 2.5 Hz), 2.67 (t, 2H, C*H*$_2$N), 1.92 (br, 2H, N*H*$_2$), 1.58 (m, 2H, CH$_2$C*H*$_2$CH$_2$), 0.98 (s, 18H, C*Me*$_3$),

0.58 (m, 2H, CH_2Si). $^{13}C\{^1H\}$ NMR ($CDCl_3$): δ 45.2 (*C*H_2N), 30.5 (CH_2*C*H_2CH_2), 28.7 (*C*Me_3), 18.8 (*C*Me_3), 5.9 (*C*H_2Si). $^{29}Si\{^1H\}$ ($CDCl_3$): δ 14.3. IR: 2082 cm^{-1} (vs, υ H-Si). MS (CI): *m/z* (relative intensity) 230(11) [M^+ + 29], 202(34) [M^+ + 1], 201(97) [M^+], 186(10) [M^+ - Me], 144(100) [M^+ - ^{t}Bu].

$(HSi^tBu_2CH_2CH_2CH_2)_3N$ (17) A solution of **15** (8.8 g, 0.028 mol) in 150 mL CH_3CN was added dropwise over 3 h to a refluxing solution of **16** (2.4 g, 0.012 mol) and excess K_2CO_3 (16 g) in 250 mL of CH_3CN. After addition of **15** was complete, the reaction mixture was refluxed for a further 3 h until ^1H NMR indicated that there was no primary or secondary amine remaining. CH_3CN was removed under reduced pressure and the residue was extracted with 200 mL of hexane. Yield: 5.1 g (75 %). ^1H NMR (C_7D_8): δ 3.56 (t, 3H, *H*Si, $^3J_{HH}$ = 2.7 Hz), 2.49 (t, 6H, CH_2N, $^3J_{HH}$ = 7.1), 1.73 (m, 6H, $CH_2CH_2CH_2$), 1.06 (s, 54H, CMe_3), 0.74 ppm (m, 6H, CH_2Si). $^{13}C\{^1H\}$ NMR (C_7D_8): δ 58.2 (*C*H_2N), 29.1 (CMe_3), 25.5 ($CH_2CH_2CH_2$), 19.1 (*C*Me_3), 7.0 (*C*H_2Si). $^{29}Si\{^1H\}$ NMR (C_7D_8): δ 19.7. IR: 2089 cm^{-1} (vs, υ H-Si). MS (CI): *m/z* (relative intensity) 568(8) [M^+ - H], 512(3) [M^+ - ^{t}Bu], 384(100) [M^+ - $CH_2CH_2CH_2Si^tBu_2H$], 328(76) [M^+ - $CH_2CH_2CH_2Si^tBu_2H$ - ^{t}Bu].

$(HOSi^tBu_2CH_2CH_2CH_2)_3N$ (18) $CuCl_2$ (8.5 g, 0.063 mol) and CuI (1.0 g, 0.0052 mol) were added to a solution of **17** (4.1 g, 0.0072 mol) in 100 mL CH_3CN and the reaction mixture stirred 3 h at room temperature. CH_3CN was removed under reduced pressure and 30 mL of 17% NH_4OH in H_2O was added. The reaction mixture was extracted with hexane (250 mL) and the extract taken to dryness under reduced pressure. The brown oil that remained was dissolved in 50 mL acetone and 1.5 g oxalic acid was added. After stirring at room temperature for 0.5 h, the acetone was removed and the residue was washed repeatedly with hexane. Aqueous KOH (10 %) was added and the solution extracted with

hexane. Removal of hexane under vacuum produced **18** as an oil. Further purification by distillation gave **18** as a viscous, light yellow oil. Yield: 3.4 g (76 %). Bp: 120-140 °C (0.1 Torr) ^{1}H NMR (C_6D_6): δ 2.35 (t, 6H, CH_2N, $^3J_{HH}$ = 7.1), 1.73 (m, 6H, $CH_2CH_2CH_2$), 1.10 (s, 54H, CMe_3), 0.59 (t, 6H, CH_2Si, $^3J_{HH}$ = 7.5). ^{13}C{^{1}H} NMR (C_6D_6): δ 58.2 (CH_2N), 28.1 (CMe_3), 21.6 (CMe_3), 20.8 ($CH_2CH_2CH_2$), 9.2 (CH_2Si). ^{29}Si{^{1}H} NMR (C_6D_6): δ 10.7. MS(EI): *m/z* (relative intensity) 619(77) [M$^+$], 560(88) [M$^+$ - ^{t}Bu], 430(100) [M$^+$ - $CH_2CH_2Si^tBu_2OH$]. Anal. Found: C, 62.64; H, 11.65; N, 2.12. Calc. for $C_{33}H_{75}NO_3Si_3$: C, 64.11; H, 12.23; N, 2.26.

Y[(OSi^{t}Bu$_2$CH$_2$CH$_2$CH$_2$)$_3$N] (19) In the glove box, a 10 mL of toluene solution of yttrium silylamide (0.36 g, 0.63 mmol) was placed into a 50 mL Erlenmeyer flask and stirred rapidly. A 10 mL toluene solution of **18** (0.38 g, 0.63 mmol) was added dropwise over a period of 5 minutes. Volatiles were removed under reduced pressure immediately after addition of **18** to afford **19** as light yellow oil which solidified over a few hours. ^{1}H NMR of **19** as THF adduct (C_6D_6): δ 4.13 (m, br, 4H, THF CH_2O), 2.74 (m, 3H, CH_{2a}N), 1.52 (m, 3H, CH_{2b}N), 1.92 (m, 3H, $CH_2CH_{2a}CH_2$), 1.65 (m, 3H, $CH_2CH_{2b}CH_2$), 1.37 (m, 4H, THF CH_2CH_2O), 1.18 (s, 27H, CMe_{3a}), 1.16 (s, 27H, CMe_{3b}), 0.80 (m, 3H, CH_{2a}Si), 0.43 (m, 3H, CH_{2b}Si). ^{13}C{^{1}H} NMR (C_6D_6): δ 71.1 (THF, CH_2O), 57.9 (CH_2N), 28.9 (CMe_{3a}), 28.6 (CMe_{3b}), 25.2 (THF, CH_2CH_2O), 23.7 ($CH_2CH_2CH_2$), 21.9 (C_aMe_3), 20.6 (C_bMe_3), 9.0 (CH_2Si). ^{29}Si{^{1}H} NMR (C_6D_6): δ -0.84. ^{89}Y NMR (C_6D_6): δ 289. MS(EI): *m/z* (relative intensity) 688 (5) [M$^+$-Me], 646 [M$^+$-^{t}Bu] (100).

Y{OSi^{t}Bu[*o*-C$_6$H$_4$(CH$_2$NMe$_2$)]$_2$}{N(SiMe$_3$)$_2$}$_2$ (20) Silanol **5** (1.83 g, 4.95 mmol) and Y[N(SiMe$_3$)$_2$]$_3$ (2.82 g, 4.95 mmol) were weighed into a 250 mL Schlenk tube and dissolved in 200 mL of toluene. The reaction mixture was refluxed overnight and the volatiles

removed under reduced pressure to yield a white solid. Recrystallization from toluene gave colorless crystals of **20**. Yield: 2.75 g (3.53 mmol, 71.3%). Mp: 158 °C. ^{1}H NMR (C_7D_8, -40 °C): δ 8.56 (d, 1H, arylC*H*, J_{HH} = 6.3 Hz), 8.07 (d, 1H, arylC*H*, J_{HH} = 6.1 Hz), 7.90 (d, 1H, arylC*H*, J_{HH} = 7.1 Hz), 7.42 (t, 1H, arylC*H*, J_{HH} = 7.3 Hz), 7.32 (t, 1H, arylC*H*, J_{HH} = 7.3 Hz), 7.0-7.15 (m, 2H, arylC*H*), 6.56 (d, 1H, arylC*H*, J_{HH} = 6.4 Hz), 4.06 (d, 1H, coordinated C*H*$_2$N, $^2J_{HH}$ = 12.5 Hz), 3.26 (d, 1H, noncoordinated C*H*$_2$N, $^2J_{HH}$ = 13.5 Hz), 2.76 (d, 1H, noncoordinated C*H*$_2$N, $^2J_{HH}$ = 13.5 Hz), 1.76 (d, 1H, coordinated C*H*$_2$N), 2.15 (s, 3H, coordinated N*Me*$_2$), 1.78 (s, 3H, coordinated N*Me*$_2$), 1.74 (s, 6H, noncoordinated N*Me*$_2$), 1.43 (s, 9H, SiC*Me*$_3$), 0.63 (s, 9H, silamide C*Me*$_3$), 0.56 (s, 9H, silamide C*Me*$_3$), 0.34 (s, 9H, silamide C*Me*$_3$), 0.22 (s, 9H, silamide C*Me*$_3$). ^{13}C{^{1}H} NMR (C_7D_8, -40 °C): δ 149.8, 149.3, 143.3, 141.5, 141.1, 137.9, 134.6, 134.2, 132.3, 131.3 (aryl*C*, two resonances were not observed), 67.3, 63.6 (*C*H$_2$N), 49.7, 45.3 (coordinated N*Me*$_2$), 44.8 (noncoordinated N*Me*$_2$), 28.1 (C*Me*$_3$), 21.1 (*C*Me$_3$), 5.7, 5.1, 4.7, 3.9 (Si*Me*$_3$). ^{29}Si{^{1}H} NMR (C_7D_8, -40 °C): δ -8.4, -9.5, -12.9, -13.1 (N(*Si*Me$_3$)$_2$), -20.5 (O*Si*^{t}BuAr$_2$, $^2J_{SiY}$ = 4.9 Hz). ^{89}Y NMR (C_6D_6): δ 479. MS(CI): *m/z* 778 (M^+), 763 (M^+ - Me), 721 (M^+ - ^{t}Bu), 644 (M^+ - $C_6H_4(CH_2NMe_2)$), 617 (M^+ - N(SiMe$_3$)$_2$). Anal. Calcd for $C_{34}H_{69}N_4OSi_5Y$: C, 52.40; H, 8.92; N, 7.19. Found: C, 51.95; H, 8.48; N, 6.72.

Y{OSi^{t}Bu[o-C$_6$H$_4$(CH$_2$NMe$_2$)]$_2$}{OC$_6$H$_3$^{t}Bu$_2$}$_2$ (21) Silylamide complex **20** (1.50 g ; 1.92 mmol) and 2,6-di-*tert*-butylphenol (0.800 g, 3.88 mmol) were weighed into a Schlenk tube and dissolved in 100 mL of toluene. The solution was refluxed overnight and the solvent stripped under vacuum. The solid white residue was recrystallized from toluene to afford colorless crystals of **21**. Yield: 1.51 g (1.74 mmol, 90.5%). Mp: 240-243 °C. ^{1}H NMR (C_7D_8, -40 °C): δ 8.63 (d, 1H, arylC*H*, J_{HH} = 6.8 Hz), 8.01 (d, 1H, arylC*H*, J_{HH} = 6.5 Hz),

7.92 (d, 1H, arylC*H*, J_{HH} = 7.3 Hz), 7.0-7.45 (m, 8H, arylC*H*), 6.89 (t, 1H, arylC*H*, J_{HH} = 7.7 Hz), 6.74 (t, 1H, arylC*H*, J_{HH} = 7.7 Hz), 6.64 (d, 1H, arylC*H*, J_{HH} = 8.5 Hz), 4.18 (d, 1H, coordinated CH_2N, $^2J_{HH}$ = 12.3 Hz), 3.33 (d, 1H, noncoordinated CH_2N, $^2J_{HH}$ = 13.2 Hz), 2.88 (d, 1H, noncoordinated CH_2N, $^2J_{HH}$ = 13.2 Hz), 2.20 (d, partially obscured, 1H, coordinated CH_2N), 2.18 (s, 3H, coordinated NMe_2), 1.99 (s, 9H, phenoxide CMe_3), 1.96 (s, 3H, coordinated NMe_2), 1.74 (s, 6H, noncoordinated NMe_2), 1.61 (s, 9H, phenoxide CMe_3), 1.41 (s, 9H, phenoxide CMe_3), 1.26 (s, 9H, SiCMe_3), 1.05 (s, 9H, phenoxide CMe_3). ^{1}H NMR (C_7D_8, 40 °C): δ 8.47 (br s, 1H, arylC*H*), 8.02 (br d, 1H, arylC*H*), 7.70 (br d, 1H, arylC*H*), 6.95-7.40 (m, 7H, arylC*H*), 6.76 (t, 2H, arylC*H*), 6.65 (t, 2H, arylC*H*), 4.22 (d, 1H, coordinated CH_2N), 3.20 (d, 1H, noncoordinated CH_2N), 2.83 (d, 1H, noncoordinated CH_2N), 2.32 (d, 1H, coordinated CH_2N), 2.28 (s, 3H, coordinated NMe_2), 2.13 (s, 3H, coordinated NMe_2), 1.74 (s, 6H, noncoordinated NMe_2), 1.65 (br s, 18H, phenoxide CMe_3), 1.29 (s, 18H, CMe_3), 1.22 (s, 9H, SiCMe_3). ^{1}H NMR (C_7D_8, 110 °C): δ 8.2 (br s, 2H, arylC*H*), 7.0-7.3 (m, 8H, arylC*H*), 6.64 (br s, 4H, arylC*H*), 2.85 (v br s, 2H, CH_2N), 2.02 (br s, 12H, NMe_2), 1.47 (s, 36H, phenoxide CMe_3), 1.22 (s, 9H, SiCMe_3). ^{13}C{^{1}H} NMR (C_7D_8, -40 °C): δ 161.9, and 161.0 (phenoxide *ipso*C), 145.3, 144.5, 139.1, 138.3, 137.0, 136.5, 133.8, 129.8, 129.3, 129.1, 129.0, 128.5, 128.4, 127.9, 126.1, and 125.7 (arylC), 117.6, and 117.3 (phenoxide arylC), 67.9 (coordinated CH_2N), 63.8 (noncoordinated CH_2N), 48.3 (coordinated NMe_2), 44.8 (noncoordinated NMe_2), 44.3 (coordinated NMe_2), 35.5, 35.4, and 34.9 (phenoxide CMe_3), 32.6, 31.8, and 30.5 (phenoxide CMe_3), 27.5 (SiCMe_3), 20.5 (SiCMe_3). Four arylC resonances were not observed. ^{29}Si{^{1}H} NMR (50/50% C_7D_8 / THF): δ -14.8 ($^2J_{SiY}$ = 5.4 Hz). ^{89}Y NMR (C_6D_6): δ 221 MS(CI): *m/z* 869 (M^+ + 1), 853 (M^+ - Me), 812 (M^+ - ^{t}Bu),

664 (M^+ - $OC_6H_3{}^tBu_2$). Anal. Calcd for $C_{50}H_{75}N_2O_3SiY$: C, 69.10; H, 8.70; N, 3.22. Found: C, 68.96; H, 8.60; N, 2.99.

$\{Y\{OSi^tBu[o\text{-}C_6H_4(CH_2NMe_2)]_2\}\{OC_6H_3{}^tBu_2\}\{CH_2SiMe_3\}_2\}^- Li^+$ (22)

Complex **21** (1.67 g, 1.92 mmol) was dissolved in 50 mL of toluene and cooled to -30°C. A solution of $LiCH_2SiMe_3$ (0.362 g, 3.85 mmol) in 20 mL of toluene was added dropwise and the reaction mixture was allowed to warm to room temperature with stirring overnight. Insoluble $LiOC_6H_3{}^tBu_2$ was filtered off and the toluene was removed from the filtrate under vacuum to yield a white powder. Recrystallization from hexane produced colorless crystals of **22** as a hexane solvate. Exposure of the crystals to vacuum resulted in loss of hexane and formation of a white microcrystalline powder. Yield: 1.57 g (1.69 mmol, 88%). $^{13}C\{^1H\}$ NMR (C_7D_8, -10 °C): δ 162.8 (phenoxide *ipsoC*, $^2J_{YC}$ = 4.5 Hz), 142.0, 141.4, 139.1, 138.5, 137.8, 137.7, 135.9, 134.4, 133.0, 129.7, 129.2, 128.4, 127.4, 127.2, 125.6, 124.9, and 116.6 (aryl*C*), 66.1, and 66.0 (coordinated CH_2N), 50.5, 47.8, 45.7, and 45.1 (coordinated NMe_2), 35.1 (phenoxide CMe_3), 31.9 (phenoxide CMe_3), 27.9 ($SiCMe_3$), 21.3 ($SiCMe_3$), 4.6, and 4.4 (CH_2SiMe_3) $^{29}Si\{^1H\}$ NMR (C_7D_8): δ -4.0 (CH_2SiMe_3), and -9.8 (OSi^tBuAr_2). ^{89}Y NMR (C_7D_8): δ 758. ^{89}Y NMR (C_7D_8, -70 °C): δ 765 and 755 (ca. 2:1 relative intensity). Anal. Calcd for $C_{47}H_{83}LiN_2O_2Si_3Y$: C, 63.55; H, 9.42; N, 3.15. Found: C, 62.97; H, 9.45; N, 3.17.

$N[CH_2CH_2CO_2Me]_3$ (23). To a 1L round bottom flask equipped with a magnetic stirrer, reflux condenser and dropping funnel was added 21 mL 28% aqueous ammonia solution (0.35mol) and 200 mL methanol. This was followed by dropwise addition of a solution of methyl acrylate (100g, 1.16 mol) in 100 mL methanol over one hour. The resulting mixture was stirred at room temperature for 3 hours followed by overnight reflux. The low boiling fraction was removed by rotary evaporation, and the

remaining oil was distilled under vacuum (130°C-152 °C / 0.1 Torr) to afford **23** as a colourless oil. Yield: 85g (88 %). NMR data are collected in Tables 8 and 9. MS(CI): m/z 286 (M^++1, 100 %), 202 (M^+ - (CH_2CO_2Me), 66 %).

$MeN[CH_2CH_2CO_2Me]_2$ (24). A 20 mL portion of 40% aqueous methylamine (0.26 mol), 200 mL methanol and 67 g (0.78 mol) methyl acrylate were placed in a round bottom flask. The reaction took place immediately and was very exothemic. The reaction mixture was stirred at room temperature for 5 hours, followed by removal of the low boiling fraction by rotary evaporation using a water aspirator. The remaining oil was vacuum distilled (120 °C / 0.1 Torr) to afford the pure diester as a colourless liquid. Yield: 50 g (95 %). NMR data are collected in Tables 8 and 9. MS(CI): m/z 204 (M^++1, 100 %), 130 (M^+ - (CH_2CO_2Me), 88).

***tert*-$BuN[CH_2CH_2CO_2Me]_2$ (25)** A solution of *tert*-butylamine (10.0 g, 0.137 mol), methyl acrylate (40g, 0.47 mol) and 100 mL methanol was placed in a 250 mL round bottom flask and the solution was refluxed for 7 days. The pure diester was separated from the monoester and excess methyl acrylate by fractional vacuum distillation (110 °C / 0.1 Torr). Yield: 17.3 g (0.0706 mol, 52 %). NMR data are collected in Table 8 and 9. MS(CI): m/z 246 (M^++1, 92 %), 230 (M^+ - Me, 15), 172 (M^+ - (CH_2CO_2Me), 100), 188 (M^+ - CMe_3, 80).

(*S*)-$PhMeC(H)N[CH_2CH_2CO_2Me]_2$ (26) A procedure analogous to that described for **25** was used to prepare diester **26** from (*S*)-$PhMeC(H)NH_2$ and methyl acrylate. Yield: 85 %. NMR data are collected in Tables 8 and 9.

$N[CH_2CH_2C(OH)Ph_2]_3$ (27) A solution of bromobenzene (9.4g, 0.060 mol) in 150 mL freshly distilled diethyl ether was added to a 500 mL oven-dried Schlenk

flask. This solution was cooled to -78°C with a dry-ice bath, and 38 mL n-butyllithium (1.6 M as a hexane solution) was added by syringe. The reaction mixture was stirred for one hour at -78 °C and then allowed to warm to room temperature before it was canula transferred to a 750 mL Schlenk flask containing an ether solution of **23** (2.5 g, 9.1 mmol) cooled to 0°C. The resulting mixture was stirred for 2 hours at room temperature and then quenched with ice water. The aqueous phase was separated, extracted repeatedly with diethyl ether (3 × 300 mL) and the combined ether extracts were dried over anhydrous $MgSO_4$ and rotary evaporated to dryness to yield a white solid. The crude material was dried over molecular sieves in toluene solution and recrystallized from toluene to afford **27** as a white crystalline solid. Yield: 5.0 g (85 %). M.P. 169 °C. NMR data are collected in Table 10 and 11. MS(CI): m/z 676 (M^++29, 16 %), 648 (M^++1, 100), 570 (M^+ - C_6H_5, 16 %).

$MeN[CH_2CH_2C(OH)Me_2]_2$ (28) A solution of **24** (3.50 g, 0.0172 mol) in 200 mL dry diethyl ether was placed under argon in a 750 mL Schlenk flask and cooled to -30 °C. Lithium wire (2.7 g, 0.39 mol) was added to the flask followed by the dropwise addition of iodomethane (21.0 g, 0.148 mmol) over a 1 h period. The reaction mixture was stirred for an additional hour at -30 °C and then quenched with ice water. The ether layer was separated and the aqueous phase extracted with CH_2Cl_2 (2 × 200 mL). The solvent was removed from the combined organic extracts by rotary evaporation. The remaining crude oil was purified by vacuum distillation and the resulting pale yellow oil was dried over molecular sieves. Yield: 2.8 g (81 %). NMR data are collected in Tables 10 and 11. MS(CI): m/z 204 (M^++1, 100%), 186 (M^+ - OH, 11), 130 (M^+ - ($CH_2C(OH)Me_2$), 71). Anal. Calcd for $C_{11}H_{25}NO_2$: C, 64.98; H, 12.39; N, 6.89 %.

Found: C, 65.31; H, 11.90; N, 7.14 %.

$MeN[CH_2CH_2C(OH)Ph_2]_2$ (29) A solution of bromobenzene (15.7 g, 0.100 mol) in 200 mL diethyl ether was placed in a 500 mL round bottom flask and cooled to -78 °C under an argon atmosphere. A 1.6 M solution of n-butyllithium (60 mL, 0.096 mol) was added to the flask by syringe and the reaction mixture was allowed to warm to room temperature over a 1 h period during which a white precipitate of phenyllithium formed. The suspension was cooled to 0 °C and a solution of **2** (4.00 g, 0.0197 mol) in 50 mL diethyl ether was added dropwise over 1 h. The reaction mixture was stirred for 2 h at room temperature and then quenched with ice water. The aqueous phase was separated and extracted with diethyl ether (3 × 300 mL) and the combined ether extracts were evaporated to dryness to yield a white solid. The crude material was dried over molecular sieves in toluene solution and finally recrystallized from a toluene-hexane mixture to afford pure diol **29**. Yield: 4.3 g (48 %). M.P. 170 °C. NMR data are collected in Tables 10 and 11. MS(CI): m/z 480 (M^++29, 20%), 452 (M^++1, 100), 374 (M^+ - C_6H_5, 12), 254 (M^+ - ($CH_2C(OH)Ph_2$), 5). Anal. Calcd for $C_{31}H_{33}NO_2$: C, 82.45; H, 7.36; N, 3.10 %. Found: C, 82.48; H, 7.43; N, 3.54 %.

***tert*-$BuN[CH_2CH_2C(OH)Me_2]_2$ (30)** This compound was prepared from **25** by a procedure analogous to that used for **28**. The colorless crystalline product was isolated in 65 % yield. M.P. 52 °C. NMR data are collected in Tables 10 and 11. MS(CI): m/z 274 (M^++29, 13%), 246 (M^++1, 100), 230 (M^+ - Me, 21), 172 (M^+ - $CH_2C(OH)Me_2$, 78). Anal. Calcd for $C_{14}H_{31}NO_2$: C, 68.52; H, 12.73; N, 5.71 %. Found: C, 68.43; H, 12.47; N, 6.18 %.

***tert*-BuN[$CH_2CH_2C(OH)Ph_2$]$_2$ (31)** The diol was isolated as a white crystalline solid in 75 % yield starting from diester **25** and using the same procedure as given for **29**. M.P. 120 °C. NMR data are collected in Tables 10 and 11. MS(CI): m/z 512 (M^++29, 15%), 494 (M^++1, 100), 296 (M^+ - $CH_2C(OH)Ph_2$, 15).

(*S*)-PhMeC(H)N[$CH_2CH_2C(OH)Me_2$]$_2$ (32) The chiral diol was prepared from diester **26** using the procedure given for **28**. The crude product was purified by column chromatography on silica gel (95:5 ethyl acetate-methanol) and dried over molecular sieves. The pure diol was isolated in a 62 % yield as a sticky, colorless oil. NMR data are collected in Tables 10 and 11. MS(CI): m/z 322 (M^++29, 12%), 294 (M^++1, 100), 278 (M^+ - Me, 8), 220 (M^+ - $CH_2C(OH)Me_2$, 71). Anal. Calcd for $C_{18}H_{31}NO_2$: C, 73.68; H, 10.65; N, 4.77 %. Found: C, 72.58; H, 10.40; N, 5.22 %.

Zr{MeN[$CH_2CH_2C(O)Me_2$]$_2$}$_2$ (33). In the glove box, a solution of **28** (1.50 g, 7.39 mmol) in 20 mL toluene was added dropwise to a solution of tetrabenzyl zirconium (1.70 g, 3.74 mmol) in 20 mL toluene with rapid stirring. The solution was allowed to stir for 30 min and the solvent was removed under reduced pressure to afford pale yellow amorphous solid **33**. Yield: 3.52 g (96%). M.P. 190-212 °C. NMR (C_6D_6, 80 °C): ^{1}H δ 2.50 (br, 4H, NC*H*$_2$,), 2.20 (s, 3H, *Me*N), 1.60 (br, 4H, C*H*$_2$CO), 1.33 (s, 12H, OC*Me*$_2$); ^{13}C{^{1}H} δ 73.3 (*C*O), 56 (br, NCH_2), 46.1 (*Me*N), 39.3 (*C*H_2CO), 31.6 (OC*Me*$_2$). Anal. Calcd for $C_{22}H_{46}N_2O_4Zr$: C, 53.51: H, 9.39; N, 5.67 %. Found: C, 53.71; H, 9.28; N, 5.94 %.

Zr{MeN[$CH_2CH_2C(O)Ph_2$]$_2$}$_2$ (34) White solid was isolated following the same procedure as for **33**. Recrystallization of this crude product from hot toluene afforded colourless crystals of **34**. Yield: 90 %. M.P. > 285 °C. NMR (C_6D_6): ^{1}H δ 8.25

(dd, 8H, *o*-arylCH_a, $^3J_{HH}$=8.4 Hz, $^4J_{HH}$ = 1.2 Hz), 8.19 (dd, 8H, *o*-arylCH_b, $^3J_{HH}$=7.3, 1.1), 6.68-7.68 (m, 24H, *o*-arylC*H*, *p*-arylC*H*), 2.94 (t, 2H, NCH_a, $^{2,3}J_{HH}$ = 12.3 Hz) 1.38 (dd, 2H, NCH_b, $^{2,3}J_{HH}$ = 17.7, 5.5 Hz) 3.14 (t, 2H, NCH_c, ^{2,3}J=12.4 Hz) 1.00 (dd, 2H, NCH_d, ^{3}J=12.7 Hz, ^{2}J=5.5 Hz) and 2.29 (dd, 2H, CH_aCO, $^3J_{HH}$ = 15.2 Hz, $^2J_{HH}$ = 11.9 Hz), 2.53 (dd, 2H, CH_bCO, $^3J_{HH}$ = 15.3 Hz, $^2J_{HH}$ = 5.3 Hz), 2.11 (dd, 2H, CH_cCO, $^3J_{HH}$ = 14.0 Hz, $^2J_{HH}$ = 5.2 Hz), 1.93 (dd, 2H, CH_dCO, $^3J_{HH}$ = 13.8 Hz, $^2J_{HH}$ = 5.1 Hz), 1.56 (s, 6H, *Me*N); ^{13}C{^{1}H} δ 152.9, 151.2, 149.6, 149.4 (arylC_{quat}), 126.3, 126.1, 126.1, 126.0 (*p*-arylCH), 129.3, 128.6, 128.5, 127.6, 127.3, 126.96,126.7, 125.5 (*o,m*-arylCH,), 83.7, 82.1 (CH_2CO), 58.3, 53.7 (NCH_2), 46.6 (*Me*N), 37.3, 36.5 (CH_2CO) Anal. Calcd for $C_{62}H_{62}N_2O_4Zr$: C, 75.19; H, 6.31; N, 2.83 %. Found: C, 75.51; H, 6.37; N, 2.78 %.

Zr{*tert*-BuN[$CH_2CH_2C(O)Me_2$]$_2$}$_2$ (35) The complex was isolated as a colorless solid using the same procedure as given for **33**. Yield: 95 %. NMR (C_6D_6): ^{1}H δ 2.58 (t, 8H, NCH_2, $^3J_{HH}$ = 6.7 Hz), 1.75 (t, 8H, CH_2CO, $^3J_{HH}$ = 6.7 Hz), 1.25 (s, 24H, COMe_2), 1.11 (s, 18H, Me_3CN); ^{13}C{^{1}H} δ 76.7 (OCMe_2), 54.7 (Me_3CN), 43.6 (NCH_2), 42.6 (CH_2CO), 31.0 (Me_3CN), 28.8 (OCMe_2).

Zr{*tert*-BuN[$CH_2CH_2C(O)Ph_2$]$_2$}$_2$ (36) A pale yellow crystalline solid was isolated using the procedure given for **33**. Yield: 95 %. M.P. 260-280 °C. NMR (C_6D_6): ^{1}H δ 7.41 (d, 16H, *o*-arylC*H*, ^{3}J=7.3), 7.11 (t, 16H, *m*-arylC*H*, $^3J_{HH}$ = 7.4 Hz), 7.02 (d, 8H, *p*-arylC*H*, $^3J_{HH}$ = 7.3 Hz), 2.51 (br, overlap, 16H, NCH_2, CH_2CO), 0.75 (s, 18H, Me_3CN); ^{13}C{^{1}H} δ 148.5 (arylC_{quat}), 128.2, 126.9, 126.7, (*o*-arylCH, *p*-arylCH, *m*-arylCH), 85.9 ($OCPh_2$), 55.9 (Me_3CN), 45.4 (NCH_2), 42.0 (CH_2CO), 21.4 (Me_3CN).

Zr{(*S*)-PhMeC(H)N[$CH_2CH_2C(O)Me_2$]$_2$}$_2$ (37). A yellow powder was isolated by the procedure given for **33**. Yield: 92 %. NMR (C_6D_6, 70 °C): ^{1}H δ 7.31-7.0

(m, 10H, arylC*H*), 4.15 (q, 2H, PhMeC(*H*), $^3J_{HH}$ = 6.7 Hz), 2.98 (m, 4H, NCH_a), 2.57 (m, 4H, NCH_b), 1.75 (m, 4H, ChaCO), 1.68 (m, 4H, CH_bCO), 1.54 (d, 6H, Ph*Me*C(H), $^3J_{HH}$ = 6.7 Hz), 1.31 (s, 12H, OC*Me*$_a$), 1.23 (s, 6H, OC*Me*$_b$); $^{13}C\{^1H\}$ δ 144.1 (arylC_{quat}), 128.7 (*o*-arylCH), 128.4 (*m*-arylCH), 127.2 (*p*-arylCH), 75.4 ($OCMe_2$), 62.0 (PhMe*C*(H)), 46.5 (NCH_2), 40.5 (CH_2CO), 32.1 (OC*Me*$_a$),30.6 (OC*Me*$_b$),22.7 (Ph*Me*C(H)). Anal. Calcd for $C_{36}H_{58}N_2O_4Zr$: C, 64.15; H, 8.67; N, 4.15 %. Found: C, 65.28; H, 8.31; N, 4.13 %.

$Zr\{N[CH_2CH_2C(O)Ph_2]_3\}\{CH_2C_6H_5\}$ (38). In the glovebox, a 10 mL toluene solution of tetrabenzyl zirconium (0.39 g, 0.86 mmol) was placed into a 50 mL Erlenmeyer flask and stirred rapidly. A 10 mL toluene solution of **27** (0.56 g, 0.86 mmol) was added dropwise over a period of 10 minutes. The reaction mixture was stirred for a further 30 minutes, and the solvent was removed under reduced pressure. The pale yellow crystalline residue was further purified by recrystallization from toluene to afford 0.59 g of **38** as colorless crystals. Yield: 83 %. M.P. 207 °C. NMR (C_6D_6): ^1H δ 7.40 (br, d, 6H, *o*-arylC*H*), 7.36 (d, 6H, *o*-arylC*H*, $^3J_{HH}$ = 7.0 Hz), 7.2-6.9 (m, 23H, aryl proton), 3.00, 2.96 (br, 2d, 2H, ZrCH_2, $^3J_{HH}$ = 6.7 Hz), 2.77, 1.10 (br, 2m, 6H, CH_2C(OZr)), 1.98 (br, m, 6H, NCH_2); $^{13}C\{^1H\}$ δ 149.1 (benzyl C_{quat}), 148.9, 146.8 (arylC_{quat}), 128.7, 128.7, 128.5, 128.4, 127.2, 126.8, 126.4, 125.9, 125.6 (aromatic carbons), 84.8 (*C*(O)), 56.29 (CH_2Zr) 54.55 (NCH_2), 39.41 ($CH_2C(OZr)$).

$Zr\{MeN[CH_2CH_2C(O)Me_2]_2\}\{CH_2C_6H_5\}_2$ (39). Tetrabenzyl zirconium (0.730 g, 1.60 mmol) was dissolved with 15 mL toluene and cooled to -30 °C. With rapid stirring, a solution of **28** (0.311 g, 1.53 mmol) in 15 mL toluene was added dropwise over a period of 10 minutes. After the addition was completed, the solution was allowed to warm up to room temperature. Removal of the solvent resulted in a yellow oily material.

NMR showed that this oil was a mixture of tetrabenzyl zirconium, **33** and **39** in 1:1:3 ratio. Attempts to isolate pure **39** by recrystallization were not successful. NMR (C_6D_6): ^{1}H δ 7.2-7.0 (m, 9H, aromatic protons), 6.72 (tt, H, *p*-benzylC*H*, $^3J_{HH}$ = 7.1 Hz, $^4J_{HH}$ = 1.4 Hz), 2.52 (dt, 2H, NCH_aCH$_2$, $^{2,3}J_{HH}$ = 13.2 Hz), 1.03 (m, 2H, *NCH*$_b$CH$_2$), 2.34, 1.62 (dt, 2H, NCH$_2$CH_a, $^{2,3}J_{HH}$ = 13.1 Hz, $^3J_{HH}$ = 1.7 Hz), 1.25 (m, 2H, NCH$_2$CH_b), 2.56 (s, 2H, CH_2Zr), 1.64 (s, 2H, CH_2Zr), 1.25 (s, 6H, CH_3CO), 1.22 (s, 6H, CH_3CO), 1.24 (s, 3H, CH_3N); ^{13}C{^{1}H} δ 150.1, 137.9 (benzyl C_{quat}), 130.3, 129.7, 129.3, 128.6 (benzyl $C_{ortho,meta}$) 122.8, 120.3 (benzyl C_{para}), 73.2 (*C*(OZr)), 58.0 (NCH$_2$) 53.4, 52.7 (*C*H$_2$Zr), 38.7 (NCH$_2$*C*H$_2$), 37.7 (*C*H$_3$N), 32.7, 30.3 (*C*H$_3$CO).

Cl$_2$Zr{MeN[CH$_2$CH$_2$C(O)Ph$_2$]$_2$} (40). Amino diol **29** (2.00 g, 4.42 mmol) and Cl$_2$Zr[N(SiMe$_3$)]$_2$ (2.13 g, 4.42 mmol) were carefully weighed into a 100 mL Erlenmeyer in the glovebox and dissolved in 30 mL toluene. The solution became cloudy but only trace precipitate formed. After the reaction mixture was heated at 70°C for 10 minutes, large amounts of white solid formed. This solid was isolated by filtration, washed with toluene (2 × 10 mL) and dried under vacuum to give **40** as a free-flowing white powder. The low solubility and volatility of this material precluded complete characterization. Yield: 82 %.

Zr{MeN[CH$_2$CH$_2$C(O)Ph$_2$]$_2$}Me$_2$ (41a). In glovebox, 0.55 g **40** (0.90 mmol) was weighed into a 250 mL Schlenk flask. Diethyl ether (20 mL) was added under argon, and the suspension was cooled to -10 °C. Addition of 1.28 mL of 1.4M methyllithium solution in diethyl ether by syringe resulted in an immediate colour change to grey and eventually to black. The volatiles were removed under vacuum, and the oily residue was extracted with toluene. ^{1}H NMR suggested that the expected product **41a**

was formed, however, further purification was not possible due to its instability. NMR (C_6D_6): ^1H δ 7.85, 7.68 (2d, 8H, *o*-arylC*H*, $^3J_{HH}$ = 7.2 Hz), 7.3-6.7 (m, 12H, aromatic protons), 2.25 (m, 2H, NCH_2CH_a), 1.60 (m, 2H, NCH_2CH_b), 2.22 (t, 4H, NCH_2 $^{2,3}J_{HH}$ = 11 Hz), 1.43 (s, 3H, CH_3N), 0.84 (s, 3H, CH_3Zr), 0.75 (s, 3H, CH_3Zr); $^{13}C\{^1H\}$ δ 150.8, 148.44 (arylC_{quat}), 128.4, 128.3, 126.7, 126.6, 126.5, 125.4 (aromatic carbons), 82.3 (*C*(OZr)), 57.4 (NCH_2), 38.5 (CH_3N), 37.9 (NCH_2CH_2), 37.6, 34.8 (CH_3Zr).

Zr{MeN[$CH_2CH_2C(O)Ph_2$]$_2$}{CH_2SiMe_3}$_2$ (41b). Addition of **40** (0.20 g, 0.33 mmol) to a vigorously stirred solution of $LiCH_2SiMe_3$ (0.061 mg, 0.66 mmol) in toluene (20 mL) resulted in immediate precipitation of a white solid. The amount of solid diminished after the suspension was stirred overnight. The remaining solid was filtered off and the clear yellow filtrate was evaporated under reduced pressure to give a yellow-brown oil, which solidified on standing. Recrystallization of the residue from hexane at -30 °C afforded **41b** as a yellow crystalline solid. Yield: 72 %. NMR (C_6D_6): ^1H δ 7.73 (d, 4H, *o*-arylCH_a, $^3J_{HH}$ = 7.2 Hz), 7.48 (d, 4H, *o*-arylCH_b, $^3J_{HH}$ = 7.2 Hz), 7.25 (t, 4H, *m*-arylCH_a, $^3J_{HH}$ = 7.8 Hz), 7.15 (t, 4H, *m*-arylCH_b, $^3J_{HH}$ = 7.8 Hz), 2.2, 2.6 (m, 8H, NCH_2CH_2), 1.62 (s, 3H, CH_3N), 0.84 (s, 2H, $ZrCH_{2a}SiMe_3$), 0.69 (s, 2H, $ZrCH_{2a}SiMe_3$), 0.33 (s, 9H, $ZrCH_2SiMe_{3a}$), 0.23 (s, 9H, $ZrCH_2SiMe_{3b}$); $^{13}C\{^1H\}$ δ 149.7, 148.1 (arylC_{quat}), 128.4, 126.8, 126.5, 126.0 (aromatic carbons), 83.6 (*C*(OZr)), 57.6 (NCH_2) 52.4, ($ZrCH_{2a}SiMe_3$), 51.8 ($ZrCH_{2b}SiMe_3$), 42.2 (CH_3N), 37.9 (NCH_2CH_2), 3.4 ($ZrCH_2SiMe_{3a}$), 3.2 ($ZrCH_2SiMe_{3b}$).

Zr{MeN[$CH_2CH_2C(O)Ph_2$]$_2$}{$CH_2C_6H_5$}$_2$ (41c). *Method 1.* **40** (0.21 g, 0.34 mmol) and $KCH_2C_6H_5$ (0.089 g, 0.69 mmol) were carefully weighed into a 50 mL Erlenmeyer flask, and 15 mL toluene was added. The reaction mixture was stirred

vigorously overnight, at which point, all the red benzyl potassium had dissolved. The white precipitate which formed was removed by filtration to afford a clear, pale yellow solution. Removal of the solvent give **41c** as a light yellow solid. *Method 2.* Tetrabenzyl zirconium (1.0 g, 2.2 mmol) was weighed into a 250 mL Schlenk flask, and 50 mL freshly distilled diethyl ether was added by syringe. The Schlenk flask was cooled with a dry ice bath, and ligand **29** (1.0 g, 2.2 mmol) was rapidly added to the solution under a high argon flow. The reaction mixture was stirred vigorously and allowed to warm to room temperature over a period of 1 hour. The diethyl ether solvent was removed under reduced pressure, and the flask was taken into the glove box. The light yellow solid residue was redissolved with a minimum amount of toluene and recrystallized at -30 °C to give **41c** as white solid. Yield: 85 %. NMR (C_6D_6): ^{1}H δ 7.62, 7.52 (2d, 8H, *o*-arylCH, $^3J_{HH}$ = 7.4 Hz), 7.3-6.7 (m, 22H, aromatic protons), 2.58 (t, 2H, NCH_2CH_a, $^{2,3}J_{HH}$ = 11.4 Hz), 1.62 (ddd, 2H, NCH_2CH_b, $^{2,3}J_{HH}$ = 11.1, 5.7, 1.7 Hz), 2.34, 2.30 (m, 4H, NCH_2), 2.67 (s, 2H, CH_2Zr), 1.95 (s, 2H, CH_2Zr), 1.32 (s, 3H, CH_3N); $^{13}C\{^1H\}$ δ 151.5, 148.4 (arylC_{quat}), 148.6, 139.2 (benzyl C_{quat}), 130.1, 130.0, 129.3, 128.6, 128.5, 128.4, 127.0, 126.8, 126.6, 125.5, 123.7, 121.3 (aromatic carbons), 82.2 (C(OZr)), 58.0 (NCH_2) 57.5, 55.4 (CH_2Zr), 39.5 (CH_3N), 36.9 (NCH_2CH_2). Anal. Calcd for $C_{45}H_{45}NO_2Zr$: C, 74.75; H, 6.27; N, 1.94 %.

Zr{*tert*-BuN[$CH_2CH_2C(O)Me_2$]$_2$}{$CH_2C_6H_5$}$_2$ (42). *Method 1.* **30** (0.461 g, 1.68 mmol) and tetrabenzyl zirconium (0.763 g, 1.68 mmol) were accurately weighed into a 50 mL Erlenmeyer flask, 20 mL toluene was added, and the resulting solution was stirred at room temperature for 10 minutes. Removal of the solvent under vacuum gave **42**

as a viscous, yellow oil in quantitative yield. *Method 2*. Equimolar amounts of **35** and tetrabenzyl zirconium (1.00 mmol) each were dissolved in 20 mL toluene and stirred for 10 minutes before the solvent was removed under vacuum. The resulting oil was pure complex **42**. NMR ($CDCl_3$): ^1H δ 7.09 (t, 4H, *m*-aryl, $^3J_{HH}$ = 7.7 Hz), 6.89 (t, 2H, *p*-aryl, $^3J_{HH}$ = 6.9 Hz), 6.79 (d, 4H, *o*-aryl $^3J_{HH}$ = 7.8 Hz), 2.77 (t, 4H, NCH_2, $^3J_{HH}$ = 7.2 Hz), 1.62 (t, 4H, $CH_2C(OZr)$, $^3J_{HH}$ = 7.2 Hz), 1.06 (s, 12H, $C(OZr)Me_2$), 1.05 (s, 9H, Me_3CN); $^{13}C\{^1H\}$ δ 144.0 (arylC_{quat}) 130.8 (*o*-aryl*C*) 126.7 (*m*-aryl*C*) 122.6 (*p*-aryl*C*) 80.5 (*C*OZr), 54.0 (Me_3CN), 52.9 (CH_2N), 43.2 (CH_2Zr) 41.6 ($CH_2C(OZr)$), 30.3 ($C(OZr)Me_2$), 28.9 (Me_3CN). MS(EI): decomposed.

Zr{*tert*-BuN[$CH_2CH_2C(O)Ph_2$]$_2$}{$CH_2C_6H_5$}$_2$ (43). The methods described above for **42** were used to prepare **43**. Complex **43** was isolated as a white powder, which can be further purified by recrystallization from toluene. M.P. 180 °C, decomposes. NMR (C_6D_6 / d_8-THF): ^1H δ 7.38 (d, 8H, *o*-aryl*CH*, $^3J_{HH}$ = 7.4 Hz), 7.15 (t, 8H, m-aryl*CH*, $^3J_{HH}$ = 7.5 Hz), 7.06-7.00 (m, 8H, aromatic protons) 6.83 (t, 2H, *p*-benzyl*CH*, $^3J_{HH}$ = 7.3 Hz), 6.73 (d, 4H, *o*-benzyl*CH*, $^3J_{HH}$ = 8.0 Hz), 2.83 (t, 4H, NCH_2, $^3J_{HH}$ = 6.8 Hz), 2.60 (t, 4H, NCH_2CH_2, $^3J_{HH}$ = 6.8 Hz), 1.99 (s, 4H, CH_2Zr), 0.92 (s, 9H, Me_3N); $^{13}C\{^1H\}$ δ 147.8 (phenylC_{quart}), 146.0 (benzylC_{qrat}), 128.9, 128.3, 127.5, 127.4, 126.8, 121.7 (aromatic carbons), 88.3 (*C*(OZr)), 56.6 (NCH_2) 54.2 (Me_3CN), 43.4 (CH_2Zr), 42.6 (NCH_2CH_2), 28.6 (Me_3CN). MS(EI): decomposed.

Zr{(*S*)-PhMeC(H)N[$CH_2CH_2C(O)Me_2$]$_2$}{$CH_2C_6H_5$}$_2$ (44). Complex **44** was prepared by the methods described for **42**. Although **44** was isolated as a colorless oil it slowly decomposes to **45** by *ortho* metallation at room temperature. NMR (C_6D_6): ^1H 7.3-6.7 (m, 15H, aromatic protons), 3.96 (quat, 1H, CH_3CHN), 2.75 (m, 2H, NCH_aCH_2),

2.29 (d, 2H, CH_aZr, $^3J_{HH}$ = 9.6 Hz), 2.13 (d, 2H, CH_bZr, 3JHH = 9.6 Hz), 1.95 (m, 2H, NCH_bCH_2), 1.65 (m, 2H, NCH_2CH_a), 1.30 (m, 2H, NCH_2CH_b), 1.25 (d, 3H, CH_3CHN, $^3J_{HH}$ = 7.0 Hz), 1.26 (s, 6H, Me_a(COZr)), 1.19 (s, 6H, Me_b(COZr)); $^{13}C\{^1H\}$ δ 146.2 ($C_{quat}CH(CH_3)N$), 141.1 ($C_{quat}CH_2Zr$), 129.3, 129.0, 128.8, 128.6, 128.2, 127.6 (aromatic carbons), 75.5 (*C*(OZr)), 58.7 (CH_2Zr), 58.64 (CH_3CHN), 50.1 (NCH_2) 40.1 (NCH_2CH_2), 31.9, 31.7, 30.1 (*Me*COZr), 21.7 (CH_3CHN).

C_6H_4-(2)-*S*-$(CH_3)CHN(CH_2CH_2CMe_2O)_2]ZrCH_2C6H_5$ (45) (metallacycle complex)

To a 30 mL toluene solution of tetrabenzyl zirconium (2.67 g, 5.87 mmol) in a 100 mL Erlenmeyer flask, was added dropwise 20 mL of a toluene solution of **32** (1.75 g, 5.87 mmol). The reaction mixture was stirred at room temperature for 30 minutes and then heated at 70 °C for 1 hour. The resulting dark brown solution was concentrated until yellow crystals began to appear. The crystals redissolved when the solution was warmed to room temperature. Cooling the mother liquor at -30 °C gave 1.65 g of **45** as pale yellow crystals. Yield: 60 %. M.P. 175 °C. NMR (C_6D_6): ^1H δ 8.16 (m, 1H, α–phenyl*H*) 7.3 (m, 2H, β,γ-phenyl*H*), 7.03 (m, 1H, δ-phenyl*H*), 7.35 (m, 1H, *o*-benzyl*H*), 7.25 (m, 1H, *m*-benzyl*H*), 6.90 (tt, *p*-benzyl*H*, $^3J_{HH}$ = 7.3 Hz, $^4J_{HH}$ = 1.2 Hz), 4.61 (q, 1H, CH_3CHN, $^3J_{HH}$ = 6.9 Hz), 3.10 (d, 1H, CH_aZr, $^3J_{HH}$ = 9.1 Hz), 3.00 (d, 1H, CH_bZr, $^3J_{HH}$ = 9.1 Hz), 2.81 (m, 1H, NCH_aCH_2), 2.71 (m, 1H, NCH_bCH_2), 1.80 (m, 2H, $NCH_{c,d}CH_2$), 1.78 (m, 1H, NCH_2CH_a), 1.58 (m, 1H, NCH_2CH_b), 1.02 (m, 1H, NCH_2CH_c), 0.92 (m, 1H, NCH_2CH_d), 0.89 (d, 3H, CH_3CHN, $^3J_{HH}$ = 6.9 Hz), 1.04 (s, 3H, Me_a(COZr)), 1.03 (s, 3H, Me_b(COZr)) 0.96 (s, 3H, Me_c(COZr)), 0.83 (s, 3H,

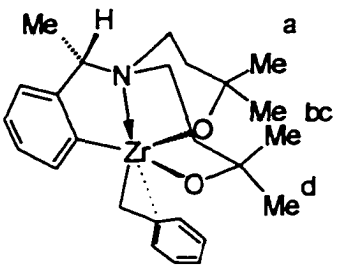

Me$_d$(COZr)); ^{13}C{^{1}H} δ 182.9 (*C*Zr), 152.2 (*C*$_{quat}$CH(CH$_3$)N), 144.1 (*C*$_{quat}$CH$_2$Zr), 139.4, 129.8, 128.9, 127.6, 125.78, 123.5, 121.5 (aromatic carbons), 76.2 (*C*$_a$(OZr)), 74.8 (*C*$_b$(OZr)), 60.5 (*C*H$_2$Zr), 59.5 (NCHCH$_3$), 46.9 (CH$_2$*C*$_a$HN), 46.7 (CH$_2$*C*$_b$HN), 37.9 (NCH$_2$*C*$_a$H$_2$), 37.6 (NCH$_2$*C*$_b$H$_2$), 32.5, 31.6, 30.3, 30.3 (*Me*COZr), 7.6 (*C*H$_3$CHN).

C$_6$H$_4$-(2)-*S*-(CH$_3$)CHN(CH$_2$CH$_2$CMe$_2$O)$_2$]ZrNH^{t}Bu (46)

To a toluene solution (10 mL) of **45** (0.102 g, 0.216 mmol), was added 1.54 mL of a 0.140 M hexane solution of *tert*-butyl amine (0.216 mmol). The reaction mixture was stirred at room temperature for 2 hours before the volatiles were removed under vacuum. The resulting yellow oil solidified when hexane was added and was recrystallized from a toluene / hexane mixture to give **46** as a pale yellow solid. Yield: 75 %. NMR (C$_6$D$_6$): ^{1}H δ 8.40 (m, 1H, α–phenyl*H*)) 7.23 (m, 2H, β,γ-phenyl*H*), 7.06 (m, 1H, δ-phenyl*H*), 5.28 (s, 1H, Me$_3$CN*H*), 4.63 (quat, 1H, CH$_3$C*H*N, ^{3}J$_{HH}$ = 6.8 Hz), 3.06 (m, 1H, NC*H*$_a$CH$_2$), 2.75 (m, 1H, NC*H*$_b$CH$_2$), 2.00 (m, 2H, NC*H*$_{c,d}$CH$_2$), 1.80, 1.0 (m, 4H, NCH$_2$C*H*$_2$), 1.45 (s, 9H, *Me*$_3$CN), 0.97 (d, 3H, C*H*$_3$CHN, ^{3}J$_{HH}$ = 6.9 Hz), 1.20 (s, 3H, *Me*$_a$(COZr)), 1.18 (s, 3H, *Me*$_b$(COZr)) 1.13 (s, 3H, *Me*$_c$(COZr)), 0.94 (s, 3H, *Me*$_d$(COZr)); ^{13}C{^{1}H} δ 181.5 (*C*Zr), 151.8 (*C*$_{quat}$CH(CH$_3$)N), 141.5, 127.7, 125.5, 123.7 (aromatic carbons), 75.6 (*C*$_a$(OZr)), 74.6 (*C*$_b$(OZr)), 59.2 (NCHCH$_3$), 53.3 (Me$_3$*C*N), 47.0 (CH$_2$*C*$_a$HN), 46.9 (CH$_2$*C*$_b$HN), 38.4 (NCH$_2$*C*$_a$H$_2$), 38.2 (NCH$_2$*C*$_b$H$_2$), 34.7 (*Me*$_3$CN), 33.0, 32.2, 31.5, 30.4 (*Me*COZr), 7.3 (*C*H$_3$CHN).

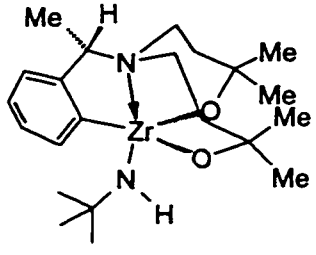

C$_6$H$_4$-(2)-*S*-(CH$_3$)CHN(CH$_2$CH$_2$CMe$_2$O)$_2$]ZrNH-(2,6)-C$_6$H$_4$ (CH$_3$)$_2$ (47)

47 was prepared from **45** and 2,6- dimethylaniline using a procedure analogous to

that described for the synthesis of **46**. NMR (C_6D_6): ^{1}H δ 8.40 (dd, 1H, α–phenyl*H*, $^2J_{HH}$ = 7.3, $^3J_{HH}$ = 1.4 Hz) 7.15–6.8 (m, 8H, aromatic protons), 6.80 (br, s, 1H, N*H*Ph), 4.60 (q, 1H, NC*H*(CH$_3$)Ph, $^3J_{HH}$ = 6.6 Hz), 3.04 (t, 1H, NCH_aCH$_2$, $^3J_{HH}$ = 13 Hz), 2.71 (dt, 1H, NCH_bCH$_2$, $^2J_{HH}$ = 1.5 Hz, $^3J_{HH}$ = 13 Hz), 2.58 (s, 6H, CH$_3$Ph) 1.90 (m, 2H, NC$H_{c,d}$CH$_2$), 1.80, 1.0 (m, 4H, NCH$_2$CH_2), 1.12 (s, 3H, *Me*$_a$(COZr)), 1.11 (s, 3H, *Me*$_b$(COZr)) 1.11 (s, 3H, *Me*$_c$(COZr)), 0.95 (s, 3H, *Me*$_d$(COZr)), 0.92 (d, 3H, CH_3CHN, $^3J_{HH}$ = 6.9 Hz);

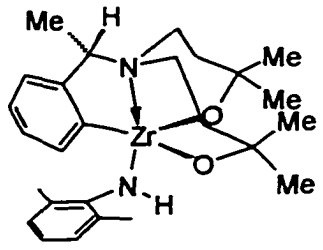

^{13}C{^{1}H} δ 182.3 (*C*Zr), 152.2 (*C*$_{quat}$CH(CH$_3$)N), 151.1 (*C*$_{quat}$NPh), 139.5 (*C*$_{quat}$PhMe), 129.3, 128.5, 126.2, 124.1, 123.6, 117.4 (aromatic carbons), 76.5 (*C*$_a$(OZr)), 75.73 (*C*$_b$(OZr)), 59.8 (N*C*HCH$_3$), 46.9 (CH$_2$*C*$_a$HN), 46.8 (CH$_2$*C*$_b$HN), 38.2 (NCH$_2$*C*$_a$H$_2$), 38.9 (NCH$_2$*C*$_b$H$_2$), 32.5, 31.6, 30.5, 30.5 (*Me*COZr), 20.3 ((*C*H$_3$)$_2$PhN), 7.4 (*C*H$_3$CHN).

{(*S*)-PhMeC(H)N[CH$_2$CH$_2$C(O)Me$_2$]Zr(μ-N^{t}Bu)}$_2$ (49a)

Complex **45** (0.253 g, 0.536 mmol), 4.60 mL of a 0.140 M hexane solution of tert-butyl amine (6.44 mmol) and 20 mL toluene were added to a 100 mL Schlenk flask equipped with a teflon valve in the glovebox. The solution was heated at 70 °C for 24 hours before solvent was removed. The NMR spectrum of the residue showed the presence of **49a** and **37** in a 9:1 ratio. Crystals of **49a** were obtained by recrystallization from toluene. Yield: 62 %. M.P. > 265 °C. NMR (C_6D_6): ^{1}H δ 7.49 (dd, 4H, *m*-arylC*H*, $^3J_{HH}$ = 7.3, 8.0 Hz), 7.22 (m, 4H, *o*-arylC*H*), 7.10 (tt, 2H, *p*-arylC*H*, $^3J_{HH}$ = 7.3, $^4J_{HH}$ = 1.5 Hz), 3.84 (q, 2H, PhMeC(*H*), $^3J_{HH}$ = 6.5 Hz), 3.36 (m, 8H, NCH_2), 2.00 (m, 8H, CH_2C(OZr), 1.39 (s, 18H, *Me*$_3$CN), 1.38

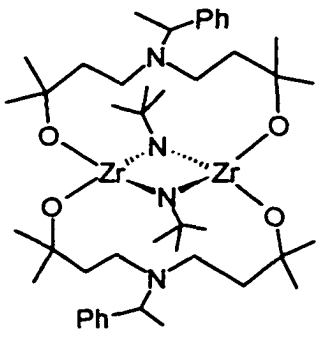

(d, 3H, PhMeC(H), $^3J_{HH}$ = 6.5 Hz), 1.20 (s, 12H, C(OZr)Me_a), 1.18 (s, 12H, C(OZr)Me_b); $^{13}C\{^1H\}$ δ 146.9 (arylC_{quat}), 128.4 (*o*-arylCH), 128.0 (*m*-arylCH), 126.9 (*p*-arylCH), 76.9 (*C*OZr), 61.5 (PhMe*C*(H)), 48.8 (NCH_2), 43.7 (CH_2C(OZr), 35.7 (Me_3CN), 31.9 (Me_3CN), 31.6 (C(OZr)Me_a), 31.6 (C(OZr)Me_b), 22.5 (PhMeC(H)). MS(EI): decomposed. Anal. Calcd for $[C_{22}H_{38}N_2O_2Zr]_2$: C, 58.23; H, 8.44; N, 6.17 %. Found: C, 56.42; H, 8.28; N, 5.54 %.

{(*S*)-PhMeC(H)N[$CH_2CH_2C(O)Me_2$]Zr(μ-N^{t}Bu)}$_2$·PMe_3 (49b). To a 100 mL Schlenk flask equipped with a teflon valve, was added **49a** as a toluene solution and dry PMe_3 (two fold excess) as a hexane solution. The resulting mixture was stirred for 10 minutes , and volatile materials were removed under vacuum to give a pale yellow viscous oil which was a 1:1 PMe_3 adduct of **49a**. NMR (C_6D_6): ^1H δ 7.55 (dd, 4H, *m*-arylC*H*, $^3J_{HH}$ = 7.3, 8.0 Hz), 7.22 (m, 4H, *o*-arylC*H*), 7.11 (tt, 2H, *p*-arylC*H*, $^3J_{HH}$ = 7.3, $^4J_{HH}$ = 1.5 Hz), 3.84 (q, 2H, PhMeC(*H*), $^3J_{HH}$ = 6.5 Hz), 3.21 (m, 8H, NCH_2), 2.15 (m, 8H, CH_2C(OZr), 1.65 (s, 18H, Me_3CN), 1.43 (d, 3H, PhMeC(H), $^3J_{HH}$ = 6.5 Hz), 1.32(s, 12H, C(OZr)Me_a), 1.29 (s, 12H, C(OZr)Me_b), 0.82 (d, 9H, PMe_3, $^2J_{PH}$ = 11 Hz); $^{31}P\{H\}$ δ 47.2 (*P*Me_3) (relative to external 85 % H_3PO_4).

{(*S*)-PhMeC(H)N[$CH_2CH_2C(O)Me_2$]Zr(μ-N-(2,6)-$C_6H_5(CH_3)_2$)}$_2$ (50). Complex **50** was prepared as described for **49a**. NMR (C_6D_6): ^1H δ 7.2–7.0 (m, 14H, aromatic protons), 6.72 (t, 2H, *p*-aniline*H*, $^3J_{HH}$ = 7.4 Hz), 3.88 (q, 2H, NC*H*(CH_3)Ph, $^3J_{HH}$ = 6.9 Hz), 2.98 (s, 12H, $(Me_3)_2$PhN), 2.9, 2.15, 1.80, 1.40, 1.30 (br, m, 16H, NCH_2CH_2), 1.21 (br, s, 24H, *Me*(COZr)), 1.14 (d, 6H, CH_3CHN, $^3J_{HH}$ = 6.7 Hz).

C_6H_4-(2)-*S*-$(CH_3)CHN(CH_2CH_2CMe_2O)_2]Zr(\mu$-N^{t}Bu)$Al(CH_3)_2$ (51)

To a 50 mL Erlenmeyer flask, was added 0.022 g **46** (0.049 mmol) and 10 mL of toluene. The solution was cooled to -30 °C, and 0.25 mL of a 0.2 M hexane solution of $AlMe_3$ was added rapidly in the glovebox. The solution was allowed to warm to room temperature, and the solvent was removed by rotary evaporation under vacuum. The residue was recrystallized from a toluene and hexane mixture to afford 0.018 mg colorless crystals of **51a** and **51b** in 6:1 ratio. Yield: 75 %. **51a** NMR (C_6D_6): ^{1}H δ 8.47 (m, 1H, α–phenyl*H*)) 7.18 (m, 2H, β,γ-phenyl*H*), 6.95 (m, 1H, δ-phenyl*H*), 4.56 (quat, 1H, CH_3(Ph)C*H*N, $^3J_{HH}$ = 6.6 Hz), 2.6, 1.8, 1.5, 1.05, 0.8 (m, 8H, NCH_2CH_2), 1.70 (s, 9H, *Me*$_3$CN), 1.27 (s, 3H, *Me*$_a$(COZr)), 1.15 (s, 3H, *Me*$_b$(COZr)) 1.12 (s, 3H, *Me*$_c$(COZr)), 0.76 (s, 3H, *Me*$_d$(COZr)), 0.80 (d, 3H, CH_3CHN, $^3J_{HH}$ = 6.9 Hz), 0.034 (s, 3H, Al*Me*$_{3a}$), -0.19 (s, 3H, Al*Me*$_{3b}$); 13C{^{1}H} δ 183.0 (*C*Zr), 149.4 (*C*$_{quat}$CH(CH_3)N), 140.6, 128.9, 126.1, 124.2 (aromatic carbons), 77.3 (*C*$_a$(OZr)), 75.6 (*C*$_b$(OZr)), 58.4 (N*C*HCH$_3$), 53.2 (Me$_3$*C*N), 48.4 (CH$_2$*C*$_a$HN), 46.6 (CH$_2$*C*$_b$HN), 39.7 (NCH$_2$*C*$_a$H$_2$), 38.4 (NCH$_2$*C*$_b$H$_2$), 36.1 (*Me*$_3$CN), 32.5, 31.9, 31.5, 27. 5 (*Me*COZr), 6.8 (*C*H$_3$CHN), -3.1, -6.5 (*Me*$_3$Al). **51b**: aromatic protons and ligand backbone protons overlap with **51a**'s except for the following protons: ^{1}H δ 8.37 (m, 1H, α–phenyl*H*)), 4.38 (quat, 1H, CH_3(Ph)C*H*N, $^3J_{HH}$ = 6.5 Hz), 1.74 (s, 9H, *Me*$_3$CN), 0.95 (d, 3H, CH_3CHN, $^3J_{HH}$ = 6.5 Hz), -0.052 (s, 3H, Al*Me*$_{3a}$), -0.185 (s, 3H, Al*Me*$_{3b}$).

Zr{MeN[$CH_2CH_2C(O)Ph_2$]$_2$}{NH-2,6-$C_6H_4Me_2$}$_2$ (52). To a 50 mL Erlenmeyer flask, was added 0.040 g **41c** (0.055 mmol), 0.95 mL of a 0.14M solution of 2,6-dimethyl aniline as a hexane solution (0.133 mmol) and 20 mL toluene. The reaction mixture was heated at 70 °C for 3 hours. The small amount of precipitate formed during the reaction was filtered off, and the filtrate was evaporated to dryness under vacuum. The residue was recrystallized from a hexane / toluene mixture to afford 0.012 g **52** as a pale yellow solid. Yield: 28 %. NMR (C_6D_6): ^{1}H δ 7.48 (d, 4H, *o*-arylCH_a, $^3J_{HH}$ = 7.3 Hz), 7.37 (d, 4H, *o*-arylCH_b, $^3J_{HH}$ = 7.3 Hz), 7.2-6.9 (m, 16H, aromatic protons), 6.78 (t, 1H, *p*-anilineCH_a, $^3J_{HH}$ = 7.4 Hz), 6.69 (t, 1H, *p*-anilineCH_b, $^3J_{HH}$ = 7.3 Hz), 6.63 (s, 1H, NH_aPh$(CH_3)_2$), 6.16 (s, 1H, NH_bPh$(CH_3)_2$), 2.51 (s, 6H, NHPh$(CH_3)_{2a}$), 2.27 (s, 6H, NHPh$(CH_3)_{2b}$), 2.2, 2.1, 1.85 (m, 8H, NC*H*2C*H*2), 1.76 (s, 3H, *Me*N). ^{13}C{^{1}H} δ 152.2, 151.0 (arylC_{quat}), 148.4, 148.2 (anilineCH_3C_{quat}), 129.3, 128.7, 128.6, 128.5, 126.9, 126.8, 125.9, 125.8, 125.6, 123.5 (aromatic carbons), 118.5, 118.2 (*p*-anilineC*H*), 84.4 (*C*(OZr)), 57.1 (N*C*H_2) 47.1 (*C*H_3N), 38.1 (NCH_2*C*H_2), 20.6, 19.8 (anilineCH_3).

Zr{MeN[$CH_2CH_2C(O)Ph_2$]$_2$}{2,6-dimethylaniline imide} polymer (53).

To a 25 mL Erlenmeyer flask, was added 0.056 g **41c** (0.077 mmol) and 0.55 mL of a 0.14 M 2,6-dimethyl aniline (0.077 mmol) solution in toluene. The solvent was quickly pumped away, and the resulting oily material was redissolved with 0.5 mL C_6D_6 and investigated by NMR. The initial NMR showed that no reaction had taken place but after heating at 80 °C overnight, a crystalline solid precipitated in the NMR tube. The C_6D_6 was removed by pipette, and pale yellow crystals of **53** (0.035, 69 %) were obtained. No NMR spectra can be recorded for **53**, because it was insoluble in all common NMR solvents. MS(EI): m/z 1318 (M^+, dimer), 1199 (M^+- aniline). Anal. Calcd for

$[C_{39}H_{40}N_2O_2Zr]_n$: C, 70.98; H, 6.11; N, 4.24 %. Found: C, 70.75; H, 6.16; N, 4.16 %.

[OCH(β-nathphyl)-(1)-C_6H_4-(2)-*S*-(CH_3)CHN$(CH_2CH_2CMe_2O)_2$]ZrCH$_2C_6H_5$ (54)

In the glovebox, 0.124 g **45** (0.263 mmol) was dissolved in 10 mL of toluene and cooled to -30 °C. To this solution, a 10 mL toluene solution of β-naphathalaldehyde (0.041 g, 0.263 mmol) was added quickly. The reaction mixture was kept at -30 °C for 1 hour, and the solvent was removed by rotary evaporation. The NMR spectrum of the resulting solid showed that it was a mixture of the two diastereomers **54a** and **54b** in 12:1 ratio. However, recrystallization from a toluene / hexane mixture afforded 0.12 g of pure **54a** as a pale yellow, crystalline solid. Yield: 71 %. NMR (C_6D_6, 50 °C): ^{1}H δ 7.8-6.9 (m, 14H, aromatic protons), 6.10 (s, 1H, C*H*OZr), 4.51 (q, 1H, CH_3CHN, $^3J_{HH}$ = 7.0 Hz), 3.02, 2.84, 1.90, 1.80, 1.60, 1.45, 1.00 (m, 8H, NCH_2CH_2), 2.69 (ab, 1H, CH_aZr, $^2J_{HH}$ = 10.2 Hz), 2.66 (ab, 1H, CH_bZr, $^2J_{HH}$ = 10.2 Hz), 1.38 (s, 3H, CH_{3a}OZr),1.09 (s, 6H, CH_{3bc}OZr), 0.65 (s, 3H, CH_{3d}OZr), 0.60 (d, 3H, CH_3CHN, $^3J_{HH}$ = 7.0 Hz); ^{13}C{^{1}H}: δ 150.4, 145.91, 143.9, 139.3, 133.7, 132.9, 132.5, 130.6, 128.3, 127.3, 127.2, 126.2, 125.8, 124.3, 123.7, 119.7 (aromatic carbons), 83.8 (*C*HOZr), 76.1, 75.5 (CH_3*C*OZr), 54.4 (PhCH_2Zr), 54.4 (CH_3*C*HN), 47.1, 46.9 (NCH_2CH_2), 40.6, 38.2 (NCH_2CH_2), 28.5, 32.7 (*C*H_3COZr), 11.4 (*C*H_3CHN).

[OCH(β-nathphyl)-(1)-C_6H_4-(2)-*S*-(CH_3)CHN$(CH_2CH_2CMe_2O)_2$]ZrOCH$_2C_6H_5$ (55)

In the glove box, 0.050 g of **54a** was dissolved with 15 mL of toluene in a 120 mL Schlenk flask fitted with a teflon valve. The flask was cooled to -78 °C, exposed to

vacuum briefly and then refilled with pre-dried H_2. The flask was warmed to room temperature and heated at 80 °C for 5 hours before the solvent was removed under vacuum. NMR of the residue showed that instead of expected zirconium hydride product, it was clean **55a** which was the product of **54a** and oxygen (possibly from trace O_2 impurity in the H_2 gas). NMR (C_6D_6, 80 °C): ^{1}H δ 8.0-7.0 (m, 14H, aromatic protons), 6.73 (s, 1H, C*H*OZr), 5.42, 4.64 (ab, 2H, PhCH_{ab}OZr, $^2J_{HH}$ = 14.3 Hz), 5.05 (q, 1H, CH_3CHN, $^3J_{HH}$ = 7.1 Hz), 3.2, 3.1, 2.1 1.85, 1.2 (m, 8H, NCH_2CH_2), 1.70 (s, 3H, CH_{3a}OZr), 1.14 (s, 6H, CH_{3b}OZr), 0.99 (s, 3H, CH_{3c}OZr), 0.52 (s, 6H, CH_{3d}OZr), 0.67 (d, 3H, CH_3CHN, $^3J_{HH}$ = 7.1 Hz); ^{13}C{^{1}H}: δ 148.2, 145.5, 144.8, 140.5, 133.8, 132.7, 132.5, 130.7, 128.5, 128.1, 127.3, 126.9, 126.9, 126.7, 125.8, 125.5, 125.0, 124.5, 123.8 (aromatic carbons), 83.3 (*C*HOZr), 75.3, 74.7 (CH_3COZr), 71.8 ($PhCH_2Zr$), 54.4 (CH_3CHN), 49.14, 47.10 (NCH_2CH_2), 40.8, 38.2 (NCH_2CH_2), 33.3, 33.2, 29.2, 28.6 (CH_3COZr), 10.6 (CH_3CHN).

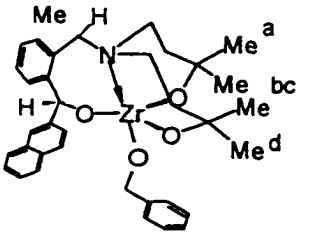

(*R* or *S*)-1-([PhCH(OH)]C_6H_4-2-(*S*)-[$CH(CH_3)N(CH_2CH_2CMe_2OH)_2$] (56)

A solution of 45 (0.045 g, 0.095 mmol) in 10 mL toluene was added to a toluene solution of benzylaldehyde (0.095 mmol) rapidly at -78 °C. The reaction mixture was allowed to warmed to room temperature after stirred at -78 °C for 30 minutes and was then quenched with water. **56** was isolated as a mixture of two isomers (*RS*:*SS* = 13:1) after aqueous work-up. *RS* isomer :^{1}H NMR ($CDCl_3$) δ 7.3-7.1 (m, 9H, arylC*H*), 5.77 (s, 1H, PhC*H*O), 3.89 (q, 1H, $^3J_{HH}$ = 7.0 Hz, CH_3CHN), 2.68, 2.40 (m, 4H, $NCH_{a,b}$), 1.60, 1.40 (m, 4H, $CH_{a,b}CO$), 1.16 (d, 3H,

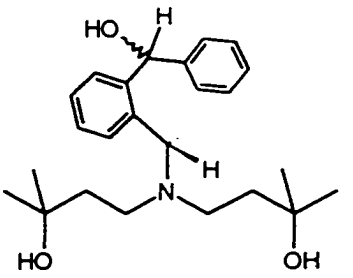

$^3J_{HH}$ = 6.8 Hz), 1.07, 1.08 (s, 12H, C$H_{3a,b}$CO). *SS* isomer: aromatic protons and ligand backbone protons overlap with those of RS isomer except for the following protons : ^{1}H NMR ($CDCl_3$) δ 6.15 (s, 1H, C*H*OPh), 4.57 (q, 1H, $^3J_{HH}$ = 6.9 Hz, CH_3CHN).

(*R*)-1-([PhC(CH$_3$)(OH)]C$_6$H$_4$-2-(*S*)-[CH(CH$_3$)N(CH$_2$CH$_2$CMe$_2$OH)$_2$] (57)

The methods described above for **56** were used to prepare **57**. Only one isomer was observed ^{1}H NMR ($CDCl_3$) δ 7.4-7.1 (m, 9H, arylC*H*), 3.73 (q, 1H, $^3J_{HH}$ = 6.9 Hz, CH_3CHN), 2.68, 2.32 (dt, 4H, NC$H_{a,b}$), 1.89 (s, 3H, CH_3C(Ph)OH), 1.60, 1.35 (m, 4H, C$H_{a,b}$CO), 1.08 (s, 12H, C$H_{3a,b}$CO), 1.06 (d, 3H, $^3J_{HH}$ = 7.0 Hz, CH_3CHN).

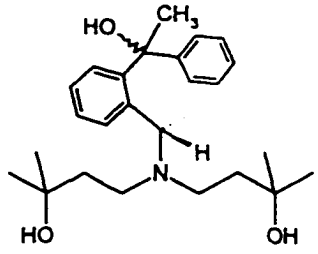

(*R* or *S*)-1-([β-(C$_{10}$H$_7$)PhCH(OH)]C$_6$H$_4$-2-(*S*)-[CH(CH$_3$)N(CH$_2$CH$_2$CMe$_2$OH)$_2$] (58)

The methods described above for **56** were used to prepare **58**. **58** was isolated as a mixture of two diastereomers. (*RS*:*SS* = 10:1). *RS* isomer :^{1}H NMR ($CDCl_3$) δ 7.9-7.1 (m, 11H, arylC*H*), 5.92 (s, 1H, PhC*H*O), 3.94 (q, 1H, $^3J_{HH}$ = 6.8 Hz, CH_3CHN), 2.70, 2.40 (m, 4H, NC$H_{a,b}$), 1.62, 1.42 (m, 4H, C$H_{a,b}$CO), 1.10 (d, 3H, $^3J_{HH}$ = 7.0 Hz), 1.08 (s, 12H, C$H_{3a,b}$CO). *SS* isomer: aromatic protons and ligand backbone protons overlap with those of *RS* isomer except for the following protons : ^{1}H NMR ($CDCl_3$) δ 6.33 (s, 1H, ArC*H*OH), 4.68 (q, 1H, $^3J_{HH}$ = 6.9 Hz, CH_3CHN).

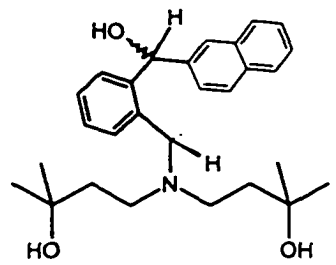

(*R* or *S*)-1-([α-(C$_{10}$H$_7$)PhCH(OH)]C$_6$H$_4$-2-(*S*)-[CH(CH$_3$)N(CH$_2$CH$_2$CMe$_2$OH)$_2$] (59)

The methods described above for **56** were used to prepare **59**. **59** was isolated as a mixture of two diastereomers. (*RS*:*SS* = 3:1). *RS* isomer :^{1}H NMR ($CDCl_3$) δ 7.9-7.1 (m,

11H, arylC*H*), 6.67 (s, 1H, ArC*H*OH), 4.15 (q, 1H, $^3J_{HH}$ = 6.9 Hz, CH_3CHN), 2.60, (m, 4H, $NCH_{a,b}$), 1.60, (m, 4H, $CH_{a,b}CO$), 1.40 (d, 3H, $^3J_{HH}$ = 7.0 Hz), 1.04 (s, 12H, $CH_{3a,b}CO$). *SS* isomer: aromatic protons and ligand backbone protons overlap with those of *RS* isomer except for the following protons: ^{1}H NMR ($CDCl_3$) δ 6.81 (s, 1H, C*H*OAr), 4.65 (q, 1H, $^3J_{HH}$ = 6.7 Hz, CH_3CHN).

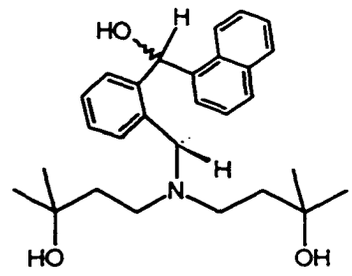

Cationic Zirconium Complexes

Cationic zirconium complexes were made by reaction of the zirconium alkyl complexes with $B(C_6F_5)_3$ in 1:1 ratio in an appropriate solvent (usually C_6D_6 or toluene). All the cationic complexes were viscous orange oils, and efforts to grow crystals from various solvents were not successful.

$Zr\{MeN[CH_2CH_2C(O)Ph_2]_2\}\{CH_2C_6H_5\}^+(C_6F_5)_3B(CH_2C_6H_5)^-$ (60). In the glove box, 0.029 g **41c** (0.040 mmol) and 0.021 g $B(C_6F_5)_3$ (0.040 mmol) were weighed into a NMR tube and 0.5 mL of C_6D_6 was added. The solution turned orange-yellow immediately upon mixing and an orange oil precipitated from solution. Addition of 0.1 mL of d_8-THF to the NMR tube resulted in dissolution of the oil. The ^{19}F spectrum of this mixture was very clean. However, the ^{1}H NMR spectrum was still very complex. NMR (C_6D_6): ^{1}H δ 7.3-6.7 (br, m, aromatic protons), 6.05 (br, d, 2H, o-benzylCH), 3.42 (br, s, BCH_2Ph) 3.2-1.3 (br, m, ligand backbone protons); $^{19}F\{^1H\}$ (C_6D_6) δ 130.3, 130.4, 130.8, 130.9, 160.4, 160.5, 160.6, 161.2, 161.3, 162.8, 163.4, 164.6, 164.7, 165.2, 165.3, 166.5, 166.9; $^{19}F\{^1H\}$ (C_6D_6/d_8-THF) δ 130.6 (d, 6F, *o*-phenylC*F*, $^3J_{FF}$ = 20 Hz), 164.1 (t, 3F, *p*-phenylC*F*, $^3J_{FF}$ = 20 Hz), 166.9 (t, 6F, *m*-phenylC*F*, $^3J_{FF}$ = 20 Hz).

$[C_6H_4$-(2)-*S*-$CH(CH_3)N(CH_2CH_2CMe_2O)_2]Zr^+\{B(C_6F_5)_3(CH_2Ph)\}^-$ (62)

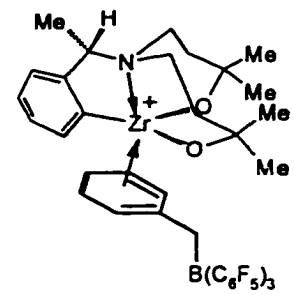

A procedure analogous to that described for **60** was used to prepare **62.** Both the ^1H and ^{19}F NMR spectra of **62** are complex in C_6D_6. However in a mixture of C_6D_6 and d_8-THF (5:1), the spectra simplified and became well resolved. NMR (C_6D_6): ^1H δ 7.1-6.1 (broad peaks for aromatic protons), 4.1, 3.1, 2.0-0.2 (broad peaks for aliphatic); $^{19}F\{^1H\}$ (C_6D_6) δ 130.7 (br, 6F, *o*-phenylC*F*), 164.0 (br, 3F, *p*-phenylC*F*), 166.9 (br, 6F, *m*-phenylC*F*). ^1H (C_6D_6/d_8-THF): δ 7.18-6.95 (m, 8H, aromatic protons), 6.83 (t, 1H, *p*-benzylC*H*, $^3J_{HH}$ = 6.7 Hz), 4.54 (br, 1H, CH_3CHN), 3.37 (br, s, 2H, $PhCH_2B$), 2.84 (br, t, 1H, NCH_aCH_2, $^3J_{HH}$ = 9.7 Hz), 2.57 (t, 1H, NCH_bCH_2, $^3J_{HH}$ = 13.0 Hz), 2.14, 1.94 (br, m, 2H, $NCH_{c,d}CH_2$), 1.88 (t, 1H, NCH_2CH_a, $^3J_{HH}$ = 13.4 Hz), 1.68 (t, 1H, NCH_2CH_b, $^3J_{HH}$ = 14.2 Hz), 1.33 (m, 1H, NCH_2CH_c), 1.10 (m, 1H, NCH_2CH_d), 1.04 (d, 3H, CH_3CHN, $^3J_{HH}$ = 6.8 Hz), 1.00 (s, 3H, Me_a(COZr)), 0.97 (s, 3H, Me_b(COZr)) 0.94 (s, 3H, Me_c(COZr)), 0.70 (s, 3H, Me_d(COZr)); $^{13}C\{^1H\}$ δ 150.8, 150.4 (br), 149.2, 147. 8 (br), 138.4 (br), 135.8 (br), 133.7, 129.2, 128.4, 127.3, 125.8, 124.4, 122.9 (aromatic carbons), 78.0 (C_a(OZr)), 77.1 (C_b(OZr)), 61.0 (br, $NCHCH_3$), 48.6 (CH_2C_aHN), 47.4 (CH_2C_bHN), 37.6 ($NCH_2C_aH_2$), 37.2 ($NCH_2C_bH_2$), 31.7, 31.6, 30.2, 29.0 (*Me*COZr), 31.5 (br, $PhCH_2B$), 7.5 (br,CH_3CHN). ^{19}F (C_6D_6/d_8-THF) $\{^1H\}$ δ 130.6 (d, 6F, *o*-phenylC*F*, $^3J_{FF}$ = 20 Hz), 164.8 (t, 3F, *p*-phenylC*F*, $^3J_{FF}$ = 20 Hz), 167.5 (t, 6F, *m*-phenylC*F*, $^3J_{FF}$ = 20 Hz).

3-acyl-4-alkyl-4-hydroxy-N-methylpiperidine (63a) To a 500 mL Schlenk flask, were added 2.00 g amino diester **24** (9.85 mmol), 16.4 g n-C_4F_9I (47.4 mmol), and 200 mL freshly distilled diethyl ether. The flask was cooled to -78 °C, and 30 mL of n-butyllithium (1.6 M as a hexane solution) was added dropwise over a period of 30 minutes. The reaction mixture was stirred at -78 °C for a further hour and quenched with ice water. The aqueous phase was separated, extracted repeatedly with diethyl ether (3 × 100 mL) and the combined ether extracts were rotary evaporated to dryness to yield a white solid. **63a** was isolated as colorless crystals by recrystallization from $CHCl_3$. Yield: 58 %. NMR ($CDCl_3$): ^{1}H δ 4.08 (s, 1H, O*H*), 3.77 (m, 1H, H_a), 2.86 (dd, 1H, H_b, $^3J_{HH}$ = 11.3 Hz, $^2J_{HH}$ = 3.6 Hz) 2.42 (t, 1H, H_b', $^3J_{HH}$ = 11.3 Hz), 2.73, 2.50 (m, 2H, H_c and H_c'), 2.32 (s, 3H, CH_3N), 1.96 (m, 2H, H_d and H_d'); ^{13}C{^{1}H} δ 197.1 (*C*=O), 77.2 (C_3), 53.6 (C_1), 48.7 (C_5), 45.2 (CH_3N), 44.3 (C_2), 29.82 (C_4); MS(CI): m/z 579, (M^+ + 1, 100 %), 559 (M^+ -F, 7 %).

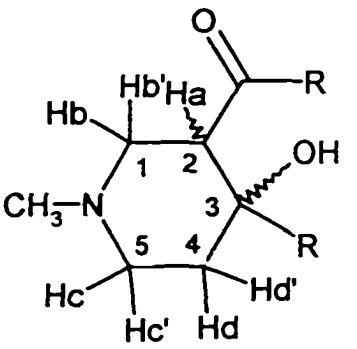

63a, R = C_4F_9
63b, R = C_6F_5
63c, R = 3,5-$C_6F_3(CF_3)_2$
63d, R = C_6H_5

63b and **c** These two compounds were synthesized by the procedure described for **63a** except that bromopentafluorobenzene (**63b**) and 3,5-bis(trifluoromethyl)bromobenzene (**63c**) were used instead of iodoperfluorobutane. Both compounds were identified by ^{1}H NMR and were not isolated. Characteristic resonances: **63b** ^{1}H NMR ($CDCl_3$): δ 4.17 (dd, 1H, H_a, $^3J_{HH}$ = 11.5 Hz, $^2J_{HH}$ = 3.4 Hz); **63c**, δ 4.32 (dd, 1H, H_a, $^3J_{HH}$ = 11.8 Hz, $^2J_{HH}$ = 3.3 Hz).

63d Bromopentafluorobenzene (1.88 g, 7.61 mmol) in 20 mL of dry DMF was added dropwisely to a vigorously stirred suspension of 1.00 g zinc powder (15.3 mmol) in 30 mL dry DMF during a period of 30 minutes. The resulting solution was canula transferred to a 250 mL flask containing 1.05 g $MeN(CH_2CH_2COPh)_2$ (3.56 mmol) in 30 mL dry DMF at 0 °C. Immediately after addition, ^1H NMR indicated clean formation of **63d**. NMR ($CDCl_3$): ^1H δ 7.8-7.1 (m, 10H, aromatic protons), 5.23 (s, 1H, O*H*), 4.38 (dd, 1H, H_a), 2.91,2.68 (m, 2H, H_b and H_b') 2.76, 2.65 (m, 2H, H_c and H_c'), 2.38 (s, 3H, CH_3N), 2.05, 1.80 (m, 2H, H_d and H_d').

$CH_3N(CH_2CH_2COOCH_3)(CH_2CH_2COC_6F_5)$ (64) 3 mL from a total 20 mL of bromopentafluorobenzene (2.65 g, 10.7 mmol) diethyl ether solution was added rapidly to 1.2 g Mg (50 mmol) in 30 ml ether with vigorous stirring. The Grignard reaction initiated immediately and the remainder of the bromopentafluorobenzene solution was added dropwise over a period of 30 minutes. The resulting solution was canula transferred to a 250 mL Schlenk flask containing 0.47 g amino diester **24** (2.3 mmol) in 30 mL ether solution at -30°C. The reaction mixture was stirred at -30 °C for two hours, and ^1H NMR showed that **64** was the main product. NMR ($CDCl_3$): ^1H δ 3.65 (s, 3H, CH_3O), 3.02 (t, 2H, H_b, $^3J_{HH}$ = 6.6 Hz), 2.78 (t, 2H, H_a, $^3J_{HH}$ = 6.6 Hz), 2.67 (t, 2H, H_a', $^3J_{HH}$ = 6.6 Hz), 2.48 (t, 2H, H_b', $^3J_{HH}$ = 6.6 Hz), 2.25 (s, 3H, CH_3N).

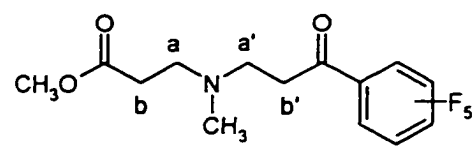

The above solution was warmed to room temperature and stirred overnight. At this point, ring product **63b** became the major component in the reaction mixture as indicated by ^1H NMR.

1,1-di(3,5-bis(trifluoromethyl)phenyl)epoxide (65) A solution of bis(3,5-bis(trifluoromethyl)phenyl) ketone (2.00 g, 4.41 mmol) in 50 mL dry THF was placed it a 250 mL Schlenk flask and cooled to -10 °C under an argon atmosphere. A

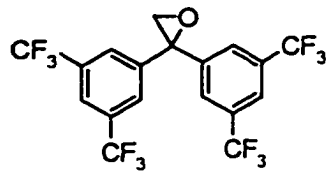

0.6 M DMSO solution of $Na^+CH_2^-SO(CH_3)_2$ (7.5 mL, 4.5 mmol) [153] was added to the flask rapidly by syringe. The reaction mixture was quenched with ice water 10 minutes after addition. The resulting mixture was extracted with diethyl ether (3 × 300 mL) and the combined ether extracts were dried over $MgSO_4$ and evaporated to yield a white solid. This solid was further dried over 4 Å molecular sieves and recrystallized from a hexane / toluene mixture to afford **65** as colorless crystals. Yield: 78 %. M.P. 46 °C. ^{1}H NMR ($CDCl_3$): δ 7.90 (s, 2H, *p*-arylC*H*), 7.79 (s, 4H, *o*-arylC*H*), 3.36 (s, 2H, CH_2); in C_6D_6: δ 7.60 (s, 2H, *p*-aryl*CH*), 7.46 (s, 4H, *o*-arylC*H*), 2.22 (s, 2H, CH_2); $^{13}C\{^1H\}$ ($CDCl_3$): δ 140.4 (s, arylC_{quat}), 132.4 (q, *m*-arylC_{quat}, $^2J_{CF}$ = 34 Hz), 127.5 (s, *o*-aryl*CH*), 122.9 (s, *p*-aryl*CH*), 122.9 (q, CF_3, $^1J_{CF}$ = 273 Hz), 77.2 (*C*O), 56.9 (CH_2O).

2-cyclopentadienyl-1,1-di(3,5-bis(trifluoromethyl)phenyl) ethanol (66)

A solution of **65** (0.80 g, 1.7 mmol) in 50 mL dry THF was placed under argon in a 250 mL Schlenk flask and cooled to -30 °C. A 0.50 M THF solution of CpNa (7.5 mL, 3.8 mmol) was added to the flask by syringe and the reaction mixture was allowed to warm to room temperature during a period of 30 minutes then stirred for an additional 2 hours. The reaction mixture was quenched with ice water and extracted with diethyl ether (3 × 200 ml). The combined organic extracts was dried over $MgSO_4$ and the solvent was removed by rotary evaporation. The crude material was dried over 4 Å molecular sieves in toluene solution and recrystallized from toluene to afford a 2:1 ratio of **66a** and **b** as pale

yellow crystals. Yield: 67 %. **66a** ^{1}H NMR (C_6D_6): δ 7.79 (s, 2H, *p*-arylC*H*), 7.58 (s, 4H, *o*-arylC*H*), 6.15 (m, 1H, H_d), 5.98 (m, 1H, H_c), 5.82 (m, 1H, H_e), 2.58 (s, 2H, CH_2), 2.16 (d, 1H, H_a, $^2J_{HH}$ = 1.4 Hz) 2.15 (d, 1H, H_a', $^2J_{HH}$ = 1.4 Hz), 1.96 (s, 1H, O*H*); $^{13}C\{^1H\}$ δ 148.5 (arylC_{quat}), 140.1 (C_f), 134.2, 134.1 133.5 (C_c, C_d and C_e), 131.9 (q, *m*-arylC), 125.1 (*o*-arylCH), 123.6 (q, CF_3, $^1J_{CF}$ = 272 Hz), 121.6 (*p*-arylCH), 76.1 (CO), 44.6 (C_b), 42.6 (C_a); **66b**: δ 7.81 (s, 2H, *p*-arylC*H*), 7.59 (s, 4H, *o*-arylC*H*), 6.00 (m, 1H, H_c), 5.67 (m, 1H, H_d), 5.56 (m, 1H, H_e), 2.58 (s, 2H, CH_2), 2.44 (d, 1H, H_a, $^2J_{HH}$ = 1.2 Hz) 2.43 (d, 1H, H_a', $^2J_{HH}$ = 1.2 Hz), 2.15 (s, 1H, O*H*); $^{13}C\{^1H\}$ δ 148.4 (arylC_{quat}), 139.6 (C_f), 134.8, 132.3, 132.0 (C_c, C_d and C_e), 131.9 (q, *m*-arylC), 127.7 (*o*-arylCH), 123.6 (q, CF_3, $^1J_{CF}$ = 272 Hz), 121.6 (*p*-arylCH), 76.0 (CO), 41.9 (C_b), 41.5 (C_a); $^{19}F\{^1H\}$ δ 62.8 (CF_3); MS(CI): m/z 516 (M^+ - H_2O, 50 %), 515 (M^+ -F, 75 %), 469 (M^+ - Cp, 20 %), 464 (M^+ - CF_3, 10 %).

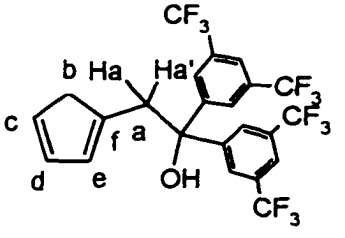

66a

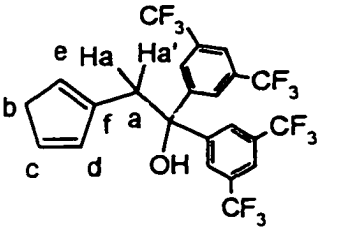

66b

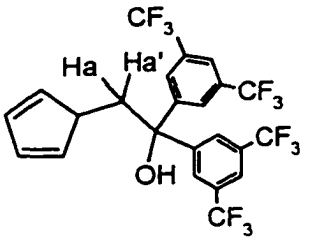

66c not observed

{η^5-CpCH$_2$C(3,5-C$_6$H$_3$)(CF$_3$)$_2$O}ZrCl$_2$.ether (67)

$Cl_2Zr(CH_2C_6H_5)_2$·ether (.172 g, 0.411 mmol) and an equilibrium mixture of **66a** and **b** (.220 g, 0.411 mmol) were weighed into a 100 mL Erlenmeyer flask in the glovebox and dissolved in 20 mL toluene. The resulting solution was heated at 30 °C for 20 minutes, and the toluene solvent was removed under vacuum. Addition of 20 mL of

hexane to the residue resulted in precipitation of **67**. Complex **67** was isolated as a light brown powder by filtration. Yield: 81 %. ^{1}H NMR (C_6D_6 / d_8-THF): δ 8.14 (s, 4H, *o*-arylC*H*), 7.73 (s, 2H, *p*-arylC*H*), 6.46 (t, 2H, Cp*H*, $^3J_{HH}$ = 2.7 Hz), 5.81 (t, 2H, Cp*H*, $^3J_{HH}$ = 2.7 Hz), 3.27 (s, 2H, CH_2); ^{13}C{^{1}H} δ 150.2 (arylC_{quat}), 132.0 (q, *m*-arylC_{quat}, $^2J_{CF}$ = 33.0 Hz), 126.9 (*o*-arylCH), 125.6 (CpC_{quat}), 124.0 (q, CF_3, $^1J_{CF}$ = 273 Hz), 121.6 (*p*-arylCH), 119.7 (CpCH), 113.3 (CpCH), 42.7 (CH_2).

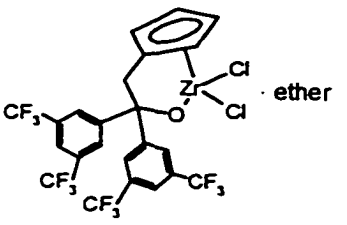

{η^5-CpCH$_2$C(3,5-C$_6$H$_3$)(CF$_3$)$_2$O}Zr(CH$_2$Ph)$_2$ (68)

67 (0.110 g, 0.143 mmol) and $KCH_2C_6H_5$ (0.040 g, 0.31 mmol) were dissolved in 20 mL of toluene. The reaction mixture was stirred vigorously for two hours, at which point, the red benzyl potassium had dissolved. The white precipitate (KCl) was removed by filtration to afford a clear yellow solution. Removal of toluene and recrystallization from hexane gave **68** as a light yellow crystalline solid. Yield: 65 %.^{1}H NMR (C_6D_6): δ 7.81 (s, 4H, *o*-arylC*H*), 7.60 (s, 2H, *p*-arylC*H*), 7.05 (t, 4H, *m*-benzylC*H*, $^3J_{HH}$ = 7.9 Hz), 6.84 (t, 2H, *p*-benzylC*H*, $^3J_{HH}$ = 7.4 Hz), 6.53 (d, 4H, *o*-benzylC*H*, $^3J_{HH}$ = 7.5 Hz), 5.58 (t, 2H, Cp*H*, $^3J_{HH}$ = 2.6 Hz), 5.26 (t, 2H, Cp*H*, $^3J_{HH}$ = 2.6 Hz), 2.77 (s, 2H, CpCH_2), 1.41 (d, 2H, benzylCH_{2a}, $^2J_{HH}$ = 9.9 Hz), 1.17 (d, 2H, benzyl$CH_{2a'}$, $^2J_{HH}$ = 9.9 Hz); ^{13}C{^{1}H} δ 151.1 (arylC_{quat}), 144.8 (benzylC_{quat}), 132.3 (q, *m*-arylC_{quat}, $^2J_{CF}$ = 33 Hz), 131.3 (*o*-benzylCH), 126.1 (*m*-benzylCH), 125.5 (*o*-arylCH), 123.7 (*p*-benzylCH), 123.7 (q, CF_3, $^1J_{CF}$ = 273 Hz), 122.2

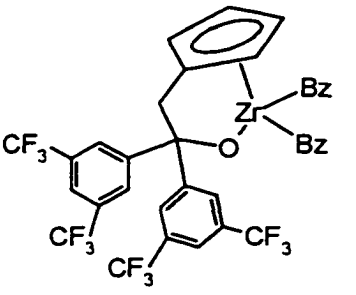

(CpC_{quat}), 121.5 (*p*-aryl*C*H), 114.3 (Cp*C*H), 110.6 (Cp*C*H), 56.6 (benzylCH_2), 41.5 (CH_2).

Alkyne cyclotrimerization

In the glove box, 0.025 g **45** (0.053 mmol), phenylacetylene (30 equivalents) and 0.5 mL of C_6D_6 were added into a NMR tube. The starting material remained unchanged at room temperature. After heated at 70 °C, the sample turned dark red and toluene formed as indicated by ^{1}H NMR spectroscopy. The sample was heated at 70 °C over night and became black. ^{1}H NMR spectrum showed no peaks correspond to phenylacetylene. This sample was quenched with H_2O and washed with HCl (1M) to afford a mixture of 1,3,5-triphenyl benzene and1,2,4-triphenyl benzene in 3:1 ratio as determined by GC-mass spectroscopy.

Olefin polymerization

Ethylene polymerization To a teflon seal 150 mL Schlenk flask was added 35 mg **60** (0.028 mmol) and 15 mL toluene. The flask was cooled to - 78 °C and evacuated. The flask was refilled with ethylene (1 atm) and warmed to room temperature. The reaction mixture was stirred at ambient temperature for 2 hours and the volatile materials were removed under vacuum. The residual solid was washed with methanol and dried to give 250 mg of white solid. Because it is hard to estimate the amount of ethylene used in the reaction, percentage conversion cannot be calculated. In this case, one equivalent of **60** polymerized about 320 equivalents of ethylene.

1-Hexene Polymerization 37 mg (0.028 mmol) of **60** and 2.2 g 1-hexene (26.2 mmol, 935 equivalent) were added to 10 mL of toluene in the glove box. After the reaction mixture was stirred at room temperature overnight, 1.5 g of polyhexene was

obtained (68 % conversion) as a sticky gel-like material. The average molecular weight of this polyhexene product was determined to be 2016 (24 units per polyhexene chain) by comparing the integration of terminal alkene protons (4.7 ppm) with the alkyl protons.

APPENDIX

CRYSTALLOGRAPHIC DATA

The crystal structures presented in this thesis were solved by Mrs. K. Beveridge, B. Chak and D. Berg. In general, the crystallographic data were obtained as follows. Crystals were loaded into glass capillaries in the glove box, sealed under argon and transferred to a Nonius CAD4F diffractometer equipped with Ni-filtered Cu K_α radiation. The unit cell was refined using 25 high angle reflections (> 35° in θ). Data were collected using 3 reference standards measured periodically during data collection. In general, decay of < 10 % in the intensity of these standards was observed. Following data reduction, an absorption correction according to an empirical Ψ scan was applied. The structure was solved using Patterson or direct methods and refined using SHELX86 or the NRCVAX structure-solving package. The structural plots were drawn using ORTEP or the ZORTEP modification.

Summary of crystallographic data, fractional atomic coordinates and equivalent isotropic temperature factors are given in the following tables.

Table I Summary of crystallographic data for **7** and **10**

	7	**10**
empirical formula	$C_{39}H_{90}N_3O_3Si_3Y$	$C_{52}H_{121}N_4O_4Si_4Yb$
fw	822.3	1151.9
cryst syst	triclinic	monoclinic
space group	P1 (No. 2)	$P2_1/n$ (No. 14)
a (Å)	13.738(2)	13.266(3)
b (Å)	15.940(3)	23.337(5)
c (Å)	13.363(2)	21.914(3)
α (deg)	93.80(1)	90
β (deg)	116.77(1)	93.94(1)
γ (deg)	74.55(1)	90
V (Å^3)	2513.3	6768.3
Z	2	4
ρ (calcd) (g cm^{-3})	1.087	1.130
μ (cm^{-1})	25.96	35.49
radiation, λ (Å)	Cu K_α, 1.542	Cu K_α, 1.542
T	ambient	ambient
$2\theta_{max}$ (deg)	60	55
no. of obsd reflcns	6850	8171
no. of unique reflcns	4395	7048
R [a]	0.0839	0.0684
R_w [b]	0.1081	0.0929

[a] $R = \Sigma(|F_o| - |F_c|) / \Sigma|F_o|$ [b] $R_w = [\Sigma w(|F_o| - |F_c|)^2 / \Sigma w(|F_o|)^2]^{1/2}$

Table II Fractional atomic coordinates [a] and equivalent isotropic temperature [b] factors for 7 (estimated standard deviations in parentheses)

atom	x	y	z	U_{eq}
Y(1)	40493(7)	26310(6)	17808(8)	543(4)
Si(1)	3566(3)	2936(2)	4320(2)	67(2)
Si(2)	6939(3)	2233(3)	2061(3)	95(2)
Si(3)	1499(3)	2814(3)	-834(3)	101(2)
O(1)	3752(5)	2852(4)	3193(5)	68(4)
O(2)	5636(5)	2562(4)	1875(5)	71(4)
O(3)	2671(5)	2531(4)	257(5)	68(3)
N(1)	1150(8)	517(6)	3269(9)	103(6)
N(2)	4632(7)	925(5)	2113(7)	83(5)
N(3)	3580(8)	4254(5)	1147(8)	81(5)
C(1)	3254(10)	1923(7)	4658(9)	80(6)
C(2)	2189(9)	1668(7)	3721(9)	79(6)
C(3)	2169(10)	786(7)	4144(10)	90(7)
C(4)	1316(14)	215(11)	2263(13)	134(11)
C(5)	926(13)	-164(9)	3790(14)	135(11)
C(6)	2311(10)	3949(7)	4127(10)	79(7)
C(7)	1355(10)	3957(8)	2914(10)	95(7)
C(8)	1822(12)	3858(10)	4962(12)	118(10)
C(9)	2603(13)	4829(8)	4238(13)	118(10)
C(10)	4965(11)	2984(8)	5591(10)	88(7)
C(11)	5849(11)	2095(9)	5732(12)	117(8)
C(12)	5429(11)	3705(9)	5355(12)	106(8)
C(13)	4858(13)	3174(11)	6719(10)	127(10)
C(14)	7548(13)	1024(11)	2748(15)	148(12)
C(15)	6727(15)	819(13)	3143(16)	177(13)
C(16)	5738(15)	533(10)	2172(20)	167(15)
C(17)	3779(19)	590(9)	1108(18)	205(16)
C(18)	4631(17)	577(10)	3118(16)	157(15)
C(19)	7065(12)	2099(9)	691(11)	98(8)
C(20)	6998(18)	2982(11)	199(14)	158(14)
C(21)	5997(13)	1823(11)	-224(12)	134(11)
C(22)	8155(14)	1459(13)	792(15)	166(13)
C(23)	7851(11)	2881(12)	3134(13)	127(10)
C(24)	7820(15)	2781(16)	4287(14)	189(15)
C(25)	9115(11)	2581(12)	3325(14)	141(10)
C(26)	7362(16)	3949(11)	2664(17)	166(14)
C(27)	867(15)	4073(11)	-880(17)	173(13)
C(28)	1681(18)	4676(12)	-604(17)	188(15)
C(29)	2333(12)	4780(10)	594(16)	133(10)
C(30)	4138(16)	4601(9)	2239(14)	159(13)
C(31)	4190(14)	4310(10)	461(15)	150(12)
C(32)	376(10)	2429(10)	-729(11)	107(8)
C(33)	702(19)	1364(14)	-742(18)	200(17)
C(34)	438(14)	2596(13)	458(14)	155(13)

C(35)	-836(11)	2748(14)	-1739(15)	187(13)
C(36)	1677(12)	2508(13)	-2152(10)	121(9)
C(37)	2697(21)	2742(25)	-2062(18)	309(28)
C(38)	673(17)	2814(25)	-3213(16)	308(24)
C(39)	1811(35)	1586(22)	-2358(30)	332(39)

[a] $x10^n$ where n = 5 for Y; n = 4 for Si, C, N, O

[b] $U_{eq} = 1/3\ \Sigma_i\Sigma_j U_{ij} a_i^* a_j^* (a_i \bullet a_j)$ $Å^2$ $x10^n$ where n = 4 for Y; n = 3 for Si, C, N, O.

Table III Bond distances (Å) for (7)

Atoms		Distance	Atoms		Distance
O(1)	-Y(1)	2.093(8)	C(3)	-C(2)	1.56(2)
O(2)	-Y(1)	2.099(8)	C(7)	-C(6)	1.56(2)
O(3)	-Y(1)	2.098(5)	C(8)	-C(6)	1.57(3)
N(2)	-Y(1)	2.629(8)	C(9)	-C(6)	1.54(2)
N(3)	-Y(1)	2.595(9)	C(11)	-C(10)	1.56(2)
O(1)	-Si(1)	1.630(9)	C(12)	-C(10)	1.56(2)
C(1)	-Si(1)	1.906(14)	C(13)	-C(10)	1.58(2)
C(6)	-Si(1)	1.954(11)	C(15)	-C(14)	1.55(3)
C(10)	-Si(1)	1.925(11)	C(16)	-C(15)	1.55(3)
O(2)	-Si(2)	1.631(8)	C(20)	-C(19)	1.56(3)
C(14)	-Si(2)	1.99(2)	C(21)	-C(19)	1.58(2)
C(19)	-Si(2)	1.91(2)	C(22)	-C(19)	1.52(2)
C(23)	-Si(2)	1.89(2)	C(24)	-C(23)	1.58(3)
O(3)	-Si(3)	1.583(6)	C(25)	-C(23)	1.58(2)
C(27)	-Si(3)	1.96(2)	C(26)	-C(23)	1.70(3)
C(32)	-Si(3)	1.87(2)	C(28)	-C(27)	1.57(3)
C(36)	-Si(3)	1.90(2)	C(29)	-C(28)	1.46(3)
C(3)	-N(1)	1.51(2)	C(33)	-C(32)	1.64(3)
C(4)	-N(1)	1.49(2)	C(34)	-C(32)	1.56(3)
C(5)	-N(1)	1.49(2)	C(35)	-C(32)	1.57(2)
C(16)	-N(2)	1.45(2)	C(37)	-C(36)	1.50(4)
C(17)	-N(2)	1.51(2)	C(38)	-C(36)	1.46(2)
C(18)	-N(2)	1.49(3)	C(39)	-C(36)	1.45(4)
C(29)	-N(3)	1.54(2)			
C(30)	-N(3)	1.46(2)			
C(31)	-N(3)	1.52(3)			
C(2)	-C(1)	1.57(2)			

Estimated standard deviations are given in parentheses.

Table IV Bond angles (deg) for (7)

Atoms			Angle	Atoms			Angle
O(2)	-Y(1)	-O(1)	121.5(3)	C(3)	-C(2)	-C(1)	106.8(8)
O(3)	-Y(1)	-O(1)	116.9(3)	C(2)	-C(3)	-N(1)	108.7(8)
O(3)	-Y(1)	-O(2)	121.6(3)	C(7)	-C(6)	-Si(1)	107.1(8)
N(2)	-Y(1)	-O(1)	93.6(3)	C(8)	-C(6)	-Si(1)	110.6(8)
N(2)	-Y(1)	-O(2)	89.5(3)	C(8)	-C(6)	-C(7)	107.3(11)
N(2)	-Y(1)	-O(3)	88.9(2)	C(9)	-C(6)	-Si(1)	114.2(10)
N(3)	-Y(1)	-O(1)	97.2(3)	C(9)	-C(6)	-C(7)	107.2(10)
N(3)	-Y(1)	-O(2)	84.1(3)	C(9)	-C(6)	-C(8)	110.2(12)
N(3)	-Y(1)	-O(3)	87.0(3)	C(11)	-C(10)	-Si(1)	107.7(8)
N(3)	-Y(1)	-N(2)	169.2(4)	C(12)	-C(10)	-Si(1)	110.2(8)
C(1)	-Si(1)	-O(1)	112.1(5)	C(12)	-C(10)	-C(11)	106.9(12)
C(6)	-Si(1)	-O(1)	109.8(5)	C(13)	-C(10)	-Si(1)	113.6(10)
C(6)	-Si(1)	-C(1)	108.9(6)	C(13)	-C(10)	-C(11)	110.0(11)
C(10)	-Si(1)	-O(1)	108.7(6)	C(13)	-C(10)	-C(12)	108.3(12)
C(10)	-Si(1)	-C(1)	104.2(5)	C(15)	-C(14)	-Si(2)	109.5(11)
C(10)	-Si(1)	-C(6)	113.1(5)	C(16)	-C(15)	-C(14)	112(2)
C(14)	-Si(2)	-O(2)	106.7(7)	C(15)	-C(16)	-N(2)	115(2)
C(19)	-Si(2)	-O(2)	113.4(5)	C(20)	-C(19)	-Si(2)	111.6(11)
C(19)	-Si(2)	-C(14)	103.2(8)	C(21)	-C(19)	-Si(2)	108.5(13)
C(23)	-Si(2)	-O(2)	111.1(6)	C(21)	-C(19)	-C(20)	104.3(11)
C(23)	-Si(2)	-C(14)	105.1(7)	C(22)	-C(19)	-Si(2)	114.4(10)
C(23)	-Si(2)	-C(19)	116.1(8)	C(22)	-C(19)	-C(20)	107(2)
C(27)	-Si(3)	-O(3)	109.0(6)	C(22)	-C(19)	-C(21)	110.8(13)
C(32)	-Si(3)	-O(3)	111.9(5)	C(24)	-C(23)	-Si(2)	109.5(14)
C(32)	-Si(3)	-C(27)	99.3(8)	C(25)	-C(23)	-Si(2)	112.2(12)
C(36)	-Si(3)	-O(3)	111.1(5)	C(25)	-C(23)	-C(24)	109.2(11)
C(36)	-Si(3)	-C(27)	110.3(9)	C(26)	-C(23)	-Si(2)	109.5(9)
C(36)	-Si(3)	-C(32)	114.5(8)	C(26)	-C(23)	-C(24)	110(2)
Si(1)	-O(1)	-Y(1)	175.1(4)	C(26)	-C(23)	-C(25)	106(2)
Si(2)	-O(2)	-Y(1)	164.3(5)	C(28)	-C(27)	-Si(3)	118.0(13)
Si(3)	-O(3)	-Y(1)	159.5(4)	C(29)	-C(28)	-C(27)	115(2)
C(4)	-N(1)	-C(3)	111.1(12)	C(28)	-C(29)	-N(3)	116(2)
C(5)	-N(1)	-C(3)	109.0(10)	C(33)	-C(32)	-Si(3)	108.0(13)
C(5)	-N(1)	-C(4)	112.2(12)	C(34)	-C(32)	-Si(3)	109.4(11)
C(16)	-N(2)	-Y(1)	111.9(9)	C(34)	-C(32)	-C(33)	103(2)
C(17)	-N(2)	-Y(1)	106.8(7)	C(35)	-C(32)	-Si(3)	114.9(13)
C(17)	-N(2)	-C(16)	107.7(14)	C(35)	-C(32)	-C(33)	105.0(14)
C(18)	-N(2)	-Y(1)	116.8(8)	C(35)	-C(32)	-C(34)	115.2(13)
C(18)	-N(2)	-C(16)	107.1(13)	C(37)	-C(36)	-Si(3)	109.2(13)
C(18)	-N(2)	-C(17)	106(2)	C(38)	-C(36)	-Si(3)	115.8(14)
C(29)	-N(3)	-Y(1)	118.2(9)	C(38)	-C(36)	-C(37)	114(2)
C(30)	-N(3)	-Y(1)	99.6(8)	C(39)	-C(36)	-Si(3)	114(2)
C(30)	-N(3)	-C(29)	107.7(12)	C(39)	-C(36)	-C(37)	108(3)
C(31)	-N(3)	-Y(1)	108.5(7)	C(39)	-C(36)	-C(38)	96(2)
C(31)	-N(3)	-C(29)	113.0(12)				
C(31)	-N(3)	-C(30)	108.8(14)				
C(2)	-C(1)	-Si(1)	116.3(7)				

Estimated standard deviations are given in parentheses.

Table V Fractional atomic coordinates [a] and equivalent isotropic temperature factors [b] for **10** (estimated standard deviations in parentheses)

atom	x	y	z	U_{eq}
Yb(1)	1115.3(3)	2049.2(2)	3354.6(2)	354(2)
Si(1)	2300(2)	3461.2(10)	3464.9(12)	523(8)
Si(2)	180(2)	1839.0(11)	1756.9(10)	501(8)
Si(3)	3007(2)	948.2(11)	3805.6(12)	577(9)
Si(4)	-1005(2)	1952.1(11)	4325.7(12)	592(10)
O(1)	1820(4)	2837(2)	3389(3)	59(2)
O(2)	580(4)	1908(3)	2455(3)	58(2)
O(3)	2135(4)	1410(3)	3659(3)	64(2)
O(4)	-102(4)	2091(3)	3900(3)	62(2)
C(11)	1528(7)	3987(4)	2968(5)	73(4)
C(12)	378(7)	3916(4)	2893(5)	72(4)
C(13)	6(8)	4280(5)	2345(7)	103(6)
N(1)	-1112(7)	4366(4)	2264(4)	73(4)
C(14)	-1542(12)	4722(6)	2753(8)	136(8)
C(15)	-1314(12)	4642(7)	1633(7)	151(9)
C(16)	2316(9)	3678(5)	4304(5)	85(5)
C(17)	3618(8)	3472(5)	3158(5)	80(4)
C(161)	1131(11)	3763(7)	4435(6)	128(7)
C(162)	2889(12)	4252(5)	4458(7)	124(7)
C(163)	2733(15)	3176(6)	4705(5)	137(8)
C(171)	4070(9)	4092(5)	3119(7)	106(6)
C(172)	3539(12)	3182(7)	2535(8)	137(8)
C(173)	4378(11)	3111(7)	3558(8)	141(8)
C(21)	-1139(7)	2151(4)	1610(4)	67(4)
C(22)	-1342(8)	2673(5)	2020(5)	71(4)
C(23)	-2372(8)	2936(5)	1802(5)	76(4)
N(2)	-2547(6)	3471(4)	2179(4)	72(3)
C(24)	-3462(8)	3758(6)	1884(7)	106(6)
C(25)	-2746(11)	3321(6)	2820(5)	109(6)
C(26)	72(8)	1038(4)	1569(5)	74(4)
C(27)	1048(7)	2258(4)	1259(4)	64(4)
C(261)	-519(11)	746(5)	2073(6)	107(6)
C(262)	1163(11)	749(5)	1564(7)	120(7)
C(263)	-490(13)	925(6)	933(6)	133(7)
C(271)	2165(8)	2088(5)	1398(7)	96(5)
C(272)	947(11)	2905(4)	1403(7)	101(6)
C(273)	766(11)	2186(6)	556(5)	106(6)
H(1)	-145(6)	404(4)	228(4)	5(3)[c]
C(31)	3933(10)	888(6)	3173(6)	114(6)
C(32)	3787(10)	1370(5)	2688(5)	101(5)
C(33)	4718(14)	1471(8)	2322(8)	150(9)
N(3)	5092(8)	1001(4)	1994(4)	88(4)
C(34)	4288(17)	825(10)	1554(9)	181(11)
C(35)	5918(14)	1150(9)	1658(9)	201(11)
C(36)	2423(9)	203(4)	3868(5)	80(4)
C(37)	3785(8)	1175(5)	4537(5)	87(5)

C(361)	3172(10)	-286(5)	3903(6)	102(6)
C(362)	1770(12)	170(6)	4417(8)	135(8)
C(363)	1750(15)	103(6)	3283(9)	172(10)
C(371)	4611(9)	739(5)	4747(7)	110(6)
C(372)	4389(13)	1728(7)	4337(9)	171(10)
C(373)	3118(12)	1331(8)	5039(6)	163(9)
C(41)	-1941(8)	2566(5)	4370(5)	82(5)
C(42)	-1504(9)	3180(5)	4327(6)	86(5)
C(43)	-2365(10)	3609(6)	4400(5)	102(6)
N(4)	-2044(9)	4198(4)	4258(5)	108(5)
C(44)	-2991(12)	4562(6)	4188(7)	140(8)
C(45)	-1295(14)	4435(7)	4725(8)	148(8)
C(46)	-1779(7)	1327(5)	3970(5)	80(5)
C(47)	-427(9)	1779(5)	5131(5)	84(5)
C(461)	-1137(10)	791(5)	3931(7)	113(6)
C(462)	-2134(11)	1527(6)	3304(6)	121(7)
C(463)	-2745(11)	1172(7)	4305(8)	139(8)
C(471)	-1230(12)	1641(7)	5595(6)	135(8)
C(472)	294(12)	1305(7)	5132(6)	134(7)
C(473)	105(16)	2343(8)	5374(7)	166(9)

[a] $x10^4$ [b] $U_{eq} = 1/3\ \Sigma_i\Sigma_j U_{ij} a_i^* a_j^* (a_i \bullet a_j)$ $Å^2$ $x10^n$ where n = 4 for Yb, Si; n = 3 for C, N, O; n = 2 for H. [c] refined isotropically.

Table VI Bond distances (Å) for **(10)**

Atoms	Distance	Atoms	Distance
O(1) -Yb(1)	2.062(6)	C(23) -C(22)	1.55(2)
O(2) -Yb(1)	2.074(6)	N(2) -C(23)	1.523(14)
O(3) -Yb(1)	2.092(6)	C(24) -N(2)	1.493(14)
O(4) -Yb(1)	2.077(6)	C(25) -N(2)	1.49(2)
O(1) -Si(1)	1.594(6)	C(261)-C(26)	1.56(2)
C(11) -Si(1)	1.895(10)	C(262)-C(26)	1.60(2)
C(16) -Si(1)	1.907(11)	C(263)-C(26)	1.56(2)
C(17) -Si(1)	1.916(12)	C(271)-C(27)	1.54(2)
O(2) -Si(2)	1.593(6)	C(272)-C(27)	1.55(2)
C(21) -Si(2)	1.903(9)	C(273)-C(27)	1.57(2)
C(26) -Si(2)	1.917(10)	C(32) -C(31)	1.55(2)
C(27) -Si(2)	1.909(10)	C(33) -C(32)	1.54(2)
O(3) -Si(3)	1.597(6)	N(3) -C(33)	1.42(2)
C(31) -Si(3)	1.921(14)	C(34) -N(3)	1.45(2)
C(36) -Si(3)	1.913(11)	C(35) -N(3)	1.41(2)
C(37) -Si(3)	1.920(12)	C(361)-C(36)	1.51(2)
O(4) -Si(4)	1.600(7)	C(362)-C(36)	1.53(2)
C(41) -Si(4)	1.902(11)	C(363)-C(36)	1.53(2)
C(46) -Si(4)	1.919(12)	C(371)-C(37)	1.54(2)
C(47) -Si(4)	1.918(11)	C(372)-C(37)	1.60(2)
C(12) -C(11)	1.532(13)	C(373)-C(37)	1.50(2)
C(13) -C(12)	1.53(2)	C(42) -C(41)	1.55(2)
N(1) -C(13)	1.495(14)	C(43) -C(42)	1.54(2)
C(14) -N(1)	1.50(2)	N(4) -C(43)	1.48(2)
C(15) -N(1)	1.53(2)	C(44) -N(4)	1.52(2)
C(161)-C(16)	1.63(2)	C(45) -N(4)	1.48(2)
C(162)-C(16)	1.57(2)	C(461)-C(46)	1.52(2)
C(163)-C(16)	1.54(2)	C(462)-C(46)	1.57(2)
C(171)-C(17)	1.57(2)	C(463)-C(46)	1.56(2)
C(172)-C(17)	1.52(2)	C(471)-C(47)	1.56(2)
C(173)-C(17)	1.54(2)	C(472)-C(47)	1.46(2)
C(22) -C(21)	1.55(2)	C(473)-C(47)	1.57(2)

Estimated standard deviations are given in parentheses.

Table VII Bond angles (deg) for **(10)**

Atoms	Angle	Atoms	Angle
O(2) -Yb(1) -O(1)	107.5(2)	C(23) -C(22) -C(21)	108.6(8)
O(3) -Yb(1) -O(1)	110.1(2)	N(2) -C(23) -C(22)	108.9(8)
O(3) -Yb(1) -O(2)	111.2(2)	C(24) -N(2) -C(23)	106.4(8)
O(4) -Yb(1) -O(1)	107.8(2)	C(25) -N(2) -C(23)	111.3(9)
O(4) -Yb(1) -O(2)	109.0(2)	C(25) -N(2) -C(24)	108.8(9)
O(4) -Yb(1) -O(3)	111.2(2)	C(261)-C(26) -Si(2)	108.0(7)
C(11) -Si(1) -O(1)	109.6(4)	C(262)-C(26) -Si(2)	111.0(7)
C(16) -Si(1) -O(1)	108.8(4)	C(262)-C(26) -C(261)	108.7(9)
C(16) -Si(1) -C(11)	110.6(5)	C(263)-C(26) -Si(2)	112.5(7)
C(17) -Si(1) -O(1)	110.1(4)	C(263)-C(26) -C(261)	109.1(10)
C(17) -Si(1) -C(11)	105.1(5)	C(263)-C(26) -C(262)	107.5(10)
C(17) -Si(1) -C(16)	112.6(5)	C(271)-C(27) -Si(2)	111.4(7)
C(21) -Si(2) -O(2)	111.4(4)	C(272)-C(27) -Si(2)	108.6(8)
C(26) -Si(2) -O(2)	108.6(4)	C(272)-C(27) -C(271)	107.8(9)
C(26) -Si(2) -C(21)	106.4(5)	C(273)-C(27) -Si(2)	113.2(8)
C(27) -Si(2) -O(2)	108.9(4)	C(273)-C(27) -C(271)	109.0(10)
C(27) -Si(2) -C(21)	107.0(4)	C(273)-C(27) -C(272)	106.6(9)
C(27) -Si(2) -C(26)	114.6(5)	C(32) -C(31) -Si(3)	112.7(9)
C(31) -Si(3) -O(3)	113.3(5)	C(33) -C(32) -C(31)	113.7(12)
C(36) -Si(3) -O(3)	109.6(4)	N(3) -C(33) -C(32)	117.8(14)
C(36) -Si(3) -C(31)	105.5(5)	C(34) -N(3) -C(33)	106.8(13)
C(37) -Si(3) -O(3)	108.8(4)	C(35) -N(3) -C(33)	112.6(13)
C(37) -Si(3) -C(31)	106.8(5)	C(35) -N(3) -C(34)	106.6(13)
C(37) -Si(3) -C(36)	112.9(5)	C(361)-C(36) -Si(3)	114.9(8)
C(41) -Si(4) -O(4)	113.3(4)	C(362)-C(36) -Si(3)	110.8(8)
C(46) -Si(4) -O(4)	108.5(4)	C(362)-C(36) -C(361)	109.0(10)
C(46) -Si(4) -C(41)	105.1(5)	C(363)-C(36) -Si(3)	107.2(8)
C(47) -Si(4) -O(4)	108.1(4)	C(363)-C(36) -C(361)	105.8(10)
C(47) -Si(4) -C(41)	109.4(5)	C(363)-C(36) -C(362)	108.8(12)
C(47) -Si(4) -C(46)	112.5(5)	C(371)-C(37) -Si(3)	113.4(8)
Si(1) -O(1) -Yb(1)	174.7(4)	C(372)-C(37) -Si(3)	104.2(9)
Si(2) -O(2) -Yb(1)	176.5(4)	C(372)-C(37) -C(371)	104.8(10)
Si(3) -O(3) -Yb(1)	171.3(4)	C(373)-C(37) -Si(3)	111.6(8)
Si(4) -O(4) -Yb(1)	165.6(4)	C(373)-C(37) -C(371)	112.5(11)
C(12) -C(11) -Si(1)	119.1(7)	C(373)-C(37) -C(372)	109.7(12)
C(13) -C(12) -C(11)	106.9(8)	C(42) -C(41) -Si(4)	116.3(8)
N(1) -C(13) -C(12)	115.7(10)	C(43) -C(42) -C(41)	108.2(10)
C(14) -N(1) -C(13)	114.4(10)	N(4) -C(43) -C(42)	110.9(11)
C(15) -N(1) -C(13)	105.9(10)	C(44) -N(4) -C(43)	107.1(11)
C(15) -N(1) -C(14)	111.2(10)	C(45) -N(4) -C(43)	113.0(11)
C(161)-C(16) -Si(1)	104.8(8)	C(45) -N(4) -C(44)	111.8(11)
C(162)-C(16) -Si(1)	114.1(8)	C(461)-C(46) -Si(4)	111.3(8)
C(162)-C(16) -C(161)	108.6(10)	C(462)-C(46) -Si(4)	105.6(8)
C(163)-C(16) -Si(1)	109.1(8)	C(462)-C(46) -C(461)	109.0(11)
C(163)-C(16) -C(161)	107.8(11)	C(463)-C(46) -Si(4)	114.7(9)
C(163)-C(16) -C(162)	112.1(10)	C(463)-C(46) -C(461)	108.5(11)
C(171)-C(17) -Si(1)	113.1(8)	C(463)-C(46) -C(462)	107.5(10)
C(172)-C(17) -Si(1)	107.5(8)	C(471)-C(47) -Si(4)	113.4(8)
C(172)-C(17) -C(171)	111.3(11)	C(472)-C(47) -Si(4)	112.4(8)
C(173)-C(17) -Si(1)	111.8(9)	C(472)-C(47) -C(471)	108.6(11)
C(173)-C(17) -C(171)	107.3(10)	C(473)-C(47) -Si(4)	106.1(9)
C(173)-C(17) -C(172)	105.6(11)	C(473)-C(47) -C(471)	105.3(11)
C(22) -C(21) -Si(2)	113.4(6)	C(473)-C(47) -C(472)	110.8(12)

Estimated standard deviations are given in parentheses.

Table VIII Summary of crystallographic data for **12a** and **12b**

	12a	**12b**
empirical formula	$C_{38}H_{96}Ba_2N_4O_2Si_6$	$C_{46}H_{112}Ba_2N_4O_4Si_6$
fw	1082.4	1228.6
cryst syst	monoclinic	monoclinic
space group	C2/c (No. 15)	$P2_1/c$ (No. 14)
a (Å)	20.451(4)	11.025(4)
b (Å)	14.277(3)	22.414(3)
c (Å)	22.258(5)	13.925(2)
α (deg)	90	90
β (deg)	101.14(2)	104.05(2)
γ (deg)	90	90
V (Å^3)	6376.1(2)	3338.0(1)
Z	4 (dimers)	2 (dimers)
ρ (calcd) (g cm^{-3})	1.130	1.222
μ (cm^{-1})	13.65	13.13
radiation, λ (Å)	Mo Kα, 0.70932	Mo Kα, 0.70932
T	ambient	ambient
$2\theta_{max}$ (deg)	45	45
no. of obsd reflcns	4158	4330
no. of unique reflcns	2484	1995
R [a]	0.069	0.090
R_w [b]	0.100	0.117

[a] $R = \Sigma(|F_o| - |F_c|) / \Sigma|F_o|$

[b] $R_w = [\Sigma w(|F_o| - |F_c|)^2 / \Sigma w(|F_o|)^2]^{1/2}$

Table IX Fractional atomic coordinates [a] and equivalent Isotropic temperature [b] factors for **12a** (estimated standard deviations in parentheses)

Atom	x/a	y/b	z/c	U_{eq}
Ba(1)	21463(6)	22756(8)	7578(5)	435(4)
Si(1)	3796(3)	3661(4)	794(2)	48(2)
Si(2)	1018(3)	4166(4)	1156(3)	61(2)
Si(3)	1213(3)	2481(4)	1972(3)	61(2)
O(1)	3189(5)	3022(8)	435(5)	45(4)
N(1)	2550(9)	4704(12)	-1054(8)	71(8)
N(2)	1350(7)	3130(10)	1381(6)	49(6)
C(1)	380(1)	487(2)	45(1)	75(9)
C(2)	357(1)	495(2)	-26(1)	78(10)
C(3)	279(1)	500(2)	-39(1)	69(9)
C(4)	277(1)	540(2)	-151(1)	102(12)
C(5)	177(1)	477(2)	-116(1)	104(13)
C(10)	464(1)	309(1)	76(1)	57(8)
C(11)	525(1)	356(2)	118(1)	88(10)
C(12)	474(1)	309(2)	9(1)	84(10)
C(13)	466(1)	204(2)	96(1)	97(13)
C(14)	369(1)	388(2)	163(1)	68(9)
C(15)	377(2)	296(2)	202(1)	120(15)
C(16)	418(1)	473(2)	194(1)	104(12)
C(17)	297(1)	433(2)	163(1)	98(12)
C(21)	125(1)	515(2)	174(1)	102(12)
C(22)	132(1)	451(2)	41(1)	81(11)
C(23)	6(1)	417(2)	95(1)	96(11)
C(31)	54(1)	156(2)	171(1)	98(12)
C(32)	101(1)	317(2)	265(1)	95(11)
C(33)	201(1)	180(2)	232(1)	91(11)

[a] Coordinates x 10^n where n = 5 for Ba, 4 for Si, O, and N, and 3 for C. Temperature parameters x10^n where n = 4 for Ba, and 3 for Si, O, N, and C.

[b] U_{eq} = the equivalent isotropic temperature parameter = $1/3 \sum_i \sum_j U_{ij} a_i^* a_j^* (a_i \cdot a_j)$

$T = \exp-(8\pi^2 U_{iso} \sin^2 \theta/\lambda^2)$

Table X Bond distances (Å) and angles (deg) for **12a** (estimated standard deviations in parentheses).

Distances			
O(1) - Ba(1)	2.602(11)	C(32)- Si(3)	1.90(2)
O(1)'- Ba(1)	2.645(12)	C(33)- Si(3)	1.92(2)
N(1)'- Ba(1)	2.94(2)	C(3) - N(1)	1.53(3)
N(2) - Ba(1)	2.630(14)	C(4) - N(1)	1.54(3)
O(1) - Si(1)	1.618(11)	C(5) - N(1)	1.56(3)
C(1) - Si(1)	1.89(2)	C(2) - C(1)	1.55(3)
C(10)- Si(1)	1.92(2)	C(3) - C(2)	1.56(3)
C(14)- Si(1)	1.93(2)	C(11)- C(10)	1.56(3)
N(2) - Si(2)	1.66(2)	C(12)- C(10)	1.54(3)
C(21)- Si(2)	1.91(2)	C(13)- C(10)	1.56(3)
C(22)- Si(2)	1.94(2)	C(15)- C(14)	1.57(3)
C(23)- Si(2)	1.93(2)	C(16)- C(14)	1.63(3)
N(2) - Si(3)	1.67(2)	C(17)- C(14)	1.62(3)
C(31)- Si(3)	1.91(2)		

Angles			
O(1) - Ba(1)- O(1)'	82.0(3)	Si(1)- O(1) - Ba(1)'	133.2(6)
O(1) - Ba(1)- N(1)'	107.5(3)	Ba(1)- O(1) - Ba(1)'	98.0(3)
O(1) - Ba(1)- N(2)	125.3(4)	C(3) - N(1) - Ba(1)'	92.6(1)
N(1)'- Ba(1)- N(2)	117.1(4)	C(4) - N(1) - Ba(1)'	133(2)
N(1)'- Ba(1)- O(1)'	94.5(3)	C(5) - N(1) - Ba(1)'	104(2)
N(2) - Ba(1)- O(1)'	122.4(3)	C(4) - N(1) - C(3)	112(2)
C(1) - Si(1)- O(1)	112.3(8)	C(5) - N(1) - C(3)	105(2)
C(10)- Si(1)- O(1)	110.3(7)	C(5) - N(1) - C(4)	106(2)
C(10)- Si(1)- C(1)	107.3(10)	Si(2)- N(2) - Ba(1)	20.8(7)
C(14)- Si(1)- O(1)	110.3(8)	Si(3)- N(2) - Ba(1)	111.8(7)
C(14)- Si(1)- C(1)	104.8(10)	Si(3)- N(2) - Si(2)	127.4(9)
C(14)- Si(1)- C(10)	111.6(9)	C(2) - C(1) - Si(1)	117(2)
C(21)- Si(2)- N(2)	114.9(11)	C(3) - C(2) - C(1)	107(2)
C(22)- Si(2)- N(2)	107.7(9)	C(2) - C(3) - N(1)	107(2)
C(22)- Si(2)- C(21)	108.4(11)	C(11)- C(10)- Si(1)	114.1(14)
C(23)- Si(2)- N(2)	114.3(9)	C(12)- C(10)- Si(1)	108.7(14)
C(23)- Si(2)- C(21)	105.1(11)	C(12)- C(10)- C(11)	110(2)
C(23)- Si(2)- C(22)	105.9(11)	C(13)- C(10)- Si(1)	112.3(14)
C(31)- Si(3)- N(2)	111.5(9)	C(13)- C(10)- C(11)	106(2)
C(32)- Si(3)- N(2)	115.5(10)	C(13)- C(10)- C(12)	105(2)
C(32)- Si(3)- C(31)	109.8(12)	C(15)- C(14)- Si(1)	113(2)
C(33)- Si(3)- N(2)	109.6(9)	C(16)- C(14)- Si(1)	111(2)
C(33)- Si(3)- C(31)	106.1(12)	C(16)- C(14)- C(15)	114(2)
C(33)- Si(3)- C(32)	103.6(11)	C(17)- C(14)- Si(1)	110(2)
Si(1)- O(1) - Ba(1)	133.2(6)	C(17)- C(14)- C(15)	109(2)
		C(17)- C(14)- C(16)	100(2)

Table XI Fractional atomic coordinates [a] and equivalent isotropic temperature [b] factors for **12b** (estimated standard deviations in parentheses)

Atom	x/a	y/b	z/c	U_{eq}
Ba(1)	21463(6)	22756(8)	7578(5)	435(4)
Ba(1)	49546(13)	91396(5)	677(10)	530(5)
Si(1)	4636(5)	10082(4)	2327(4)	62(3)
Si(2)	1625(7)	9004(4)	-1077(6)	76(3)
Si(3)	2933(8)	7824(4)	-672(6)	80(3)
O(1)	469(1)	1005(1)	117(1)	6(1)
O(2)	686(2)	841(1)	112(1)	9(1)
N(1)	886(3)	890(1)	403(2)	12(1)
N(2)	289(2)	859(1)	-68(1)	7(1)
C(1)	620(2)	999(2)	323(2)	9(1)
C(2)	680(3)	941(2)	324(2)	10(2)
C(3)	818(3)	945(2)	400(3)	11(2)
C(4)	1015(3)	901(2)	430(4)	18(3)
C(5)	843(4)	847(2)	466(3)	16(2)
C(10)	417(3)	1087(1)	262(2)	8(1)
C(11)	382(4)	1094(2)	364(3)	15(2)
C(12)	315(3)	1112(1)	181(2)	9(1)
C(13)	534(3)	1130(1)	272(2)	11(2)
C(14)	343(3)	950(1)	259(2)	8(1)
C(15)	373(4)	941(2)	376(2)	12(2)
C(16)	370(4)	891(1)	210(2)	10(2)
C(17)	215(3)	971(2)	221(2)	9(1)
C(21)	211(3)	982(1)	-87(2)	9(1)
C(22)	83(3)	895(1)	-249(2)	10(1)
C(23)	37(3)	887(2)	-39(2)	11(2)
C(31)	176(3)	746(1)	-177(2)	10(1)
C(32)	460(3)	754(2)	-68(3)	15(2)
C(33)	260(4)	751(2)	47(3)	16(2)
C(41)	812(3)	852(2)	102(4)	15(2)
C(42)	889(3)	803(2)	146(3)	13(2)
C(43)	799(5)	764(2)	188(3)	17(3)
C(44)	681(3)	794(1)	183(2)	10(1)

[a] Coordinates x 10^n where n = 5 for Ba, 4 for Si, and 3 for O, N, and C. Temperature parameters x10^n where n = 4 for Ba, 3 for Si, and 2 for O, N, and C.

[b] U_{eq} = the equivalent isotropic temperature parameter = $1/3 \sum_i \sum_j U_{ij} a_i^* a_j^* (a_i \cdot a_j)$

$T = \exp(-8\pi^2 U_{iso} \sin^2 \theta/\lambda^2)$

Table XII Bond distances (Å) and angles (deg) for **12b**

Distances

O(1) - Ba(1)	2.603(14)	C(41)- O(2)	1.46(3)
O(1)'- Ba(1)	2.596(14)	C(44)- O(2)	1.45(3)
N(2) - Ba(1)	2.58(2)	C(3) - N(1)	1.43(4)
O(2) - Ba(1)	2.78(2)	C(4) - N(1)	1.41(4)
O(1) - Si(1)	1.637(14)	C(5) - N(1)	1.46(4)
C(1) - Si(1)	1.88(3)	C(2) - C(1)	1.47(4)
C(10)- Si(1)	1.91(3)	C(3) - C(2)	1.63(4)
C(14)- Si(1)	1.96(3)	C(11)- C(10)	1.56(4)
N(2) - Si(2)	1.65(2)	C(12)- C(10)	1.50(4)
C(21)- Si(2)	1.90(3)	C(13)- C(10)	1.59(4)
C(22)- Si(2)	1.96(3)	C(15)- C(14)	1.59(4)
C(23)- Si(2)	1.88(3)	C(16)- C(14)	1.55(4)
N(2) - Si(3)	1.71(2)	C(17)- C(14)	1.46(4)
C(31)- Si(3)	1.92(2)	C(42)- C(41)	1.42(4)
C(32)- Si(3)	1.95(4)	C(43)- C(42)	1.54(5)
C(33)- Si(3)	1.85(3)	C(44)- C(43)	1.46(5)

Angles

N(2) - Ba(1)- O(1)	113.5(5)	C44)- O(2) - Ba(1)	132(3)
N(2) - Ba(1)- O(1)'	109.7(7)	C(41)- O(2) - Ba(1)	122(2)
N(2) - Ba(1)- O(2)	115.6(9)	C(4) - N(1) - C(3)	111(3)
O(2) - Ba(1)- O(1)	109.8(7)	C(5) - N(1) - C(3)	110(3)
O(2) - Ba(1)- O(1)'	121.1(7)	C(5) - N(1) - C(4)	114(4)
Ba(1)- O(1) - Ba(1)	96.0(7)	Si(2)- N(2) - Ba(1)	117(10)
C(1) - Si(1)- O(1)	113.9(11)	Si(3)- N(2) - Ba(1)	117(10)
C(10)- Si(1)- O(1)	109.4(10)	Si(3)- N(2) - Si(2)	126(12)
C(10)- Si(1)- C(1)	102.1(14)	C(2) - C(1) - Si(1)	117(2)
C(14)- Si(1)- O(1)	110.2(10)	C(3) - C(2) - C(1)	108(3)
C(14)- Si(1)- C(1)	110.8(14)	C(2) - C(3) - N(1)	112(3)
C(14)- Si(1)- C(10)	110.1(11)	C(11)- C(10)- Si(1)	115(2)
C(21)- Si(2)- N(2)	108.0(12)	C(12)- C(10)- Si(1)	112(2)
C(22)- Si(2)- N(2)	115.7(13)	C(12)- C(10)- C(11)	110(2)
C(22)- Si(2)- C(21)	104.6(14)	C(13)- C(10)- Si(1)	109(2)
C(23)- Si(2)- N(2)	114.0(12)	C(13)- C(10)- C(11)	104(3)
C(23)- Si(2)- C(21)	107(2)	C(13)- C(10)- C(12)	106(3)
C(23)- Si(2)- C(22)	107.1(13)	C(15)- C(14)- Si(1)	108(2)
C(31)- Si(3)- N(2)	113.6(13)	C(16)- C(14)- Si(1)	106(2)
C(32)- Si(3)- N(2)	111.0(13)	C(16)- C(14)- C(15)	108(2)
C(32)- Si(3)- C(31)	108(2)	C(17)- C(14)- Si(1)	111(2)
C(33)- Si(3)- N(2)	111.8(14)	C(17)- C(14)- C(15)	111(2)
C(33)- Si(3)- C(31)	107(2)	C(17)- C(14)- C(16)	112(3)
C(33)- Si(3)- C(32)	106(2)	C(42)- C(41)- O(2)	108(3)
Si(1)- O(1) - Ba(1)	130.8(8)	C(43)- C(42)- C(41)	104(3)
Si(1)'-O(1)'- Ba(1)	131.5(12)	C(44)- C(43)- C(42)	111(3)
O(1) - Ba(1)- O(1)	84.0(6)	C(43)- C(44)- O(2)	101(2)
C(44)- O(2) - C(41)	112(2)		

Estimated standard deviations are given in parentheses.

Table XIII Summary of crystallographic data for **20**

empirical formula	$C_{34}H_{69}N_4OSi_5Y$	Z	8
fw	779.3	ρ (calcd) (g cm^{-3})	1.139
cryst syst	monoclinic	μ (cm^{-1})	33.34
space group	I2/a (No. 15)	radiation, λ (Å)	Cu K_α, 1.542
a (Å)	20.709(3)	T	295 K
b (Å)	9.511(1)	$2\theta_{max}$ (deg)	60
c (Å)	46.579(6)	no. of obsd reflcns	5986
α (deg)	90	no. of unique reflcns	3543
β (deg)	98.04(1)	R [a]	0.078
γ (deg)	90	R_w [b]	0.101
V (Å^3)	9084.6		

[a] $R = \Sigma(|F_o| - |F_c|) / \Sigma|F_o|$

[b] $R_w = [\Sigma w(|F_o| - |F_c|)^2 / \Sigma w(|F_o|)^2]^{1/2}$

Table XIV Fractional atomic coordinates [a] and equivalent isotropic temperature [b] factors for **20** (estimated standard deviations in parentheses)

Atom	x/a	y/b	z/c	Ueq
Y(1)	8012(5)	20650(12)	10505(2)	466(4)
Si(1)	831(2)	3450(4)	1747(1)	46(1)
Si(2)	-821(2)	2403(5)	772(1)	72(2)
Si(3)	-398(2)	-269(4)	1089(1)	58(1)
Si(4)	1231(2)	1592(5)	396(1)	82(2)
Si(5)	1388(2)	4565(5)	584(1)	89(2)
O(1)	85.8(3)	344.1(8)	140.4(1)	49(3)
N(1)	189.8(4)	112.6(1)	133.0(2)	59(4)
N(2)	168.7(5)	382.2(12)	273.9(2)	65(4)
N(3)	-23.3(4)	132.9(10)	96.2(2)	49(4)
N(4)	117.8(5)	283.7(11)	65.6(2)	60(4)
C(1)	94.5(5)	155.5(12)	187.3(2)	43(4)
C(2)	148.8(6)	74.2(14)	181.5(2)	48(5)
C(3)	159.6(7)	-59(2)	192.5(3)	62(6)
C(4)	115.5(7)	-125(2)	208.6(3)	66(6)
C(5)	60.5(7)	-51(2)	213.8(3)	65(6)
C(6)	50.0(6)	86.7(14)	203.4(3)	54(5)
C(7)	200.1(5)	142.6(14)	164.7(2)	52(5)
C(8)	237.6(6)	217(2)	121.0(3)	92(7)
C(9)	207.2(7)	-39(2)	126.8(3)	84(7)
C(10)	156.1(6)	452.4(12)	192.9(2)	46(5)
C(11)	184.5(6)	440.3(13)	221.9(3)	52(5)
C(12)	241.7(6)	518.3(14)	232.6(3)	65(6)

C(13)	270.9(6)	600(2)	213.2(3)	67(6)
C(14)	243.5(7)	614.4(14)	183.7(3)	64(6)
C(15)	185.3(6)	538.3(13)	173.7(3)	56(5)
C(16)	157.0(6)	338.3(13)	2433(2)	57(5)
C(17)	146.1(7)	270(2)	291.4(3)	76(6)
C(18)	135.6(7)	520(2)	278.2(3)	76(6)
C(19)	3.0(6)	433.5(13)	181.2(3)	56(5)
C(20)	3.2(7)	577(2)	165.9(3)	75(6)
C(21)	-4.5(7)	458(2)	213.6(3)	77(6)
C(22)	-57.2(6)	341(2)	165.7(3)	73(6)
C(23)	-163.9(7)	233(2)	92.1(4)	127(9)
C(24)	-98.1(9)	188(2)	37.3(3)	116(8)
C(25)	-53.6(8)	423(2)	79.2(4)	113(8)
C(26)	43.7(6)	-110(2)	123.8(3)	72(6)
C(27)	-86.8(7)	-26(2)	141.4(3)	77(6)
C(28)	-84.0(8)	-151(2)	81.2(3)	100(7)
C(29)	80.1(12)	203(2)	2.4(3)	150(11)
C(30)	85.3(8)	-11.6(14)	51.1(3)	84(7)
C(31)	208.7(8)	101(2)	35.4(4)	133(10)
C(32)	222.3(12)	468(2)	45.6(6)	182(13)
C(33)	143.4(10)	565(2)	91.2(3)	109(8)
C(34)	77.3(12)	548(2)	30.4(4)	180(13)

[a] $x10^n$ where n = 5 for Y; n = 4 for Si; n = 3 for O, N, C

[b] $U_{eq} = 1/3 \sum_i \sum_j U_{ij} a_i^* a_j^* (a_i . a_j)$ Å $x10^n$ where n = 4 for Y; n = 3 for Si, O, N, C.

Table XV Bond distances (Å) and angles (deg) for **20**

Atoms		Distance	Atoms		Distance
O(1)	-Y(1)	2.093(7)	C(34)	-Si(5)	1.90(2)
N(1)	-Y(1)	2.611(9)	C(7)	-N(1)	1.49(2)
N(3)	-Y(1)	2.237(9)	C(8)	-N(1)	1.56(2)
N(4)	-Y(1)	2.221(9)	C(9)	-N(1)	1.52(2)
O(1)	-Si(1)	1.606(7)	C(16)	-N(2)	1.473(14)
C(1)	-Si(1)	1.901(12)	C(17)	-N(2)	1.46(2)
C(10)	-Si(1)	1.923(12)	C(18)	-N(2)	1.50(2)
C(19)	-Si(1)	1.921(13)	C(2)	-C(1)	1.42(2)
N(3)	-Si(2)	1.733(10)	C(6)	-C(1)	1.43(2)
C(23)	-Si(2)	1.92(2)	C(3)	-C(2)	1.37(2)
C(24)	-Si(2)	1.909(14)	C(7)	-C(2)	1.55(2)
C(25)	-Si(2)	1.84(2)	C(4)	-C(3)	1.41(2)
N(3)	-Si(3)	1.679(10)	C(5)	-C(4)	1.39(2)
C(26)	-Si(3)	1.940(13)	C(6)	-C(5)	1.40(2)
C(27)	-Si(3)	1.909(14)	C(11)	-C(10)	1.40(2)
C(28)	-Si(3)	1.89(2)	C(15)	-C(10)	1.41(2)
N(4)	-Si(4)	1.705(11)	C(12)	-C(11)	1.43(2)
C(29)	-Si(4)	1.88(2)	C(16)	-C(11)	1.56(2)

C(30)	-Si(4)	1.91(2)	C(13)	-C(12)	1.39(2)
C(31)	-Si(4)	1.89(2)	C(14)	-C(13)	1.42(2)
N(4)	-Si(5)	1.744(12)	C(15)	-C(14)	1.43(2)
C(32)	-Si(5)	1.91(3)	C(20)	-C(19)	1.54(2)
C(33)	-Si(5)	1.84(2)	C(21)	-C(19)	1.56(2)
			C(22)	-C(19)	1.61(2)

Angles

N(1)	-Y(1)	-O(1)	82.7(3)	C(9)	-N(1)	-Y(1)	116.3(7)
N(3)	-Y(1)	-O(1)	106.7(3)	C(9)	-N(1)	-C(7)	111.2(10)
N(3)	-Y(1)	-N(1)	136.8(3)	C(9)	-N(1)	-C(8)	110.8(10)
N(4)	-Y(1)	-O(1)	117.2(3)	C(17)	-N(2)	-C(16)	108.1(10)
N(4)	-Y(1)	-N(1)	98.2(3)	C(18)	-N(2)	-C(16)	111.0(9)
N(4)	-Y(1)	-N(3)	112.9(3)	C(18)	-N(2)	-C(17)	112.1(10)
C(1)	-Si(1)	-O(1)	106.4(5)	Si(2)	-N(3)	-Y(1)	119.7(5)
C(10)	-Si(1)	-O(1)	107.9(5)	Si(3)	-N(3)	-Y(1)	117.0(5)
C(10)	-Si(1)	-C(1)	108.1(5)	Si(3)	-N(3)	-Si(2)	123.3(6)
C(19)	-Si(1)	-O(1)	108.1(5)	Si(4)	-N(4)	-Y(1)	114.9(6)
C(19)	-Si(1)	-C(1)	116.1(5)	Si(5)	-N(4)	-Y(1)	126.6(5)
C(19)	-Si(1)	-C(10)	110.0(5)	Si(5)	-N(4)	-Si(4)	118.5(6)
C(23)	-Si(2)	-N(3)	112.8(7)	C(2)	-C(1)	-Si(1)	121.7(9)
C(24)	-Si(2)	-N(3)	110.8(7)	C(6)	-C(1)	-Si(1)	122.4(9)
C(24)	-Si(2)	-C(23)	107.5(8)	C(6)	-C(1)	-C(2)	115.9(11)
C(25)	-Si(2)	-N(3)	109.6(6)	C(3)	-C(2)	-C(1)	121.6(12)
C(25)	-Si(2)	-C(23)	108.0(9)	C(7)	-C(2)	-C(1)	119.0(11)
C(25)	-Si(2)	-C(24)	108.0(8)	C(7)	-C(2)	-C(3)	119.2(11)
C(26)	-Si(3)	-N(3)	106.3(5)	C(4)	-C(3)	-C(2)	121.8(13)
C(27)	-Si(3)	-N(3)	115.5(6)	C(5)	-C(4)	-C(3)	118.2(13)
C(27)	-Si(3)	-C(26)	104.1(6)	C(6)	-C(5)	-C(4)	120.5(13)
C(28)	-Si(3)	-N(3)	115.3(6)	C(5)	-C(6)	-C(1)	121.9(12)
C(28)	-Si(3)	-C(26)	108.0(7)	C(2)	-C(7)	-N(1)	114.1(9)
C(28)	-Si(3)	-C(27)	106.8(7)	C(11)	-C(10)	-Si(1)	125.5(9)
C(29)	-Si(4)	-N(4)	115.5(7)	C(15)	-C(10)	-Si(1)	114.1(8)
C(30)	-Si(4)	-N(4)	108.9(6)	C(15)	-C(10)	-C(11)	120.1(11)
C(30)	-Si(4)	-C(29)	106.6(8)	C(12)	-C(11)	-C(10)	120.7(12)
C(31)	-Si(4)	-N(4)	115.4(7)	C(16)	-C(11)	-C(10)	121.8(10)
C(31)	-Si(4)	-C(29)	107.4(9)	C(16)	-C(11)	-C(12)	117.5(10)
C(31)	-Si(4)	-C(30)	101.9(8)	C(13)	-C(12)	-C(11)	118.6(12)
C(32)	-Si(5)	-N(4)	112.0(8)	C(14)	-C(13)	-C(12)	122.1(12)
C(33)	-Si(5)	-N(4)	110.8(6)	C(15)	-C(14)	-C(13)	118.2(13)
C(33)	-Si(5)	-C(32)	106.6(10)	C(14)	-C(15)	-C(10)	120.3(11)
C(34)	-Si(5)	-N(4)	113.6(7)	C(11)	-C(16)	-N(2)	114.8(10)
C(34)	-Si(5)	-C(32)	108.1(11)	C(20)	-C(19)	-Si(1)	104.9(9)
C(34)	-Si(5)	-C(33)	105.4(8)	C(21)	-C(19)	-Si(1)	115.0(8)
Si(1)	-O(1)	-Y(1)	141.2(4)	C(21)	-C(19)	-C(20)	108.9(11)
C(7)	-N(1)	-Y(1)	114.9(7)	C(22)	-C(19)	-Si(1)	108.7(8)
C(8)	-N(1)	-Y(1)	99.1(7)	C(22)	-C(19)	-C(20)	109.4(10)
C(8)	-N(1)	-C(7)	102.9(9)	C(22)	-C(19)	-C(21)	109.7(10)

Estimated standard deviations in parentheses.

Table XVI Summary of crystallographic data for **45**

formula	$C_{36}H_{43}NO_3Zr$	ρ (calcd) (g cm^{-3})	1.253
fw	628.95	μ (cm^{-1})	29.8
cryst syst	orthorhombic	radiation, λ (Å)	Cu Kα, 1.542
space group	$P2_12_12_1$ (No.)	T	ambient
a (Å)	9.535(2)	$2\theta_{max}$ (deg)	110
b (Å)	17.675(3)	no. obsd reflcns	1647
c (Å)	19.786(2)	no. of unique reflcns	2389
α (deg)	90	R^a	0.050
β (deg)	90	$R_w{}^b$	0.054
γ (deg)	90		
V (Å^3)	3334.4(9)		
Z	4		

[a] $R = \Sigma(|F_o|-|F_c|)/\Sigma|F_o|$. [b] $R_w = [\Sigma w(|F_o|-|F_c|^2)/\Sigma w(|F_o|)^2]^{1/2}$.

Table XVII Fractional atomic coordinates and temperature parameters of complexes **45**

Atom	x/a	y/b	z/c	Ueq
Zr(1)	-74323(15)	-96388(10)	-92313(5)	589(4)
O(1)	-7009(10)	-8169(9)	-8828(4)	76(4)
O(2)	-7181(11)	-11213(9)	-8918(5)	82(4)
N(1)	-4970(12)	-9696(13)	-9307(6)	67(5)
C(1)	-4652(18)	-8945(17)	-9794(7)	77(7)
C(2)	-4327(21)	-9266(16)	-8735(11)	99(9)
C(3)	-4650(22)	-7934(16)	-8588(10)	92(8)
C(4)	-6136(20)	-7726(15)	-8393(8)	90(7)
C(5)	-4440(18)	-10969(14)	-9401(8)	83(7)
C(6)	-4820(18)	-11863(15)	-8932(8)	76(6)

C(7)	-6350(20)	-12217(13)	-8916(7)	83(7)
C(8)	-9691(16)	-9538(27)	-9522(8)	91(8)
C(11)	-5494(19)	-9390(15)	-10315(7)	83(7)
C(12)	-6862(18)	-9588(15)	-10194(6)	71(6)
C(13)	-7738(22)	-9986(15)	-10661(6)	94(7)
C(14)	-7168(28)	-10113(20)	-11246(9)	121(10)
C(15)	-5775(27)	-9845(26)	-11340(9)	132(12)
C(16)	-4956(23)	-9498(20)	-10908(9)	110(9)
C(41)	-6289(27)	-6341(17)	-8380(10)	136(11)
C(42)	-6536(25)	-8319(20)	-7799(7)	121(10)
C(71)	-6772(25)	-12953(19)	-9481(10)	138(10)
C(72)	-6679(26)	-12900(20)	-8317(10)	140(11)
C(81)	-10214(18)	-9640(20)	-8919(8)	85(8)
C(82)	-10514(26)	-10776(22)	-8716(11)	153(14)
C(83)	-10947(46)	-10914(23)	-8150(14)	213(24)
C(84)	-11215(48)	-9930(29)	-7811(13)	294(43)
C(85)	-10912(30)	-8799(26)	-8011(10)	231(25)
C(86)	-10427(23)	-8650(20)	-8567(10)	115(11)
C(111)	-3071(19)	-8829(19)	-9897(10)	116(9)

Estimated standard deviations are given in parentheses.

Coordinates x10n where n = 5,4,4,4 for Zr,O,N,C.

Temperature parameters x10n where n = 4,3,3,3 for Zr,O,N,C.

Ueq = the equivalent isotropic temperature parameter.

$Ueq = 1/3\ \Sigma_i\Sigma_j U_{ij} a_i^* a_j^* (a_i . a_j)$

$T = \exp-(8\pi^2 U_{iso} \sin^2 \theta/\lambda^2)$

Table XVIII Bond distances (Å) and bond angles (deg) of complexes 45

Distance

N(1)	-Zr(1)	2.419(12)	C(6)	-C(5)	1.517(23)
O(1)	-Zr(1)	1.938(9)	C(7)	-C(6)	1.551(24)
O(2)	-Zr(1)	1.927(10)	C(71)	-C(7)	1.592(25)
C(8)	-Zr(1)	2.313(16)	C(72)	-C(7)	1.605(24)
C(12)	-Zr(1)	2.275(14)	C(81)	-C(8)	1.478(23)
C(81)	-Zr(1)	2.817(19)	C(12)	-C(11)	1.386(22)
C(1)	-N(1)	1.433(19)	C(16)	-C(11)	1.463(23)
C(2)	-N(1)	1.531(24)	C(13)	-C(12)	1.443(22)
C(5)	-N(1)	1.538(20)	C(14)	-C(13)	1.459(27)
C(4)	-O(1)	1.404(18)	C(15)	-C(14)	1.413(31)
C(7)	-O(2)	1.392(17)	C(16)	-C(15)	1.332(29)
C(11)	-C(1)	1.536(23)	C(82)	-C(81)	1.391(19)
C(111)	-C(1)	1.572(25)	C(86)	-C(81)	1.391(18)
C(3)	-C(2)	1.568(25)	C(83)	-C(82)	1.373(18)
C(4)	-C(3)	1.540(27)	C(84)	-C(83)	1.377(20)
C(41)	-C(4)	1.565(24)	C(85)	-C(84)	1.384(19)
C(42)	-C(4)	1.566(24)	C(86)	-C(85)	1.371(17)

Angles

O(1)	-Zr(1)	-N(1)	81.0(5)	C(3)	-C(4)	-O(1)	108.4(15)
O(2)	-Zr(1)	-N(1)	82.8(5)	C(41)	-C(4)	-O(1)	108.0(15)
O(2)	-Zr(1)	-O(1)	125.4(4)	C(41)	-C(4)	-C(3)	104.3(17)
C(8)	-Zr(1)	-N(1)	159.1(6)	C(42)	-C(4)	-O(1)	108.3(15)
C(8)	-Zr(1)	-O(1)	107.5(8)	C(42)	-C(4)	-C(3)	115.1(17)
C(8)	-Zr(1)	-O(2)	105.9(8)	C(42)	-C(4)	-C(41)	112.4(17)
C(12)	-Zr(1)	-N(1)	71.7(5)	C(6)	-C(5)	-N(1)	115.8(13)
C(12)	-Zr(1)	-O(1)	112.8(5)	C(7)	-C(6)	-C(5)	115.1(14)
C(12)	-Zr(1)	-O(2)	110.7(5)	C(6)	-C(7)	-O(2)	110.9(12)
C(12)	-Zr(1)	-C(8)	87.4(6)	C(71)	-C(7)	-O(2)	105.5(14)
C(81)	-Zr(1)	-N(1)	169.3(5)	C(71)	-C(7)	-C(6)	111.4(17)
C(81)	-Zr(1)	-O(1)	95.0(5)	C(72)	-C(7)	-O(2)	105.9(15)
C(81)	-Zr(1)	-O(2)	91.6(5)	C(72)	-C(7)	-C(6)	109.7(16)
C(81)	-Zr(1)	-C(8)	31.6(5)	C(72)	-C(7)	-C(71)	113.3(16)
C(81)	-Zr(1)	-C(12)	118.9(6)	C(81)	-C(8)	-Zr(1)	93.4(11)
C(1)	-N(1)	-Zr(1)	104.8(10)	C(12)	-C(11)	-C(1)	114.5(15)
C(2)	-N(1)	-Zr(1)	109.9(11)	C(16)	-C(11)	-C(1)	123.8(17)
C(2)	-N(1)	-C(1)	112.9(13)	C(16)	-C(11)	-C(12)	121.4(18)
C(5)	-N(1)	-Zr(1)	111.8(10)	C(11)	-C(12)	-Zr(1)	115.8(12)
C(5)	-N(1)	-C(1)	111.5(13)	C(13)	-C(12)	-Zr(1)	124.4(12)
C(5)	-N(1)	-C(2)	106.0(13)	C(13)	-C(12)	-C(11)	118.4(16)
C(4)	-O(1)	-Zr(1)	140.4(10)	C(14)	-C(13)	-C(12)	118.9(19)
C(7)	-O(2)	-Zr(1)	145.2(10)	C(15)	-C(14)	-C(13)	119.2(19)
C(11)	-C(1)	-N(1)	107.2(14)	C(16)	-C(15)	-C(14)	122.1(20)
C(111)	-C(1)	-N(1)	112.3(15)	C(15)	-C(16)	-C(11)	119.8(20)
C(111)	-C(1)	-C(11)	116.0(16)	C(8)	-C(81)	-Zr(1)	55.1(9)
C(3)	-C(2)	-N(1)	113.8(16)	C(82)	-C(81)	-Zr(1)	106.8(14)
C(4)	-C(3)	-C(2)	113.4(16)	C(82)	-C(81)	-C(8)	117.2(23)

C(86) -C(81) -Zr(1)	107.0(14)	C(84) -C(83) -C(82)	120.0(14)
C(86) -C(81) -C(8)	122.1(22)	C(85) -C(84) -C(83)	120.8(14)
C(86) -C(81) -C(82)	120.6(15)	C(86) -C(85) -C(84)	119.6(12)
C(83) -C(82) -C(81)	119.0(15)	C(85) -C(86) -C(81)	119.6(14)

Estimated standard deviations are given in parentheses.

Table XIX Summary of crystallographic data for **51a**

formula	$C_{24}H_{43}N_2O_2AlZr$	ρ(calcd) (g cm^{-3})	1.218
fw	509.81	μ (cm^{-1})	37.4
cryst syst	monoclinic	radiation, λ (Å)	Cu Kα, 1.542
space group	$P2_1$ (No.)	T	ambient
a (Å)	11.069(2)	$2\theta_{max}$ (deg)	120
b (Å)	11.320(2)	no. obsd reflcns	2033
c (Å)	11.222(3)	no. of unique reflcns	2181
α (deg)	90	R^a	0.043
β (deg)	98.62(2)	R_w^b	0.057
γ (deg)	90		
V (Å^3)	1390.2(5)		
Z	2		

[a] $R = \Sigma(|F_o|-|F_c|)/\Sigma|F_o|$. [b] $R_w = [\Sigma w(|F_o|-|F_c|^2)/\Sigma w(|F_o|)^2]^{1/2}$.

Table XX Atomic parameters x,y,z and Biso for **51a**

	x	y	z	Biso
ZR1	0.29548(7)	0.25000(8)	0.17718(7)	3.43(4)
AL1	0.2369 (3)	0.3103 (4)	0.4162 (3)	4.97(17)
O1	0.2836 (7)	0.3985 (7)	0.2844 (7)	4.1 (4)
O2	0.2050 (8)	0.1765 (8)	0.0331 (7)	5.3 (4)
N1	0.3504 (9)	0.3860 (9)	0.0233 (9)	4.5 (4)
N2	0.2439 (8)	0.1704 (9)	0.3206 (8)	3.9 (4)
C1	0.3308 (16)	0.5189 (13)	0.2881 (14)	6.0 (8)
C2	0.3137 (15)	0.5598 (11)	0.1523 (14)	6.3 (8)
C3	0.3921 (14)	0.5025 (12)	0.0709 (13)	5.6 (7)
C4	0.2456 (12)	0.4011 (15)	-0.0782 (12)	6.2 (7)
C5	0.1962 (13)	0.2931 (15)	-0.1461 (11)	6.5 (9)
C6	0.1311 (13)	0.2000 (14)	-0.0774 (12)	6.1 (7)
C7	0.2467 (19)	0.5982 (15)	0.3515 (15)	7.6 (10)
C8	0.4597 (14)	0.5209 (16)	0.3456 (15)	7.6 (9)
C9	0.0084 (12)	0.244 (3)	-0.0546 (13)	8.2 (9)
C10	0.1101 (18)	0.0855 (17)	-0.1513 (15)	8.4 (10)
C11	0.4581 (10)	0.3210 (11)	-0.0170 (10)	4.3 (5)
C12	0.5126 (13)	0.3900 (15)	-0.1131 (12)	6.3 (7)
C13	0.5470 (10)	0.2829 (9)	0.0938 (10)	3.9 (5)
C14	0.5008 (9)	0.2218 (7)	0.1884 (9)	3.1 (5)
C15	0.5819 (11)	0.1814 (12)	0.2828 (11)	4.9 (6)
C16	0.7083 (12)	0.1974 (14)	0.2887 (12)	6.4 (7)
C17	0.7507 (10)	0.2630 (24)	0.1963 (13)	6.6 (8)
C18	0.6737 (11)	0.2991 (12)	0.1002 (11)	5.0 (6)
C19	0.0663 (16)	0.3561 (18)	0.4420 (18)	9.6 (11)
C20	0.3668 (16)	0.3248 (17)	0.5577 (13)	7.7 (9)
C21	0.1894 (11)	0.0571 (12)	0.3511 (11)	4.7 (6)
C22	0.2078 (15)	0.0375 (18)	0.4890 (14)	8.1 (10)
C23	0.0519 (13)	0.0529 (16)	0.2997 (14)	7.2 (8)
C24	0.2556 (21)	-0.0408 (14)	0.2970 (20)	9.1 (13)

Biso is the Mean of the Principal Axes of the Thermal Ellipsoid

Table XXI Bond distances (Å) and angles (deg) of complexes **51a**

Distances			
Zr(1)-Al(1)	2.933(4)	C(11)-C(12)	1.526(17)
Zr(1)-O(1)	2.083(8)	C(11)-C(13)	1.528(16)
Zr(1)-O(2)	1.956(8)	C(13)-C(14)	1.424(14)
Zr(1)-N(1)	2.457(9)	C(13)-C(18)	1.406(16)
Zr(1)-N(2)	2.001(9)	C(14)-C(15)	1.361(16)
Zr(1)-C(14)	2.279(10)	C(15)-C(16)	1.403(18)
Al(1)-O(1)	1.919(9)	C(16)-C(17)	1.412(24)
Al(1)-N(2)	1.921(11)	C(17)-C(18)	1.335(21)
Al(1)-C(19)	2.020(15)	C(21)-C(23)	1.546(19)
Al(1)-C(20)	1.983(16)	C(4)-C(5)	1.500(24)
O(1)-C(1)	1.458(18)	C(21)-C(22)	1.547(19)
O(2)-C(6)	1.404(15)	C(5)-C(6)	1.547(22)
N(1)-C(3)	1.471(18)	C(21)-C(24)	1.506(22)
N(1)-C(4)	1.508(16)	C(6)-C(9)	1.505(22)
N(1)-C(11)	1.526(15)	C(6)-C(10)	1.538(23)
N(2)-C(21)	1.479(16)	C(1)-C(2)	1.577(22)
C(1)-C(7)	1.543(22)	C(1)-C(8)	1.475(23)
C(2)-C(3)	1.499(21)		
Angles			
Al(1)-Zr(1)-O(1)	0.72(24)	Al(1)-Zr(1)-O(2)	134.4(3)
Al(1)-Zr(1)-N(1)	127.5(3)	Al(1)-Zr(1)-N(2)	40.6(3)
Al(1)-Zr(1)-C(14)	109.7(3)	O(1)-Zr(1)-O(2)	138.8(4)
O(1)-Zr(1)-N(1)	86.8(3)	O(1)-Zr(1)-N(2)	81.3(4)
O(1)-Zr(1)-C(14)	103.3(3)	O(2)-Zr(1)-N(1)	80.5(3)
O(2)-Zr(1)-N(2)	107.5(4)	N(2)-Zr(1)-C(14)	107.1(4)
N(1)-Zr(1)-C(14)	77.1(3)	N(1)-C(11)-C(13)	109.3(9)
Zr(1)-Al(1)-O(1)	45.08(25)	N(1)-C(11)-C(12)	111.8(10)
Zr(1)-Al(1)-N(2)	42.6(3)	C(12)-C(11)-C(13)	116.4(10)
Zr(1)-Al(1)-C(19)	122.0(6)	C(11)-C(13)-C(14)	119.0(9)
Zr(1)-Al(1)-C(20)	121.2(5)	O(1)-Al(1)-N(2)	87.7(4)
O(1)-Al(1)-C(19)	110.0(7)	O(1)-Al(1)-C(20)	109.1(6)
N(2)-Al(1)-C(19)	114.1(7)	N(2)-Al(1)-C(20)	115.5(6)
C(19)-Al(1)-C(20)	116.4(8)	Zr(1)-O(1)-Al(1)	94.2(4)
Zr(1)-O(1)-C(1)	135.8(8)	Al(1)-O(1)-C(1)	126.9(8)
Zr(1)-O(2)-C(6)	143.9(9)	C(11)-C(13)-C(18)	121.4(10)
Zr(1)-N(1)-C(3)	113.8(7)	C(14)-C(13)-C(18)	119.5(10)
Zr(1)-N(1)-C(4)	111.0(7)	Zr(1)-C(14)-C(13)	110.9(7)
Zr(1)-N(1)-C(11)	101.1(6)	Zr(1)-C(14)-C(15)	128.8(8)
C(3)-N(1)-C(4)	109.6(11)	C(13)-C(14)-C(15)	118.3(10)
C(3)-N(1)-C(11)	108.9(10)	C(14)-C(15)-C(16)	122.0(11)
C(4)-N(1)-C(11)	112.2(10)	Zr(1)-N(2)-Al(1)	96.8(5)
Zr(1)-N(2)-C(21)	138.8(8)	C(15)-C(16)-C(17)	118.2(11)
Al(1)-N(2)-C(21)	122.2(7)	O(1)-C(1)-C(2)	104.9(11)
O(1)-C(1)-C(7)	108.6(13)	C(16)-C(17)-C(18)	120.8(11)
O(1)-C(1)-C(8)	110.3(12)	C(2)-C(1)-C(7)	106.3(12)
C(2)-C(1)-C(8)	112.8(14)	C(13)-C(18)-C(17)	120.9(11)
C(7)-C(1)-C(8)	113.6(14)	C(1)-C(2)-C(3)	117.7(12)
N(1)-C(3)-C(2)	115.5(11)	N(1)-C(4)-C(5)	118.1(12)
N(2)-C(21)-C(22)	111.1(12)	N(2)-C(21)-C(23)	110.7(11)

N(2)-C(21)-C(24)	107.8(10)	C(22)-C(21)-C(23)	110.1(11)
C(22)-C(21)-C(24)	107.3(14)	O(2)-C(6)-C(5)	108.4(10)
C(4)-C(5)-C(6)	117.7(11)	C(23)-C(21)-C(24)	109.8(15)
O(2)-C(6)-C(9)	109.6(11)	O(2)-C(6)-C(10)	109.8(13)
C(5)-C(6)-C(9)	110.9(16)	C(5)-C(6)-C(10)	110.5(12)
C(9)-C(6)-C(10)	107.8(15)		

Estimated standard deviations are given in parentheses.

Table XXII Summary of crystallographic data for **55a**

formula	$C_{36}H_{43}NO_3Zr$	ρ (calcd) (g cm^{-3})	1.253
fw	628.95	μ (cm^{-1})	29.8
cryst syst	orthorhombic	radiation, λ (Å)	Cu Kα, 1.542
space group	$P2_12_12_1$ (No.)	T	ambient
a (Å)	9.535(2)	$2\theta_{max}$ (deg)	110
b (Å)	17.675(3)	no. obsd reflcns	1647
c (Å)	19.786(2)	no. of unique reflcns	2389
α (deg)	90	R^a	0.050
β (deg)	90	R_w^b	0.054
γ (deg)	90		
V (Å^3)	3334.4(9)		
Z	4		

[a] $R = \Sigma(|F_o|-|F_c|)/\Sigma|F_o|$. [b] $R_w = [\Sigma w(|F_o|-|F_c|^2)/\Sigma w(|F_o|)^2]^{1/2}$.

Table XXIII Atomic parameters x,y,z and Biso for 55a

	x	y	z	Biso
ZR1	0.87348(14)	0.05260(7)	0.97697(7)	4.52(6)
O1	0.7351 (10)	0.1319 (5)	0.9827 (7)	6.7 (6)
O2	0.8147 (9)	-0.0509 (5)	0.9711 (5)	5.7 (5)
O3	1.0551 (10)	0.0733 (5)	0.9363 (5)	5.5 (5)
N1	0.7836 (11)	0.0501 (8)	0.8519 (6)	5.3 (6)
C1	0.6164 (18)	0.1680 (7)	0.9527 (9)	6.0 (9)
C2	0.5034 (21)	0.1699 (14)	1.0080 (14)	12.1 (16)
C3	0.6607 (23)	0.2477 (11)	0.9371 (13)	11.3 (17)
C4	0.5700 (19)	0.1270 (9)	0.8908 (10)	6.8 (10)
C5	0.6804 (18)	0.1119 (10)	0.8364 (11)	6.6 (10)
C6	0.7060 (18)	-0.0233 (9)	0.8423 (10)	6.5 (9)
C7	0.7793 (18)	-0.0944 (9)	0.8593 (10)	6.6 (10)
C8	0.7804 (18)	-0.1148 (9)	0.9339 (9)	6.1 (9)
C9	0.6354 (22)	-0.1417 (9)	0.9580 (11)	8.5 (12)
C10	0.8851 (22)	-0.1771 (9)	0.9454 (11)	8.7 (12)
C11	0.9076 (14)	0.0545 (12)	0.8009 (8)	5.8 (8)
C12	0.8750 (21)	0.0272 (11)	0.7295 (7)	7.9 (11)
C13	0.9787 (19)	0.1318 (11)	0.8003 (8)	6.1 (9)
C14	0.9325 (19)	0.1859 (12)	0.7551 (10)	7.8 (11)
C15	0.996 (3)	0.2561 (14)	0.7505 (14)	10.7 (16)
C16	1.108 (3)	0.2747 (12)	0.7892 (13)	10.1 (15)
C17	1.1574 (23)	0.2199 (12)	0.8361 (10)	8.3 (12)
C18	1.1003 (19)	0.1486 (9)	0.8406 (8)	5.8 (9)
C19	1.1555 (16)	0.0918 (9)	0.8895 (8)	5.0 (8)
C20	1.2236 (17)	0.0225 (10)	0.8575 (9)	5.5 (9)
C21	1.2248 (15)	-0.0444 (11)	0.8907 (8)	5.7 (8)
C22	1.2883 (18)	-0.1109 (11)	0.8598 (10)	5.9 (10)
C23	1.2848 (18)	-0.1796 (12)	0.8930 (11)	7.6 (12)
C24	1.3456 (24)	-0.2398 (12)	0.8625 (12)	8.7 (13)
C25	1.4123 (22)	-0.2363 (13)	0.7991 (14)	8.8 (14)
C26	1.4177 (22)	-0.1663 (16)	0.7651 (11)	9.5 (14)
C27	1.3525 (19)	-0.1006 (11)	0.7970 (9)	5.9 (9)

C28	1.3536 (20)	-0.0306 (11)	0.7634 (8)	6.5 (10)
C29	1.2920 (18)	0.0304 (10)	0.7928 (9)	6.1 (9)
C30	0.9512 (16)	0.0530 (10)	1.0861 (8)	5.4 (8)
C31	1.0698 (21)	0.0025 (9)	1.0934 (9)	5.9 (9)
C32	1.2104 (21)	0.0252 (11)	1.0835 (10)	6.9 (10)
C33	1.3216 (23)	-0.0243 (13)	1.0858 (13)	9.6 (14)
C34	1.298 (3)	-0.0974 (14)	1.1000 (13)	9.0 (14)
C35	1.164 (3)	-0.1227 (10)	1.1120 (15)	10.4 (18)
C36	1.0536 (22)	-0.0741 (9)	1.1075 (12)	8.1 (12)

Biso is the Mean of the Principal Axes of the Thermal Ellipsoid

Table XXIV Bond distances (Å) and bond angles (deg) of 55a

Distances

Zr(1)-O(1)	1.928(9)	C(13)-C(18)	1.44(3)
Zr(1)-O(2)	1.917(9)	C(14)-C(15)	1.38(3)
Zr(1)-O(3)	1.945(10)	C(15)-C(16)	1.35(4)
Zr(1)-C(30)	2.284(15)	C(16)-C(17)	1.42(3)
O(1) -C(1)	1.429(19)	C(35)-C(36)	1.36(3)
O(2) -C(8)	1.387(18)	C(17)-C(18)	1.38(3)
O(3) -C(19)	1.370(19)	C(18)-C(19)	1.490(22)
N(1) -C(5)	1.502(22)	C(19)-C(20)	1.524(24)
N(1) -C(6)	1.505(20)	C(20)-C(21)	1.35(3)
N(1) -C(11)	1.557(18)	C(11)-C(13)	1.52(3)
C(1) -C(2)	1.54(3)	C(25)-C(26)	1.41(4)
C(1) -C(3)	1.503(24)	C(6) -C(7)	1.477(24)
C(1) -C(4)	1.490(25)	C(26)-C(27)	1.46(3)
C(20)-C(29)	1.44(3)	C(27)-C(28)	1.40(3)
C(21)-C(22)	1.46(3)	C(7) -C(8)	1.52(3)
C(22)-C(23)	1.38(3)	C(28)-C(29)	1.36(3)
C(22)-C(27)	1.40(3)	C(8) -C(9)	1.54(3)
C(23)-C(24)	1.35(3)	C(30)-C(31)	1.45(3)
C(4) -C(5)	1.53(3)	C(34)-C(35)	1.37(4)
C(24)-C(25)	1.41(4)	C(13)-C(14)	1.383(25)
C(8) -C(10)	1.504(25)	C(11)-C(12)	1.526(22)
C(31)-C(32)	1.41(3)	C(33)-C(34)	1.34(3)
C(31)-C(36)	1.391(24)	C(32)-C(33)	1.38(3)

Angles

O(1)-Zr(1)-O(2)	119.8(4)	C(11)-C(13)-C(14)	118.9(16)
O(1)-Zr(1)-O(3)	119.8(4)	C(11)-C(13)-C(18)	122.7(15)
O(1)-Zr(1)-C(30)	99.4(6)	C(14)-C(13)-C(18)	118.2(17)
O(2)-Zr(1)-O(3)	114.5(4)	C(13)-C(14)-C(15)	121.5(19)

O(2)-Zr(1)-C(30)	98.9(5)	C(14)-C(15)-C(16)	121.9(20)
O(3)-Zr(1)-C(30)	95.8(5)	C(15)-C(16)-C(17)	117.6(20)
Zr(1)-O(1)-C(1)	147.4(10)	C(16)-C(17)-C(18)	122.4(19)
Zr(1)-O(2)-C(8)	151.4(10)	C(17)-C(18)-C(19)	121.3(16)
Zr(1)-O(3)-C(19)	161.1(9)	C(18)-C(19)-C(20)	114.9(14)
C(5)-N(1)-C(6)	106.2(11)	C(19)-C(20)-C(21)	120.3(16)
C(5)-N(1)-C(11)	109.2(13)	C(20)-C(21)-C(22)	120.4(15
C(6)-N(1)-C(11)	109.5(13)	C(19)-C(20)-C(29)	119.0(15)
O(1)-C(1)-C(2)	105.6(15)	C(1)-C(4)-C(5)	117.3(15))
O(1)-C(1)-C(3)	106.3(13)	C(21)-C(22)-C(23)	120.0(18)
O(1)-C(1)-C(4)	111.1(13)	C(21)-C(20)-C(29)	120.7(16)
C(21)-C(22)-C(27)	116.7(17)	C(23)-C(22)-C(27)	23.3(18)
C(2)-C(1)-C(3)	108.8(16)	C(2)-C(1)-C(4)	112.8(16)
Zr(1)-C(30)-C(31)	110.2(11)	C(3)-C(1)-C(4)	111.8(15)
O(3)-C(19)-C(18)	110.6(13)	C(13)-C(18)-C(19)	120.4(14)
O(3)-C(19)-C(20)	112.7(13)	C(23)-C(24)-C(25)	123.8(21)
N(1)-C(5)-C(4)	115.6(15)	C(22)-C(23)-C(24)	117.9(20)
N(1)-C(6)-C(7)	118.2(14)	C(24)-C(25)-C(26)	118.7(19)
C(25)-C(26)-C(27)	118.4(20)	C(22)-C(27)-C(28)	122.7(17)
C(6)-C(7)-C(8)	115.2(15)	C(22)-C(27)-C(26)	117.8(19)
C(26)-C(27)-C(28)	119.5(18)	C(13)-C(18)-C(17)	118.2(16)
O(2)-C(8)-C(7)	108.9(13)	C(20)-C(29)-C(28)	119.9(16)
O(2)-C(8)-C(9)	107.4(14)	C(33)-C(34)-C(35)	120.2(21)
O(2)-C(8)-C(10)	111.1(14)	C(34)-C(35)-C(36)	120.2(18)
C(7)-C(8)-C(9)	111.6(15)	C(12)-C(11)-C(13)	111.6(14)
C(7)-C(8)-C(10)	108.9(15)	C(31)-C(36)-C(35)	122.7(19)
C(9)-C(8)-C(10)	108.9(14)	C(32)-C(33)-C(34)	119.6(21)
C(30)-C(31)-C(32)	123.4(16)	C(31)-C(32)-C(33)	123.0(18)
N(1)-C(11)-C(12)	115.5(13)	C(30)-C(31)-C(36)	122.3(18)
N(1)-C(11)-C(13)	112.8(14)	C(32)-C(31)-C(36)	114.2(18)

Estimated standard deviations are given in parentheses.

REFERENCES

1. (a) J.J Ebelman and M. Bouquet, *Ann. Chim. Phys.*, **17**, 54 (1846); (b) J.J. Ebelman, *Ann.* **57**, 331 (1846).

2. J.H. Gladstone and A. Tribe, *J. Chem. Soc.*, **39**, 4 (1881).

3. (a) R. Hornbergger, *Ann.*, **181**, 232 (1876); (b) O. Hinsberg, *Ann.*, **239**, 253 (1887).

4. D.C. Bradley and W. Wardlaw, *Nature*, **165**, 75 (1950).

5. R.J. Meyer and M. Koss, *Chem. Ber.*, 2622 (1902).

6. D.C. Bradley, R.C. Mehrotra and D.P. Gaur, "Metal Alkoxide", Academic Press, London, 1978.

7. W. Tischtschenko, *Chem. Zentr.*, 77, 1309, 1556, 1558 (1906).

8. (a) A. Verley, *Bull. Soc. Chim.*, **37**, 537 (1925); (b) H. Meerwein and R. Schmidt, *Ann.*, **444**, 221 (1925); (c) W. Ponndorf, *Z. Angew. Chem.*, **39**, 138 (1926); (d) W.G. Young, B. Von Bock, B. Kirschnick, W. Lenz and A. Migge, *J. Prakt. Chem.*, **147**, 211 (1926).

9. (a) D.C. Bradley, *Chem. Rev.*, **89**, 1317 (1989); (b) K.G. Caulton and L.G. Hubert-Pfalzgraf, *Chem. Rev.*, **90**, 969 (1990); (c) L.G. Hubert-Pfalzgraf, *Appl. Organomet. Chem.*, **6**, 627 (1992); (d) C.D. Chandler, C. Roger and M.J. Hampden-Smith, *Chem. Rev.*, **93**, 1206 (1993).

10. W.A. Herrmann, N.W. Huber and O. Runte, *Angew. Chem. Int. Ed. Engl.*, **34**, 2187 (1995).

11. (a) B. Weidmann and D. Seebach, *Angew. Chem., Int. Ed. Engl.*, **22**, 31 (1983); (b) D. Seebach, A.K. Beck, M. Schiess, L. Wilder and A. Wonnacott, *Pure Appl. Chem.*, **55**, 1087 (1983); (c) N.W. Eilerts and J.A. Heppert, *Polyhedron*, **14**, 3255 (1995); M.A. Lockwood, M.C. Potyen, B.D. Steffey, P.E. Fanwick and I.P. Rothwell, *polyhedron*, **14**, 3293 (1995); (d) P.T. Wolczanski, *Polyhedron*, **14**, 3335 (1995).

12. R.E. LaPointe, P.T. Wolczanski and G.D. Van Duyne, *Organometallics*, **4**, 1810 (1985).

13. C.A. Tolman, *Chem. Rev.*, 77 313 (1977).

14. (a) D.C. Bradley, R.C. Mehrotra and W. Wardlaw, *J. Chem. Soc.*, 2027 (1952); (b) D.C. Bradley, R.C. Mehrotra and W. Wardlaw, *J. Chem. Soc.*, 4204 (1952).

15. (a) D.C. Bradley, H. Chudzynska D.F. Frigo, M.E. Hammond and M.B. Hursthouse, *Polyhedron*, **9**, 719 (1990); (b) G. Helgesson, S. Jagner, O. Poncelt and L.G. Hubert-Pfalzgraf, *Polyhedron*, **10**, 1559 (1991); (c) O. Poncelet, W.J. Sartain, L.G. Hubert-Pfalzgraf, K. Folting and K.G. Caulton, *Inorg. Chem.*, **28**, 263 (1989).

16. D.C. Bradley, R.C Mehrotra, J.D. Swanwick and W. Wardlaw, *J. Chem. Soc.*, 2025 (1953).

17. (a) D.C. Bradley, H.Chudzynska, M.B. Hursthouse and M. Motevalli, *Polyhedron*, **10**, 1049 (1991); (b) W.A. Herrmann, R. Anwander, M. Kleine and W. Scherer, *Chem. Ber.* **125**, 1971 (1992); (c) W.A. Herrmann, R. Anwander and W. Scherer, *Chem. Ber.* **126**, 1533 (1993).

18. A.L. Allred, *J. Inorg. Nuclear Chem.*, **17**, 215 (1961).

19. (a) M.H. Chisholm and I.P. Rothwell, in *Comprehensive coordination chemistry* (Edited by G. Wilkinson, R.D. Gillaard and J.A. McCleverty), Charpt 15.3, Pergamon Press, Oxford (1987); (b) T.W. Coffindaffer, B.D. Steffey, I.P. Rothwell and J.C. Huffman, *J. Am. Chem. Soc.*, **111**, 4742 (1989); (c) J.L. Kerschner, P.E. Fanwick, I.P. Rothwell and J.C. Huffman, *Inorg. Chem.*, **28**, 780 (1989).

20. B.D. Steffey, P.E. Fanwick and I.P. Pothwell, *Polyhedron*, **9**, 963 (1990).

21. R.O. Duthaler and A. Hafner, *Chem. Rev.*, **92**, 807 (1992).

22. L. Chamberlain, J.C. Huffman, J. Keddington and I.P. Rothwell, *J. Chem. Soc. Commun.* 805 (1982).

23. (a) S.L. Latesky, A.K. McMullen, G.P. Niccolai and I.P. Rothwell, *Organometallics*, **4**, 902 (1985); (b) P.E. Fanwick, A.E. Ogilvy and I.P. Rothwell, *Organometallics*, **6**, 73 (1987); (c) L.M. Kobriger, A.K. McMullen, P.E. Fanwick and I.P. Rothwell, *Polyhedron*, **8**, 77 (1989).

24. O.W. Steward and D.R. Fussaro, *J. Organomet. Chem.*, **129**, C28 (1977).

25. (a) K.J. Covert, P.T. Wolczanski, S.A. Hill and P.J. Krusic, *Inorg. Chem.*, **31**, 66 (1992); (b) K.J. Covert and P.T. Wolczanski, *Inorg. Chem*, **28** , 4565 (1989).

26. (a) T.V.Lubben, P.T. Wolczanski and G.D. Van Duyne, *Organometallics* **3**, 977 (1984); (b) R.E Lapointe, P.T. Wolczanski and G.D. Van Duyne, *Organometallics*, **4**, 1810 (1985).

27. S. Patai and Z. Rappaport (Eds.), "*The Chemistry of Organic Silicon Compounds*" Wiley and Sons, New York (1989).

28. T.V. Lubben, P.T. Wolczanski and G.D. Duyne, *Organometallics*, **3**, 977 (1984).

29. (a) R.J.P. Corriu and M. Henner, *J. Organomet. Chem.*, **74**, 1 (1974); (b) H.F. Schaefer, *Acc. Chem. Res.*, **15**, 283 (1982); (c) C. Eabon, *J. Organomet. Chem.*, **100**, 43 (1975).

30. (a) K.J. Covert, D.R. Neithammer and P.T. Wolczanski, *Inorg. Chem.*, **30**, 2494 (1991); (b) R. Toreki, R.E. LaPointe and P.T. Wolczanski *J. Am. Chem. Soc.* **109**, 7558 (1987); (c) D.F. Eppley, P.T. Wolczanski and G.D. Van Duyne, *Angew. Chem. Int. Ed. Engl.* **30**, 584 (1991).

31. (a) W.A. Herrmann, R. Anwander, M. Kleine and W. Scherer, *Chem. Ber.*, **125**, 1971 (1992); (b) W.A. Herrmann and W. Scherer, *Chem. Ber.*, **126**, 1533 (1993).

32. (a) and A. Singh, *J. Chem. Soc. Commun.* 1499 (1983); (b) P.B. Hitchcock, M.F. Lappert and R.G. Smith, *Inorg. Chim. Acta.*, **139**, 183 (1987); (c) H.A. Stecher, A. Sen. And A.L. Rheingold, *Inorg. Chem.* **27**, 1130 (1988); (d) G.B. Deacon, T. Feng, S. Nickel and A.H. White, *Aust. J. Chem.* **45**, 671 (1992).

33. (a) A.P Purdy, A.D. Berry, R.T. Holm, M. Fatemi and D.K. Gaskill, *Inorg. Chem.*, **28**, 2799 (1989); (b) J. Zha., K.H. Dahmen, T.J. Marks, B.M. Wessels and C.R. Kannewurf, *Appl. Phys. Lett.*, **53**, 1750 (1989); (c) R. Gardiner, D.W. Brown, P.S. Kirlin and A. Rheingold, *Chem, Mater.*, **3**, 45 (1991).

34. (a) D.C. Bradley, J. Chudzynska, M.B. Husthouse and M. Motevalli, *Polyhedron*, **10**, 1 (1991); (b) D.C. Bradley, J. Chudzynska, M.B. Husthouse and M. Motevalli, *Polyhedron*, **10**, 1049 (1991);

35. J.A. Samuels, E.B. Lobkovsky, W.E. Streib, K. Folting, F.C. Huffman and K.G. Caulton, *J. Am. Chem. Soc.*, **115**, 5093 (1993).

36. L. Pauling, *Die Natur der Chemischen Bindung*, 3rd ed., Verlag Chemie, Weinheim, 1989

37. M. Hudlicky, "Chemistry of Organic Fluorine Compounds", 2nd Ed., Ellis Horwood Ltd. (1976).

38. (a) D. Streitwieser and C. Nebenzahl, *J. Am. Chem. Soc.*, **98**, 2188 (1976); (b) A. Henne and C. Fox, *J. Am. Chem. Soc.*, **75**, 991 (1953).

39. R. Filler and R.M. Schure, *J. Org. Chem.*, **32**, 1217 (1967).

40. R.C. Mehrotra and A. Singh, *Chemtracts Inorg. Chem.*, **6**, 27 (1994).

41. J.D. Cotton, M.D. Cundy, D.H. Harris, M.F. Lappert and P.W. Lednor, *J. Chem. Soc. Chem. Commum.*, 651 (1974).

42. H.A. Stecher, A. Sen and A.L.Rheingold, *Inorg. Chem.*, **28**, 3280 (1989).

43. H.S. Horowitz, S.J. Mclane, A.W. Sleight, J.D. Druliner, P.L. Gai, M.J. VanKavelaar, J.L. Wagner, B.D. Biggs and S.J. Poon, *Science*, **243**, 66, (1989).

44. W.A. Herrmann, N.W. Huber, R. Anwander and T. Preirmeier, *Chem. Ber.*, **126**, 1127 (1993).

45. W.A. Herrmann, N.W. Huber and T.Priermeier, *Angew. Chem. Int. Ed. Engl.*, **33**, 105 (1994).

46. (a) F.T. Edelmann, *Angew. Chem. Int. Ed. Engl.*, **34**, 2466 (1995); (b) H. Schumann, *Angew. Chem. Int. Ed. Engl.*, **23**, 474 (1984); (c) C.J. Schaverien, *Adv. Organomet.Chem.*, **36**, 283 (1994); (d) F.T. Edelmann, in *Comprehensive Organometallic Chemistry II*; E.W. Abel, F.G. Stone and G. Wilkinson Eds.; Pergamon (1995); (e) H. Schumann, J.A. Meese-Marktscheffel and L. Esser, *Chem. Rev.*, **95**, 865 (1995).

47. (a) K. Narasaka, *Synthesis*, 1 (1991); (b) M. A. Lockwood, M.C. Potyen, P.E. Fanwick and I.P. Rothwell, *Polyhedron*, **14**, 3293 (1995).

48. P. Shao, D. Berg and G.W. Bushnell, *Inorg. Chem.*, **33**, 6334 (1994).

49. (a) M. Hayashi, K. Kohmura and N. Oguni, *Synlett.*, 744 (1991); (b) M. Emziane, K.I. Sutowardoyo and D.J. Sinou, *J. Organomet. Chem.*, **346**, C7 (1988).

50. (a) W.A. Nugent and R.L. Harlow, *J. Am.. Chem. Soc.*, **116**, 6142 (1994); (b) H. Takemura, M. Komeshima, I. Takahashi and S. Hashimoto, *Tetrahedron Lett.*, **28**, 5687 (1987).

51. Y. Gao, R.M. Hanson, J.M. Klunder, S.Y. Ko, H. Masamune and K. B. Sharpless, *J. Am. Chem. Soc.*, **109**, 5765 (1987).

52. (a) W.A. Nugent, *J. Am. Chem. Soc.*, **114**, 2768 (1992); (b) M.D. Fryzuk, T.S. Haddad and S.J. Rettig; *J. Am. Chem. Soc.*, **112**, 8158 (1990); (c) M.D. Fryzuk, T.S. Haddad, M. Mylvaganam, D.M. McConville and S.J. Rettig, *J. Am. Chem. Soc.*, **115**, 2782 (1993).

53. (a) H.J. Heers, A. Meetsma and J.H. Teuben, *J. Chem. Soc. Chem. Commun.*, 962 (1988); (b) H.J. Heers, A. Meetsma, J.H. Teuben and R.D. Rogers, *Organometallics*, **9**, 2637 (1989).

54. L. Hasinoff, J. Takats, X.W. Zhang, A.H. Bond and R.D. Rodgers, *J. Am. Chem. Soc.*, **116**, 8833 (1994).

55. K. Ziegler, E. Holzkamp, H. Breil and H. Martin, *Angew. Chem.*, **67**, 541 (1955); (b) K. Ziegler, *Angew. Chem.*, **76**, 545 (1964).

56. (a) G. Natta, *Angew. Chem.*, **68**, 393 (1956); (b) G. Natta, *Angew. Chem.*, **76**, 553 (1964);

57. (a) N. Kashiwa, Polymer, **12**, 602 (1980); (b) N. Kashiwa and J. Yoshitake, Makromol. Chem., **185**, 1133 (1984); (c) *Synthesis, Structural and Industrial Aspects of Stereospecific polymerization, Makromol. Chem. Macromol. Symp.* 89 (1995): Eds. R. Tritto and U. Giannini.

58. G. Wilkinson, P.L. Pauson, J.M. Birmingham and F.A. Cotton, *J. Am. Chem. Soc.*, **75**, 1011 (1953).

59. (a) K.H. Reichert and K.R. Meyer, *Makromol. Chem.*, **169**, 163 (1973); (b) A.A. Andersen, J.G. Cordes, W. Kaminsky, A. Merck, H. Sinn and H.J. Vollmer, *Angew. Chem. Int. Ed. Engl.*, **15**, 630 (1976); (c) H. Sinn and W. Kaminsky, *Adv. Organomet.Chem.*, **18**,99 (1980).

60. (a) R. Jordan, *Advances in Organometallic Chemistry*, **32**, 325 (1991); (b) T.J. Marks, *Acc. Chem. Res.*, **25**, 57 (1992).

61. (a) M. Bochmann, *J. Chem. Soc. Dalton Trans.*, 255 (1996); (b) H.H. Brintzinger, D. Fischer, R. Mulhaupt, B. Rieger and R.M. Waymouth, *Angew. Chem. Int. Ed. Engl.*, **34**, 1143 (1995); (c) W. Kaminsky, *Catal. Today*, **20**, 257 (1994).

62. (a) P.J. Shapiro, E. Bunel, W.P. Schaefer and J.E. Bercaw, *Organometallics*, **9**, 867 (1990); (b) J.C. Stevens and F.J. Timmers, D.R. Wilson, G.F. SchmidtG.W. Knight and S.Y. Lai, Eur. Pat. Applic., EP 416815 (1990); (c) J.A.M. Canich, US Pat. Appic. 5,026,789 and 5,055,438, (1993); (d) J.A.M. Canich, Eur. Pat. Applic., EP 420436 (1990).

63. (a) J.D. Scollard, D.H. McConville and J.J. Vittal, *Organometallics*, **14**, 5478 (1995); (b) F. Guerin, D.H., McConville and J.J. Vittal, *Organometallics*, **14**, 3154 (1995).

64. (a) F.Geoffrey, N. Cloke, P.B. Hitchcock and J. Love, *J. Chem. Soc. Dalton Trans.*, 25 (1995); (b) A.D. Horton, J. De With, A.J. Van der Linder and H. Van de Weg, *Organometallics*, **15**, 2672 (1996).

65. (a) L. Lee, D. Berg and G. Bushnell, *Organometallics*, **14**, 8 (1995); (b) L. Lee, D. Berg and G. Bushnell, *Organometallics*, **16**, 2556 (1997); (c) L. Lee, D. Berg and G. Bushnell, *Inorg. Chem.*, **33**, 5302 (1994).

66. (a) R. Uhrhammer, D.G. Black, T.G. Gardner, J.D. Olsen and R.F. Jordan, *J. Am. Chem. Soc.*, **115**, 8493 (1993); (b) D.G. Black, D.C. Swenson, R.F. Jordan and R.D. Rogers, *Organometallics*, **14**, 3539 (1995).

67. (a) T. Miyatake, K. Mizunuma, Y.Seki and M. Kakugo, *Makromol. Chem., Radip Commun.* **10**, 349 (1989); (b) Mitsue Toatsu Chem. Inc. JP 05230133-A

68. A. van der Linden, C.J. Schaverien, N.Meijboom, C. Ganter and A.Guy Orpen, *J. Am. Chem. Soc.*, **117**, 3008 (1995).

69. (a) P.L. Waston, *J. Am. Chem. Soc.*, **104**, 337 (1982); (b) J. Mauermann, P.N. Swepston and T.J. Marks, *Organometallics*, **4**, 200 (1985); (c) G Keske, H. Lauke, J. Mauermann, P.N. Swepston, H. Schumann and T.J. Marks, *J. Am. Chem. Soc.*, **107**, 8091 (1985).

70. E.B. Coughlin and J.E. Bercaw, *J. Am. Chem. Soc.*, **114**, 7606 (1992).

71. C.J. Schaverien, *Organometallics*, **13**, 69 (1994).

72. (a) R.C. Mehrotra, A. Singh and S. Sogiani, *Chem. Soc. Rev.*, **215**, 225 (1994); (b) R.C. Mehrotra, A. Singh and U.M. Tripathi, *Chem. Rev.*, **91**, 1287 (1991).

73. (a) M.F. Lappert, *Chem. Rev.*, **56**, 959 (1956); (b) G.O. Doak and L.D. Freedman, *Chem. Rev.*, **61**, 31 (1961); (c) P.N. Kapoor and R.C. Mehrotra, Coord. *Chem. Rev.*, **14**, 1 (1974).

74. S.N. Misra, T.N. Misra and R.C. Mehrotra, *J. Inorg. Nucl. Chem.*, **27**, 105 (1965).

75. D.C. Bradley, F.M. Halim and W. Wardlaw, *J. Chem. Soc.*, 3450 (1950).

76. D.F. Herman, U.S. Patent, 2,654,770; 2,655,523; (1953).

77. (a) J.M. Batwara, U.D. Tripathi and R.C. Mehrotra, *J. Chem. Soc.*, (A), 991 (1967). (b) R.J. Speer, *J. Org. Chem.*, **14**, 655 (1949).

78. W.G. Bartley and W. Wardlaw, *J. Chem. Soc.*, 421 (1958).

79. D.C. Bradley, J.S. Ghotra and F.Hart, *J. Chem. Soc. Dalton*, 1021 (1973).

80. B.A. Vaartstra, J.C. Huffman, W.E. Streib and K.G. Caulton, *Inorg. Chem.*, **30**, 121 (1991).

81. U. Zucchini, E. Albizzati and U. Giannini, *J. Organomet. Chem.*, **26**, 357 (1971).

82. (a) R.A. Andersen, *Inorg. Chem.*, **18**, 1724 (1979); (b) *J. Chem. Soc. Dalton*, 2010 (1980).

83. (a) D.C. Bradley and W. Wardlaw, *Nature*, **165**, 75 (1950); (b) R.C. Mehrotra, *J. Am. Chem. Soc.*, **76**, 2266 (1954).

84. (a) M.K. Wu, J.R. Ashburn, C.J. Thorng, P.H. Hor, R.L. Gao, Z.J. Huang, and C.W. Chu, *Phys. Rev. Lett.*, **58**, 908 (1987). (b) K.G. Caulton and L.G. Hubert-Pfalzgraf, *Chem. Rew.*, **90**, 969 (1990)

85. (a) P. Shao, D.J. Berg and G.W. Bushnell, *Inorg. Chem.*, **33**, 3452 (1994); (b) P. Shao, D.J. Berg and G.W. Bushnell, *Can. J. Chem.*, **73**, 1 (1995).

86. J.L. Kiplinger, T. G. Richmond and C.E. Osterberg, *Chem. Rev.*, **94**, 373 (1994).

87. (a) P.B. Hitchcock, M.F. Lappert, I.A. MacKinnon, *J. Chem. Soc., Chem. Commun.* 1557 (1988); (b) W.A. Herrmann, R. Anwander, and M. Denk, *Chem. Ber.*, **125**, 2399 (1992).

88. L.E. Manzer, *J. Am. Chem. Soc.*, **100**, 8068 (1978).

89. (a) McGeary, M.J.; Coan, P.S.; Folting, K.; Streib, W.E.; Caulton, K.G. *Inorg. Chem.***30**, 1723 (1991); (b) Coan, P.S.; Hubert-Pfalzgraf, L.G.; Caulton, K.G. *Inorg. Chem.*, **31**, 1262 (1992).

90. (a) B.A. Vaarstra, J.C. Huffman, P.S. Gradeff, L.G. Hubert-Pfalzgraf, J.C. Daran, S. Parraud, K.Yunlu, and K.G. Caulton, *Inorg. Chem.* **29**, 3126 (1990); (b) H.A. Stecher, A. Sen and A.L. Rheingold, *Inorg. Chem.* **28**, 3280, (1989); (c) A. Sen, H.A. Stecher and A.L. Rheingold, *Inorg. Chem.* **31**, 473 (1992); (d) M. Wedler, J. Gilje, U. Pieper, D. Stalke, M. Noltemayer and F.T. Edelmann, *Chem. Ber.*, **124**, 1163 (1991); (e) W.A. Herrmann, R. Anwander, M. Kleine and W. Scherer, *Chem. Ber.*, **125**, 1971 (1992); (f) W.A. Herrmann, R. Anwander and W. Scherer, *Chem. Ber.*, **126**, 1533 (1993).

91. R.D. Shannon, *Acta Crystallogr.*, **A32**, 751 (1976).

92. (a) D.R. Niethamer, L. Parkanyi, J.F. Mitchell and P.T. Wolczanski, *J. Am. Chem. Soc.*, **110**, 4421 (1988); (b) R. Toreki, R.E. LaPointe, P.T. Wolczanski, *J. Am. Chem. Soc.*, **108**, 6382 (1986).

93. L. DeCola, D.L. Smailes, L.M. and Vallarino, *Inorg. Chem.*, **25**, 1729 (1986).

94. D.C. Bradley, R.C. Mehrotra, J.D. Swanwick and W. Wardlaw, *J. Chem. Soc.*, 2025 (1953).

95. D.L. Clark, J.G. Watkin and J.C. Huffman, *Inorg. Chem.*, **31**, 1556 (1991).

96. M.H. Chisholm, J.C. Huffman and J.L. Wesemann, *Polyhedron*, **10**, 1367 (1991).

97. K.F. Tesh, D.J. Burkey and T.P. Hanusa, *J. Am. Chem. Soc.*, **116**, 2409 (1994).

98. M.J. McCormick, S.C. Sockwell, C.E.H. Davies, T.P. Hanusa and J.C. Huffman, *Organometallics*, **8**, 2044 (1989).

99. (a) D.C. Bradley, H. Chudzynska, M.B. Hursthouse and M. Motevalli, *Polyhedron*, **10**, 1049 (1991); (b) D.C. Bradley, H. Chudzynska, M.E. Hammond, M.B. Hursthouse, M. Motevalli and W. Ruowen, *Polyhedron*, **11**, 375 (1992).

100. (a) A.A. Naiini, W.M. Menge and J.G. Verkade, *Inorg. Chem*, **30**, 5009 (1991); (b) W.M. Menge and J.G. Verkade, *Inorg. Chem.*, **30**, 4628 (1991); (c) A.A. Naiini, S.L. Ringrose, Y. Su, A. Jacobson and J.G. Verkade, Inorg. Chem., *Inorg. Chem.*, **32**, 1290 (1993).

101. (a) C.C. Cummins, R.R. Schrock, and W.M. Davis, *Organometallics*, **11**, 1452 (1992); (b) C.C. Cummins, J. Lee, R.R. Schrock, and W.M. Davis, *Angew. Chem. Int. Ed. Engl.*, **31**, 1501 (1992); (c) S. Friedrich, H. Memmler, L.H. Gade, W. Li and M. McPartlin, *Angew. Chem. Int. Ed. Engl.*, **33**, 676 (1994).

102. H.C. Brown, N.R. De Lue, G.W. Kabalka and H.C. Hedgecock, Jr. *J. Am. Chem. Soc.*, **98**, 1291 (1976).

103. H.C. Brown, "Organic Syntheses Via Boranes", Wiley, New York, 1975, p 102.

104. M.S. Gibson, R.W. Bradshaw *Angew. Chem. Int. Ed. Engl.*, 7, 919 (1968).

105. A. Kunai, T. Kawakami, E. Toyoda and M. Ishikawa, *Organometallics*, **11**, 2708 (1992).

106. (a) F.A. Cotton and G. Wilkinson, "Advanced Inorganic Chemistry", 5th Ed., John Wiley and Sons, New York, 1988. (b) E.W. Abel, F.G. Stone and G. Wilkinson,

Eds. "Comprehensive Organometallic Chemistry" Vol. 4., Pergamon, New York, 1995. (c) C. Elschenbroich and A. Salzer, "Organometallics", 2nd Ed., VCH Verlagsgesellschaft mbH, Weinheim, 1992.

107. (a) W.J. Evans, *Adv. Organomet. Chem.* **24**, 131 (1985). (b) H. Schumann, *Angew. Chem. Int. Ed. Engl.*, **110**, 145 (1985). (c) W.J. Evans, *Polyhedron*, **6**, 803 (1987).

108. (a) P.B. Hitchcock, M.F. Lappert, R.G. Smith, R.A. Bartlett and P.P. Power, *J. Chem. Soc. Chem. Commun.*, 1007 (1988); (b) C.J. Schaverien, and A. Orpen, *Inorg. Chem.*, **30**, 4968 (1991); (c) J.L. Atwood, M.F. Lappert, R.G. Smith and H. Zhang, *J. Chem. Soc. Chem. Commun.*, 1309 (1988).

109. C.J. Schaverien, and A. Orpen, *J. Chem. Soc. Chem. Commun.*, 124 (1992).

110. Z. Shen, *Inorg. Chim. Acta*, **140**, 7 (1987).

111. M.F. Lappert, A. Singh, and R.G. Smith, *Inorg. Synth.* **27**, 164 (1990).

112. (a) W.J. Evans, R.E. Golden and J.W. Ziller, *Inorg. Chem.*, **30**, 4963 (1991). (b) M.J. McGeary, P.S. Coan, K. Folting, W.E. Streib and K.G. Caulton, *Inorg. Chem.* **30**, 1723 (1991). (c) P.S. Gradeff, K.Yunlu, T.J. Deming, J.M. Olofson, R.J. Doedens and W.J. Evans, *Inorg. Chem.* **29**, 420 (1990). (d) M.J. McGeary, P.S. Coan, K. Folting, W.E. Streib and K.G. Caulton, *Inorg. Chem.*, *28*, 3283 (1989); (e) P.S. Gradeff, K. Yunlu, A. Gleizes and J. Galy, *Polyhedron*, **8**, 1001 (1989).

113. J. Sandstrom, "Dynamic NMR Spectroscopy", Pergamon, London, 1982.

114. (a) J.M. Berg, D.L. Clark, J.C. Huffman, D.E. Morris, A.P. Sattelberger, W.E. Streib, W.G. Van der Sluys and J.G.Watkin, *J. Am. Chem. Soc.* **114**, 10811 (1992). (b) D.C. Bradley, J.S. Ghotra, F.A. Hart, M.B. Hursthouse and P.R. Raithby, *J. Chem. Soc., Dalton Trans.*, 1166 (1977). (c) H.C. Aspinall, S.R. Moore and A.K. Smith, *J. Chem. soc., Dalton Trans.*, 153 (1992). (d) M. Allen, H.C. Aspinall, S.R. Moore, M.B. Hursthouse and A.I. Karvalov, *Polyhedron*, **11**, 409 (1992). (e) H.A. Stecher, A. Sen and A.L. Rheingold, *Inorg. Chem.*, **27**, 1130 (1988).

115. L. Lee, D.J. Berg and G.W. Bushnell, *Organometallics*, **14**, 5021 (1995).

116. (a) E.W. Abel, F.G. Stone and G. Wilkinson, Eds. "Comprehensive Organometallic Chemistry" Vol. 12., Pergamon, New York, 1995. (b) K. Maruoka, Y. Araki and H. Yamamoto, *J. Am. Chem. Soc.*, **110**, 2650 (1988); (c) K. Mikami, Y. Motoyama and M. Terada, *J. Am. Chem. Soc.*, **116**, 2812 (1994); (d) N.W. Eilerts and J.A. Heppert, *Polyhedron*, **14**, 3255 (1995).

117. S.R. Buc and Ford, *J. Am. Chem. Soc.*, **69**, 844 (1947).

118. (a) D.W. Stephan, *Organometallics*, **10**, 2037 (1991). (b) D.W. Stephan, *Organometallics*, **9**, 2718 (1990); (c) G. Erker and R. Noe, *J. Chem. Soc. Dalton Trans.*, 685 (1991).

119. H. Clark, F.G. Cloke, P.B. Hitchcock, J.B. Love and A.P. Wainwright, *J. Organom. Chem.*, **501**, 333 (1995).

120. E. C.Ashby, and G. F. Willard, *J.Org.Chem.* **43**, 4750 (1978).

121. B.A. Vaartstra, J.C. Huffman, P.S. Gradeff, L.G. Hubert-Pfalzgraf, J. Daran, S. Parraud, K. Yunlu and K.G. Caulton, *Inorg. Chem.* **29**, 3126 (1990).

122. S.L. Latesky, A. McMullen, I.P. Pothwell and J. Huffman, *J. Am. Chem. Soc.*, **102**, 5981 (1985).

123. C. McDade, J.C. Green and J.E. Bercaw, *Organometallics*, **1**, 1629 (1982); A. R. Bulls, W.P. Schaefer, M. Serfas and J.E. Bercaw, *Organometallics*, **6**, 1219 (1987); L. Chamberlain, I.P. Rothwell and J.C. Huffman, *J. Am. Chem. Soc.*, **104**, 7338 (1982).

124. M.D. Fryzuk, T.S. Haddad and S.J. Rettig, *Organometallics*, **10**, 2026 (1991).

125. (a) P.C. Wailes and H. Weigold, *J. Organom. Chem.*, **24**, 405 (1970); (b) P.C. Wailes, H. Weigold and A.P. Bell, *J. Organom. Chem.*, **43**, C32 (1972); (c) J. Shwartz and J. Labinger, *Angew. Chem. Int. Ed. Eng.*, **15**, 333 (1976); (d) J.A. Labinger, "Comprehensive Organic Synthesis", B.M. Trost and I. Fleming Eds., Pergamon, New York, Vol. 9, 667 (1991).

126. E. Negishi, "Comprehensive Organic Synthesis", L. Paqutte Eds., Pergamon, New York, Vol. 5, 1163 (1991); (b) E. Negishi and T. Takahashi, *Acc. Chem. Res.*, **27**, 124 (1994).

127. (a) G. Erker, *J. Organomet. Chem.*, **134**, 189 (1977); (b) S. Buchwald, R.D. Brone, *Science*, **261**, 1696 (1993); (c) S. Buchwald and R. Neilsen *Chem. Rev.*, **88**, 1047 (1988).

128. (a) C.A. Willoyghby and S. Buchwald, *J. Am. Chem. Soc.*, **116**, 11703 (1994); (b) R.D. Broene and S. Buchwald, *J. Am. Chem. Soc.*, **115**, 12569 (1993).

129. W.A. Nugent and J.M. Mayer, "Metal-Ligand Multiple Bonds", John Wiley & Sons, New York, (1988).

130. W.A. Nugent, R.J. McKinney, R.V. Kasowski and F.A. Van-Catledge, *Inorg. Chim. Acta*, **65**, L91 (1982).

131. (a) R.R. Schrock, R.T. DePue, J. Feldman, C.J. Schaverrien, J.C. Dewan and A.H. Liu, *J. Am. Chem. Soc.*, **110**, 1423 (1988); (b) M. Kol, R. Schrock, R. Kempe and W.M. Davis, *J. Am. Chem. Soc.*, **116**, 4382 (1994); (c) R. O'Dell, D.H. McConville, G.E. Hofmeister and R.R. Schrock, *J. Am. Chem. Soc.*, **116**, 3414 (1994).

132. (a) P.J. Walsh, F.J. Hollander and R.G. Bergman, *J. Am. Chem. Soc*, **110**, 8729 (1988); (b) P.J. Walsh, A.M Baranger and R.G. Berrgman, *J. Am. Chem. Soc.*, **114**, 1708 (1992); (c) K.E. Meyer, P.J. Walsh and R.G. Bergman, *J. Am. Chem. Soc.*, **117**, 974 (1995).

133. G.I. Nikonov, A.J. Blake and P. Mountford, *Inorg. Chem.*, **36**, 1107 (1997).

134. (a) C.C. Cummins, S.M. Baxter and P.T. Wolzanski, *J. Am. Soc. Chem*, **110**, 8731 (1988); (b) C.C. Cummins, C.P. Schaller, G.D. Vanduyne, P.T. Wolzanski, A.W. Chan and R. Hoffmann, *J. Am. Soc. Chem*, **113**, 2985 (1991).

135. "Handbook of Phosphorus-31 Nuclear Magnetic Resonance Data", J.C. Tebby Ed., CRC Press Inc., 1991

136. R. Cram, "Fundamentals of Carbonanion Chemistry", Academic Press. Inc., New York, 1965.

137. D.L. Thorn, W.A. Nugent and R.L. Harlow, *J. Am. Chem. Soc.*, **103**, 357 (1981).

138. (a) N.Y. Turova, V.A. Kozunov, A.I. Yanovskii, N.G. Bokii, Yu Struchkov and B.L. Tamopolskii, *J. Inorg. Nucl. Chem.*, **41**, 5 (1979); (b) K Folting, W.E. Caulton, O. Poncelet and L.G. Hubert-Pfalzgraf, *Polyhedron*, **10**, 1639 (1991).

139. M.T. Reetz, "Organotitanium Reagents in Organic Synthesis, Springer Verlag, Berlin, 1986; (b) B. Weidmann, D. Seebach, *Angew. Chem. Int. Ed. Engl.* **22**, 31 (1983).

140. B. Schmidt and D. Seebach, *Angew. Chem. Int. Ed. Engl.*, **30**, 99 (1991).

141. R.O. Duthaler, A. Hafner and M. Riediker, *Pure Appl. Chem.*, **62**, 631 (1990).

142. "NMR and Chemistry - An Introduction to Modern NMR Spectroscopy", 3rd. Ed., J.W. Akitt, Chapman & Hall, 1992.

143. K.P.C. Vollhardt, *Angew. Chem. Int. Ed. Engl.*, **23**, 539 (1984).

144. N.E. Schore, *Chem. Rev.*, **88**, 1081 (1988). (b) W. Hubel and C. Hoogzand, *Chem. Ber.*, **93**, 103 (1960); (c) R.S. Dickson and P.J. Fraser, *Adv. Organomet. Chem.*, **12**, 323 (1974); (d) Y. Ito, M. Inouye, M. Murakami and M. Shiro, *J. Organomet.*

Chem., **385**, 399 (1990); (e) K.S. Jerome and E.J. Parsons, *Organometallics*, **12**, 2991 (1993).

145. J.E. Hill, G. Balaich, P.E. Fanwick and I.P. Rothwell, *Organometallics*, **12**, 2911 (1993)

146. (a) J.L. Atwood, W.E. Hunter, H.G. Alt and M.D. Rausch, *J. Am. Chem. Soc.*, **98**, 2425 (1976); (b) W.A. Nugent, D.L. Thorn and R.L. Harlow, *J. Am. Chem. Soc.*, **109**, 2788 (1987); (c) G. Erker, R. Zwettler, C. Kruger and R. Gleiter, *Organometallics*, **9**, 524 (1990); (d) S.L. Buchwald, K.A. Kreutzer and R.A. Fisher, *J. Am. Chem. Soc.*, **112**, 4600 (1990).

147. (a) J.R. Strickler, P.A. Wexler and D.E. Wigley, *Organometallics*, 7, 2067 (1988); D.P. Smith, J.R. Strickler, S.D. Gray, M.A. Bruck, R.S. Holmes and D.E. Wigley, *Organometallics*, **11**, 1275 (1992).

148. (a) J.C. Green, M.L.H. Green and C.K. Prout, *J. Chem. Soc. Chem. Commun.*, 421 (1972); (b) J.L. Petersen, D.L. Lichtenberger, R.F. Fenske and L. Dahl, *J. Am. Chem. Soc.*, **97**, 6433 (1975); (c) J.W. Lauher and R. Hoffmann, *J. Am. Chem. Soc.*, **98**, 1729 (1976); (d) L. Zen and N.M. Kostic, *J. Organomet. Chem.*, **335**, 395 (1987).

149. (a) X. Yang, C.L. Stern and T.J. Marks, *J. Am. Chem. Soc.*, **113**, 3623 (1991); (b) X. Yang, C.L. Stern and T.J. Marks, *J. Am. Chem. Soc.*, **116**, 10015 (1994).

150. (a) I.K. Lee, W.J. Gauthier, J.M. Ball, B. Iyengar and S. Collins, *Organometallics*, **11**, 2115 (1992); (b) N. Piccolrovazzi, P. Pino, G. Consiglio, A. Sironi and M. Moert, *Organometallics*, **9**, 3098 (1990); (c) D.E. Richardson, N.G. Alameddin, M.F. Ryan, T. Hayes, J.R. Eyler and A.R. Siedle, *J. Am. Chem. Soc.*, **118**, 11244 (1996).

151. D.M. Roddick and R.C. Schnabel, "Inorganic Fluorine Chemistry, Toward the 21st Centry", Edt. J.S. Thrasher and S.H. Strauss, Chapter 27, ACS Symposium Series 555.

152. (a) M. Kol, R.R. Schrock, R. Kempe and W.M. Davis, *J. Am. Chem. Soc.*, **116**, 4382 (1994); (b) R.R. Schrock, J. Murdezek, G.C. Bazan, J. Robbins, M. DiMare and M. O'Regan, *J. Am. Chem. Soc.*, **112**, 3875 (1990).

153. S. Danishefsky and M. Bednarski, *Tetrahedron Lett.*, **25**, 721 (1984).

154. L. Clouston, C. Spino and D. Berg, *Can . J. Chem.*, **74**, 1762 (1996).

155. (a) O. Fujimura, F. Javier De La Mata and R.H. Grubbs, *Organometallics*, **15**, 1865 (1996); (b) O. Fujimura, and R.H. Grubbs, *J. Am. Chem. Soc.*, **118**, 2499 (1996).

156. E.J. Corey and M. Chaykovsky, *J. Am. Chem. Soc.*, **87**, 1353 (1965).

157. H. Ohta, T. Kobori and T. Fujisawa, *J. Org. Chem.*, **42**, 1231 (1977).

158. J.D. Coombes and D.D. Eley, *J. Chem. Soc.*, 3700 (1957).

159. O. Nuyken and S.D. Pask, "New Methods for Polymer Synthesis", Chapter 4, W.J. Mijs Edt., Plenum Press, New York, 1992.

160. G.M. Sheldrick, SHELX86, Programs for Crystal Structure Determination. University of Cambridge, 1986.

161. A.C. Larson, F.L. Lee, Y. Lepage, M. Webster, J.P. Charland and E.J. Gabe, NRC, Canada, 1991

162. C.K. Johnson, ORTEPII, Oak Ridge National Laboratory: Oak Ridge, TN, 1976.

163. L. Zsolnai, ZORTEP, University of Heidelberg, Heidelberg, Germany, 1995.